Imperial College of Science, Technology & Medicine

University of London

THE NON-INTRUSIVE MODAL TESTING OF DELICATE AND CRITICAL STRUCTURES

Philip Ind

A thesis submitted to the University of London for the

degree of Doctor of Philosophy

For Donna, Scott & Taylor

ABSTRACT

The thesis focuses on the application of non-intrusive modal test methods to a class of structures that require careful handling due to their delicate or critical nature. The test related problems associated with these types of structure are discussed, as are the requirements for their accurate dynamic characterisation. Previous works on non-intrusive test methods are reviewed against these requirements and conclusions are drawn as to where more research or alternative approaches are necessary.

From the review, the Laser Doppler Vibrometer (LDV) is selected as the most versatile and easy to deploy of the available non-contacting response measurement methods. The LDV's continuously scanning capability is explored and extended to encompass axi-symmetric structures such as cylinders and cones, which are common shapes for the structures of specific interest. The application of the LDV in conjunction with hammer testing is also demonstrated on a delicate structure, illustrating how this minimally intrusive test configuration can provide the high quality of data required for model validation purposes.

The review also highlights the problems associated with existing, non-contacting excitation methods and in particular those associated with force measurement. The theory for indirect testing, a possible alternative approach to completely non-contacting testing, is introduced. The concept of indirect testing is explored through virtual testing, the simulation and rehearsal of experiments in a computer. These virtual tests demonstrate that the calculations used for the indirect testing of structures can behave erratically if the test fixtures used are not carefully designed. Criteria for the design of indirect test fixtures are established and two possible indirect testing

methods (FRF-based and “model-and-remove”) are introduced. These two methods are then demonstrated in two case studies, a simple free-free beam, and a more complex, purpose built structure, which is similar to the structures of specific interest.

Finally, conclusions as to the successes/failures of the techniques introduced in the thesis are given and suggestions for areas of further study are made.

Acknowledgements

The author gratefully acknowledges the support of his supervisor, Prof. D.J. Ewins for his encouragement, advice and direction over the past few years. I would also like to thank Tony Stanbridge for his technical advice and friendship during the course of my studies. My thanks must also go to the many AWE staff who have offered technical and moral support, and in particular, Charles Kernthaler, Brian Tyler, Carole Reece and Dr. Gurdip Kalsi each of whom have contributed to the completion of this work in some way. I must also acknowledge the support of my family, especially my wife, whose patience and support (particularly in the final months) has been much appreciated.

The author also gratefully acknowledges the financial support of both AWE and the EPSRC, without which this work would not have been possible.

CONTENTS

CHAPTER 1. INTRODUCTION **18**

1.1 BACKGROUND 18

1.2 DELICATE AND CRITICAL COMPONENTS 20

1.3 DEFINITIONS 24

1.3.1 Non-intrusive testing 24

1.3.2 Indirect testing 24

1.3.3 Non-contact testing 25

1.4 THE IMPORTANCE OF MASS NORMALISATION FOR DTA LEVEL 3 AND 4 MODAL ANALYSIS APPLICATIONS 25

1.5 ON THE RELEVANCE OF VIRTUAL TESTING TO DELICATE AND CRITICAL COMPONENTS 28

1.6 EVALUATION CRITERIA FOR NON-INTRUSIVE MODAL TESTING METHODS FOR DTA LEVEL 3 AND 4 APPLICATIONS 29

1.6.1 General comment 29

1.6.2 The transfer function relationships 29

1.6.3 Generic requirements of response/force measurement equipment 31

1.6.4 Response Measurement Requirements 32

1.6.5 Force Measurement Requirements 32

1.6.6 Force Application Requirements 33

1.6.7 Concluding remarks 36

1.6.8 A note on test requirements for the structures of specific interest 37

1.7 THESIS SCOPE AND STRUCTURE 38

1.7.1 Scope 38

1.7.2 Structure 38

CHAPTER 2. A REVIEW OF NON-INTRUSIVE MODAL TESTING **41**

2.1 INTRODUCTION 41

2.2 OVERVIEW 41

2.3 NON-CONTACT RESPONSE MEASUREMENT DEVICES 42

2.3.1 General comment on non-contacting measurement devices 42

2.3.2 LDVs 42

2.3.3 Holography 47

2.3.4 Moiré Techniques 49

2.3.5 Laser Triangulation Methods 50

2.3.6 Acoustic Measurement Methods 50

2.3.7 Proximity Detection 52

2.3.8 Stress/Strain Measurement Techniques 53

2.4 NON-CONTACTING EXCITATION DEVICES 53

2.4.1 General comment on non-contacting excitation devices 53

2.4.2 Acoustic excitation methods 54
2.4.3 Pulsed air excitation 56
2.4.4 Non-contacting magnetic excitation 56
2.4.5 Eddy current excitation 58
2.4.6 Laser pulse excitation 59
2.4.7 Electrical spark excitation 60
2.5 NON-INTRUSIVE AND MINIMALLY-INVASIVE EXCITATION TECHNIQUES 61
2.5.1 Minimally-invasive excitation techniques 61
2.5.2 Non-intrusive excitation techniques 63
2.6 INDIRECT EXCITATION/RESPONSE MEASUREMENT METHODS 65
2.6.1 The measurement of Rotational Degrees of Freedom (RDOFs) 65
2.6.2 The Dynamic Characteristics of Internal Components 66
2.7 CONCLUSIONS 67
2.8 SPECIFIC OBJECTIVES 68

CHAPTER 3. PRACTICAL APPLICATION OF THE LDV 70

3.1 INTRODUCTION 70
3.2 SINGLE POINT LDV 70
3.2.1 General comment 70
3.2.2 Case study: minimally intrusive modal testing of a delicate component 71
3.3 CONTINUOUSLY SCANNING LDV 86
3.3.1 General Comment 86
3.3.2 Fundamental theory for CSLDV sinusoidal straight line and area scans 86
3.3.3 Application of continuous area scanning to cylindrical structures 97
3.4 CONCLUDING REMARKS ON THE LDV DEVICE AS A RESPONSE TRANSDUCER 111

CHAPTER 4. INDIRECT TESTING 114

4.1 INTRODUCTION 114
4.2 THE INDIRECT TESTING METHOD 115
4.3 SUBSTRUCTURE COUPLING 116
4.3.1 Spatial sub-structuring 116
4.3.2 FRF sub-structuring 117
4.3.3 CMS sub-structuring 119
4.3.4 Two common problems 120
4.4 UNCOUPLING AS A METHOD FOR THE INDIRECT TESTING OF STRUCTURES 123
4.4.1 Development of an FRF uncoupling analysis 123
4.4.2 Further refinements 126
4.4.3 On the practical implementation of the uncoupling equations 128
4.5 NUMERICAL EXAMPLE 128
4.5.1 Purpose of the numerical tests 128
4.5.2 Model data for the structures 129

4.5.3 Investigation into the selection of remote DOFs and the omission of Point RDOF measurements *131*
4.5.4 Results *131*
4.5.5 Investigation of the effects of noise on the indirect testing calculation *135*
4.5.6 Discussion *136*
4.6 THE DESIGN OF INDIRECT TEST FIXTURES 147
4.6.1 Mathematical basis *147*
4.6.2 Practical implementation *148*
4.6.3 Numerical example revisited *152*
4.7 CONSIDERATIONS FOR THE PRACTICAL IMPLEMENTATION OF THE FRF UNCOUPLING METHOD 162
4.7.1 The choice of exciter *162*
4.8 A SUMMARY OF THE STATE-OF-THE-ART IN FRF BASED INDIRECT TESTING 163
4.9 AN ALTERNATIVE INDIRECT TESTING METHOD 166
4.9.1 Spatial uncoupling: the "model-and-remove" approach *166*
4.10 CONCLUSIONS 169
4.10.1 Indirect modal testing of structures *169*
4.10.2 Ramifications for the inference of information on internal components *170*
CHAPTER 5. APPLICATION OF INDIRECT TESTING MODAL TESTING 171
5.1 INTRODUCTION 171
5.2 CASE STUDY ONE: FREE-FREE BEAM 171
5.2.1 Background *171*
5.2.2 Method and results *173*
5.2.3 Discussion *180*
5.2.4 Conclusions. *187*
5.3 CASE STUDY TWO: THE MACE CASE 188
5.3.1 Background *188*
5.3.2 Indirect testing of the MACE Case using FRF uncoupling technique *189*
5.3.3 Development and application of the model and remove approach *196*
CHAPTER 6. CONCLUSIONS AND RECOMMENDATIONS FOR FURTHER STUDY 224
6.1 CONCLUSIONS 224
6.1.1 Overview *224*
6.1.2 Minimally-invasive modal testing using impact hammer excitation and LDV response measurement *224*
6.1.3 Application of CSLDV method to axi-symmetric structures *225*
6.1.4 The indirect modal testing of structures *226*
6.1.5 The use of LDV for indirect test measurements *229*
6.2 RECOMMENDATIONS FOR FURTHER STUDY 230
6.2.1 Application of FRF-based indirect testing for sub-structuring applications *230*

6.2.2 Stiff spring ill-conditioning *230*
6.3 CLOSURE 233

LIST OF FIGURES

Figure 2.3.1. Examples of LDV scanning techniques, results, and analysis: a) Circular scanning and; b) area scanning. 46
Figure 3.2.1. The structure under test: (a) actual structure; (b) initial finite element model....71
Figure 3.2.2. Best hammer excitation locations for the structure-under-test 73
Figure 3.2.3. Best accelerometer locations for the structure-under-test....74
Figure 3.2.4. (a) The selected test geometry and (b) its corresponding Auto-MAC....77
Figure 3.2.5. Overlay of true point FRF (black) and approximation to the point FRF given by excitation on the structures interior (red) showing small differences in the locations of the anti-resonances. 79
Figure 3.2.6. Test configuration used for minimally invasive modal testing of the structure under test. 80
Figure 3.2.7. (a) The point FRF H_{1r1r} ; (b) example of reciprocity check (H_{1r17r} (blue) and H_{17r1r} (green)); (c) example of response time history; (d) example coherence function.....81
Figure 3.2.8. (a) Full FRF data set; (b) natural frequency and MAC correlation of experimental model (set 1) and finite element model (set 2). 82
Figure 3.2.9. (a) Original shell element representation of the leg; (b) Improved brick element representation of the leg. 83
Figure 3.2.10. Natural frequency and MAC correlation of experimental model (set 1) and improved finite element model (set 2)....84
Figure 3.2.11. Natural frequency and MAC correlation of experimental model (set 1) and updated finite element model (set 2). 84
Figure 3.2.12. FRF calculated from FE model $H_{1r,1r}$ (red) and corresponding measured FRF $H_{1r,1r}$ (green). 85
Figure 3.3.1. Example cubic polynomial. 88
Figure 3.3.2. Side-band structure for example polynomial of Figure 3.3.1. (ω = 100Hz , Ω =10 Hz). .89
Figure 3.3.3. Simulated time-history computed for example polynomial (Figure 3.3.1). 91
Figure 3.3.4. Polynomial recovered from CSLDV analysis of time-history shown in Figure 3.3.3.....91

Figure 3.3.5. Example of side-band structure resulting from an area scan with Ω_x=10Hz and Ω_y=1.1Hz 93
Figure 3.3.6. Result of line scan on black carbon fibre composite with a scan rate of 10Hz, showing noise peaks caused by signal drop-out. 96
Figure 3.3.7. Result of line scan on black carbon fibre composite with a scan rate of 5Hz. 96
Figure 3.3.8. Illustration of the internal radius or "light-house scan".....97
Figure 3.3.9. Schematic CSLDV configuration for scanning cylindrical structures.....99
Figure 3.3.10. Illustration of LDV positioning for 6DOF scanning of a conical structure. 101
Figure 3.3.11. Illustration of geometry for scanning of a cone.....101
Figure 3.3.12. Geometry for deriving the mirror drive signal $\theta(t)$.....102
Figure 3.3.13. Test configuration for scanning of a cylinder using the rotary-stage method; (a) over-all configuration; (b) detail of internally mounted shaker; (c) detail of flexures used to constrain the test piece.....106
Figure 3.3.14. Modulation of the LDV signal due to misalignment: (a) scan not aligned with the axis of rotation; (b) scan not aligned with axis of rotation and skewed relative to the axis of rotation. .107
Figure 3.3.15. ODS obtained from CSLDV scanning of a cylinder: (a) (2,0) ODS at 231.1 Hz; (b) (2,1) ODS at 266.0Hz; (c) (3,1) ODS at 646Hz; (d) (3,1) ODS at 701Hz. 108
Figure 3.3.16. Qualitative comparison of experimental ODS at 701Hz and FE mode at 698Hz.....108
Figure 3.3.17. ODS obtained from scanning of a mis-tuned cylinder: (a) ODS at 211 Hz; (b) ODS at 778 Hz; (c) ODS at 532.4 Hz;(d) ODS at 847 Hz. 108
Figure 4.2.1. Illustration of the indirect testing problem 115
Figure 4.3.1. Schematic representation of the FRF coupling process. 118
Figure 4.5.1. The Frame structures for the numerical tests. 130
Figure 4.5.2. Nodes used in node sets 1, 2 and 3. 132
Figure 4.5.3. The result of the uncoupling calculation using node set 1. 132
Figure 4.5.4. The result of the uncoupling calculation using node set 2. 133
Figure 4.5.5. The result of the uncoupling calculation using node set 3. 133
Figure 4.5.6. Fourth node set, incorporating an additional point, so to provide an over-determined set of FRFs for use in the uncoupling equation. 134
Figure 4.5.7. The result of the uncoupling calculation using the over-determined node set 4. 134

Figure 4.5.8. Example of an FRF contaminated by 1% "peak" noise.....135

Figure 4.5.9. The effect of 1% "peak" noise on the uncoupling calculation.....136

Figure 4.5.10. The effect of 1% "peak" noise on the coupling calculation.....136

Figure 4.5.11. Condition number with respect to inversion against frequency plot for node sets 1, 2, 3 and 4.....138

Figure 4.5.12. Example of the difference between an FRF calculated from an FE model of the assembled structure (structure C) and the same FRF generated by via FRF coupling of structures A and B. 139

Figure 4.5.13. Optimum remote DOFs selected by iterative Matlab procedure. 142

Figure 4.5.14. Condition number with respect to inversion against frequency plot for the selected optimum DOFs and previous node set 142

Figure 4.5.15. Results of effective independence calculation for the first two modes of structure A: a) *x* direction; b) *y* direction. 144

Figure 4.5.16. Systems containing a stiff spring between two connection DOFs.....145

Figure 4.6.1. Possible solutions to the problem of constraining relative motion.....149

Figure 4.6.2. Redesigned indirect test fixture, incorporating additional masses.....150

Figure 4.6.3. Indirect testing fixture redesigned as two separate components.....152

Figure 4.6.4. Condition number vs. frequency for the original, and improved designs.....153

Figure 4.6.5. Estimation of HB1x1x by uncoupling using design 3, in the presence of 1% noise. 154

Figure 4.6.6. DOFs used for generation of FRFs for the virtual test 155

Figure 4.6.7. Example FRFs contaminated with 5% noise: a) H^{A}_{3x3x}; b) H^{C}_{3x3x}; c) H^{A}_{9x9x} 156

Figure 4.6.8. Example of FRFs regenerated from modal curve-fit data overlaid on the (true) FE curves: a) H^{A}_{3x3x}; b) H^{C}_{3x3x}; c) H^{A}_{9x9x} 157

Figure 4.6.9. Estimate of $T_{7x,7x}$ calculate via uncoupling (blue) overlaid on the actual curve (green) given by $H^{A}_{7x7x} + H^{B}_{1x1x}$. 159

Figure 4.6.10. FRF plot illustrating how "breakthroughs" in the calculated curve occur at the natural frequencies of the test fixture and assembled structures. 159

Figure 4.6.11. The FRF H^{B}_{1x1x} calculated using the uncoupling calculation overlaid on the actual FRF H^{B}_{1x1x} 160

Figure 4.6.12. Curve fitting of the "true" resonance calculated using uncoupling 161

Figure 5.2.1. Illustration of the indirect testing of a beam (beam B) showing the required measurements on beams A and C. 172

Figure 5.2.2. Test configurations use for the indirect testing of a beam: (a) experimental set-up for beam A; (b) experimental set-up for beam C. 173

Figure 5.2.3. Estimates of translational (red) and rotational (green) FRFs: (a) $H^{A}_{1x,3x}$ and $H^{A}_{1x,3\theta z}$; (b) $H^{A}_{2x,3x}$ and $H^{A}_{2x,3\theta z}$ 175

Figure 5.2.4. Estimate of $T_{3x,3x}$ (overlaid on $H^{A}_{1x,1x}$ and $H^{C}_{1x,1x}$) showing at least 4 new resonant peaks. 175

Figure 5.2.5. Zoomed portion of Figure 5.2.4 showing an example of noise on the new peaks. 176

Figure 5.2.6. Example of modal curve fits (red) overlaid on raw FRF data (green) for FRFs: (a) $H^{A}_{1x,1x}$; (b) $H^{A}_{1x,3\theta z}$; (c) $H^{C}_{1x,1x}$ 177

Figure 5.2.7. Estimate of $T_{3x,3x}$ overlaid on the curve given by $H^{A}_{1x,1x} + H^{C}_{1x,1x}$ 178

Figure 5.2.8. Example estimates of the free-free FRFs of beam B calculated via the indirect testing method 179

Figure 5.2.9. Examples of mode shapes obtained from modal analysis of FRFs obtained via the indirect testing calculation: (a) mode at 280 Hz; (b) mode at 1291 Hz. 180

Figure 5.2.10. Analytically derived condition number with respect to inversion Vs. Frequency plot for the uncoupling of beam A and beam B. 181

Figure 5.2.11. Examples of curve-fitted translational and rotational FRFs derived using Equation 5.2.1 overlaid on FRF curves derived from an FE model. 182

Figure 5.2.12. Example of reciprocity achieved with the test configuration, H^{A}_{1x2x} (green) and H^{A}_{2x1x} (red). 183

Figure 5.2.13. Illustration of how incorrect assumptions relating to excitation and reference locations lead to reciprocity errors. 184

Figure 5.2.14. Key node locations (finite element model numbering) for the virtual test investigation into the effects of assuming reciprocity. 185
Figure 5.2.15. Examples of analytical FRFs including reciprocity errors (blue) overlaid on true FRF curves (green).....186
Figure 5.2.16. Estimate of an element ($T_{est3y3y}$)of the coupled system matrix [T_{est}] overlaid on the true curve (T_{3y3y}).....187
Figure 5.3.1. The MACE assembly. 188
Figure 5.3.2. Problems in meeting the flexibility and strength requirements for the ITF when designed as 4 individual components.....190
Figure 5.3.3. Example mode (536 Hz) of rigidly grounded ITF showing relative motion between the connection locations.....191
Figure 5.3.4. Purpose designed bolt for connecting the MACE Case to the ITF.....191
Figure 5.3.5. Indirect testing of the MACE Case: (a) the Indirect Testing Fixture (ITF); (b) the MACE Case; (c) the ITF/MACE Case assembly. 192
Figure 5.3.6. Plot of EI showing how the best remote measurement DOFs are located on the diagonal cross braces of the ITF. 193
Figure 5.3.7. Measurement geometry for FRF-based indirect testing. 194
Figure 5.3.8. Example FRFs from test on the ITF and ITF/MACE Case assembly: a) H^{A}_{1x1x}; b) H^{A}_{1y1y}; c) H^{C}_{1x1x} ; d) H^{C}_{1y1y} 195
Figure 5.3.9. Example estimate of an element of the coupled structure matrix [T] 196
Figure 5.3.10. The initial FE model of the ITF.....199
Figure 5.3.11. Test planning for the ITF: a) Best Suspension locations (shown in dark blue) and ; (b) best impact locations (shown in maroon/red).....199
Figure 5.3.12. Best accelerometer locations for the ITF in a free-free configuration.....201
Figure 5.3.13. The final test geometry for the free-free ITF.....201
Figure 5.3.14. Analytically derived Auto-MAC for the final test geometry.....201
Figure 5.3.15. Auto-MAC of the experimentally obtained mode shapes. 202
Figure 5.3.16. Correlation between the experimental (set 1) and analytical (set 2) mode shapes achieved with the initial FE model.....203
Figure 5.3.17. Detail of the ITF model showing the dimension which required correction. 203

Figure 5.3.18. Correlation between the experimental (set 1) and analytical (set 2) mode shapes achieved with the improved leg FE model. 204
Figure 5.3.19. Close up of ITF showing large welds used to secure the cross braces (a) and approximation to these welds included in the FE model. 204
Figure 5.3.20. Correlation between the experimental (set 1) and analytical (set 2) mode shapes achieved with the FE model (legs corrected and approximations to major welds). 205
Figure 5.3.21. Close-ups of the ITF model, showing region where dimensional error was found (a) and the inclusion of all welds (b). 206
Figure 5.3.22. Correlation between the experimental (set 1) and analytical (set 2) mode shapes achieved with the FE model (all errors corrected, all welds included (E=69 GN/m^2) and mean values of measured thickness used). 207
Figure 5.3.23. Correlation between the experimental (set 1) and analytical (set 2) mode shapes achieved with the FE model (all errors corrected, all welds included (E=69 MN/m^2) and mean values of measured thickness used). 207
Figure 5.3.24. a) Best accelerometer locations for the ITF in fixed-base configuration showing clustering of measurement locations; b) analytical auto-MAC for the EI determined, best measurement locations. 209
Figure 5.3.25. Final test geometry (a) and its corresponding (analytical) auto-MAC (b). 209
Figure 5.3.26. Auto-MAC of the experimentally derived modes. 210
Figure 5.3.27. a) Close up of ITF showing the compliant elements (blue) used to represent the leg/ground interface stiffness; b) actual clamping arrangement used to fix the ITF to the seismic block. 211
Figure 5.3.28. Natural Frequency and MAC plot for the experimental and analytical ITF (in fixed base configuration) modal models: (a) all modes included; (b) modes 1-21 (0-1210Hz) included. ... 212
Figure 5.3.29. a) MACE Case model; b) ITF/MACE Case assembly model; c) detail of assembly model showing ITF/MACE Case interface and representation of a connection bolt. 213
Figure 5.3.30. Measurement geometry for modal test on the ITF/MACE Case assembly. 214
Figure 5.3.31. Example of an FRF taken from the ITF/Mace case assembly showing multiple resonances. 214
Figure 5.3.32. Example Case mode at 1805Hz. 215

Figure 5.3.33. Natural Frequency and MAC plot for the experimental (set 1) and analytical (set 2) modal models of the ITF/MACE Case assembly model. 215

Figure 5.3.34. Natural frequency and MAC plot of assembled structure (Case modes only, all measured DOFs included).....216

Figure 5.3.35. Natural frequency and MAC plot of assembled structure (DOFs on Case only, Case modes only).....216

Figure 5.3.36. % change in frequency of the first 46 Modes of the ITF/MACE Case assembly caused by halving and doubling the original leg/ground interface stiffness (69MN/m^2).....217

Figure 5.3.37. Systems containing a stiff spring between two connection DOFs.....218

Figure 5.3.38. % change in frequency of the first 46 Modes of the ITF/MACE Case assembly caused by halving and doubling the original ITF/ MACE Case interface stiffness (69GN/m^2). 219

Figure 5.3.39. Natural frequency and MAC plot showing for the free-free MACE Case. Set 1=Experimental model , set 2= FE model.....220

Figure 5.3.40. FE Model of MACE Case/Seal Plate Assembly containing approximately 2 million 20 node brick elements (courtesy of Trevor Hensley (AWE)).....223

Figure 6.2.1. Ill-posed force determination example: it is not possible to uniquely determine the three applied forces, even though five response measurements are made since the system only possesses two degrees of freedom.....231

Figure 6.2.2. The sub-structuring problem becomes ill-conditioned when both structures include FRFs measured at one or more apparently redundant co-ordinates. 231

LIST OF TABLES

Table 3.2-1. The effect of mass loading on the structure-under-test.....75

Table 3.2-2. Results of experimental modal analysis compared with analytical results from updated FE model.....84

NOMENCLATURE

x, y, z	translational degrees of freedom / co-ordinates (time varying)
$\theta_x, \theta_y, \theta_z$	rotational degrees of freedom
X, Y, Z	translational degrees of freedom / co-ordinates (frequency varying)
F	Force (frequency varying)
n, m	current mode/co-ordinate/value
N, M	total number of modes/co-ordinates/values
j, k	integers
r	current mode number
ω	frequency variable
$[M]$	mass matrix
$[K]$	stiffness matrix
$[\Psi]$	eigenvector matrix (un-normalised)
$[\Phi]$	mass normalised eigenvector matrix
ϕ_{jr}	mass normalised eigenvector element
${}_r A_{jk}$	modal constant of the r^{th} mode (given by $\phi_{jr}\phi_{kr}$)
ω_r	natural frequency or the r^{th} mode
$[Q]$	ordinary polynomial to Chebyshev polynomial conversion matrix
$[T]$	Chebyshev to ordinary polynomial conversion (i.e $[Q]^{-1}$) or coupled system matrix
$[H]$	FRF Matrix
H_{jk}	individual element of an FRF matrix

A, B	sub-structure superscripts
C	coupled structure / assembly superscript
a, b	remote/slave DOF on sub-structure/assembly
c	connection/master DOF on sub-structure/assembly
$[H^A], [H^B]$	sub-system FRF matrices
$[H^C]$	coupled system FRF matrix
$[H^A_{aa}], [H^A_{ac}], [H^A_{cc}]$	sub-matrices of partitioned FRF matrix (for sub-structure A, for example)
λ	condition number with respect to inversion (ratio of the highest singular value to the lowest)

CHAPTER 1. INTRODUCTION

1.1 Background

Over the past two decades or so, the near exponential growth in computer performance, coupled with advances in the field of Finite Element Modelling (FEM), has allowed industry to explore a new route to delivering their products to market. Increasingly the time-consuming and expensive, "iterative loops" within the design cycle are being conducted within the computer in an effort to remove the need for expensive prototypes. Traditionally, the design cycle included several prototype-testing phases, which were used to develop the product until it could meet the requirements of its specification. If it was expected that the product would be exposed to shock or vibration environments during its service life, this could mean numerous, and often lengthy, phases of dynamic testing. The safety and quality of the final design with respect to dynamic loading were, and in many cases still are, underwritten by such tests. The financial cost of these trials can be huge, especially in industries such as aero-engine manufacture or space flight, where product safety and quality are of paramount importance. With the recent advances in computing power and FEM codes, industry has begun not only to use FE models to aid the design optimisation process but, also, as an alternative means of underwriting of the safety and quality of products. This approach offers considerable savings by foregoing the need to manufacture and test prototype designs, but places considerable demands on the reliability of the model's predictions.

The use of analytical models for this purpose has given rise to the term "model validation", which Ewins [1] describes as, "the process of demonstrating or attaining

the condition that the coefficients in a model are sufficiently accurate to enable that model to provide an acceptably correct description of the subject structure's dynamic behaviour".

In the field of experimental structural dynamics, modal testing and analysis has developed as an essential tool for the validation of FE models, and is viewed as the primary source of information for evaluating, improving, and eventually underwriting the accuracy of the mass and stiffness matrices generated by FE models in a linear / weakly non-linear regime. For individual components, which can now be modelled with extremely high fidelity and faithfulness to the structure's geometry, these validation tests provide a method of checking for any errors on the part of the analyst or shortcomings in the model's details. For more complex structural assemblies, validation tests currently provide the main source of information for updating of the interface or joint stiffness parameters, which are usually difficult to assign a priori. In addition, more advanced modal testing and analysis methods such as substructure coupling are seen as offering a method of introducing experimentally-derived models of parts, which are computationally too expensive to model with existing technology into validated FE models.

The applications of modal testing and analysis were categorised by Ewins op. cit and the Dynamic Testing Agency (DTA) [2], with validation and structural sub-structuring being amongst the highest-level applications of modal testing. The DTA test levels are defined as:

Level 0: estimation of natural frequencies and damping factors; response levels measured at few points; very short test times.

Level 1: estimation of natural frequencies and damping factors; mode shapes defined qualitatively rather than quantitatively.

Level 2: measurements of all modal parameters suitable for tabulation and mode shape display, albeit un-normalised.

Level 3: measurements of all modal parameters, including normalised mode shapes; full quality checks performed and model usable for model validation.

Level 4: measurements of all modal parameters and residual effects for out-of-range modes; full quality checks and model usable for response based applications, including modification, coupling and response predictions.

These definitions will be used throughout this work as a means of determining how useful the data obtained using a particular test method can be.

1.2 Delicate and critical components

Although for the vast majority of structures modal testing to DTA levels 3 and 4 is possible using conventional excitation techniques (such as an attached shaker) and response measurement techniques (such as attached accelerometers), a class of structures exists to which these commonly used techniques cannot be so readily applied. This class of structures is comprised of items to which it is difficult, or impossible, to attach the required excitation and measuring equipment. There are a

variety of reasons why it may not be possible to use a contacting test configuration. Two of the more commonly occurring ones are associated with the testing of very small structures and of rotating structures.

In the case of miniature structures, such as Micro-Electro-Mechanical Systems (MEMS) devices it is not currently possible to find contacting test equipment that will not severely affect the structure's dynamic response characteristics due to mass loading. Mass loading is an effect that occurs when the apparent mass of a structure at a given DOF is similar to or less than the mass of the attached transducer. The effect causes the natural frequencies of the structure/transducer assembly to vary as the transducer is moved around the structure. The amount of frequency-shift is dependent upon the transducer's mass and whether it is positioned close to a node for a particular mode where the apparent mass will be high and the frequency-shift will be at a minimum. Conversely, near an anti-node for the mode, where the structure's apparent mass is low, the amount of frequency-shift will be at a maximum. FRF data sets that show distortion due to mass loading cannot be considered reliable or suitable for the purposes of model validation, or indeed for any of the DTA test levels. It must also be said that, in the case of microstructures, it may well be impossible to find a contacting transducer that is small enough to attach to the structure in the first place.

Rotating structures pose a more rudimentary problem: how to ensure that the transducers and excitation equipment remain attached? Slip-rings can be employed to allow the signals generated by transducers to be fed back to the analysis system, but the signals can be noisy, and there are limits on the allowable angular velocities of such systems. Moreover, the problem of how to apply excitation at a fixed location

remains, and is often currently overcome by applying the excitation through a bearing, or other stationary part of the structure.

The modal testing of these two types of structure has been the subject of considerable previous research as can be seen in the literature review presented in Chapter 2. However, there are other structures for which valid models are sought and for which contacting modal testing is not appropriate, albeit for different reasons. These structures are those which are themselves delicate or critical, or which have some delicate or critical feature associated with the surfaces of specific interest.

Examples of such structures include:

- those with a specialised surface finish, which risk being damaged by the attachment and removal of test equipment, or chipped by impacts. The cost of re-certification of such components as fit for purpose after a contacting modal test has been conducted on it may mean that such a test is not financially viable; or

- assemblies containing hazardous materials which must be handled in accordance with strict safety regulations. These regulations may impose limits on the levels of acceptable electrical charge in close proximity to the item, or on prolonged human contact with it. Such restrictions may mean that it is extremely difficult to test the item in a contacting way without breaching applicable health and safety legislation.

It should be noted that some of the structures for which the research in this thesis is intended fall into both of the above categories, and new, inherently safe, modal testing

techniques are required to enable FE models of these structures to be validated. Contact with these structures is limited to a few prescribed locations and these are not on the surfaces of specific interest.

A further problem which is common, but not exclusive, to these types of structure, is that the problem component or components are usually encased within a protective structure, either to shield them from the environment, vice versa, or both. Usually, response measurements on the protective case are possible, although these are likely to be the regions or components of least concern, but there are currently few means of inferring information about the dynamic responses or physical condition of the internal structures from the data that such "external only" tests provide. For this reason, it is common practice to embed instrumentation within the assembly, a process that may require significant modification to allow for the passage of instrumentation cables. In general environmental testing these alterations lead to the expressions "as built" and "as tested" as a recognition of the changes they may cause to a structure's dynamic response.

While it may be difficult to apply modal testing methods to structures of the types outlined above, it is often the case that the feature which makes them difficult to test makes it all the more important to have an accurate knowledge of their response to vibration environments. Some level of compromise usually resolves the dilemma posed by, on the one hand, the need for test data and, on the other, the difficulties in collecting it. Dependent upon the nature of the problem component, the compromise solution may, for example, take the form of replacing potentially hazardous components with dummy replicas or, in extreme cases, building two nominally-

identical structures, one for testing and the other for deployment. Such compromise solutions are not ideal and in some cases are impractical, either because the information provided by tests does not give a true representation of the as-issued structure, or because of the financial cost of duplicating what would otherwise be a one-off assembly.

The fundamental aims of the research reported within this thesis are to establish methods of testing delicate and critical structures for which it is impossible to have direct contact with the surfaces of interest, both for the purposes of excitation and response measurement. Furthermore, methods are sought which allow information about the dynamic characteristics of internal / inaccessible components to be inferred from measurements made on external / accessible parts.

1.3 Definitions

Having explained the reasons for, and overall aims of this work, it is important to define what some commonly-used terms will mean throughout the remainder of the thesis. These are “non-intrusive”, “indirect” and “non-contacting” tests and are defined as follows.

1.3.1 Non-intrusive testing

The term “non-intrusive” is used to describe both indirect tests (see 1.3.2 below) and non-contacting tests (see 1.3.3 below). It also includes tests that combine both indirect and non-contacting test methods.

1.3.2 Indirect testing

Throughout the remainder of the work an “indirect” test will be a test in which the structure of interest is excited indirectly via either an attached test fixture, or another

more robust component of an assembly. Indirect response measurements may also be made on the fixture/component, and the results of such a test will allow the properties of the structure of interest to be inferred rather than measured directly.

1.3.3 Non-contact testing

In a "non-contact" test, the structure is excited by some means that does not require any attachment between the structure and the exciter. In order to be a completely non-contact excitation method, there should also be no need to attach "targets" to the structure of interest. Non-contact response measurements will also require no part of any response transducer to be attached to the structure of interest.

1.4 The importance of mass normalisation for DTA level 3 and 4 modal analysis applications

In addition to demanding that full quality checks (signal quality and fidelity reciprocity, linearity, measurement repeatability and reliability, data consistency, Ewins op. cit.) be made, DTA level 3 and 4 test criteria place a further important demand on the test data, in that the data set must contain a measurement that allows the eigenvectors obtained from modal analysis to be mass-normalised. The mass-normalisation process makes use of the orthogonality properties of the modal model, and scales the non-unique eigenvectors (usually denoted as [Ψ]) such that:

$$[\Phi] = [\Psi]\left([\Psi]^T [M][\Psi]\right)^{-\frac{1}{2}} \tag{1.4.1}$$

so that

$$[\Phi]^T [M][\Phi] = [I] \tag{1.4.2}$$

and

$$[\Phi]^T [K][\Phi] = [\overline{\omega}_r^2] \tag{1.4.3}$$

Equation 1.4.1 represents the way in which mass-normalised eigenvectors are typically obtained from an FE model, in which the full system mass matrix is available. However, it is a requirement for mass-normalisation of the eigenvectors from the test data, which is of greater interest here. The requirement for mass-normalisation makes specific demands on the information that must be included in the data set if the information obtained from the test is to fulfil the requirements of DTA level 3 and above. The specific requirement is most easily revealed if we consider the mathematical description of the modal constant that forms one of the outputs of any modal parameter extraction routine. This constant, for a particular excitation DOF (k), response DOF (j) and mode (r) is given by

$$_r A_{jk} = \phi_{jr} \phi_{kr} \tag{1.4.4}$$

Most importantly, if the excitation and response DOFs are the same then Equation 1.4.4 becomes;

$$_r A_{jj} = \phi_{jr} \phi_{jr} \tag{1.4.5}$$

from which,

$$\phi_{jr} = \sqrt{_r A_{jj}} \tag{1.4.6}$$

This result (Equation 1.4.6) allows the mass-normalised eigenvectors to be extracted from the full FRF data set, if an FRF can be supplied for which the excitation and response DOFs are the same, the so called “point FRF”.

A second common way to scale the eigenvectors is to scale them such that the largest element of each has unit magnitude. However, eigenvectors scaled in this way are not suitable for use in FE to experiment correlation, since the largest eigenvector elements found from the model (in which there may be many thousands of DOFs) may differ considerably from those extracted from the experimental data in which measurements are made at only a relatively few locations. Mass-normalisation, on the other hand, leads to a unique set of eigenvectors from the FE model and from the test data and these may be quantitatively compared, DOF by DOF.

The importance of such a quantitative comparison is noticed not only in the generation of a Modal Assurance Criterion (MAC) plot (which illustrates the degree of correlation between the analytical and experimental mode shapes) but, also, because it allows the eigenvector data to be included in any model updating process that may be required. The use of the eigenvectors at the updating stage in the validation process may be essential in ensuring that an over-determined set of updating equations can be formed. This over-determination allows a least-squares-error solution to the model updating problem that minimises the differences between the model and observations of the actual structures behaviour. The advantages of over-determination of the updating problem may be difficult to achieve based upon eigenvalue information alone, and in fact, it may be impossible to form the problem in

anything but an underdetermined way, as there are likely to be more updating variables than observed natural frequencies.

1.5 On the relevance of virtual testing to delicate and critical components

One issue which is often associated with delicate, critical or potentially hazardous structures is that, because of their nature, there tend to be very short time windows in which they are available for testing. Because of this, there is often little or no time to develop test methods on the items themselves. Furthermore, regulations governing how the items may be handled mean that experimenting with different test configurations, in the way one might with a more standard structure, is not possible because of the need to have each different configuration approved by those in charge of quality or safety. One solution to this problem is to use prototypes or dummy replicas as test beds for the development of a test strategy which will yield the required information in as shorter a time as possible, although this is an empirical and time consuming approach. A second approach that has been made possible by improved computational power is that of virtual testing. Virtual testing is, according to Ewins op. cit., "… a set of processes which help us to decide, first and foremost, which data should be measured and which data are not required and, secondly, how best to support and excite the structure so that all the critical data are observed and accessed with a uniform reliability". The concept of virtual testing differs from modal test planning in that it is not solely concerned with the best excitation, suspension and measurement DOFs but, rather, with which data need to be measured and how these data should be analysed. It also allows the test engineer to investigate how known deficiencies in test equipment will affect the results of tests and thereby to make judgements as to how equipment is best employed in order to minimise the potential errors. This method of rehearsing experimental techniques within the computer,

before entering the laboratory, is a powerful technique regardless of the type of structure, but it is particularly valuable when dealing with structures that require careful handling. The use of virtual testing for test / analysis optimisation will be a recurring theme throughout this work.

1.6 Evaluation criteria for non-intrusive modal testing methods for DTA level 3 and 4 applications

1.6.1 General comment

Throughout this work, methods for the modal testing of delicate and critical structures to DTA level 3 and 4 will be discussed. However, if these methods are to be evaluated, it is necessary to develop criteria against which such an evaluation is possible. It is difficult to define a "normal" or "usual" modal testing method, a fact reflected by the absence of any broadly-accepted recognised standard in the subject. It is possible, though, to develop a list of characteristics that are desirable in modal testing equipment and to use this as a means of evaluating the usefulness of the test methods that are reviewed or developed.

1.6.2 The transfer function relationships

Essentially, a modal test aims to make measurements that provide two of the three unknowns in the fundamental relationship

$$response = properties \times input$$

Since it is impossible to measure the properties directly, they are usually determined by calculating the quotient of the response (displacement, velocity or acceleration) and input force, giving rise to the transfer function relationships commonly written as

$$\alpha_{jk}(\omega) = \frac{X_j(\omega)}{F_k(\omega)} \qquad \text{(Receptance)} \qquad (1.6.1)$$

$$Y_{jk}(\omega) = \frac{\dot{X}_j(\omega)}{F_k(\omega)} \qquad \text{(Mobility)} \qquad (1.6.2)$$

$$A_{jk}(\omega) = \frac{\ddot{X}_j(\omega)}{F_k(\omega)} \qquad \text{(Accelerance)} \qquad (1.6.3)$$

Although it is common to see these relationships presented as above (and it is clear from them that we must measure **both** the response parameter and the applied force), it is important to recognise that the transfer function relationships are actually more stringent, demanding that, in the case of a receptance, for example:

$$\alpha_{jk}(\omega) = \frac{X_j(\omega)}{F_k(\omega)}; \qquad \text{where } F_m = 0;\ m = 1, N; \neq k \qquad (1.6.4)$$

This relationship places much greater demands on the tester since they must now ensure not only that the input force is measured, but also, that it is the **sole** input to the system. In practice, fully meeting this requirement is often extremely difficult, such that much of the test preparation is likely to be devoted to ensuring any extraneous forces acting upon the structure have been removed or minimised. However, it is the exclusion of all forces, but for the intended excitation, which separates modal testing from more general vibration studies such as Operating Deflecting Shape (ODS) measurement.

1.6.3 Generic requirements of response/force measurement equipment

In order to completely fulfil the theoretical requirements described above it would of course be necessary to impart only a single force into the structure and also measure the required parameters precisely. Since no measurement is ever one hundred percent accurate, the best that can be achieved is an approximation. However, the selection of the measurement devices employed for the test will have a bearing on how accurate that estimate is, and as such, there are some generic parameters associated with transducers which may influence their selection, these are in no particular order of precedence:

1) dynamic range, the amplitude range over which the transducer can measure accurately;
2) transverse or cross-axis sensitivity, the proportion of the transducer output which may be attributed to motion in directions other than the intended sensing direction;
3) the frequency range over which the transducer can accurately measure;
4) stability, whether the gauge's sensitivity varies with environmental factors, such as temperature or humidity and,
5) linearity, whether the gauge's sensitivity varies depending upon the level of the measurement parameter.

In selecting any transducer (force or response) it is essential that these parameters satisfy our test conditions, or that the test conditions can be controlled to minimise the possible errors they introduce.

Having considered the general factors in the selection of transducers for modal testing, it is worth reviewing each aspect of the transfer function requirement that must be met. In order of increasing complexity, these are:

1) response measurement
2) force measurement
3) force application

1.6.4 Response Measurement Requirements

One of the primary concerns when selecting a response transducer is that it can be accurately positioned at the measurement location of interest. Since there is often a requirement to move response gauges around the structure, it follows that this positioning should be fairly easy to accomplish. For transfer FRF measurements the positioning of the response transducer is usually straightforward, but for the point FRF measurement (which given the earlier discussion on the importance of mass normalisation is arguably the most important), it is critical that the transducer can be positioned as closely as possible to the point at which the force is being applied. This may have a bearing on the selection of a suitable transducer for this measurement.

1.6.5 Force Measurement Requirements

The measurement of the input force is slightly more complex than that of response in that it must be made at the point of application of the force. Ewins op. cit., discusses this point in some detail, concluding that it is essential to measure the force as close to the structure's surface as possible in order that a reliable estimate of the excitation force applied to the structure is obtained. Furthermore, he stresses that it is not suitable to infer the force applied to the structure by measuring either the voltage or current supplied to the exciter since these provide a measure of the force applied to the structure/exciter assembly.

It is worth mentioning at this stage the consequences of not measuring the input force, even if all of the other requirements of Equation 1.6.4 are met. Firstly, the true natural frequencies of the system are close to the maxima of the FRF curve (their actual location cannot be determined unless the contribution of all the other modes is taken into account) and are not indicated by the maxima of the response auto-spectra alone, which may in the case of shaker excitation, vary with location of the exciter, Ewins, op. cit. Secondly, without a measurement of the force, and therefore no point FRF measurement, the shape-vectors obtained from analysis of such curves cannot easily be mass normalised (although mass normalisation may be possible, as will be discussed in Chapter 2). The lack of scaling will render the information extracted from such response only data insufficient for use in DTA applications of level 3 and 4.

1.6.6 Force Application Requirements

As has already been mentioned, meeting the force application requirements of modal testing is extremely difficult and in practice it is likely that it will not be completely met. However, a closer examination of the mathematics reveals that there are some situations that are tolerable and others that must be avoided. These situations are revealed if the matrix form of Equation 1.6.4 is considered:

$$[\alpha(\omega)] = [X(\omega)] \cdot [F(\omega)]^{-1} \qquad (1.6.5)$$

Where the force matrix **[*F*(ω)]** contains the auto and cross-spectral density functions of all the forces involved, with any one of these being the intended force, that is:

$$\left[F(\omega)\right]_{N\times N} = \begin{bmatrix} S_{f1,f1} & S_{f1,f2} & S_{f1,f3..N} \\ S_{f2,f1} & S_{f2,f2} & S_{f2,f3..N} \\ S_{f3..N,f1} & S_{f3..N,f2} & S_{f3..N,f3..N} \end{bmatrix} \qquad (1.6.6)$$

Three possibilities are of interest; firstly, that each extraneous force is an uncorrelated, non-systematic occurrence, secondly that, each extraneous forces is an uncorrelated, systematic occurrence, and thirdly that, each extraneous force is a correlated, systematic event.

In the case of non-systematic, un-correlated, random forces (passing traffic, for example) being present it is clear that each of the elements involving these sources will tend to zero with increasing numbers of averages. These kinds of forces may be justifiably ignored in the calculation if sufficient averages are used.

In the case of systematic, un-correlated, random forces (from an acoustic source, for example) being present, then each of the cross-spectral elements involving these forces will tend to zero with increasing numbers of averages, leaving only the auto-spectral term on the leading diagonal. If these forces are small in comparison with the actual excitation force, it may be considered justifiable to ignore them. If these forces are of the same order of magnitude as the intended force, and are **truly un-correlated,** then since the matrix would have terms only on its leading diagonal it would always possess an inverse[1]. This implies that if the forces could be measured it would always be possible to determine the response of the system caused by the intended source, a fact that Multi-Point Random (MPR) and appropriation modal tests

[1] Except, of course, in the case where all of the forces are zero.

attempt to exploit, Ewins, op. cit. If the forces are large and cannot be measured, then it is necessary to eliminate them from the test configuration.

The case of systematic, correlated, extraneous forces (generating an unmeasured applied moment through a drive-rod, for example) acting upon the system provides the worst-case scenario in terms of modal testing. In this case, none of the elements of the matrix tend to zero with increasing averaging and there is an increased risk of the force matrix containing linearly dependent rows and columns. This risk is greatest close to natural frequencies of the system (the regions of greatest interest in a modal test), but it is entirely possible that the force matrix will contain such linearly dependent rows and columns across the entire frequency range of interest. This effect will cause the force matrix to be singular, implying that even if the forces involved could be measured it would not be possible to determine which of them was responsible for a particular response. If such forces are present they will cause serious errors in the estimation of the FRFs and it is for this reason that the modal test engineer strives to eliminate the possibility of such forces from their measurement set-up.

A further requirement on force application is that the selected method should be able to provide excitation across the frequency band of interest. It is also desirable, although not essential, that it can impart this excitation using different types of signal depending upon whether the test aims to establish the structures response over one broad or several narrow bands of frequency range.

1.6.7 Concluding remarks

Hopefully, the preceding discussion makes it clear why contacting accelerometers and electro-dynamic shakers provide the mainstay of modal testing equipment for general structures. It also highlights the requirements, which as technical or regulatory constraints prohibiting contact with the item are imposed on the test configuration, any non-intrusive test equipment must fulfil.

In the case of non-intrusive response measurement techniques devices are sought which:

1) have a wide dynamic range;
2) are easily calibrated;
3) can measure over a broad frequency range;
4) are stable and linear;
5) have a low cross-axis sensitivity;
6) can be easily and accurately positioned, and
7) have a small target footprint.

Since it is essential that we measure the input force, force transducers are required to fulfil the same basic requirements as response transducers with the additional constraint that they measure the force at the location to which it is applied.

Finally, the excitation source must provide:

1) a point excitation;
2) a sufficient level of excitation force across the range of interest;

3) be the only source, or be capable of imparting multiple uncorrelated sources (for MPR testing or appropriation testing).

It is also desirable that the excitation source can:

4) impart the excitation with a variety of different time signals (sine, random, chirp, for example);

5) be moved with minimal effort, from point to point on the structure.

Having defined these requirements it is possible to review the methods of non-intrusive modal testing that have been reported in the literature discussed in the next chapter, and those that are newly developed in this thesis.

1.6.8 A note on test requirements for the structures of specific interest

Although section 1.6.7 has established a set of requirements which are generally desirable, irrespective of the structure under test, it is also important to consider requirements which are specific to the test item itself. In the case of the structures of specific interest, because their design has evolved based upon experimentally derived evidence it is desirable (although not essential) that a like for like comparison between new and archive data is possible. Traditionally, modal tests conducted on dummy replicas of the structures of interest have made use of FRFs defined over the frequency range 0-2000Hz, these have been collected via FFT analysers and so ideally, any new measurement system would be able capable of producing similar FRFs. Also, since the aim of testing the as-issued structures is primarily to qualitatively compare mode shape data and natural frequencies[2] then there is no requirement for well defined anti-resonances, and a noise floor at –40dB is found to be more than sufficient.

[2] Extracted from both experimental data collected on dummy assemblies and from FE calculations.

1.7 Thesis scope and structure

1.7.1 Scope

This work will attempt to develop new modal testing methods for structures which require careful handling due to their delicate or critical nature and for which the attachment of conventional test equipment is either impossible, or constrained to a very limited number of possible connection points. The data collected from these test methods must, at a minimum, be suitable for use in model validation and updating applications.

New methods are also sought which allow information about the dynamic characteristics of internal or inaccessible components to be inferred from measurements made on exterior or accessible parts. Once again, the information provided by these methods should be suitable for use in modal analysis applications such as model updating.

In addition, the work explores the application of presently available methods for non-intrusive testing and aims to extend the application of some of these techniques.

1.7.2 Structure

In Chapter 2, current methods for non-contact and indirect modal testing are critically reviewed against the requirements discussed in Chapter 1. The Laser Doppler Vibrometer emerges from this review as the most versatile and easy device to deploy of the currently available non-contact response transducers, and it is concluded that such devices have the potential to solve the problem of non-contact response measurement. Conversely, the review finds that the problems associated with the non-contacting and indirect excitation of structures have not been solved and that the

problems associated with the accurate measurement of the input force are the main obstacle in the use of these methods for DTA level 3 modal testing applications.

In Chapter 3 the practical application of the LDV as a response transducer is reported. A case study on the application of the LDV and impact hammer testing to acquire data for the validation and updating of a finite element model is presented. Through virtual testing, the case study shows that the structure of interest demands a minimally intrusive test method and using virtual tests, a test strategy for the structure is developed. The case study demonstrates how the LDV and impact hammer method can provide data that are suitable for model validation purposes and also serves to demonstrate how mass loading can affect even relatively large structures.
The use of the continuously scanning mode of the LDV is also discussed and the area scanning method is extended to allow for the scanning of axi-symmetric structures such as cylinders and cones. The theory for 6DOF measurements on such structures is developed but the practical application of this technique is limited by the LDV's current configuration.

In Chapter 4, the theory for indirect modal testing of structures is developed as an alternative to fully non-contact excitation methods. Two possible methods are considered: firstly, the FRF uncoupling technique and secondly, the use of validated, high fidelity FE models (the "model-and-remove" approach). The indirect excitation problem is shown to be highly ill-conditioned and the physical cause of this ill-conditioning is identified. Importantly, it is shown that the source of this ill-conditioning cannot be removed without careful consideration at the design stage, a

fact which has severe ramifications both for the design of indirect test fixtures and for the determination of information on interior components.

Chapter 5 reports on the application of the indirect testing methods developed in Chapter 4. Two case studies are reported: the indirect testing of a free-free beam and; the application of indirect testing to the MACE Case.

Chapter 6 presents the overall conclusions of the work and gives recommendations for areas of further study.

CHAPTER 2. A REVIEW OF NON-INTRUSIVE MODAL TESTING

2.1 Introduction

In this chapter, methods of non-contacting, indirect and minimally-invasive response measurement and excitation for modal testing, which have previously been reported, are evaluated against the requirements discussed in Chapter 1. Conclusions are drawn as to which methods are most suitable for modal testing to DTA level 4 and in which areas further or new research is required. This review of the start-of-the-art identifies gaps in the existing technology and leads to the development of the specific objectives of the research reported in this thesis.

2.2 Overview

A versatile, non-intrusive, modal testing method has been sought for some considerable time, not least because of the benefits it affords in the removal of mass loading and localised stiffening effects. The majority of research in this area has concentrated on two main types of structure, the modal testing of micro-systems and of rotating machinery. A rapidly growing and fairly recent addition to the state-of-the-art has been ‘in-operation’ or ‘output-only’ modal testing. These methods make use of the relatively easily obtained response measurements and make assumptions about the forcing functions that cause them. The forces concerned are often those that the structure sees in normal operating conditions, although this is not a prerequisite of the methods. The ‘output-only’ techniques are applicable to any type of structure, but the information acquired from them will only be sound as long as the assumptions about the forcing function hold true.

The objective of this review is to identify and to critically evaluate each of the currently available methods by which non-intrusive testing can be achieved, against the criteria specified in Chapter 1. It then aims to identify areas in which existing capabilities may be enhanced or where a different approach may be required.

The review is divided into four different sections, focusing on non-contacting response measurement methods, non-contacting excitation devices, non-invasive/minimally-invasive excitation techniques and indirect test methods, respectively.

2.3 Non-contact response measurement devices

2.3.1 General comment on non-contacting measurement devices

The numerous types of non-contacting measurement devices available today may be broadly divided into four main groups, optical, acoustic, proximity detection and stress/strain measurement and each of these groups will be examined in turn. By far the most widely used of these methods fall into the optical class. The Laser Doppler Vibrometer (LDV), in particular, has been the subject of much research in the specific area of modal testing. It is for this reason that this examination of currently available non-contacting response transducers begins with the LDV.

2.3.2 LDVs

Early LDVs were not practical for modal testing on two grounds, firstly because they needed to be set-up in an optical laboratory and secondly because the Doppler principle on which they are based is insensitive to direction. Modern, commercial LDVs are easily portable and incorporate a Bragg cell in the reference beam, which allows the direction of motion to be determined. The exact workings of LDV devices

are described in references such as [3], but satisfactory explanations are readily available in manufactures' pamphlets [4]. It will suffice to say here, that the LDV produces a signal that is proportional to the velocity of the target at the point of incidence with the beam and in line with the beam. In theory, the LDV has no cross-axis sensitivity since it is insensitive to in-plane vibration. However, in practice slight misalignment between the beam and the structure will lead to a cross-axis error related to the severity of the misalignment. Bell and Rothberg [5] studied this feature of the LDV in some detail. With careful alignment to ensure that the beam is normal to the target, the cross-axis sensitivity of these devices can be made at least as low as could be expected with a conventional accelerometer.

Further enhancements to the LDV device include the addition of mirror drives that control the position of the laser beam [4], and LDVs incorporating such mirror drives are now commercially available ("scanning" LDVs). The incorporation of these mirrors into the laser-head allow the beam to be rapidly positioned on the target surface, dwell for the measurement time and then be repositioned at the next measurement location. This allows a high-spatial density grid on the structure to be measured much faster than would be possible with accelerometers, for example. It is worth noting that the mirrors control the angle of the beam and therefore measurements made in this fashion may require correction for cosine errors [4]: commercial driving software includes a correction facility for such errors. Also, if the structure exhibits any in-plane motion then this will make up a proportion of the signal that will vary dependant upon the beams angle of incidence with the structure. FRF measurements made when this is the case are unlikely to provide data that are suitable for model correlation purposes.

Where significant in-plane motion does occur, the use of a 3D-LDV may be considered appropriate. These devices include three separate LDVs, which are focused by a lens on to a single point, with the beams angled so as to maximise the optical signal to noise ratio, [6]. Typical stand off distances for such devices are 160mm and 320mm. The most recent advance in this field is the scanning 3D-LDV manufactured by Polytec [7].

Other adaptations of the LDV include fibre-optic attachments to reduce the target spot size and to allow access to otherwise inaccessible points on a structure and microscopes have also been employed to allow measurements on micro-systems. LDV devices also commonly used to make general vibration measurements on structures operating at high temperatures [4].

It is reasonable to say that LDV offers a realistic alternative to accelerometers for the purpose of modal testing, although there is a sacrifice in dynamic range and there are obvious Line-Of-Sight (LOS) requirements, which may mean the LDV or structure may need to be repositioned. Reference is often made to the problem of speckle pattern noise, which can cause signal dropouts at certain points on a structure [3]. Commercial LDV software usually includes a facility to reposition the LDV beam close to the intended measurement point several times and thereby average out speckle-pattern effects. In any case, so long as there is sufficient signal strength, the resonant peaks in the FRF curve are usually clean enough to allow a successful modal analysis.

Castellini et al [8, 9] have also used the LDV in a point mode to track a single point on a moving structure. This type of tracking LDV is accomplished by controlling the drive mirrors by generating a feedback signal from the moving structure and has been used in the cases of both linear and rotary motion.

No review of the LDV would be complete without mentioning some fairly recent and unique developments. It has already been mentioned that the LDV can include positioning mirrors, which allow the beam to be moved around on the surface of interest. In the standard mode of operation of such a device, the beam dwells at a point for a time sufficient to allow a measurement, with the dwell time varying depending on the frequency range of interest. Under sinusoidal excitation conditions, however, the need to dwell at a single point can be removed and the laser beam can be moved in a continuous scan across the surface, Ewins, op. cit. This application was first developed for the measurement of Rotational Degrees of Freedom (RDOFs), in which first short line and then small radius circle scans were employed [10]. Later tri-axial measurements were made using conical scans, in which the single beam was moved in a circle and focused through a lens [11]. Longer line scans and also area scans have also been developed [12,13] and in these cases the first differential of the ODS obtained after analysis can be used to infer information about the RDOFs [14]. Stanbridge has also demonstrated the technique on highly curved surfaces [12] suggesting the use of a geometrical correction. However, the method proposed is suitable only for the line scanning technique.

In all continuous scanning measurements, the parameters of interest are given by relationships in the distribution and magnitude of spectral components or “side-

bands" which result from a Fourier decomposition of the measured time history. Typically, these side-bands will be centred around the excitation frequency and examples of the spectra from circular and area scans and the relationships used to obtain the required information from them is shown in Figure 2.3.1.

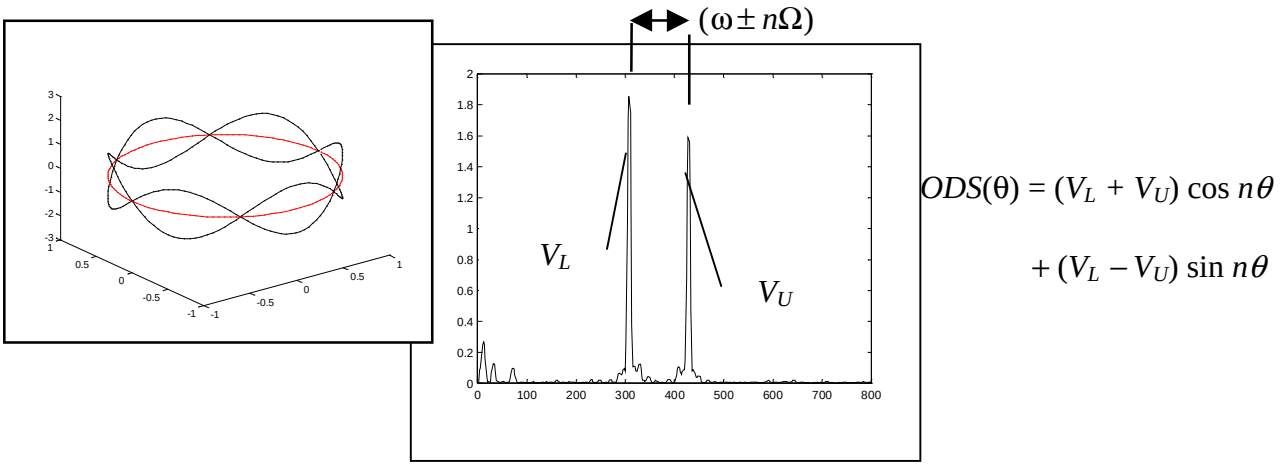

(a)

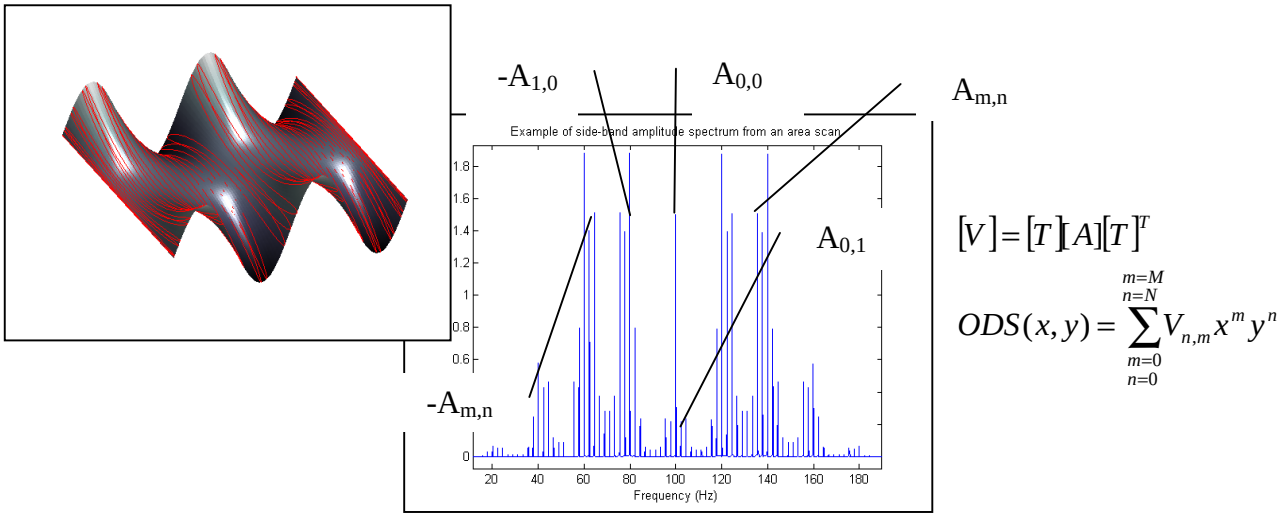

(b)

Figure 2.3.1. Examples of LDV scanning techniques, results, and analysis: a) Circular scanning and; b) area scanning.

Other excitation techniques have also been demonstrated to work with continuous scanning including narrow-band random and impact hammer, [15], although hammer excitation requires that the target be grounded so that large near DC components do

not dominate the response. Modal analysis of the side-band spectra has also been used to derive modal constant terms for a polynomial approximation to a structure's eigenfunctions,[3].

In general then, the LDV provides a transducer that is comparable to the conventional accelerometer in many ways. The problems associated with the LOS requirement can sometimes be overstated, since, when testing real assemblies as opposed to prototypes, it is often not possible to embed conventional transducers into the structure. In addition, it provides unique capabilities in its tracking and continuously scanning modes.

2.3.3 Holography

In a similar way to the LDV, holographic vibration measurement techniques have developed to a stage whereby they can be fielded outside of an optical laboratory and are available commercially. The principle of operation is similar to the LDV in the sense that it uses interferometric principles, albeit in a different way. In holography, the coherent laser beam is split into an object and reference beam, with the object beam being used to illuminate the structure while it undergoes excitation at a single frequency. The reference beam and the scattered light from the vibrating structure are reflected onto a holographic plate, and thus the relative interference between the reference and object beam is recorded for an instant in time. The fringe patterns of this image provide a full-field description of the three-dimensional displacement of the structure at a point in time.

An advancement to the technique, Electronic Speckle Pattern Interferometry (ESPI), uses the same basic principle but includes real-time video and display [16]. ESPI

systems rely on complex image processing techniques to obtain displacement time histories. Although this type of speckle pattern interferometry is useful for producing images of displacement fringes at resonant frequencies, they are of little use in modal testing due to the absence of phase data, Ewins op. cit.

The introduction of Double Pulsed ESPI **does** allow the necessary phase information for modal parameter extraction to be obtained and details of this process and its application to modal testing can be found in references [17, 18]. One notable feature of the use of Double Pulsed ESPI technique is the sheer quantity of data that it produces. Although seemingly advantageous, the large data sets can be problematic for modal parameter extraction routines, a fact that may demand the reduction of the data-set to a few choice locations. Reference [19] discusses the operation and application of automated data reduction methods for this purpose.

Insofar as holography's application to DTA level 3 and 4 types of modal test is concerned, the literature shows that the requirements for level 3 testing can be met using this method. However the level 4 requirements for compensation for out-of-range modes using residuals will be very difficult to meet using any device that relies on single frequency excitation. This is because it is necessary to provide information about response at off-resonant frequencies and if possible the anti-resonances, Ewins op. cit. The frequency location of these anti-resonances varies from point to point on the structure and so numerous measurements would be required in order to characterise them for just a few locations. With holography alone, this would be a time consuming undertaking requiring a large amount of computational storage.

2.3.4 Moiré Techniques

Moiré interferometry is similar to the holographic method described above, although it does not require a collimated light source such as a laser. The system relies on two dense and regular gratings which when super-imposed form a Moiré pattern. Displacements can be measured by imposing a grating (the "model grating") on the structure of interest and observing the changing Moiré pattern through a second grating (the "master grating"). The way in which the model grating is applied to the structure leads to three types of Moiré analysis:

1) intrinsic Moiré (model grating etched onto the structure), providing the displacements of the points with no reference to their initial position;
2) projection or shadow Moiré (model grating projected on to the structure), providing displacements of the points on observed surface with respect to a reference surface, and;
3) reflection Moiré (projection Moiré applied to a reflective as opposed to diffusing surface), which provides the slopes of the surface with respect to the reference state.

Sciammarella's comprehensive review [20] of the theory of Moiré methods discusses the pros and cons of each of these methods in detail.

Shadow Moiré systems are now available commercially from suppliers such as Electro-Optical-Information Systems and are used primarily for general vibration studies or static stress/strain measurements. Mitchell and Harvie [21] performed a modal test on a cantilevered plate using projection Moiré to obtain the structure's

response. Strictly, the results they obtained were Operating Deflection Shapes (ODS), but for lightly damped structures such as their plate, these closely approximate the mode shape at a resonant frequency. The method by which these ODS were extracted was complex, although a level of automation was achieved.

The comments regarding the use of holography for DTA level 3 and 4 testing apply to the Moiré methods also, since they again rely on single frequency excitation. Furthermore, in the case of Moiré interferometry phase information is not available and therefore even the level 3 requirements cannot be met in full.

2.3.5 Laser Triangulation Methods

This method of non-contacting response measurement was reviewed by Patton and Trethewey [22] during their research into the modal testing of ultra-light weight structures. They concluded that while the laser triangulation method was of considerable use in general vibration measurement, it was not ideally suited to modal testing due to the need for re-calibration at every new measurement location. This characteristic of the laser triangulation method means that it is best suited to a roving exciter test, although the structure under test may need to be constrained to stop large, low-frequency displacements.

2.3.6 Acoustic Measurement Methods

Acoustic methods are based on the principle that the sound radiation emitted from a vibrating structure is proportional to the surface velocity. In Patton and Trethewey's research of 1987, [40], it was found that modal tests using this technique were being conducted and reported as early as 1972 [23].

One of the main drawbacks in using microphones as transducers is the non-directional nature of the signals obtained from them. In structural vibration work, the sound field close to the structure is greatly affected by the deformation of the structure surrounding the measurement position. The sound pressure may therefore not be truly proportional to the vibration characteristics of the structure at any given point. To overcome these problems a method employing finite difference approximation was proposed and implemented by Forssen and Crocker in 1983 [24]. Since then, three dimensional acoustic intensity measurements have been achieved by using four microphones [25]. It should be noted however, that these require considerable set-up times and that calibration is difficult. The method described by Okubo et al in [25] could only be used in practice on fixed-free structures.

Efforts to understand the relationship between results obtained via acoustic intensity measurements and the results of contacting modal tests have been reported in papers such as [26] and [27] and these highlight some of the difficulties in using acoustic response data for modal testing purposes.

As a general evaluation of the acoustic response measurement methods, it has been demonstrated that they can be used for basic modal testing purposes, but they rely on approximation of the structures' actual response and are highly susceptible to external noise. These features mean that they do not meet the equipment requirements for DTA level 3 and 4 tests. It is also interesting to note the overall decline in interest (shown by falling numbers of papers) in these methods since techniques such as LDV and Holography have become more robust and more readily available.

2.3.7 Proximity Detection

There are two types of non-contacting proximity probe (capacitive and eddy-current) which might be used to measure vibration response data [2]. However, neither method is particularly appropriate for modal testing purposes, as discussed in [22]. Eddy current probes induce eddy currents in conductive targets by generating a high frequency magnetic field inside the transducer head. The distance between the transducer head and the target affects the behaviour of the exciter coil and changes in this behaviour can be measured. This transduction method is highly non-linear and the signal must be corrected by analysing circuitry provided with the transducer. The transducer must be calibrated both for the target material type and stand off distance, and it is therefore essential that the same stand off distance be used for all measurements. For very precise measurements, the stand off distance may be very small (<1mm) and this will affect the allowable amplitude of vibration. The need to maintain the same stand off distance is likely to force a fixed boundary condition on the test, and also that a roving exciter test method must be used. It is possible that these limitations are the reason why no literature on the application of these probes to modal testing could be found.

The capacitive proximity detection probe works by measuring changes in the air-gap between the transducer and the target. These variations cause a change in the capacitance of the system that can be converted into a voltage or current by relevant analyser circuitry. The resulting signal is more linear than that of the eddy current probe and stand off distances can vary between 0.0025m and 1m [2]. The target must be conducting and must also be "wired" into the analyser circuit in order for the method to work. Once again, the difficulties of calibration and gauge mobility are

likely to be the main reasons why no reports on the success or failure of these devices for modal testing purposes could be found.

2.3.8 Stress/Strain Measurement Techniques

It is possible to make measurements of stress or strain in a non-contacting manner using the SPATE technique [28]. This system detects minute changes in the temperature of the target, which are analogous to the cyclic heating or pressurising of a gas. Under certain thermodynamic conditions these small changes are proportional to the strain in the target material. The SPATE system outputs a calibrated, full-field, stress / strain map of the target object. Common uses include defect detection and fatigue monitoring.

Although strain is not one of the common properties to be measured in a modal test, Hillary and Ewins [29] proposed a method of using strain data in modal analysis in 1984. Since then, numerous papers have appeared on the subject of strain-based modal analysis, of which [30, 31, 32] are typical examples. The increased availability of laser methods such as holography and LDV in conjunction with the relatively complex analysis procedures for strain based modal data, are the likely cause for the lack of research into the use of SPATE as a modal testing response transducer.

2.4 Non-Contacting Excitation Devices

2.4.1 General comment on non-contacting excitation devices

Over the years, a wide range of non-contacting excitation devices have been demonstrated with varying degrees of success. Amongst the most commonly reported are: acoustic excitation, non-contacting magnetic excitation and laser pulses. Several others offer variations on these themes and a few employ more exotic techniques. As

has already been discussed in Chapter 1, the excitation of the structure is only half the problem in conducting a modal test. The other, more problematic half, is the measurement of the force applied to the structure at the point of application. It is in this area, as will be seen in this review, that many of the non-contacting excitation techniques falter for the purpose of modal testing.

2.4.2 Acoustic excitation methods

One of the simplest (non-contacting) ways of causing a structure to vibrate is to expose it to a sound field of some description. Since sound and vibration are closely associated, then in a similar way that it is possible to infer information about a structure's modal properties by "listening" to it, so it is possible to excite them by the reverse process.

All of the excitation signals commonly used for modal testing (sine, random, burst random, for example) can be generated acoustically, and this is a feature that has attracted several researchers interested in non-contacting excitation to their use. In Weaver and Dowdell's paper of 1984 [33] they discuss the use of speaker excitation for the modal testing of a plate. One interesting comment the paper makes is

"The speaker excitation can be considered to be multiple input excitation in the sense that the acoustic waves strike the plate over its entire surface and not just at one place as is the case of the attached shaker. Thus the normal concern of locating the exciter at a node of the structure can be alleviated."

However, the authors make no mention of the fact that the acoustic waves striking the plate are of identical frequency composition. Therefore if the waves can be considered

as multiple input excitations, then they represent a series of correlated inputs, which will (as described in Chapter 1) make it impossible to determine which force is responsible for a particular response. The measurements that are made are therefore ODS' and in fact un-scaled ODS' since no input force is measured. The paper does illustrate well one of the major problems with speaker excitation, however: namely that the acoustic excitation acts over an area as opposed to a point and will therefore be of limited use for accurate modal testing.

Musson and Stevens conducted similar tests in 1985 [34] and also attempted a fully non-contacting excitation and response test using acoustical methods in 1986 [27]. The later work concluded that the method was satisfactory when precise modal definitions were not required.

In order to circumvent the problem of distributed acoustic loads in application to activate frescoes, Castellini et al [36] focused the acoustic energy provided by a speaker using parabolic mirrors in order to provide a point excitation. This method was reported to be successful in their damage detection application, although no force measurement was possible, or necessary.

In general, then, acoustic sources can be used to excite structures and may even be focused to provide a quasi-point excitation. The excitation signals available in acoustic excitation are also identical to those that might be used in shaker tests. The force generated on the structure however, cannot be measured in a non-contacting way and so the standard mass-normalisation procedure cannot be used. This lack of scaling will mean that tests conducted in this way will be unsuitable for applications

above DTA level 2. It is worth mentioning at this stage that an alternative mass-normalisation procedure has been proposed by Parloo et al, [37], and a full discussion of this method is presented in Section 2.5.2.

2.4.3 Pulsed air excitation

The use of pulsed air to excite a structure is a variation on acoustic excitation and a distinction is only made here since the excitation is achieved using short bursts as opposed to continuous signals. Also, an air-stream of constant mass flow rate can be used on rotating structures, for which constant stationary loads can induce vibration, Ewins op. cit.

French, Knittel and Wyszynski [38] employed short bursts of air, in conjunction with LDV response measurements, for their tests on prototype automotive seats. The method suffered from the same problems of force measurement which have been mentioned in the previous section and the group were forced to base their conclusions on the ODSs obtained from the experiments. The group stressed the need to find a method for determining the force applied to the structure in order that the data obtained could be used for higher-level modal analysis applications.

2.4.4 Non-contacting magnetic excitation

Electro-dynamic shakers are commonly used to generate the forces required for conventional modal testing. In a standard test, the electrical output of a power amplifier is transferred to a mechanical output from the shaker armature by the generation of a magnetic field between the shaker core and the armature winding. The force so provided is usually transmitted from the shaker to the structure via a stinger or push-rod.

Under certain conditions, the principle of electrical-to-mechanical energy conversion via a magnetic field can be applied directly to a structure, rather than via a shaker and attached push-rod. Most obviously, the intended target must be ferromagnetic, or have a ferromagnetic target attached to it. Also, both magnet and structure must be grounded to prevent the DC component of the magnet simply drawing the exciter and structure together: Ewins, op. cit. If these conditions can be met, then the structure can be excited in a completely non-contacting manner, assuming that no magnetic target is required.

All of the common types of forcing functions can be generated via this method, although sinusoidal excitation is more complicated than usual due to the current-squared relationship of the applied force to the input signal. This relationship means that a sinusoidally varying input will produce a much more complex harmonic force to be applied to the signal. It is possible to overcome this problem by providing a modified signal to the exciter and thereby generating a purely sinusoidal force signal.

Perhaps the most alluring characteristic of non-contacting magnetic excitation is that a measurement of the force applied to the structure is possible. At present there are three methods by which this measurement can be made.

In the simplest of these methods, a load cell is placed underneath the magnetic exciter and the reaction force is measured. Both Bogy and Wilson [39] and Patton and Trethewey [40] used this method to calibrate their excitation systems for measurements on miniature structures. To employ this method, the exciter and load

cell assembly must be rigidly grounded in order to ensure that the measured reaction force is an accurate representation of the actual force applied to the structure.

A more complex (and rarely employed) method is to measure the magnetic flux density in the air gap. If this method is used then the rigidly grounded constraint is removed. Uncertainties arise, however, both from making only a point measurement of the flux, and because of the varying air gap size between the exciter and the structure.

The most recently proposed method for force measurement is to measure the reaction loads at the supports of a flexible beam [41]. A complex measurement system is required to measure the reaction at the ends of the simply supported beam and the displacement of the exciter coil. This system is employed so that the inertial contribution of the magnet can be determined and then subtracted from the force measured at the beam supports.

Magnetic excitation then, has almost all of the desirable characteristics discussed in Chapter 1. The two main drawbacks to the method are the requirement for a ferromagnetic target and the need to ground the test structure. Nonetheless, the method has been demonstrated to work on both rotating machinery [42] and cantilevered microstructures [40].

2.4.5 Eddy current excitation

Eddy current excitation also uses an electromagnetic field to excite the structure-under-test, although the principles differ from those of magnetic excitation. The use

of the eddy current proximity probe has already been discussed, and as in the case of acoustic transducers, it is again found that the process may be reversed to provide an excitation force.

Saldner reviewed the use of eddy current excitation [43] as a tool for modal analysis in 1994. The method uses an electromagnetic coil and a permanent magnet. These are placed in close proximity to a conductive target, in Saldner's case a thin metal plate. A sinusoidal current in the coil introduces harmonic eddy currents in the conductive target. The electromagnetic fields of these eddy currents interfere with the stationary field of the permanent magnet and generate a force. The force generated depends upon the electrical conductivity of the target, the distance between the target and the exciter and the thickness of the object. It is possible to calibrate this type of exciter, but a new calibration is required for each position at which the structure is to be excited.

The eddy current exciter has similar properties to the non-contacting magnetic exciter but is less demanding in its requirements. The method is not restricted to ferromagnetic materials, but can be used on any reasonably conductive material. There are drawbacks to the method also, most notably the limited excitation signals available and the comparative complexity of calibration.

2.4.6 Laser pulse excitation

In terms of vibration studies this is a relatively new technique in which bursts from a powerful laser (typically an ND YAG type) are used to excite structures. Their relevance to modal testing is that the bursts provide a point excitation much like an impact hammer. Koss and Tobin [44] first reported their use for modal testing in

1983. In their tests, the energy levels involved were sufficient to ablate the targets surface. The rapid ejection of molten material caused an impulsive reaction of the structure at levels sufficient for modal testing. One fairly obvious problem with this type of excitation is that the structure of interest is permanently damaged by the test. Koss and Tobin circumvented this problem by attaching ablative targets to the structure thereby sacrificing the fully non-contacting nature of the test method.

Philip, Booth and Perry, revisited the technique in 1995 [45], and managed to excite modal level responses in structures weighing up to 57 kg using energy levels that were below the ablation threshold of the structure. The excitation in this case was caused by a thermo-mechanical effect, which caused local bending of the structure at the target point. This method avoided the use of ablative targets, but as in the case of the earlier ablative method, no force measurement was possible.

Castellini et al [46] examined the uses of sub-ablative laser pulses for modal testing with specific reference to the mass-normalisation of the mode shapes. The first of these methods used a thermal FE analysis to provide an approximation to the force, the second, more complex method was via a "laser equivalent force" calculated via mobility FRFs and weighted velocity measurements [47]. Neither of these methods are particularly viable since the first relies on a numerical calculation based on the FE model which is to be validated and the second, in order to be effective requires an additional impact hammer test on the structure of interest.

2.4.7 Electrical spark excitation

Zhang et al [48] used this method to measure the vibration properties of a miniature silicon sensor. The technique was also used by Chou and Wang, [49], for their studies

on microstructures. In both cases the method was employed because the structures had low masses and very high stiffnesses meaning they required high frequency excitation. Electrical spark excitation is capable of imparting forces with the high frequency content required but no measurement of the force is possible. In both papers an output only modal analysis technique assuming uniform white noise excitation was used and un-scaled mode shapes were obtained.

2.5 Non-intrusive and minimally-invasive excitation techniques

2.5.1 Minimally-invasive excitation techniques

Two methods of minimally-invasive excitation are commonly used in modal testing, impact hammer and step relaxation. Both provide a means of structural excitation that causes minimal disruption to a structure's normal condition by imparting a force of very short duration.

Hammer testing is a widely used excitation technique, the theory and practice of which has been reported in many texts, Ewins, op. cit. and [50], being good examples. Essentially, the method makes use of an impact hammer with an integral force gauge. The hammers used are supplied with a range of tips made from various materials (rubber, nylon and steel, for example), these tips allow the width of the impact pulse to be varied allowing some control of the pulse's frequency content. The problems associated with the method stem from the lack of control over the precise location of the impact and level of the force imparted by it. The coherence function obtained if averaging is used can indicate how consistent the location of successive impacts was and pendulum hammers can be used to increase both the consistency of the impact location and the level of applied force.

One further potential problem is the need for the structure's response to die away within the sample time. This can be a problem when impact testing is applied to lightly damped structures. Several methods exist for overcoming this problem, including: increasing the sample time if the number of spectral lines in the analyser is not fixed; using a zoom FFT Ewins, op. cit. and taking advantage of the increased sample time; or using an exponential window to force the response to die away within the sample time. The last of these methods is not recommended for high quality modal tests since the exponential window adds artificial damping to the FRF obtained and this affects the natural frequencies obtained from analysis. The removal of this artificial damping is possible via calculation, theoretically, although the situation is often further complicated by the use of an impulse window on the force signal [50].

Step relaxation excitation is also well reported in works such as Ewins, op. cit. and [50]. The method is frequently used on very large engineering structures such as bridges, although its application to structures as small as violins have been reported [51]. The structure is usually gradually loaded by means of a cable, which is used to induce a deflection in the structure. Alternatively, a dead weight may be suspended below the structure. In either case, the static load is suddenly released by means of an explosive bolt or failure of the cable at some known tension. The applied load can be measured using a load cell in the cable or by making use of the known failure load of the cable. Woodhouse [51] for example, used high quality fishing line with an accurate and repeatable failure load to excite vibrations in violins. One problem arises in that the force and deflection are finite at t=0, a fact that contravenes the causality conditions of the Fourier transform. Ewins, op. cit., describes two ways of solving this problem:

1) the whole record of the slow loading phase is included in the time histories of both force and resulting deflection, or;
2) the signals are differentiated so that it is the rate of change of force that is used as the input, and the velocity rather than the displacement (or acceleration rather than the velocity) which is used for the response. If this method is used, the step change in the force is converted into an impulsive signal which can be processed in the same manner as the signals obtained via hammer testing.

Clearly, in order for step relaxation to work the test structure must be in a grounded condition.

Of the two minimally invasive excitation techniques, hammer testing is the least demanding and invasive, since it requires no attachment to the structure-under-test and the excitation can be imparted repeatedly with little extra cost in time or money.

2.5.2 Non-intrusive excitation techniques

It is possible to cite two non-intrusive excitation methods that are commonly used in modal testing, the base excitation method and operational or output-only modal testing.

The fundamental theory for the base excitation technique is presented in Ewins, op. cit. and it will suffice to say here that the structure is mounted on a rigid base to which the excitation force is applied. The excitation force is not measured, but instead, transmissibility data relating the response at one DOF to that of another is used to develop a function which may be analysed in exactly the same way as a normal FRF. This function is only valid if the condition that only one lightly damped mode

dominates the response near resonance holds. It should also be noted that radial modes of axi-symmetric structures are immune to base excitation. Also, since no force is measured, the eigenvectors obtained cannot be mass normalised.

Base excitation has been used to identify the modes of model buildings for earthquake assessment [52] and for the determination of the dynamic characteristics of spacecraft components, [53]. Sinapius, [54], developed a method of determining the free-free responses of structures via base excitation using a multi-axis shaker table and a device for measuring the interface forces, however, the inferred free-free properties of the structure under test had to be viewed with caution because of local stiffening effects. Chen et al [55] used base excitation for their measurements on delicate miniature objects, with their results demonstrating the applicability of base excitation to very small structures.

In recent years operational or output-only modal testing has reached a level of maturity, which is such that commercially available software (Artemis, B&K Pulse for example) include the facility to conduct an output only modal analysis. The various methods of output only modal testing and analysis are summarised in [56] which also examines the practical application of each method to full-scale problems and presents criteria for their selection. Basically, the methods rely only on measured response data and an assumption about the nature of the excitation force. The application of output only methods to real structures is discussed in several papers, [58 and 59] being examples. These papers cover a range of structures, from cars to buildings, demonstrating that the output only methods are generally applicable to any structure, although not for DTA level 3 and 4 applications.

There are some problems with output only methods that stem from assumptions being made about the applied force/forces. Firstly, no force measurement is made so mass-normalisation via the conventional route is impossible; secondly there can be problems if the excitation signal contains non-random elements such as helicopter rotor frequencies or engine harmonics [56]; finally, the forces involved may act over an area as opposed to a point, meaning that the results are, strictly, ODSs and not mode shapes.

It has been mentioned previously that in output-only modal tests a mass normalisation via the conventional method is not possible. In recent years however, it has become possible to mass normalise the mode shapes obtained from output-only testing, or for that matter, from any test method in which no force measurement is made. The procedure was introduced by Parloo et al, op. cit, and makes use of the eigenvalue /vector sensitivity functions [1] and requires a second test with a known mass attached to the structure. The method has been enhanced by Brincker, [60], who used the mass loading caused by the response transducers as a basis for determining the mass normalised mode shapes. Although this is a useful technique that has enhanced the capability of output-only testing, it also means that the tests must be conducted using contacting and relatively large transducers.

2.6 Indirect excitation/response measurement methods

2.6.1 The measurement of Rotational Degrees of Freedom (RDOFs)

There is one area of modal testing in which the FRFs are commonly inferred from measurements on an attached test fixture and that is in the measurement of RDOFs. The measurement of RDOFs is particularly important for applications such as sub-

structuring [61] and the measurement of point RDOF FRFs (moment input, angular acceleration output, for example) is usually achieved using a rigid block attachment as described in Ewins, op. cit. The more advanced of the rigid block attachment methods [62] include a method for removing the mass loading and inertial effects of the attached block from the derived FRFs as part of the calculation procedure. One of the latest versions of the method proposed by Mottershead et al, [63], also compensates for the fact that the attachments used are never truly rigid by allowing the block's flexibility to be included in the calculation. The problem typically encountered is that the calculation is extremely ill-conditioned: firstly, due to the orders of magnitude differences between the translational and rotational responses of a structure at low frequency and, secondly, because the excitation points on the structure are close in comparison to the wavelengths of the modes excited in the structure meaning that the FRFs measured on the attached structure are similar, Mottershead op. cit. This ill-conditioning means that the calculations involved are extremely sensitive to errors and in particular, cross-axis sensitivity errors which may be of the same order of magnitude as the differences in the translational FRFs. It is probably fair to say that the successful application of the "rigid-block" method is one of the most demanding tasks in modal testing.

2.6.2 The Dynamic Characteristics of Internal Components

There are few papers concerning the derivation of the dynamic properties of internal components based upon measurements on their external housings, although the subject was of considerable interest to Salter [64] who examined SDOF methods. In more recent years Jorgensen et al, [65] has researched the problem, although his paper contains only a general approach to the problem and not a solution to it. Limited research has also been conducted into how the properties of in-operation turbine

components can be inferred from measurements on the external stationary components. Maia and Silva have also investigated the use of indirect methods for the characterisation of joints [66] with their method being similar to that employed by Mottershead et al [63] for determining RDOFs.

2.7 Conclusions

From the preceding review of non-intrusive measurement techniques it is possible to conclude that the problem of non-contacting response measurement has been largely solved, with the LDV representing the most versatile and easy to deploy of all the non-contacting measurement solutions available. The LDV not only meets the requirements for response transducers as discussed in Chapter 1, but also offers an extended capability in the form of CSLDV and tracking measurements. These features of the LDV combined with its greater availability account for the increasing use of the LDV in the field of modal testing. Of particular interest within the work reported here is the application of CSLDV to highly curved surfaces such as cylinders and cones. These are common shapes for some of the structures of specific interest and the problems associated with the scanning of such axi-symmetric structures have not yet been solved.

It is also possible to conclude that the problems associated with non-intrusive excitation have not been solved in a way that is generally applicable to a broad range of structures, and this represents the most significant gap in the existing technologies for the non-intrusive modal testing of structures. In fact, only magnetic excitation with its limited target types and eddy current excitation with its limited signal types, allows the tester to progress to making measurements for DTA level 3 and above, without any contact with the structure. The main problem is in obtaining a measure of

the force applied to the structure, and it is here that most of the non-contacting methods discussed fall short of the requirements presented in Chapter 1. Accurate force measurement is likely to remain a major problem for completely non-contacting excitation since, as stated in Chapter 1, it is necessary to ensure that the force is measured at a location that is as close as possible to the surface of interest. This implies that the measuring of reaction forces on the exciter (if this is even possible) may be inaccurate, particularly over long distances. If the measurement of reaction forces is not possible, then the only other option is to measure the force (or some fraction of it) through a device with known properties, as in the case of a force or pressure gauge. Some degree of contact with the structure is implicit in any such method.

Finally, a solution to the problems associated with force measurement may be possible via indirect testing methods. Some of the theory for these methods already exists for simple indirect test fixtures. It is possible that with some extension of the basic theory, indirect testing may provide a general method for the excitation of delicate and critical structures, and the development of indirect testing technologies (presented in Chapter 4) will provide the main contribution of this work.

2.8 Specific Objectives

Having reviewed the state-of-the-art in the non-intrusive modal testing of structures and identified a gap between the requirements and the capabilities available, it is possible to establish the specific objectives of this research. These are:

1) to investigate the use of LDV in conjunction with non-intrusive excitation methods to make measurements for DTA level 3 and 4 applications;

2) the extension of CSLDV methods for application to structures with highly curved surfaces, and;
3) the development of the theory of indirect testing as a possible alternative to completely non-contacting testing, and as a means of inferring information about the dynamic characteristics of internal components. The development of indirect testing techniques is a key requirement of this research.

CHAPTER 3. PRACTICAL APPLICATION OF THE LDV

3.1 Introduction

This chapter reports on the new uses of the LDV as a response transducer for modal testing. Two of its modes of operation are explored, the single point measurement mode and the continuously scanning mode. A case study on a delicate component is used to demonstrate how the LDV device can be used in conjunction with hammer testing to provide a minimally invasive modal testing method capable of producing data suitable for use in DTA level 3 and 4 applications. Also, a novel method which allows the continuous area-scanning of axi-symmetric structures such as cylinders and cones is demonstrated.

3.2 Single point LDV

3.2.1 General comment

In single point mode, the LDV can be employed as an alternative to contacting accelerometers for the purpose of modal testing. The use of the LDV in this mode can incur some problems if the structure is not planar, since it may be necessary to reposition the structure or the LDV for each new measurement. The use of a roving exciter method, where it is appropriate, can remove this problem and achieve test times which are identical to those achieved when a contacting transducer is used. If a roving exciter technique cannot be employed, a significant increase in test times may be incurred and this will need to be justified against any technical requirements. As is demonstrated in the case study presented in this section, careful planning of the test before entering the laboratory can ensure that the LDV is used in an optimal manner,

reducing the test time, while ensuring the acquired data are sufficient for the application.

3.2.2 Case study: minimally intrusive modal testing of a delicate component

3.2.2.1 Background

The structure under test is shown in Figure 3.2.1(a), it is fabricated from titanium and at its largest point has a diameter of approximately 150mm. The lower section (as labelled in Figure 3.2.1(b)) includes a thin-walled region, in which the wall thickness is approximately 0.5mm. A valid model of the structure was required for use in an FRF sub-structuring application, in which the analytical model of the structure would be coupled with an experimentally derived model of another component [67]. For this reason, the model was required to provide a good estimate of the real structure's FRFs over the frequency range 0-2000Hz. The initial FE model had previously been used for explicit transient dynamic calculations. Although the model was reasonably faithful to the structure's geometry and included all its major features (such as the cut-outs and threads) the legs, which have a complex geometry requiring a fine mesh, had been represented simply with shell elements so that the time-step used in the explicit analysis did not become too small.

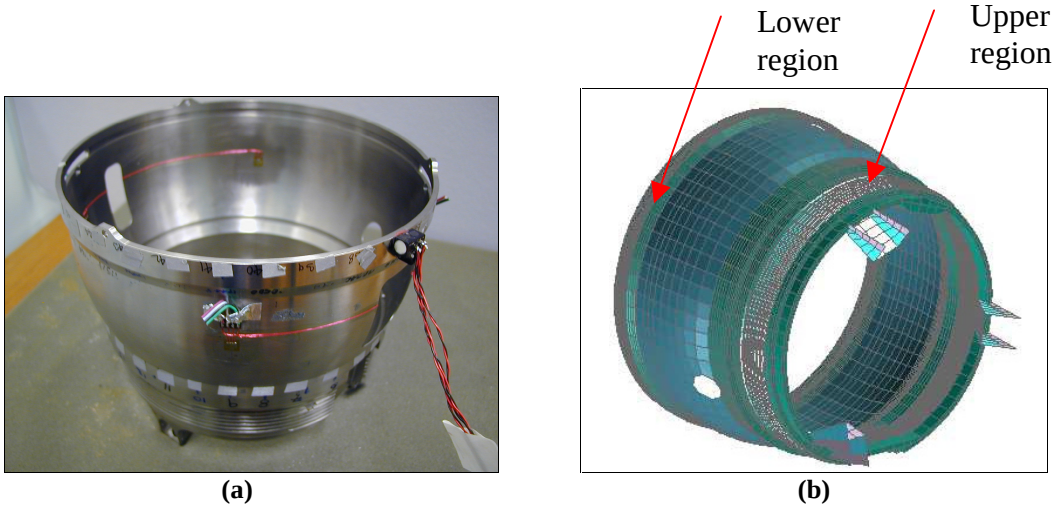

(a) **(b)**

Figure 3.2.1. The structure under test: (a) actual structure; (b) initial finite element model

Tests had previously been conducted on the structure as part of the AWE Modal Analysis Coupling Exercise (MACE) [68]. These tests were conducted using the "typical" attached shaker and roving accelerometer method. The structure proved difficult to test using a shaker due to force "drop out" at the structure's natural frequencies. This problem is often associated with lightly damped structures, and occurs in the vicinity of resonance when the (true) applied excitation force becomes small. The severity of the effect varies dependent upon the shaker mass (a fixed quantity) and the proximity of the shaker's attachment location to a node or anti-node, Ewins op. cit. In an effort to counter the force "drop out" problem, the tests were conducted using stepped-sine testing which allows greater control over the excitation frequencies than random noise, potentially allowing the tester to circumvent the problem of force drop-out. Even using stepped-sine testing the results proved extremely difficult to analyse due to inconsistency in the location of the resonances between FRFs measured at different points. In order to validate the FE model such that it was fit for use in the sub-structuring application, a different test strategy was required.

3.2.2.2 Test strategy development using virtual testing

Given the difficulties which had previously been reported in testing the structure it was decided to develop a test strategy for the structure based upon the FE model. Since shaker testing using random excitation had proved difficult and because the model was required to regenerate FRFs well not only at the resonances, but also away from resonance, it was decided to use the impact hammer technique of excitation. The impact hammer technique does not suffer from the force "drop out" problem as the force is applied transiently to a stationary as opposed to vibrating structure, Ewins op. cit. However, it is necessary to ensure that the force pulse applied has a

sufficiently short duration to provide a flat input spectrum across the frequency range of interest and this is a function of the stiffness of the hammer tip and structure's stiffness at the impact location. Suitable locations for hammer impacts can be determined from the model by calculating the ratio of the Non-Optimum Driving Point (NOPD, given by $\min_r \left\{ \left\| \phi_{jr} \right\| \right\}$ [69]) and the Average Driving point DOF for velocity (ADDOF-V, as discussed on page 73), [69]. High values of this ratio indicate locations where the structure is sufficiently stiff to impart a pulse of short duration that will excite each mode in the frequency range evenly but, where the structure's reaction to applied loading is slow enough to avoid multiple hammer impacts. A plot of the best hammer excitation points for the structure is shown in Figure 3.2.2 and shows how the best excitation locations (shown in maroon and red) are situated on the stiff upper region of the structure. It should be noted here that these locations apply for a single excitation location only. If a roving hammer test were being considered, DOFs would need to be selected which had not only the aforementioned properties but, also, gave a unique description of each mode shape. The excitation location was selected from the possible high valued (maroon/red) locations shown in Figure 3.2.2, and the final excitation location was selected on the basis that it was easy to locate on the real structure.

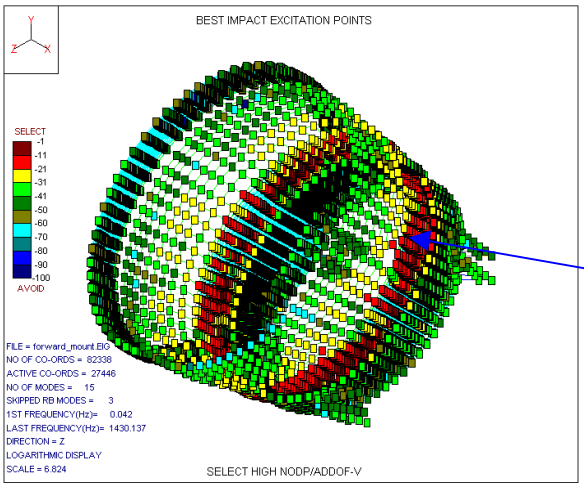

Figure 3.2.2. Best hammer excitation locations for the structure-under-test

Having determined the excitation location, the best response measurement DOFs were considered. The method used to determine the best locations is based upon the Effective Independence (EI) calculation [70]. This calculation ranks the DOFs according to their contribution to the global rank of the mode shape matrix. High values of EI indicated DOFs which will provide a unique spatial description of each mode shape within the frequency range of interest. Since the high-value EI DOFs are generally close to anti-nodes for particular modes, at which accurate measurement is difficult, the best transducer locations are determined by weighting the value of EI to take account of the measurement parameters of the intended transducer(s). The Average Driving DOF for a particular measurement parameter (ADDOF-P, where P is the measurement parameter) is defined as $\sum_{r=1}^{m} \frac{\phi_{jr}^2}{P}$ where $P = \omega_r^2$ for displacement; ω_r for velocity; and 1 for acceleration. The best measurement locations are therefore computed as $EI \times (ADDOF - P)$. The best accelerometer locations plot for the structure of interest is shown in Figure 3.2.3.

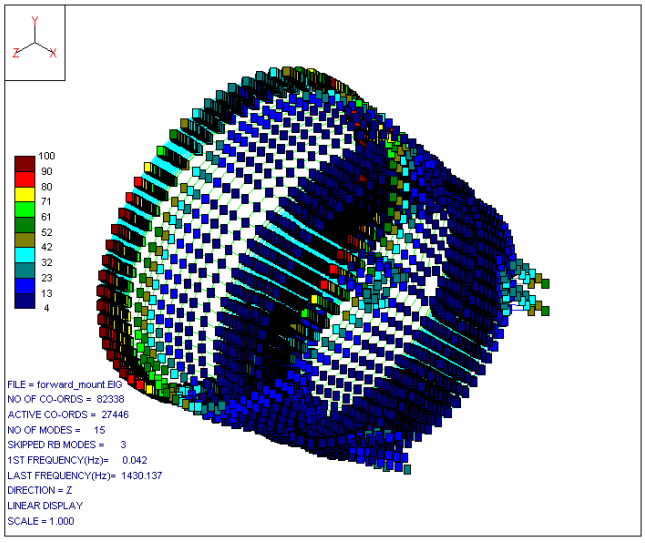

Figure 3.2.3. Best accelerometer locations for the structure-under-test

From Figure 3.2.3 it can be seen that the majority of high-valued DOFs (shown in maroon /red) are located on the lower region of the structure. This is an unsurprising result given that this is the region in which most of the mode shapes within the frequency range have their maximum displacement. However, the test planning calculations do not take account of any mass loading effects caused by the transducers used to make the measurements. Since mass loading was the suspected cause of the inconsistencies observed in the previous tests a simple virtual test was used to investigate the susceptibility of the structure to mass loading. A point mass of 0.5g (corresponding to the mass of an Endeveco type 2222c single axis transducer[3]) was applied to a node arbitrarily selected from the best measurement DOFs illustrated in Figure 3.2.3. This mass was then "removed", and the model was re-analysed with the point mass applied at a second arbitrarily selected node from the best accelerometer locations. The first ten natural frequencies calculated in these two FE runs are tabulated against the first ten modes of the unperturbed FE model in Table 3.2-1. The results shown in Table 3.2-1 clearly illustrate the susceptibility of the structure to mass loading, even if very light-weight transducers are employed.

Unperturbed natural frequency (Hz)	Mass loaded (position 1) natural frequency (Hz)	Mass loaded (position 2) natural frequency (Hz)
303	295	298
312	310	307
490	489	490
501	501	500
608	588	602
630	625	608
942	913	914
954	947	943
1237	1237	1237
1397	1380	1382

Table 3.2-1. The effect of mass loading on the structure-under-test

[3] Note that the synthesised mass loading does not include rotational inertia properties as these were not available in the transducer data sheet supplied by the manufacturer.

There are three possible approaches to the problems caused by mass-loading:

1) use a roving hammer test method, in which case the location of the contacting response transducer does not change. The use of this approach ensures that while the structure is mass loaded, the effect of the mass loading remains consistent throughout the test. A representation of the transducer can be included in the model and removed when a satisfactory level of correlation between the mass loaded FE model and test model is achieved; or

2) place accelerometers and/or dummy masses at all the locations of interest on the real structure and include representations of these in the FE model. During the test the accelerometers are moved around the structure, their positions being interchanged with those of the dummy masses in an effort to maintain the consistency of the mass-loading and thereby the consistency of the measured data. The mass-loaded model can be compared and updated based upon the observations made on the mass-loaded structure. When a satisfactory level of correlation has been achieved between the two models the masses can be removed from the theoretical model. This is a long standing method for overcoming the mass-loading problem which is often used when non-contacting transducer(s) are not available.

3) Use a non-contacting response measurement device so that a “roving gauge” test method is possible.

The first of these methods could not be used on the structure under test as the lower region of the structure was not sufficiently stiff to allow a flat force spectrum to be obtained over the frequency range of interest (note the low value of $\frac{NODP}{ADDOF-V}$ for these locations in Figure 3.2.2) and therefore a roving hammer test was not

appropriate. The second of the methods is a simple version of the model-and-remove approach discussed in more detail in Chapter 4, and is likely to include some assumptions relating to the actual masses applied and, in particular, their rotational inertia. The errors associated with assumptions about the mass property parameters will be more apparent at higher frequencies where their contribution becomes larger. Furthermore, the second method is time consuming as the repositioning of the gauges and dummy masses must be undertaken with care. The use of a non-contacting response transducer is the optimal solution to the mass loading problem and so an LDV was selected as the response measurement device.

Based on the test planning information and a review of all the mode shapes in the frequency range 0-2000Hz, the test geometry was selected and consisted of 64 locations. This number of points allowed for good visualisation of the mode shapes and was also demonstrated to provide a good Auto-MAC with no off-diagonal components greater than 60 % (Figure 3.2.4(b)). The selected measurement locations formed two equi-spaced rings on the structure on the lower and upper regions, as shown in Figure 3.2.4(a).

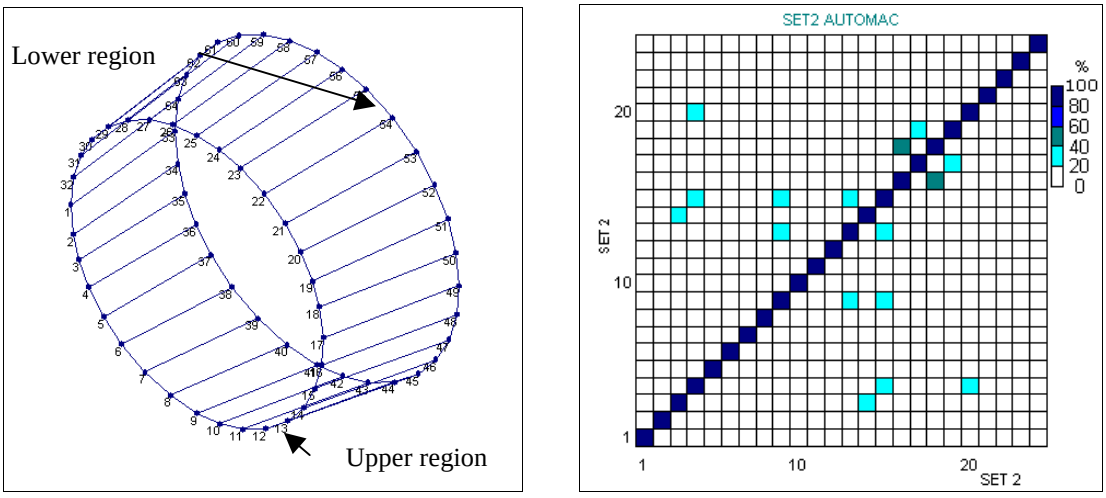

(a) **(b)**

Figure 3.2.4. (a) The selected test geometry and (b) its corresponding Auto-MAC

3.2.2.3 Practical Considerations

The use of the LDV on a highly curved surface, such as the structure of interest, does present the problem of Line Of Sight (LOS). In cases where it is possible to use a roving exciter excitation method, this problem is overcome and there is no need to reposition the LDV head or the structure. However, as mentioned previously (Section 3.2.2.2) the lower section of the structure-under-test was not sufficiently stiff to allow a flat force spectrum to be obtained over the frequency range of interest and it was necessary to reposition either the LDV or the structure. Since the structure was light-weight, it was deemed easier to reposition it for each new measurement, and this required the item to be supported on soft foam. In fact, supporting the structure in this way also mitigated against a second problem associated with large low-frequency displacement of the test item. The suspension provided by the foam was sufficiently soft not to interfere with the structure's modes, but removed the problem of the test item swaying at low frequency, which can be encountered when an elastic suspension is used. Such low-frequency swaying motion can cause uncertainty in LDV measurements since the point of incidence of the LDV on the target moves during the period of acquisition and the response measurement is not made at a single point. This problem is sometimes referred to as "blurring" and is the reason that Stanbridge [15] grounded his structures when he used impact hammer excitation for CSLDV measurements. In addition, realignment of the beam on the target point for the purpose of measurement averaging can be a difficult and time-consuming process when an elastic suspension is used.

The importance of obtaining a good point FRF measurement was explained in Chapter 1. When hammer testing is used in conjunction with an LDV this can be a

difficult measurement to make, since the hammer can interfere with the laser's LOS as it impacts the target. In the case of the structure of interest, it was possible to impact on the interior surface of the structure, opposite to the point of incidence of the LDV beam. The validity of using this method was demonstrated using virtual testing by synthesising the intended "point" FRF measurement, and comparing it to the actual point FRF obtained when force and response were taken on the same node. The calculation of the FRFs used the mode superposition method of harmonic analysis and included the first 200 modes calculated from the model. The FRF obtained when the force is applied to an interior node of the structure, opposite the response node, is plotted over the true point FRF for the force/response node in Figure 3.2.5. This result clearly demonstrates the validity of the point FRF measurement technique used for the structure under test, as there is little visible difference between the two FRF curves.

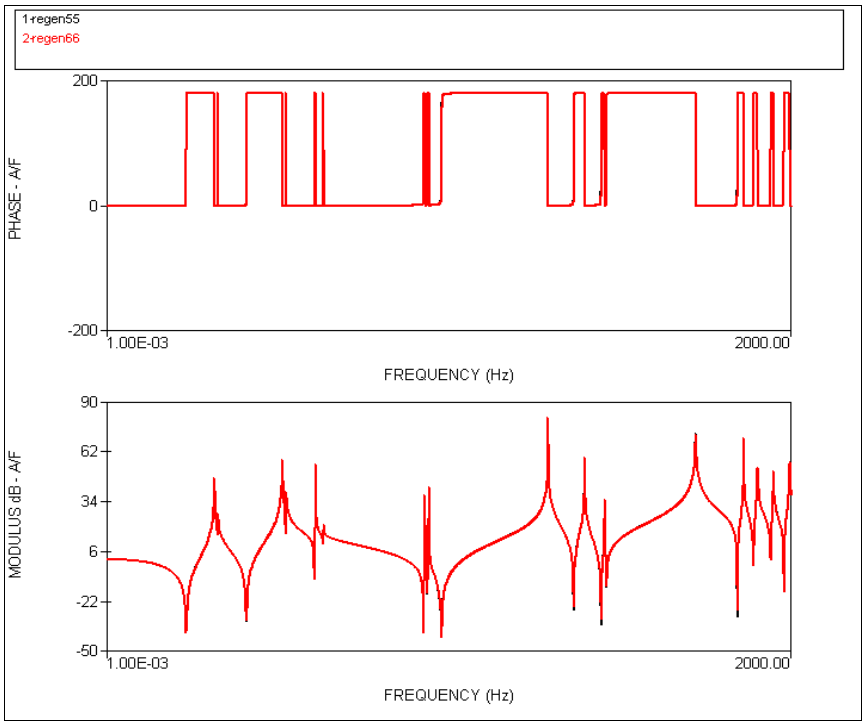

Figure 3.2.5. Overlay of true point FRF (black) and approximation to the point FRF given by excitation on the structures interior (red) showing small differences in the locations of the anti-resonances.

3.2.2.4 Modal testing of the structure

The test configuration is shown in Figure 3.2.6. Pre-test checks were conducted to ensure that each resonance of the point FRF was followed by an anti-resonance (Figure 3.2.7 (a)) and that a reasonable level of reciprocity could be demonstrated. Checks were also performed to ensure that the repositioning of the structure to align it with the laser did not cause any inconsistency in the data (Figure 3.2.7(b)) and that the structure's response died away within the measurement time of 1.27 seconds (Figure 3.2.7 (c)). Having completed the pre-test checks, the actual measurements were made. Three averages were used in acquiring each FRF: this provided some smoothing and also allowed the consistency of the hammer impact location to be assessed using the coherence function (see Figure 3.2.7(d) for an example of the coherence functions obtained).

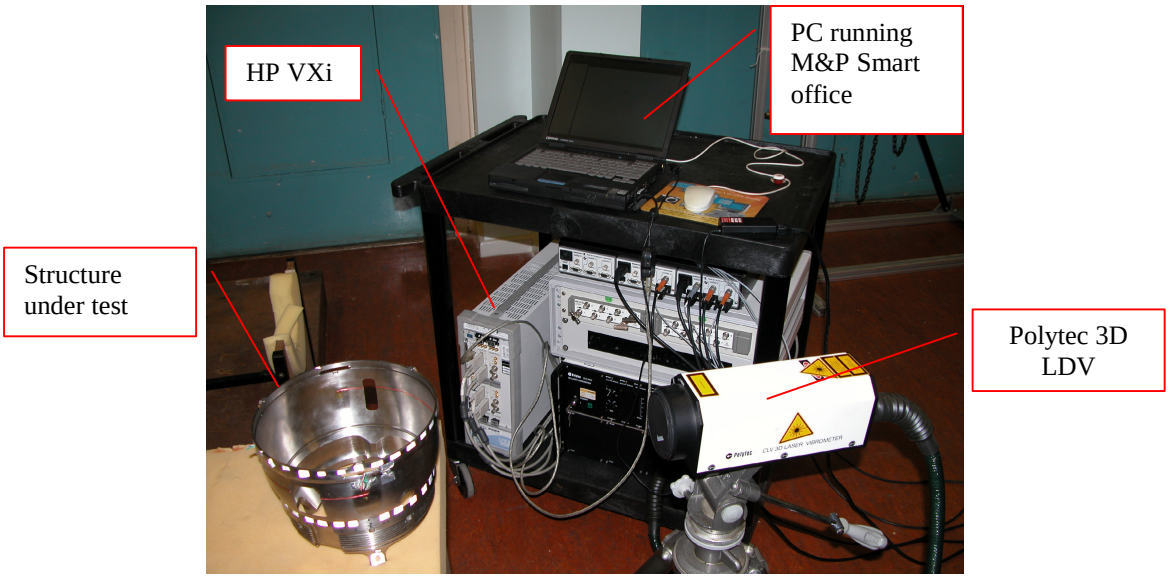

Figure 3.2.6. Test configuration used for minimally invasive modal testing of the structure under test.

3.2.2.5 Results

An overlay plot of FRFs collected using the LDV and impact hammer test method are shown in Figure 3.2.8(a). These data were analysed using the Global-M parameter

extraction method provided in the ICATS Modent software [69]. All of the mode-shapes found in the range 0-2000Hz were correlated against the FE mode shapes, the resulting MAC and natural frequency plot are shown Figure 3.2.8(b).

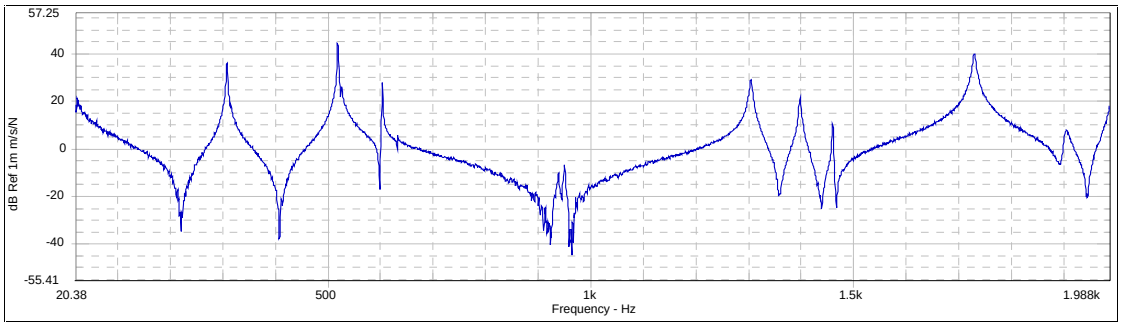

(a)

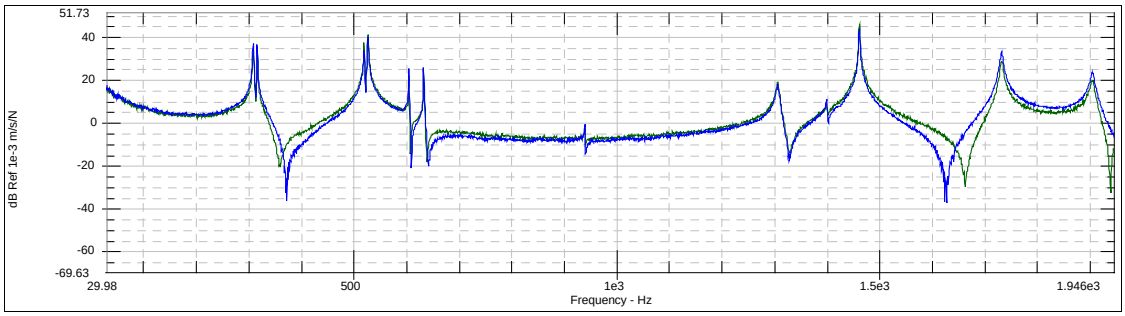

(b)

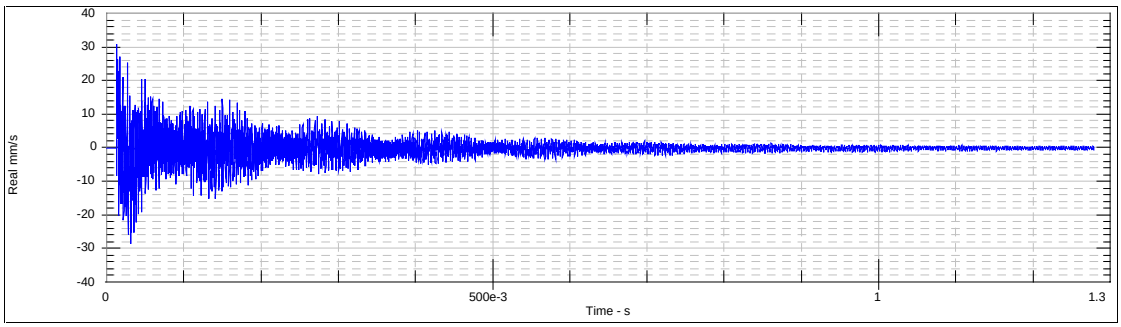

(c)

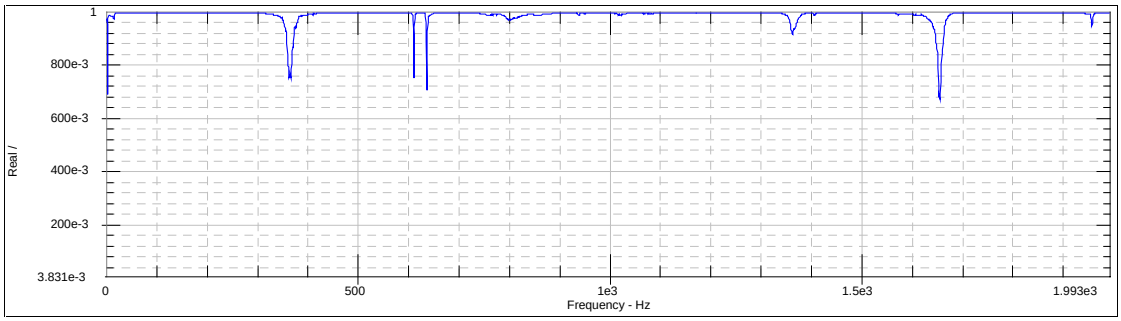

(d)

Figure 3.2.7. (a) The point FRF H_{1r1r} ; (b) example of reciprocity check (H_{1r17r} (blue) and H_{17r1r} (green)); (c) example of response time history; (d) example coherence function.

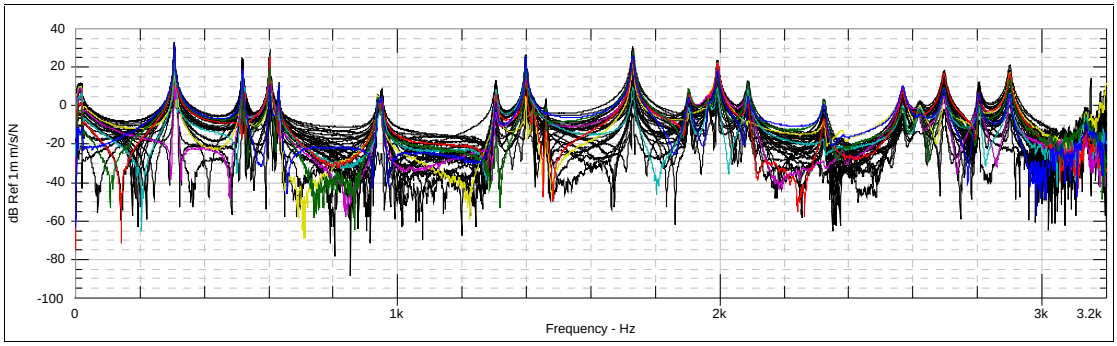

(a)

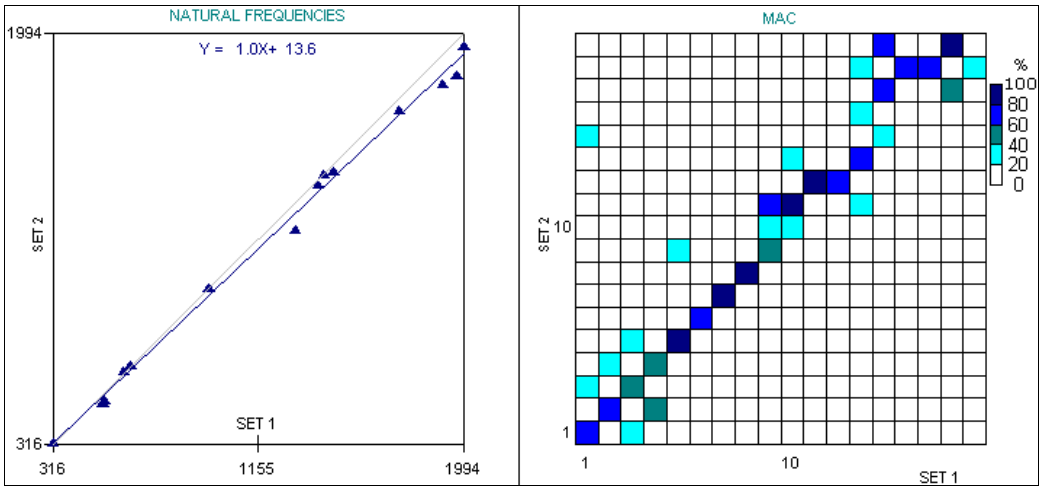

(b)

Figure 3.2.8. (a) Full FRF data set; (b) natural frequency and MAC correlation of experimental model (set 1) and finite element model (set 2).

3.2.2.6 Validation of the FE model

The MAC plot of Figure 3.2.8(b) showed that there were considerable differences between the modes obtained from the experiment and those obtained from the FE model. The first stage of the validation procedure was to minimise the differences between the model's geometry and that of the structure. The model was altered to include a brick element representation of the legs, as shown in Figure 3.2.9. When compared to the experimental data the improved leg model gave the natural frequency and MAC plot shown in Figure 3.2.10. The MAC plot of Figure 3.2.10 shows that there is some mode switching and that there is poor correlation between some of the higher modes. However, a review of the mode shapes showed that where there were

discrepancies between the FE and experimental results the mode shapes included motion of the stiff upper region of the structure. Increasing the Young's modulus of the material in the upper region by 5% led to the natural frequency and MAC plot shown in Figure 3.2.11. It is likely that the real cause of the stiffness discrepancy is a small variation in thickness of the upper region, although this possibility has not yet been explored. Table 3.2-2 gives a comparison of the experimental and analytical results for the updated model. A few modes remain with low MACs, but these relate to modes that were weakly excited in the test. A second test using a different excitation location could have been used to obtain better estimates of the modal parameters associated with these modes. However, the model was capable of giving a reasonable prediction of the structure's response (from 0-1800 Hz), as shown in Figure 3.2.12, and so a second test was deemed to be unnecessary.

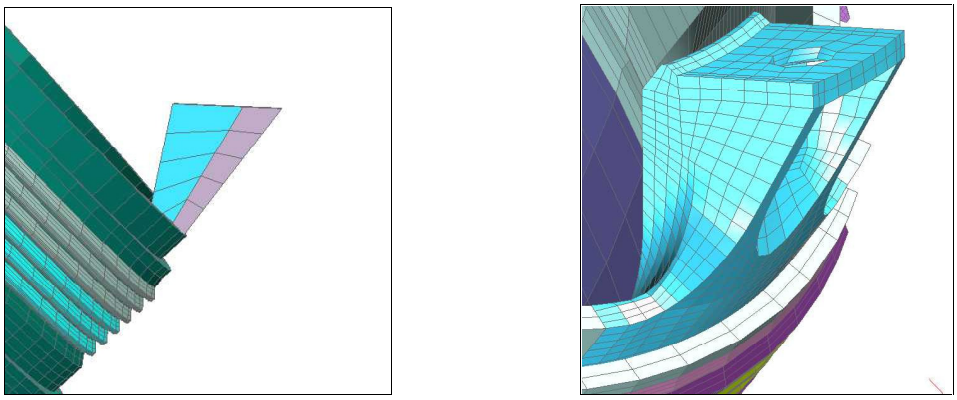

(a) **(b)**

Figure 3.2.9. (a) Original shell element representation of the leg; (b) Improved brick element representation of the leg.

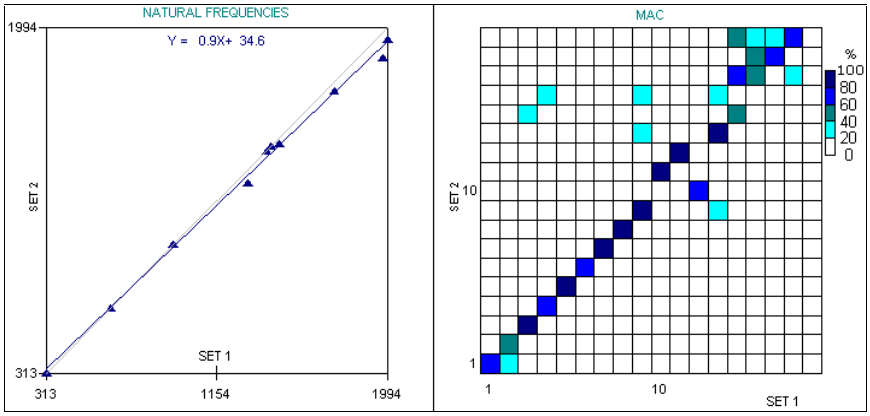

Figure 3.2.10. Natural frequency and MAC correlation of experimental model (set 1) and improved finite element model (set 2).

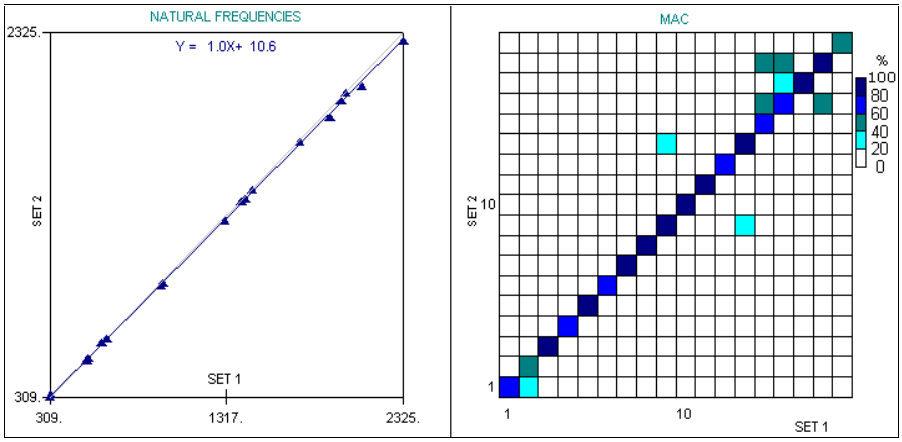

Figure 3.2.11. Natural frequency and MAC correlation of experimental model (set 1) and updated finite element model (set 2).

Mode No.	Experimental Natural Frequency (Hz)	Analytical Natural Frequency (Hz)	Difference (%)	MAC (%)
1	309	312	1.1	74.4
2	316	322	2.0	44.1
3	520	510	1.8	80.8
4	527	522	0.9	77.4
5	605	609	0.7	84.9
6	633	630	0.4	70.8
7	940	928	1.3	90.9
8	951	939	1.3	90.2
9	1306	1287	1.4	90.7
10	1399	1395	0.3	95.9
11	1423	1404	1.3	85.9
12	1461	1454	0.5	78.8
13	1732	1719	0.7	82.3
14	1905	1860	2.4	69.2
15	1970	1947	1.2	76.8
16	1995	1994	0.05	83.7

Table 3.2-2. Results of experimental modal analysis compared with analytical results from updated FE model.

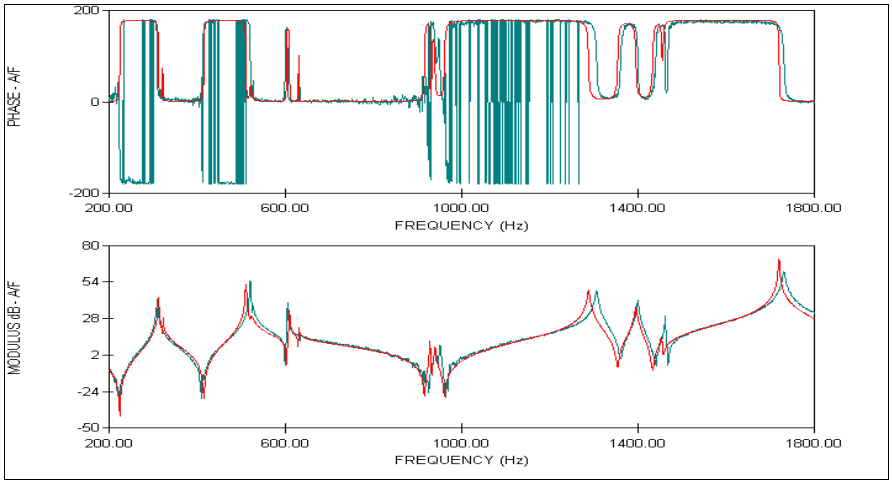

Figure 3.2.12. FRF calculated from FE model $H_{1r,1r}$ (red) and corresponding measured FRF $H_{1r,1r}$ (green).

3.2.2.7 Conclusions

This case study has demonstrated that the LDV can be used in conjunction with impact hammer testing to provide data for DTA level 3 and 4 applications. Although the excitation and response methods employed are both well established techniques, their combined application is not widely reported, with researchers favouring the use of shaker excitation in conjunction with LDV response measurements. Hammer excitation was not ideally suited for use with LDV on the structure tested here, primarily because of LOS issues associated with the axi-symmetric structure and the need to move either the laser or the structure in order to make a new measurement. It must be said that the need for re-alignment is more of a hindrance than a real problem, especially in the light of the minimally intrusive test method the impact hammer and LDV provide. It should be noted that, even though careful repositioning and alignment of the structure was required, the total test time and analysis time was less than 3 hours. For high quality measurements, some consideration must be paid to the suspension used for the test, especially if the structure is light-weight, since the hammer impact causes large low frequency displacements if the structure is suspended using elastic. It must also be noted that if an elastic suspension is used,

then it is necessary to reposition the laser as opposed to the structure for every new measurement and this may significantly increase test times.

The case-study also demonstrates the value of virtual testing in making decisions relating to the test method. In the example presented here, careful planning conducted prior to entering the laboratory both reduced the required test time and meant that no additional or repeat tests were required to validate the model to a level sufficient for its intended application.

3.3 Continuously Scanning LDV

3.3.1 General Comment

In its continuously scanning mode, the LDV can be used to obtain ODSs or mode shapes with a spatial density that is competitive with holography and which is better than FE. Since the analysis of the acquired data extracts the shapes as either a polynomial expression or a limited Fourier series [13] the problems associated with the analysis and storage of very large data sets can be avoided. Many different types of scan have previously been demonstrated and the reader is referred to references [11,12,13] for the theory of these techniques. However, since the continuous scanning of cylindrical structures presented in this section is based upon the CSLDV sinusoidal straight line and area scanning techniques [17,18] , a brief review of the theory of these methods is appropriate.

3.3.2 Fundamental theory for CSLDV sinusoidal straight line and area scans

CSLDV line and area scanning techniques are based upon the fact that for a continuous structure, excited by a force at frequency ω, the vibration at some point x

on the surface of the structure may be written (assuming linearity), without loss of generality as :

$$v_{\Re}(x,t) = \left(\sum_{n=0}^{N} V_{\Re n} x^n \right) \cos(2\pi\omega t) \tag{3.3.1}$$

for the in-phase (real part); and

$$v_{\Im}(x,t) = \left(\sum_{n=0}^{N} V_{\Im n} x^n \right) \sin(2\pi\omega t) \tag{3.3.2}$$

for the in-quadrature (imaginary part).

In the case of sinusoidal straight line scans, the LDV probe is scanned across the surface of the structure such that its point of incidence on the structure is[4]:

$$x(t) = \cos(2\pi\Omega t) \tag{3.3.3}$$

in which Ω is the scan frequency. Therefore on substitution for *x*:

$$v_{\Re}(t) = \sum_{n=0}^{N} V_{\Re n} \cos(2\pi\omega t) \cos^n(2\pi\Omega t); \tag{3.3.4}$$

and

$$V_{\Im}(t) = \sum_{n=0}^{N} V_{\Im n} \cos(2\pi\omega t) \sin^n(2\pi\Omega t) \tag{3.3.5}$$

In the case of a (real) 3rd order polynomial, such as that shown in Figure 3.3.1, for example, we have:

$$v(t) = V_0 \cos(2\pi\omega t) + V_1 \cos(2\pi\omega t)\cos(2\pi\Omega t) + V_2 \cos(2\pi\omega t)\cos^2(2\pi\Omega t) + \ldots \\ \ldots V_3 \cos(2\pi\omega t)\cos^3(2\pi\Omega t) \tag{3.3.6}$$

[4] Note that the selection of $x(t) = \cos(2\pi\Omega t)$ normalises the scan distance to the interval –1 to 1.

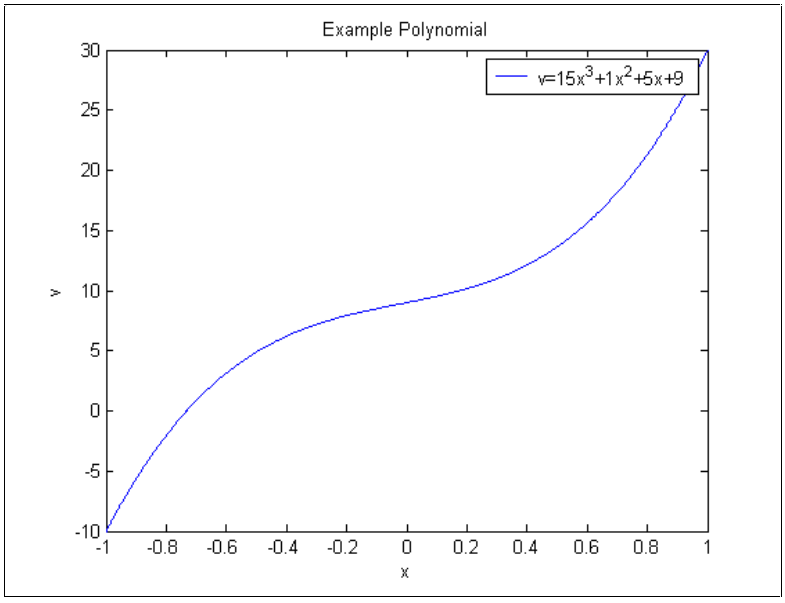

Figure 3.3.1. Example cubic polynomial.

On expanding the cosine terms (readily accomplished using Euler's relation, $\cos(\theta) = \frac{e^{j\theta} + e^{-j\theta}}{2}$):

$$v(t) = V_0 \cos(2\pi\omega) + \frac{V_1}{2}\cos(2\pi(\omega \pm \Omega))t + \frac{V_2}{2}\cos(2\pi\omega t)..$$
$$+ \frac{V_2}{4}\cos(2\pi(\omega \pm 2\Omega)t) + \frac{3V_3}{8}\cos(2\pi(\omega \pm \Omega)t) + \frac{V_3}{8}\cos((2\pi(\omega \pm 3\Omega)t) \quad (3.3.7)$$

The frequency spectrum of this function, illustrated for the case of the cubic expression shown in Figure 3.3.1 (with Ω=10 Hz and ω=100 Hz), exhibits a symmetric side-band structure centred on the excitation frequency, and having side bands at frequencies $2\pi(\omega \pm n\Omega)$, (where, in the case of the example, *n*=1 to 3) as shown in Figure 3.3.2. The amplitudes of the frequency components are (calculated for the case of the cubic equation of Figure 3.3.1):

$$
\begin{aligned}
a_0 &= V_0 + \frac{V_2}{2} = 9 + \frac{1}{2} = 9.5 \\
a_1 &= \frac{V_1}{2} + \frac{3V_3}{8} = \frac{5}{2} + \frac{45}{8} = 8.125 \\
a_2 &= \frac{V_2}{4} = \frac{1}{4} = 0.25 \\
a_3 &= \frac{V_3}{8} = \frac{15}{8} = 1.875
\end{aligned}
\tag{3.3.8}
$$

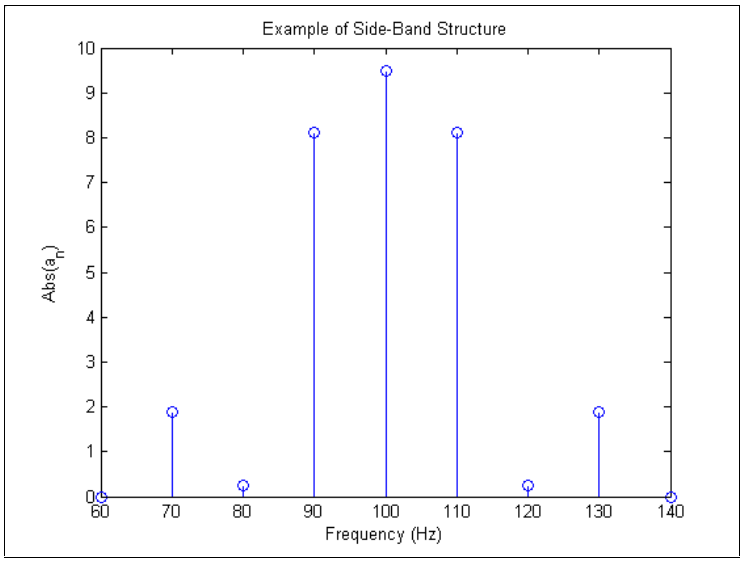

Figure 3.3.2. Side-band structure for example polynomial of Figure 3.3.1. (ω = 100Hz , Ω =10 Hz).

These side-amplitudes give directly the coefficients for a Chebyshev polynomial expression (Equation 3.3.9) :

$$
v = a_0 + \sum_{n=1}^{N} 2a_n \cos(n \cos^{-1} x) \tag{3.3.9}
$$

But, it is more common to convert the side-band amplitudes into the coefficients of two ordinary polynomials (one real and one imaginary) in *x*. This conversion is achieved by writing the expressions of Equation 3.3.7 in matrix form:

$$
\{a\} = [Q]\{V\} \text{ where } [Q] = \begin{bmatrix} 1 & 0 & \frac{1}{2} & 0 \\ 0 & \frac{1}{2} & 0 & \frac{3}{8} \\ 0 & 0 & \frac{1}{4} & 0 \\ 0 & 0 & 0 & \frac{3}{8} \end{bmatrix} \tag{3.3.10}
$$

Therefore:

$$\{V\} = [Q]^{-1}\{a\} \tag{3.3.11}$$

Stanbridge et al, [12], have computed the matrix $[Q]$ by expanding Equation 3.3.4/3.35 to the 14th term thus allowing the transformation of up to 13th order polynomials. Since Q (and therefore its inverse, usually denoted as $[T]$) are invariant smaller subsets of the matrix can be used where there are smaller numbers of side-band coefficients.

In practice of course, the CSLDV measurement generates a signal such as that shown in Figure 3.3.3 (computed using 30000 samples for the cubic polynomial example of Figure 3.3.1). The amplitude and phase spectra are determined by multiplying the acquired time history by cosine and sine waves (for the in-phase and in-quadrature components of the ODS respectively) at frequencies of $2\pi(\omega \pm n\Omega)$ where *n* is the side-band number, and determining the mean value of the thus modified signal. Since the maximum value of *n* is usually unknown, an FFT is commonly used to estimate the spectral content of the signal so that the maximum number of side-band pairs for analysis can be determined. The side-band amplitudes are then converted to provide the coefficients of a polynomial in *x* as described previously. In the case of the example polynomial (which is purely real), the coefficients recovered using this method were as given in Figure 3.3.4 and compare very well with the actual values given in Figure 3.3.1

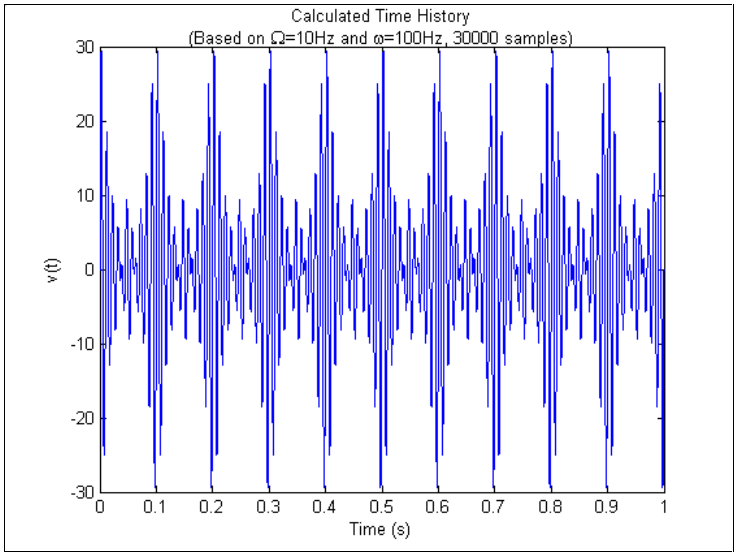

Figure 3.3.3. Simulated time-history computed for example polynomial (Figure 3.3.1).

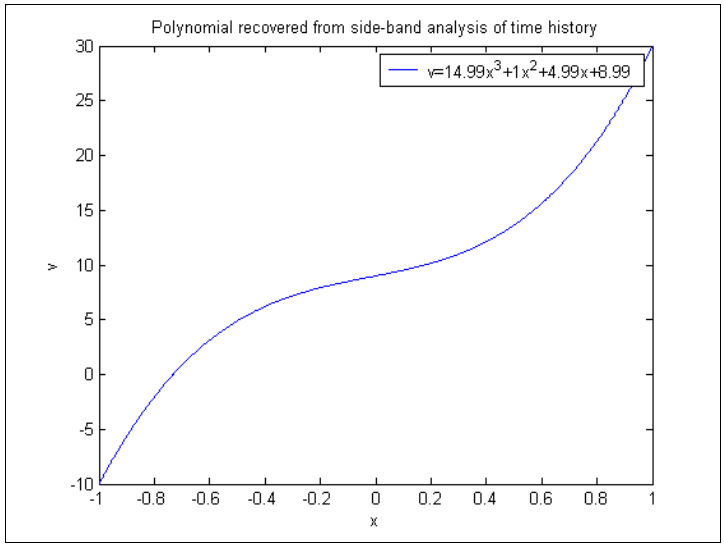

Figure 3.3.4. Polynomial recovered from CSLDV analysis of time-history shown in Figure 3.3.3

Two important features of the way in which the coefficients are extracted from the time history data are that: first, the Fourier series analysis method employed acts as an integrating filter averaging out noise effects when more than one complete scan cycle is included; and second, the theoretically symmetrical structure of the side-bands allows for further averaging so that it is usual to compute $\hat{a}_{n(\omega\pm n\Omega)} = \frac{a_{n(\omega-n\Omega)} + a_{n(\omega+n\Omega)}}{2}$.

These averaging properties mean that smooth ODSs can be obtained from what may be a very noisy spectrum when computed using the FFT.

A similar, although more lengthy, derivation to that for the sinusoidal straight line scan is possible for the case where the LDV beam moves over an area of the surface of the structure such that $x(t) = \cos(2\pi\Omega_x t)$ and $y(t) = \cos(2\pi\Omega_y t)$ [12]. The ODS is then described by the two-dimensional polynomial:

$$v(x,y) = \sum_{\substack{m=0 \\ n=0}}^{\substack{m=M \\ n=N}} V_{n,m} x^m y^n \tag{3.3.12}$$

so that

$$v(t) = \sum_{\substack{n=-n_N \\ m=-m_M}}^{\substack{+n_N \\ +m_M}} \left(V_{mn} \cos\left(2\pi\left(\omega + n\Omega_x + m\Omega_y\right)t\right) + V_{mn} \sin\left(2\pi\left(\omega + n\Omega_x + m\Omega_y\right)t\right)\right) \tag{3.3.13}$$

One of the scan frequencies is selected such that it is at a lower frequency than the other and such that it is not a simple fractional relation of the higher scan frequency. As long as the two scan speeds are not simple fractional relations[5], the spectrum of such area scans is found to contain two sets of side-bands (as shown in Figure 3.3.5). Once again these are centred on the excitation frequency, the first set spaced at ±integer multiples of the faster scan frequency and the second set spaced around the first set at ±integer multiples of the slower scan frequency. The side-bands amplitudes are assigned a double index A_{nm} and are positioned in a matrix $[A]$ accordingly. The ordinary polynomial coefficients form for the ODS is determined for the real and imaginary part of the ODS by applying the transformation matrix twice (once for the side-bands relating to *x* and once for those relating to *y*), so that:

$$[V] = [T][A_{\Re}][T]^T \text{ and } [V] = [T][A_{\Im}][T]^T \text{ where } [T] = [Q]^{-1} \tag{3.3.14}$$

[5] In which case some of the side-bands associated with the two scan rates overlap each other.

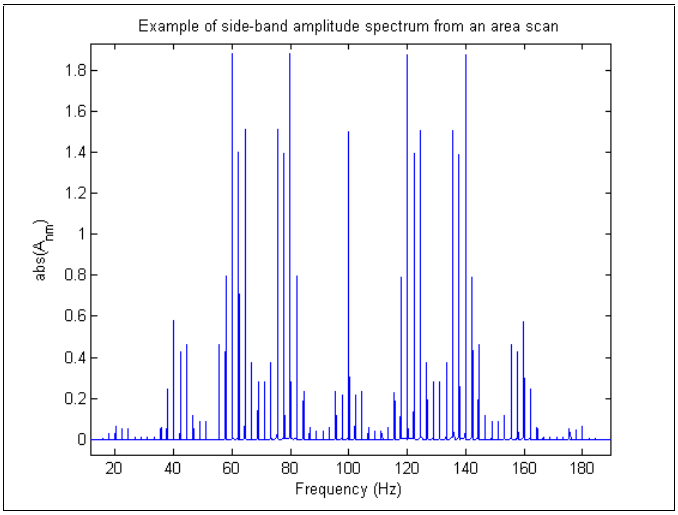

Figure 3.3.5. Example of side-band structure resulting from an area scan with Ω_x=10Hz and Ω_y=1.1Hz

The way in which the side-band amplitudes are determined from the CSLDV signal is also similar to the simpler line scan, except that the signal is multiplied by cosine and sine waves at frequencies of $2\pi\left(\omega \pm n\Omega_x \pm m\Omega_y\right)$ which leads to the A_{nm} element of the full matrix of side-band amplitudes.

It should be noted that while extraction of the amplitude information is a relatively straightforward task, based on the analysis procedure that has been described, the extraction of the phase information is slightly more complex. The main problem in extracting the phase information is that of phase-wrapping, which can cause what should be a symmetrical spectrum to appear otherwise. When deriving the phase angle it is therefore essential that the quadrant of the Argand diagram in which the complex number lies is taken into account. It is also worth mentioning that the ODS measured on many structures will possess only a real part and that complexity of the ODS should only be observed when a structure exhibits close modes and non-proportional damping.

3.3.2.1 Practical CSLDV line and area scanning.

The practical implementation of the CSLDV techniques differs very little from the theory described in the previous section. The LDV head is positioned some distance from the structure, and the scan mirrors are driven with sinusoidal input voltages at the desired scan frequencies[6], the amplitudes of these voltages being set such that beam scans the required line/area. One of the more notable problems encountered derives from the fact that it is extremely difficult to ensure that both scans are at their mid-point at the commencement of scanning and that this coincides exactly with the start of a vibration cycle. This lack of synchronisation leads to a phase error which must be accounted for in the analysis. Most often, the solution to the phase problem is to record the mirror-drive signals simultaneously with the CSLDV signal, triggering the measurement at the centre of one of the scans. The required phase corrections can be estimated from the relative phases of these three signals. The relevant spectral components of the CLSLDV signal are then determined by multiplying it by the phase shifted cosine and sine waves:

$\cos(2\pi(\omega + n\Omega x + m\Omega y)t + n\delta_x + m\delta_y)$; and $\sin(2\pi(\omega + n\Omega x + m\Omega y)t + n\delta_x + m\delta_y)$.

A second problem with measured LDV signals is that they inevitably contain some noise. As was discussed earlier, the method by which the signal is decomposed is very good at averaging out noise effects at the specific frequencies of interest. However, it must be borne in mind that averaging will remove only random noise. In LDV measurements some of the noise can be attributed to speckle drop-outs which

[6] Note that in order to produce a sinusoidal scan on the surface, the beam must be positioned such that it is normal to the target surface and that the surface must (strictly) be planar.

occur when the interaction of the coherent laser light on the vibrating surface leads to a “dark speckle” on the photo detector so that there is little optical signal. In single point operation speckle pattern noise typically leads to a noise floor at around -40dB [3]. Also in single point mode, when specific points on the structure are found to return little optical signal (“speckle drop-out”) the LDV control software is used to reposition the beam (slightly) in an effort to find a region of “bright speckle” where the optical signal is greater. In the CSLDV mode of operation however, the locations at which speckle drop-outs occur are scanned over several times in the scan cycle the drop-outs tend to become periodic [3] and the spectral content of the signal is found to have “noise peaks” at harmonics of the scan frequencies. Such noise peaks are clearly visible in Figure 3.3.6, which shows the result of a line scan made on a structure fabricated from a black, lacquered carbon fibre composite. Two common approaches to the speckle drop-out problem are: (i) to treat the structure with retro-reflective paint or tape which can reduce the problem of speckle drop-out; and/or, (ii) to select the scan frequencies such that they are not simple multiples of the vibration frequency. This ensures that the systematic “noise peaks” do not occur at the side band frequencies [3], and is usually easy to achieve so long as the side band components of the spectrum are well separated. Only the second option was used in the tests on the carbon-fibre structure since quality regulations meant that the structure’s surface had to be left untreated. It has also been noted that the severity of the noise peaks is related to the scan frequency and empirical relationships have been proposed by Martarelli, op. cit., for example. Figure 3.3.7 shows the spectrum obtained from a 5Hz scan along the same line on the carbon-fibre structure from which the reduction in amplitude of the noise peaks is clear.

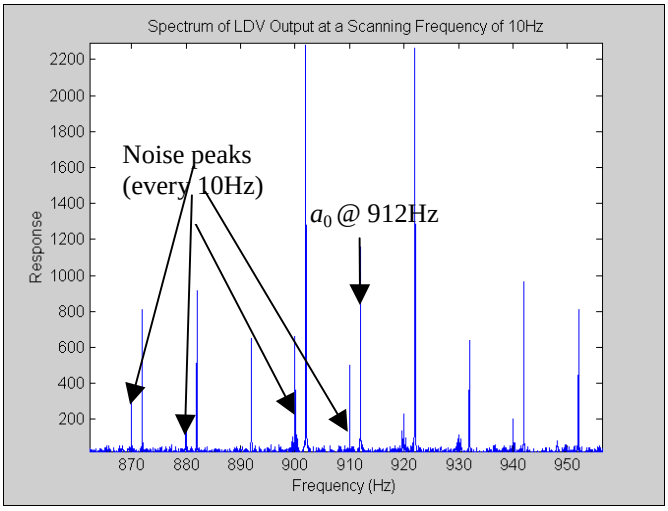

Figure 3.3.6. Result of line scan on black carbon fibre composite with a scan rate of 10Hz, showing noise peaks caused by signal drop-out.

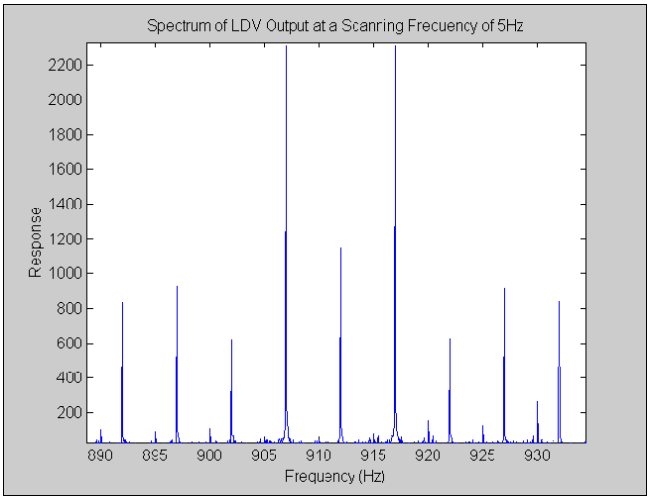

Figure 3.3.7. Result of line scan on black carbon fibre composite with a scan rate of 5Hz.

Two further considerations in the practical implementation of CSLDV include:

- ensuring that the sample time is long enough to allow frequency components spaced at the lower scan frequency to be resolved;
- sampling fast enough to ensure that the spectral components can be resolved without aliasing (related to the excitation frequency and the number of non-trivial side-bands).

3.3.3 Application of continuous area scanning to cylindrical structures

3.3.3.1 Background

The majority of previous work on continuous scanning and, in particular, area scanning has been focused on its application to planar / near-planar structures, such as vehicle body panels. Many engineering structures, such as aero-engine casings and the structure pictured in Figure 3.2.1(a), for example, are essentially cylindrical, though they are not usually completely axi-symmetric. Stanbridge et al, [87], have demonstrated the application of the internal radius or so-called "light-house scan" to cylindrical structures. In this type of scan the LDV beam is scanned round the interior of a cylindrical object, by means of a mirror angled at 45° which is driven continuously at some speed ($2\pi\Omega$). The "light-house scan" set up is shown in Figure 3.3.8.

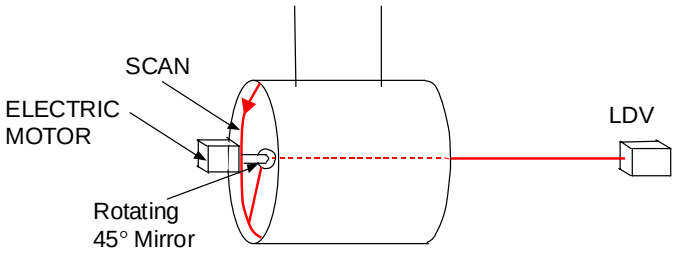

Figure 3.3.8. Illustration of the internal radius or "light-house scan".

The light-house scan exploits the fact that radial modes of cylinders exist in orthogonal pairs, their shapes being described by $v_{\cos p\theta} = A\cos(2\pi p\theta)$ and $v_{\sin p\theta} = A\sin(2\pi p\theta)$ where p is the number of nodal diameters and θ (in degrees) is the angular position around the circumference. Therefore, when continuously scanned, in the case when only the $A\cos(2\pi p\theta)$ mode is excited, for example, $v(t) = A\cos(2\pi p\Omega t)\cos(2\pi\omega t)$. The mode shape is therefore modulated by the

excitation frequency, resulting in a pair of side-bands centred on the excitation frequency and separated by a frequency difference of $4\pi p\Omega$, from which the number of nodal diameters the mode possesses can be determined directly. When it is reasonable to assume symmetry, the light-house scan can be used in conjunction with a single straight-line scan along the cylinder's axis, which yields the number of nodal-lines (q) the mode of interest exhibits. Together p and q and their associated amplitude information give a unique description of each of a cylindrical structures modes, as discussed in [87]. If however, it is not reasonable to assume symmetry, it is clear that the simple p, q description of the mode shape is not an adequate method of describing the structure's more complex vibration pattern: what is needed is an area-scan.

In [12] Stanbridge et al, discuss the application of line and area scanning techniques to non-flat surfaces. This paper demonstrates a method for developing functions relating the voltage required to position the laser at specific points on the target surface and using these to calculate correction factors for the ODS obtained from LDV scans. Although the method used was demonstrated to be general enough to cope with distorted shapes (such as the out-of-round paper bin used as a test item!) only line scans were really practicable because of the length of time required to set up for measurement. Also, the correction factors used were only applicable if the structure exhibited pure out-of-plane motion and furthermore full 360° scans were not possible because of LOS limitations. As in the earlier case study of 3.2.2 the major problem here is the LOS requirement of the LDV.

3.3.3.2 Development of a new cylindrical scanning method

As discussed in the previous case study (Section 3.2.2), there are two possible solutions to the LOS problem, either the laser-beam or the structure must be repositioned. In applications such as laser metrology, similar LOS problems exist and are usually overcome using computer-controlled actuators which allow the target object to be repositioned in front of the laser probe. In the case of the scanning of cylindrical structures a similar approach is possible, although a compromise is necessary on the structure's boundary conditions. A simple solution to the problem is to mount the structure on a computer controlled rotary-stage as shown schematically in Figure 3.3.9.

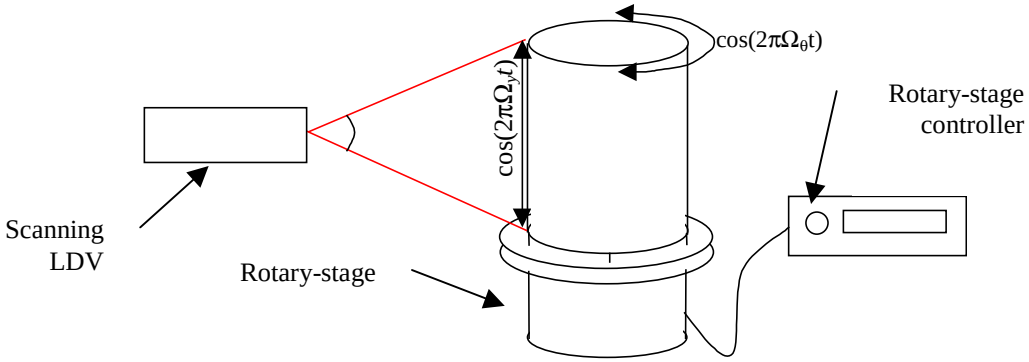

Figure 3.3.9. Schematic CSLDV configuration for scanning cylindrical structures.

The controller is programmed to rotate the stage sinusoidally at frequency, Ω_θ, through ±180°. One of the laser positioning mirrors is driven using a sine wave at a different frequency, Ω_y, such that it scans continuously up and down the target structure. The structure is excited at a single frequency, ω, using an internally mounted shaker which is connected to the structure using a push-rod. The signal measured by the laser will be given by:

$$v(t) = \sum_{\substack{n=-n_N \\ m=-m_M}}^{\substack{+n_N \\ +m_M}} \left(V_{m,n} \cos\left(2\pi\left(\omega + n\Omega_\theta + m\Omega_y\right)t\right) + V_{m,n} \sin\left(2\pi\left(\omega + n\Omega_\theta + m\Omega_y\right)t\right)\right)$$

Therefore if the rotary-stage set-up can be achieved, the resulting scan is exactly analogous to the scanning of a flat rectangular plate and so the analysis procedure discussed in 3.3.2 can be applied. The result of the scan will be an ordinary polynomial in a cylindrical co-ordinate system (y,θ). If at all possible, the shaker should be mounted inside the structure, so that a full 360 degree coverage of the structure's external surface is possible. Mounting the shaker inside the structure also reduces the eccentricity of the load on the rotary-stage, potentially allowing higher oscillation frequencies to be used. Since the motion of the stage is oscillatory, there will be no problems with the cables twisting as long as they are of sufficient length.

3.3.3.3 On the possibility of 6DOF CSLDV scans

An interesting feature of the rotary-stage method is that it would be theoretically possible to make a 6DOF measurement of a structure's vibration using three continuous scans. Only three scans would be required, since a good approximation to the RDOFs is given by the derivative of the polynomial representation of the ODS [14]. In earlier works such as [71] attempts to measure the three translational components of vibration were hampered by the problem of accurate registration of the LDV beam on the target surface. With the rotary-stage system the registration of the beam on the surface would be considerably easier to achieve. Thus three scans could be conducted from three different positions, as shown in Figure 3.3.10 in which the scanning of a conical structure is considered.

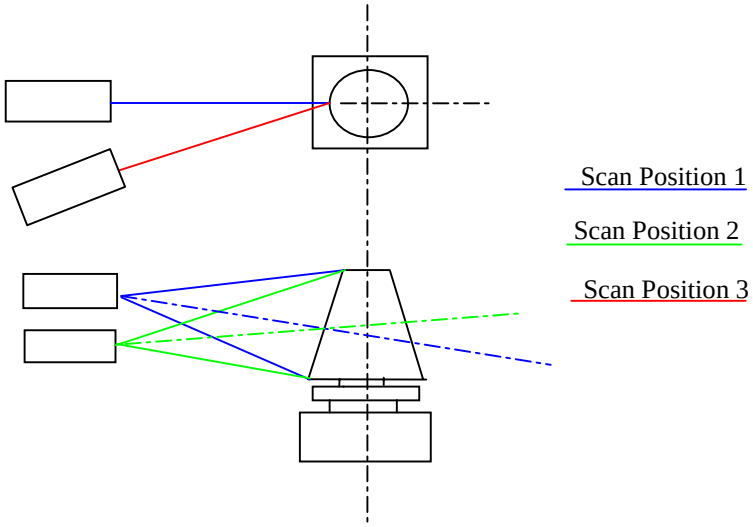

Figure 3.3.10. Illustration of LDV positioning for 6DOF scanning of a conical structure.

In the case of a cone, a sinusoidal input to the mirror drive does not produce a sinusoidal scan on the surface (unless the LDV beam is normal to the target surface at the scan's centre). Therefore, two scans made from different vertical positions cannot be synchronised. The lack of synchronisation makes it difficult to form the simultaneous equations required to separate the signal into orthogonal components. The synchronisation problem is easily overcome, however, since (with reference to Figure 3.3.11) it is possible to derive input signals for the drive mirrors which will lead to a sinusoidal scan on the surface as follows:

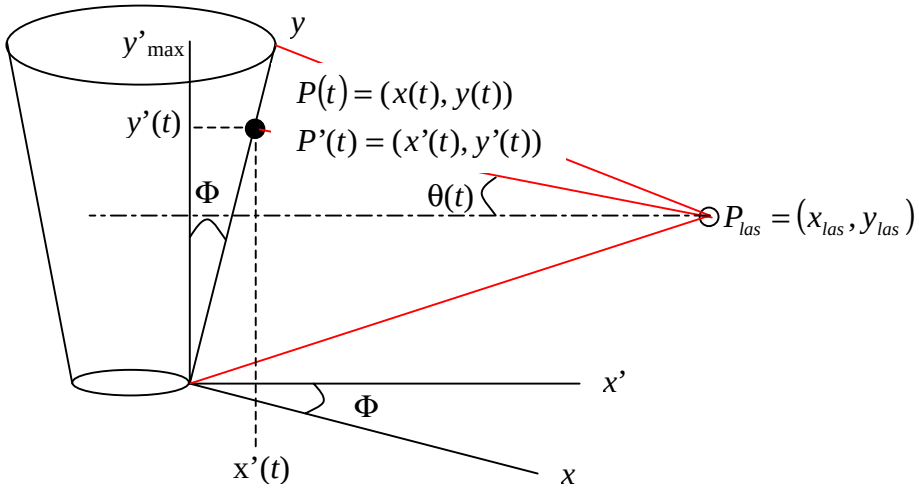

Figure 3.3.11. Illustration of geometry for scanning of a cone.

Let $P(t) = \begin{bmatrix} 0 \\ A\sin(\omega t) + A \end{bmatrix}$ where $A = \frac{1}{2}\frac{y'_{\max}}{\cos(\Phi)}$;

Where *P(t)* is the position of the laser spot in global Cartesian space at time *t*, y'_{max} is the maximum scan length, Φ is the cone angle and ω is the scan frequency in rad/s.

Then using the co-ordinate system transformation

$$[P'(t)] = [B][P(t)] \text{ where } [B] = \begin{bmatrix} \cos(\Phi) & \sin(\Phi) \\ -\sin(\Phi) & \cos(\Phi) \end{bmatrix};$$

where P'(t) is the position of the laser spot in a local co-ordinate system aligned with slant of the cone, then

$$\begin{bmatrix} x'(t) \\ y'(t) \end{bmatrix} = \begin{bmatrix} \cos(\Phi) & \sin(\Phi) \\ -\sin(\Phi) & \cos(\Phi) \end{bmatrix} \begin{bmatrix} 0 \\ A\sin(\omega t) + A \end{bmatrix}$$

so that $x'(t) = \sin(\Phi)(A\sin(\omega t) + A)$ and $y'(t) = \cos(\Phi)(A\sin(\omega t) + A)$.

With reference to Figure 3.3.12 is can be seen that:

$$\theta(t) = \tan^{-1}\left(\frac{\Delta y'(t)}{x'(t)}\right)$$

Where $\theta(t)$ is the required mirror drive angle at time *t*, *y'las* and *x'las* are the co-ordinates of the laser in the local co-ordinate system (aligned with the cone angle) such that:

$$\Delta y'(t) = y'(t) - y'_{las} \text{ and } x'(t) = x'_{las} + \left(y'_{las} - y'(t)\right)\tan(\Phi).$$

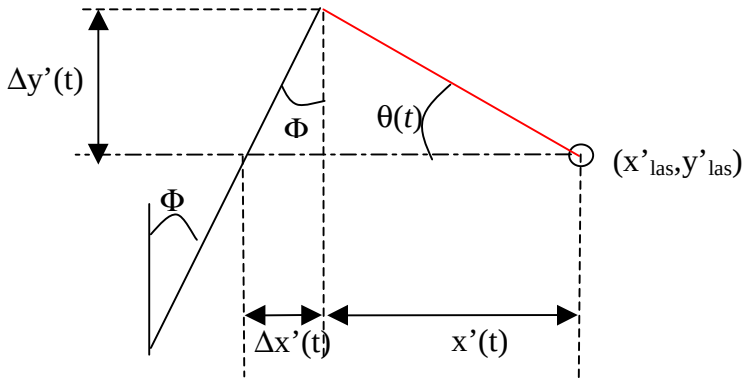

Figure 3.3.12. Geometry for deriving the mirror drive signal θ(*t*).

From which:

$$\theta(t) = \tan^{-1}\left(\frac{y'(t) - y'_{las}}{x'_{las} + (y'_{las} - y'(t))\tan(\Phi)}\right) = \tan^{-1}\left(\frac{1}{\frac{x'_{las}}{(y'_{las} - y'(t))} + \tan(\Phi)}\right) \qquad (3.3.15)$$

Using Equation 3.3.15, and with a knowledge of the cone angle and the point of origin of the LDV beam, it would be possible to synchronise scans from two different points of origin. The simultaneous equation to separate the signals from the two scans into orthogonal components can therefore be written as:

$$V_1(t) = \left(Vx(t)\cos(\theta_1(t)) + Vy(t)\sin(\theta_1(t))\right)\cos(\Phi)$$

$$V_2(t) = \left(Vx(t)\cos(\theta_2(t)) + Vy(t)\sin(\theta_2(t))\right)\cos(\Phi)$$

Where, $V_1(t)$ and $V_2(t)$ are measured velocities from scans conducted from two different heights (y'_{las}), $V_x(t)$ *and* $V_y(t)$ are the velocities resolved into global Cartesian space, from which:

$$Vx(t) = \frac{V_2(t)\sin(\theta_1(t)) - V_2(t)\sin(\theta_2(t))}{\cos(\Phi)\left(\cos(\theta_2(t))\sin(\theta_1(t)) - \cos(\theta_1(t))\sin(\theta_2(t))\right)} \qquad \text{(a)}$$

$$Vy(t) = \frac{V_1(t)}{\cos(\Phi)\sin(\theta_1(t))} - Vx(t)\cot(\theta_1(t)) \qquad \text{(b)}$$

(3.3.16)[7]

A similar derivation is possible for the case the three scans shown in Figure 3.3.10. However, in the case of the third scan, this **cannot** be normal / close to normal to the axis of rotation. Since the LDV measures velocity in line with the beam, the CSLDV

[7] Equations 3.3.16 (a) and (b) need not necessarily be applied to the time domain data as they are equally applicable to the ODS approximation obtained after spectral analysis.

signal will contain a velocity component at the drive frequency of the rotary-stage. Theoretically the presence of this component is not problematic since $\Omega_\theta << \omega$ so its presence does not interfere with the side bands associated with the structure's ODS. In practice, however, the component associated with the rotational velocity will be of much greater amplitude than the vibration amplitudes of the components associated with the ODS, either drowning them out or overloading the LDV's measurement circuitry. This is a problem which is common in vibration measurements on structures rotating at constant angular velocities as noted by Bell and Rothberg [5]. In order to overcome the problem, it would be necessary to cancel or filter out the component of the signal at the rotary-stage drive frequency within the LDV measurement system. Such a facility is not currently available in commercial LDVs and so it was not possible to demonstrate this method in practice.

3.3.3.4 Cylinder scanning test configuration

The structure-under-test was a cylinder 180mm in diameter, 300mm long and 3.4mm thick. The structure was mounted on an aluminium base-plate using 0.35mm thick flexures that were designed to provide a stiffness sufficient to constrain the structure circumferentially while offering minimal restraint in the radial direction (see Figure 3.3.13(c)). The shaker was also attached to the base-plate, inside the structure-under-test, as shown in Figure 3.3.13(b). The shaker was connected to the structure via a force gauge using a push-rod. The cables (to power the shaker, and to transmit the signal from the force gauge) which are visible in Figure 3.3.13(a) were suspended from a laboratory stand so that they were not in contact with the structure when the tests were performed. The structure, base-plate and shaker assembly were connected to a second adapter plate (which was bolted to the rotary-stage) using Anti-Vibration (AV) mounts. These AV mounts were incorporated into the design so that excitation

frequencies above around 50Hz, but much lower than the excitation frequencies required for the structure, were not transmitted into the rotary-stage which may have been damaged by them. The scanning LDV was positioned approximately 2m from the structure and the sinusoidal mirror drive signal amplitude was set such that the scan covered the full height of the cylinder. In the case of the rotary-stage it was not easily possible to obtain a signal output which could be recorded simultaneously with the CSLDV and mirror drive signal. Although the phase shift associated with the mirror drive could be approximated from a simultaneously captured mirror drive signal, an optical probe (visible in Figure 3.3.13(a)) was used to trigger the measurement at (approximately) the centre of oscillation, in an effort to minimise the phase error associated with the circumferential scan . The analysis software used to compute the ODS from the scan, (Stanbridge, [72]), also included the facility to manually alter the applied phase shifts in order to minimise the imaginary part of the resulting ODS.

After all equipment had been set up, the rotary-stage was set to oscillate at 0.3 Hz through $\pm 180^{\circ}$ and the LDV was set to scan at 10Hz. Some experimentation was required to ensure that the oscillation frequency of the stage did not cause unacceptably large angular velocities and accelerations which would trip safety switches in the stage's drive software. It should also be noted that for larger, heavier, structures the maximum available drive torque will impose an upper limit on the maximum oscillation frequency. In a continuous area scanning, the total measurement time is dictated by the lower of the scan frequencies: in this case, the frequency of oscillation of the rotary-stage (0.3 Hz). The frequency spectrum must have sufficient resolution to allow the side band pairs associated with the slower scan

rate to be resolved. For the scanning of the cylinder, this meant a minimum measurement time of 21s. However, in order to take advantage of the noise filtering properties of the ODS extraction software, a measurement time of 30s was used so that ten full scan cycles were completed. For scanning of the cylinder, the combination of a long sample time and high sampling frequencies naturally led to large time-history files, containing a minimum of 30000 samples.

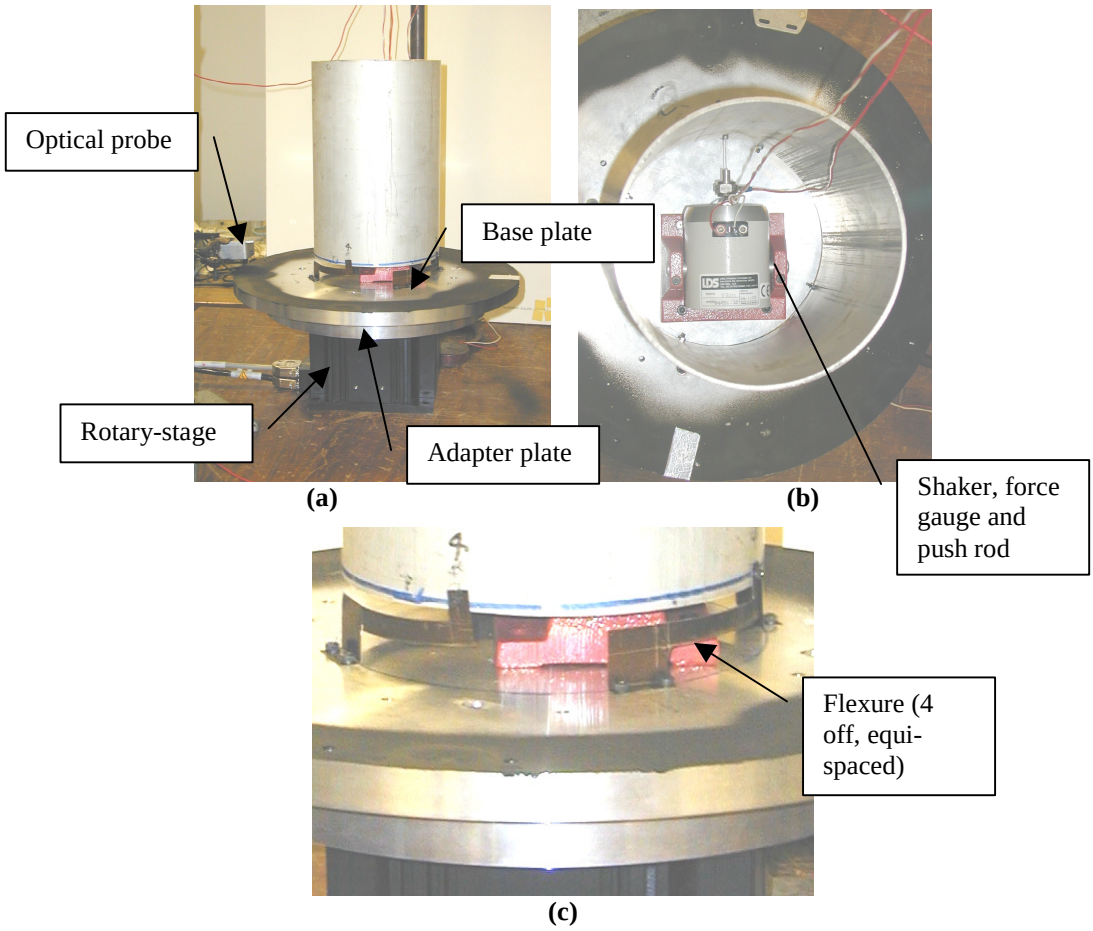

Figure 3.3.13. Test configuration for scanning of a cylinder using the rotary-stage method; (a) over-all configuration; (b) detail of internally mounted shaker; (c) detail of flexures used to constrain the test piece.

3.3.3.5 Alignment of the LDV scan

As was discussed in section 3.3.3.3, misalignment of the LDV with respect to the centre of rotation of the structure will cause the LDV to measure a component of the structure's rotational velocity. Figure 3.3.14(a) shows the signal obtained from the

LDV when it is not aligned with the axis of rotation so that the LDV signal is modulated at 0.3Hz. Also, if the scan is skewed relative to the axis of rotation, then the signal is also modulated at the mirror drive frequency (10 Hz), as shown in Figure 3.3.14(b). By minimising the observed modulation on the signals, the scan can be aligned and even if small signals remain, they are not problematic as the components associated do not interfere with the side-bands of interest and will be ignored when the data is analysed.

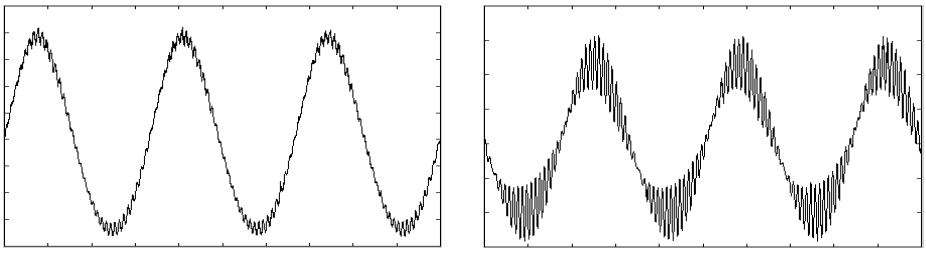

(a) **(b)**

Figure 3.3.14. Modulation of the LDV signal due to misalignment: (a) scan not aligned with the axis of rotation; (b) scan not aligned with axis of rotation and skewed relative to the axis of rotation.

3.3.3.6 Results

Figure 3.3.15 shows a few examples of ODSs obtained from scans on the cylinder. These flat ODS can easily be mapped on to the cylinder's geometry using a Cylindrical to Cartesian co-ordinate transformation, and this allows a qualitative comparison of the scan results with FE results, as shown in Figure 3.3.16.

A second series of tests were also conducted in which two 100g masses were attached inside the structure close to the top and bottom. The masses were offset circumferentially from one another by 35° so that the resulting structure was asymmetric. Continuous scans were then conducted at the new natural frequencies of the cylinder/mass assembly. Examples of the distorted ODSs obtained from these scans are shown in Figure 3.3.17.

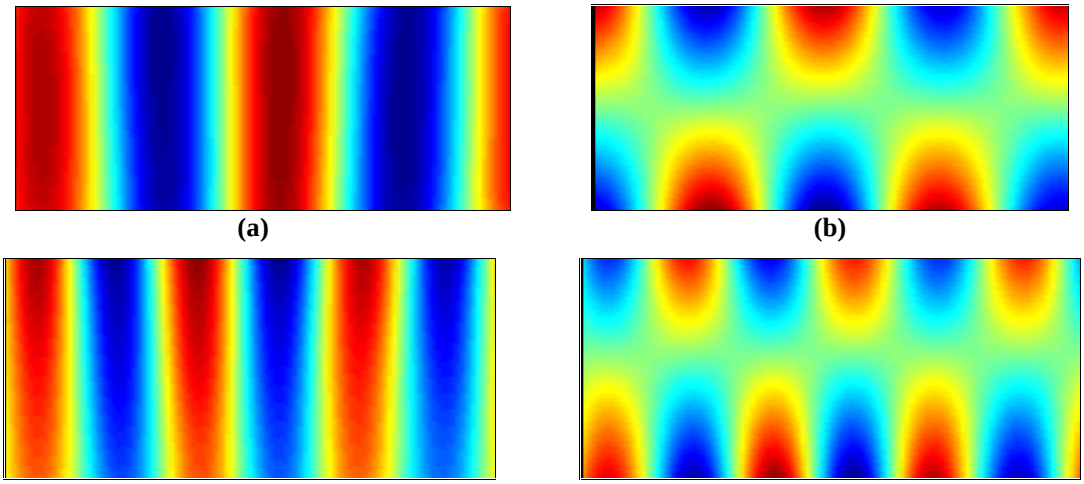

(a) **(b)**

(c) **(d)**

Figure 3.3.15. ODS obtained from CSLDV scanning of a cylinder: (a) (2,0) ODS at 231.1 Hz; (b) (2,1) ODS at 266.0Hz; (c) (3,1) ODS at 646Hz; (d) (3,1) ODS at 701Hz.

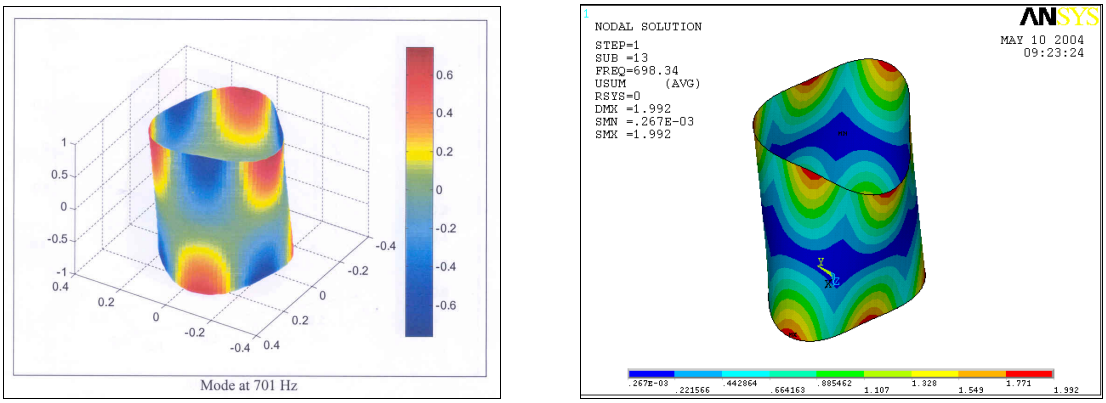

Figure 3.3.16. Qualitative comparison of experimental ODS at 701Hz and FE mode at 698Hz

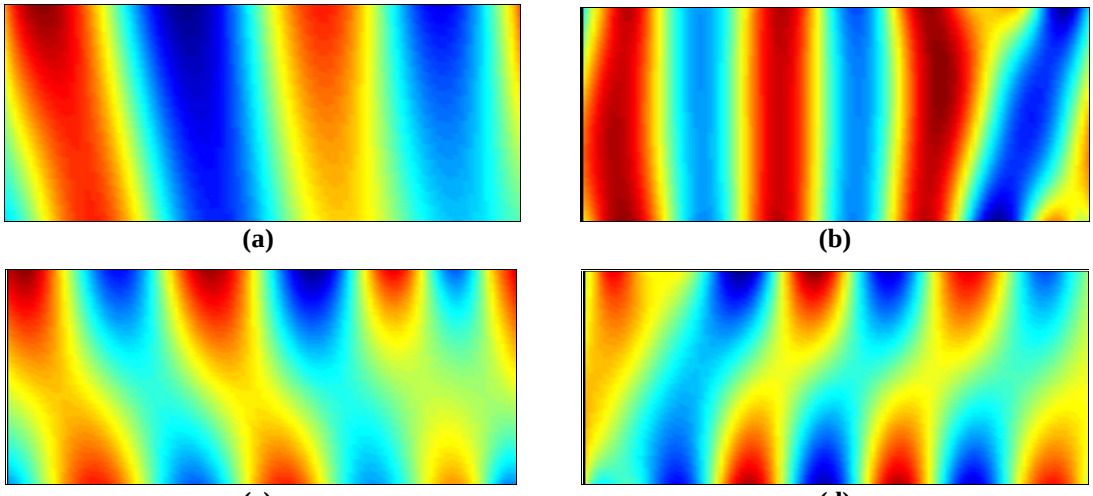

(a) **(b)**

(c) **(d)**

Figure 3.3.17. ODS obtained from scanning of a mis-tuned cylinder: (a) ODS at 211 Hz; (b) ODS at 778 Hz; (c) ODS at 532.4 Hz;(d) ODS at 847 Hz.

3.3.3.7 Discussion

From the results that have been presented above it is clear that the method proposed for the continuous scanning of cylindrical structures works effectively and that it is applicable to structures which are cylindrical but that exhibit non-symmetric ODSs because of mis-tuning caused by non-symmetric internal features. In the case of the light-weight cylinder presented, it was possible to use flexures to support the structure which had a minimal effect on the natural frequencies associated with its radial modes. For larger, heavier structures, however, it will be difficult to design flexures that are capable of withstanding the large circumferential forces generated by the oscillation of the structure. The rotary-stage method is therefore best suited to structures which can be tested in a fixed base configuration. It should also be noted that in the case of heavier structures, the oscillation frequency of the rotary-stage will need to be reduced so that the torque generated does not exceed the maximum available torque for the motor. Since lower oscillation frequencies require greater sample times, the rotary-stage method is likely to generate very large data files for each mode when heavy items are tested.

As the rotary-stage method uses an identical analysis procedure to that used for the scanning of planar structures, theoretically, a full modal analysis of the data would be possible using an identical method to that used by Martarelli, [3]. In order to undertake a full modal analysis it is necessary to complete scans at a few (typically at least 5), closely spaced, discrete excitation frequencies around the resonant frequency of interest. By doing so, it is possible to build up a "side-band FRF" for the mode of interest and each pair of side-bands may be curve-fitted (as they step around resonance) using, for example, the circle-fitting modal parameter extraction routine.

The results of this modal analysis give the natural frequency of the mode, its damping ratio and the modal constant (expressed in terms of a polynomial coefficient) associated with each side-band pair. However, one requirement of this method is that there is adequate frequency spacing between the side-band pairs to enable scans at several different frequencies around the resonance without "overlapping" them. Since the separation between the side bands associated with the circumferential ODS was only 0.3Hz, sweeping round the resonance without overlapping the side-bands was not possible. Also, despite the simplicity of the results shown in Figure 3.3.15, it is important to note that in the circumferential direction there will be as many side-bands as are required to provide a polynomial approximation to the function $\sin(2\pi p\theta)$ where p is the number of nodal diameters. Even for the low order modes of cylindrical structures this requires high-order polynomials[8] and so the extraction of mode shapes would be a time-consuming task.

It is suggested that in the case of lightly damped structures (such as the cylinder presented) the optimum use of the method would be to use scanning to provide a high fidelity image of the structure's ODS for qualitative comparison against FE results (as shown in Figure 3.3.16); and to use single-point modal testing conducted at a few choice locations to provide the natural frequencies, damping ratios, and mode shape data for correlation with the model. This represents an efficient use of the continuous scanning technique since one of the CSLDV method's greatest advantages is that it reveals (in the number of non-trivial side-bands) the order of the modes involved and this information can be used in deciding just how many response points need to be

[8] Theoretically an infinite number of terms are required, although the higher terms diminish into insignificance.

measured. It is also suggested that for high-order modes, exhibiting many side-bands that a series of smaller scans be used to build up the ODS as a series of segments. For example, conducting four scans over $\pm 45°$ degrees will dramatically reduce the side-bands that are required to describe each 90° segment of a cylinder's higher order ODSs. Also, scanning the structure in segments will allow (slightly) higher stage oscillation frequencies thus allowing a lower sample time to be used and also increasing the separation of the side-bands.

3.3.3.8 Conclusions

A method for the scanning of cylindrical / conical structures has been demonstrated. The method presented provides a full-field description of the structure's ODS at resonance but, requires that the structure be attached to a base plate. For this reason, it is best suited to structures which can be tested in a fixed base configuration. The low oscillation frequencies associated with the rotary-stage used make it difficult to complete a full modal analysis and also mean that long sample times must be used. Since the allowable torque of the rotary-stage is a limiting factor on the allowable angular acceleration, the method may be impractical for some heavy items, as very low oscillation frequencies would be required so that the motor was not overloaded. Nonetheless, the method can provide data that can be qualitatively compared to results from FE models (DTA level 2 applications) and may be useful when high spatial density ODSs are required.

3.4 Concluding remarks on the LDV device as a response transducer

The LDV device has been demonstrated as a suitable response transducer for DTA level 3 and 4 applications. The results which can be obtained with such LDV devices are comparable with those which can be obtained with conventional, contacting

accelerometers. Although there can be disadvantages associated with the LOS requirements of the LDV which may require the repositioning of the structure or the LDV, these must be weighed against the completely non-contacting nature of the measurement system. For example, the model-and-remove solution to the mass loading problem, described in Section 3.2.2.2, would certainly have required a longer test time than that required using the LDV, and would have introduced numerous assumptions into the validation process. It has also been demonstrated that the LDV and hammer testing can be used to provide high quality data for the purpose of model validation. The combination of the LDV and impact hammer is suitable for use on many different structures, such as that reported on in the case study of Section 3.2 However the method does rely on the structure under test having sufficiently stiff regions to use as excitation locations and some consideration must be given to the suspension arrangement if high quality data are required.

A method for the continuous scanning of cylindrical structures has also been demonstrated. Although the method requires the structure to be constrained circumferentially (and almost certainly radially, for heavier structures) it has produced the first experimentally derived full-field description of a cylindrical structure's ODS and as such represents a significant advance. The area ODS of the cylinder were measured over the structures full length and circumference in one continuous scan, this would not have been possible with any other existing measurement technique such as holography. The spatial resolution of the ODS is competitive with that of holography, but, the ODS is described succinctly by a 2 dimensional polynomial in a cylindrical co-ordinate system which can easily be mapped onto the structure's geometry.

The angular velocity, acceleration and torque limits on the rotary-stage oscillation frequency mean that relatively long sample times are required and that the side-band structure of the spectrum is closely packed making a modal analysis of the side-band data difficult. The method also leads to a rather inefficient description of the structure's ODS as it uses a polynomial approximation to a sinusoid requiring many coefficients to describe an essentially simple form. However, these two drawbacks are not insurmountable since it is possible to define the ODS as a series of smaller segments. Completing the scan in this way will reduce the number of side-bands and increase the maximum allowable circumferential scan frequency.

It is worth noting that Stanbridge et al, [73], have proposed an alternative method for the scanning of the internal radius of cylindrical structures which leads to a Fourier series description of the ODS in the circumferential direction and a polynomial description in the axial direction. This is achieved using a similar technique set up to the "light-house" scan of Figure 3.3.8, except that the motor and mirror assembly are mounted on a computer-controlled linear actuator, which can be driven sinusoidally. This alternative method for the scanning of cylindrical structures means that only two side-bands are required to describe the radial vibration of the cylinder and does not require the structure to be constrained. The technique has yet to be demonstrated in practice, although the theory for the analysis of the resulting scan is presented in [73].

CHAPTER 4. INDIRECT TESTING

4.1 Introduction

The literature review of Chapter 2 revealed how the main problem with the non-intrusive testing of structures, lay not with the measurement of response data, nor necessarily with the imparting of a force, but with the measurement of the force applied to the structure. The measurement of this force is essential if the modal information extracted from the test data is to be used in an application that requires a quantitative assessment of an FE model's validity. This chapter presents an alternative to completely non-contacting modal testing, indirect modal testing, which has the potential to fill the gap in existing non-intrusive test methods (force measurement) and as such represents the major contribution of this thesis.

Typically, researchers attempting to devise non-intrusive test methods have explored the use of completely non-contact excitation methods. As has been seen from the literature review, with the exception of a few methods such as non-contact magnetic excitation with its limited target types, force measurement is extremely difficult, if not impossible, with these techniques. For this reason, the present chapter considers a different approach to the problem of non-intrusive excitation, indirect excitation. In indirect excitation, the structure of interest is not excited by direct application of a force applied to its surface, but, rather, excitation is applied through an attached test fixture that can be excited using standard excitation techniques. In effect the indirect excitation of a structure is exactly analogous to the case in which information is required on interior components. In this situation, the exterior surfaces on which measurements can be made may simply be considered as an indirect testing fixture.

4.2 The indirect testing method

The indirect testing method is illustrated in Figure 4.2.1. In this example, information is sought on the dynamic behaviour of structure B, but data can only be gathered from measurements made on structure A, which forms part of the assembled structure C. Illustrating the method in this way demonstrates the close relationship between the indirect testing method and substructure coupling problems. This is a relationship that can be exploited in order to provide an alternative, indirect modal testing method suitable for use on delicate and critical structures (such as those discussed in 1.2) to which it is impossible to apply forces directly.

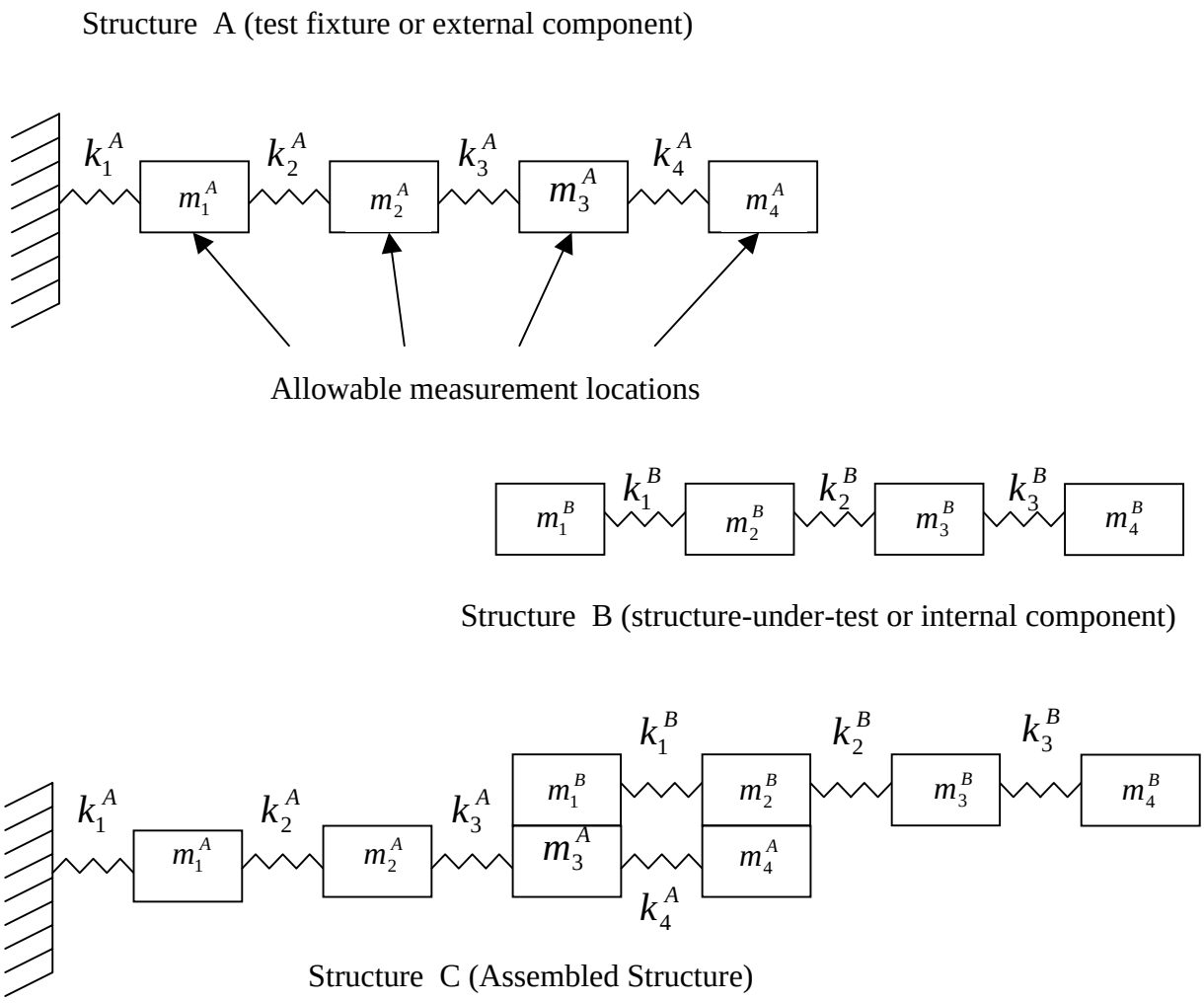

Figure 4.2.1. Illustration of the indirect testing problem

4.3 Substructure Coupling

Research into substructure coupling has been ongoing since the 1960s, and is potentially one of the most useful, although difficult, applications of modal testing. Given the close relationship between indirect testing and substructure coupling it is worth reviewing the development of substructure coupling in each of its guises.

There are three potential methods of substructure coupling, spatial, FRF (also sometimes called “admittance” or “impedance” method) and modal (the most common of which is referred to as Component Mode Synthesis (CMS)).

4.3.1 Spatial sub-structuring

Spatial sub-structuring is the simplest of the methods and is the one most commonly employed within FE models. In spatial sub-structuring the assembled mass and stiffness matrices for structure C, formed by coupling components A and B (see Figure 4.2.1), would be given by Equations 4.3.1 and 4.3.2 respectively. This is not an intuitive representation, however, since the effect on the DOFs not involved in the coupling are not immediately clear.

$$\left[M^{C}\right]=\begin{bmatrix} m_1^A & 0 & 0 & 0 & 0 & 0 \\ 0 & m_2^A & 0 & 0 & 0 & 0 \\ 0 & 0 & m_3^A+m_1^B & 0 & 0 & 0 \\ 0 & 0 & 0 & m_4^A+m_2^B & 0 & 0 \\ 0 & 0 & 0 & 0 & m_3^B & 0 \\ 0 & 0 & 0 & 0 & 0 & m_4^B \end{bmatrix} \quad \textbf{(4.3.1)}$$

$$\left[K^{C}\right]=\begin{bmatrix} k_1^A+k_2^A & -k_2^A & 0 & 0 & 0 & 0 \\ -k_2^A & k_2^A+k_3^A & -k_3^A & 0 & 0 & 0 \\ 0 & -k_3^A & k_3^A+k_4^A+k_1^B & -(k_4^A+k_1^B) & 0 & 0 \\ 0 & 0 & -(k_4^A+k_1^B) & k_4^A+k_1^B+k_2^B & -k_2^B & 0 \\ 0 & 0 & 0 & -k_2^B & k_2^B+k_3^B & -k_3^B \\ 0 & 0 & 0 & 0 & -k_3^B & k_3^B \end{bmatrix} \quad (4.3.2)$$

In any case, the spatial coupling method is of no use to the experimentalist since the matrices [M] and [K] cannot be measured directly. For this reason, the emphasis of most experimental research has been on the FRF and CMS methods of sub-structuring.

4.3.2 FRF sub-structuring

The modern FRF coupling technique stems from the work of Bishop and Johnson [75], who developed a method for predicting the responses of multi-beam assemblies from the response curves of their individual beam elements. Since their pioneering work, there have been major improvements to the response or FRF coupling method. The most significant improvement to the FRF coupling formulation can be attributed to Jetmundsen, Bielawa and Flannelly [76], who reformulated the coupling equation such that only a single matrix inversion was required and that the order of the matrix for inversion was equal to the number of DOFs at the coupling co-ordinates, simultaneously improving both its numerical efficiency and stability. Further refinements were devised by Urgueira [77], who used the SVD and QR Factorisation to pre-determine the number of active coupling DOFs and to select the most suitable of those available for use in the matrix inversion. Jetmundsen, Bielawa and Flannelly's FRF coupling formulation is quoted here as Equation 4.3.3.

$$\begin{bmatrix} H_{aa}^{C} & H_{ac}^{C} & H_{ab}^{C} \\ H_{ca}^{C} & H_{cc}^{C} & H_{cb}^{C} \\ H_{ba}^{C} & H_{bc}^{C} & H_{bb}^{C} \end{bmatrix} = \begin{bmatrix} H_{aa}^{A} & H_{ac}^{A} & 0 \\ H_{ca}^{A} & H_{cc}^{A} & 0 \\ 0 & 0 & H_{bb}^{B} \end{bmatrix} - \begin{bmatrix} H_{ac}^{A} \\ H_{cc}^{A} \\ -H_{bc}^{B} \end{bmatrix} \cdot \left(\left[H_{cc}^{B} \right] + \left[H_{cc}^{A} \right] \right)^{-1} \cdot \begin{bmatrix} H_{ac}^{A} \\ H_{cc}^{A} \\ -H_{bc}^{B} \end{bmatrix}^{T} \qquad (4.3.3)$$

Equation 4.3.3 is the most computationally efficient and numerically stable version of the FRF coupling equation developed to date. The derivation of Equation 4.3.3 is achieved by partitioning the full sub-system FRF matrices for structures A and B ($\lfloor H^A \rfloor$ and $\lfloor H^B \rfloor$) into sub-matrices relating to the "coupling" (denoted by the subscript *c*) and "slave" (denoted by the subscript[9] *a* or *b*) DOFs, such that:

$\lfloor H^A \rfloor = \begin{bmatrix} H^A_{aa} & H^A_{ac} \\ H^A_{ca} & H^A_{cc} \end{bmatrix}$ and $\lfloor H^B \rfloor = \begin{bmatrix} H^B_{bb} & H^B_{bc} \\ H^B_{cb} & H^B_{cc} \end{bmatrix}$. The FRF sub-structuring process is illustrated schematically in Figure 4.3.1.

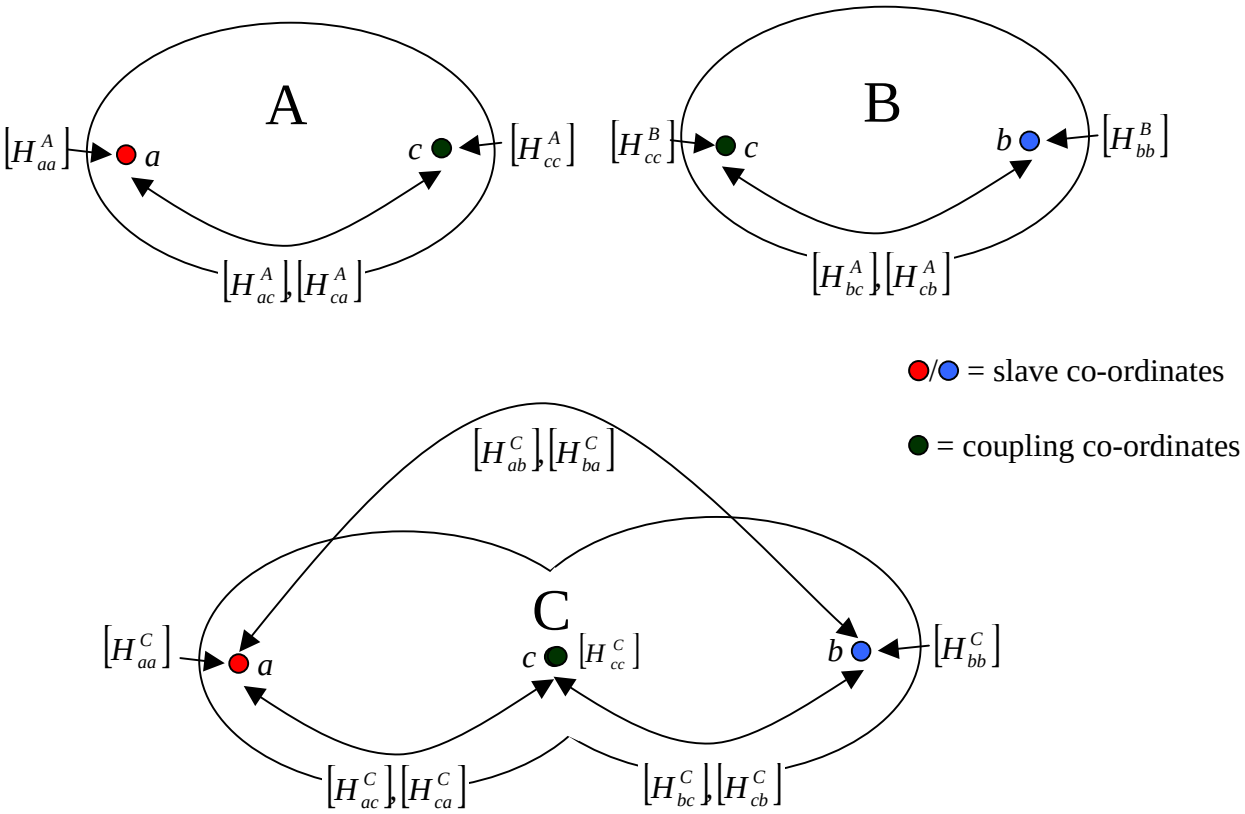

Figure 4.3.1. Schematic representation of the FRF coupling process.

[9] Depending upon which of the two subsystems the slave DOF is located.

4.3.3 CMS sub-structuring

The CMS method was originally developed for use in FE modelling at a time when creating large structural assembly models was difficult due to limitations in computing power. Even today, the CMS method is still incorporated in FE codes such as ANSYS [78], partly for this purpose, and partly as a means to allow experimentally derived structural models to be incorporated into FE calculations.

The method employs a transformation of the equations of motion into a modal co-ordinate system leading to Equation 4.3.4:

$$[I]\begin{Bmatrix}\ddot{p}_A\\ \ddot{p}_B\end{Bmatrix}+\left(\begin{bmatrix}\Phi_A^T & 0\\ 0 & \Phi_B^T\end{bmatrix}[K_{cc}]\begin{bmatrix}\Phi_A & 0\\ 0 & \Phi_B\end{bmatrix}+\begin{bmatrix}\omega_A^2 & 0\\ 0 & \omega_B^2\end{bmatrix}\right)\begin{Bmatrix}p_A\\ p_B\end{Bmatrix}=\{0\} \qquad (4.3.4)$$

In which $[\Phi_A^T]$ and $[\Phi_B^T]$ are the free-interface mode shapes of the interface DOFs and $[K_{cc}]$ is the connection stiffness matrix, which is usually used to account for the residual flexibility of the sub-structures at the connection DOFs (see Equations 4.3.5-4.3.7). The natural frequencies and mode shapes of the coupled system are given by the eigensolution of Equation 4.3.6. Strictly, all modes of the sub-systems must be included for the solution to be correct. However, this is rarely possible when experimentally-derived models are used, since the structures will always be tested to some finite frequency limit, which will almost certainly not encompass all of the structure's modes. In FE codes the problems associated with truncation of the modal database to a few free-interface modes, can be overcome by augmenting the limited information they provide with an additional set of modes, typically the "fixed interface" or "constraint modes". These modes are derived by sequentially grounding

each of the coupling DOFs one at a time, a trivial task in the theoretical model, but a major, and practically impossible, one in the real world. For experimental data, the truncation problem is usually overcome by including estimates of the residual flexibility terms, which are used to derive the connection stiffness matrix $[K_{cc}]$ as follows:

$$[R_A] = [\phi_{ce}^A][\omega_{re}^A][\phi_{ce}^A]^T \quad \text{and} \quad [R_B] = [\phi_{ce}^B][\omega_{re}^B][\phi_{ce}^B]^T \qquad 4.3.5$$

$$[R_{cc}] = ([R_A] + [R_B]) \qquad 4.3.6$$

$$[K_{cc}] = \begin{bmatrix} [R_{cc}]^{-1} & -[R_{cc}]^{-1} \\ -[R_{cc}]^{-1} & [R_{cc}]^{-1} \end{bmatrix} \qquad 4.3.7$$

It should also be noted here, that the CMS method was originally derived as an approach intended for use on theoretical models in which there is no damping and therefore no possibility of complex modes and this can limit its applicability to experimental data. Modifications to the basic theory to deal with these real-world phenomena are possible, but complicate the process and according to Ewins, op. cit., the successful implementation of such extensions is "not universally achieved".

4.3.4 Two common problems

While discussing experimental methods for sub-structuring it is worth mentioning two (closely-related) problems, which make sub-structuring one of the most demanding applications for modal test data. It has already been mentioned that the FRF coupling method requires the **full** FRF matrix for the DOFs involved in the coupling and, by definition, this matrix includes information on both the translational and rotational

DOFs. In fact, potentially seventy five percent of this matrix will be made up of FRFs that require either moment excitation to be imparted, rotational responses to be measured or a combination of both. The FRFs relating to these RDOFs are not easily acquired experimentally.

The measurement of rotational responses is generally considered to be the easier part of this problem, but it must be borne in mind that even this task is considerably more difficult than acquiring translational FRFs. The complexity of measuring rotational responses is primarily due to the way in which they are usually derived, by differencing two translational measurements. Typically, at low frequencies, the contribution of the rotational DOFs is small, around 1-2% of the translational component [1]. Since translational transducers, such as accelerometers typically have a cross axis sensitivity of around the same order, differencing the signals from two may entail an error in the order of 100% and, in fact, may simply provide a measure of the differences between the two transducers. Nonetheless, success has been reported using this technique,[62] and [88]: Stanbridge and Ewins [10] have demonstrated the possibility of measuring rotational responses using a circular scanning LDV, although, the technique requires single-frequency sinusoidal excitation and this limits its use in FRF coupling for reasons to be discussed shortly. The more complex problem of imparting moment excitation has also been the subject of much research, with Tretheway [79], amongst others, reporting the development of pure moment exciters, although these are still very much in the experimental design phase. The most common approach is to use a rigid block attachment [62], and as was mentioned in the literature review, the most advanced applications of this method are in themselves a form of indirect measurement.

The second problem, which is often cited in work on sub-structuring, is the so-called "residual problem". This problem is associated with the truncation of FRF measurements to the limited frequency range that is used for the test. It is possible to regenerate an FRF from modal information extracted from FRF measurements that form a single row or column of the response matrix [80], under the condition that information about **all** of the modes is included. However, since the observed frequency range is unlikely to encompass all of a structure's modes, the lack of information concerning the out-of-range modes leads to an error - the "residual error",- in the synthesised response curves. At present, it is not possible to compensate for this error unless an FRF measurement has been made, in which case additional terms may be calculated from the discrepancy between the measured data and the synthesised curve and these terms can be included in the FRF summation, Ewins, op. cit. These will often take the form of additional modal mass and stiffness terms, or -more commonly nowadays- pseudo-mode approximations, [69]. In practice, the residual problem means that the full FRF matrix must be measured at every frequency of interest, a fact that would make the use of any single-frequency excitation method of rotational response measurement extremely arduous for coupling applications. Furthermore, the residual problem means that the difficult moment-excitation-input/ angular-response-output FRFs **must** be measured if physically meaningful results are to be obtained from the coupling calculation. This applies to both the CMS and the FRF coupling techniques.

Having discussed the available methods for the addition of one or more structures, it is possible to examine the process of subtraction (or uncoupling) that offers a potential method for the indirect testing of structures.

4.4 Uncoupling as a method for the indirect testing of structures

4.4.1 Development of an FRF uncoupling analysis

To begin with, the FRF route to an indirect testing method will be considered here since this can utilise the data obtained from a modal test directly. However, before commencing this discussion it is worth noting the equivalence that exists between all three of the descriptions of the system (spatial, response, modal), assuming that information on all modes and DOFs is present, that is:

$$[H(\omega)] = \left([K] - \omega^2[M]\right)^{-1} = [\Theta]^T \left([\omega_r^2] - \omega^2\right)[\Theta] \qquad (4.4.1)$$

The equivalence of the three different models stems from the fact that they are only different representations of the same information and, because of this, a solution to the indirect testing problem using one of the methods will have a direct equivalent in the other two. Most importantly, though, an advantage or problem which exists within one representation will also exist in the other two, although it may manifest itself in a different way.

Maia et al [66] have explored the use of FRF uncoupling as a means of deriving information on joints. Previously they had examined the use of simple uncoupling formulations as a means of removing the mass loading effects caused by transducers and had also developed the Mass Uncoupling Method (MUM) [86]. Using the MUM approach it was demonstrated that the complete translational FRF matrix (including

residuals) could be calculated from measurements of a single row or column of the FRF matrix using an additive mass. Their earlier work on removing mass loading effects and the MUM technique essentially required only relatively simple SDOF techniques. For their later work on the properties of joints however, they exploited a feature of the FRF coupling Equation of 4.3.3. using the following derivation[10]:

-by considering only the upper-left corner of the coupled system FRF matrix in this equation, we may write

$$\left[H_{aa}^{C}\right]=\left[H_{aa}^{A}\right]-\left[H_{ac}^{A}\right]\left(\left[H_{cc}^{B}\right]+\left[H_{cc}^{A}\right]\right)^{-1}\left[H_{ca}^{A}\right] \qquad (4.4.2)$$

so that

$$\left[H_{aa}^{A}\right]-\left[H_{aa}^{C}\right]=\left[H_{ac}^{A}\right]\left(\left[H_{cc}^{B}\right]+\left[H_{cc}^{A}\right]\right)^{-1}\left[H_{ca}^{A}\right] \qquad (4.4.3)$$

and, by pre and post multiplication:

$$\left[H_{ac}^{A}\right]^{-1}\left(\left[H_{aa}^{A}\right]-\left[H_{aa}^{C}\right]\right)\left[H_{ca}^{A}\right]^{-1}=\left(\left[H_{cc}^{B}\right]+\left[H_{cc}^{A}\right]\right)^{-1} \qquad (4.4.4)$$

On taking the inverse, we have

$$\left[H_{ca}^{A}\right]\left(\left[H_{aa}^{A}\right]-\left[H_{aa}^{C}\right]\right)^{-1}\left[H_{ac}^{A}\right]=\left[H_{cc}^{B}\right]+\left[H_{cc}^{A}\right] \qquad (4.4.5)$$

Finally, subtraction yields

$$\left[H_{cc}^{B}\right]=\left[H_{ca}^{A}\right]\left(\left[H_{aa}^{A}\right]-\left[H_{aa}^{C}\right]\right)^{-1}\left[H_{ac}^{A}\right]-\left[H_{cc}^{A}\right] \qquad (4.4.6)$$

---

[10] It is worth noting the synergy between Maia et al's research [76] and that of McConnell et al [74] since the equations they develop are identical.

Equation 4.4.6 implies that the FRF matrix of structure B at its connection DOFs, $\left[H_{cc}^{B}\right]$, may be inferred from measurements made on DOFs which are remote from the connection DOFs of the coupled structure. Furthermore, these remote DOFs could all be located on structure A and, as such, Equation 4.4.6 provides the underpinning equation for the indirect testing of structures.

In their work neither Maia et al, [66], or Dong and McConnell, [74], had any requirement for the FRF matrix relating excitation at the connection DOFs to responses at DOFs on structure B $\left[H_{cb}^{B}\right]$. Obtaining this matrix (or a single row or column of it) allows a modal analysis of the data to be performed which, in theory, will provide the free-free modes of structure B. The derivation of this matrix begins by considering only the lower left hand corner of the coupled system FRF matrix given by Equation 4.3.3:

$$\left[H_{ba}^{C}\right]=\left[H_{bc}^{B}\right]\left(\left[H_{cc}^{B}\right]+\left[H_{cc}^{A}\right]\right)^{-1}\left[H_{ca}^{A}\right] \tag{4.4.7}$$

from which

$$\left[H_{bc}^{B}\right]^{-1}\left[H_{ba}^{C}\right]\left[H_{ca}^{A}\right]^{-1}=\left(\left[H_{cc}^{B}\right]+\left[H_{cc}^{A}\right]\right)^{-1} \tag{4.4.8}$$

thus,

$$\left[H_{bc}^{B}\right]^{-1}=\left(\left[H_{cc}^{B}\right]+\left[H_{cc}^{A}\right]\right)^{-1}\left[H_{ba}^{C}\right]^{-1}\left[H_{ca}^{A}\right] \tag{4.4.9}$$

and on taking the inverse of (4.49), we have;

$$\left[H_{bc}^{B}\right]=\left[H_{ba}^{C}\right]\left[H_{ca}^{A}\right]^{-1}\left(\left[H_{cc}^{B}\right]+\left[H_{cc}^{A}\right]\right) \tag{4.4.10}$$

Together, Equations 4.4.6 and 4.4.10 provide a means of obtaining the free-free FRFs of a structure, based upon excitation on an attached test fixture or other (perhaps more robust) component within an assembly. In the case of internal components, only the auto-FRF matrix, $\left[H_{cc}^{B}\right]$, of the structure of interest at its connection points can be obtained and the extracted mode shape information may be limited to a few spatial co-ordinates. For components that can have response measurements made on them, using an LDV for example, it may be possible to obtain spatially well-defined mode shapes.

4.4.2 Further refinements

One important feature of Equation 4.4.6 is that the matrices inside the bracketed expression may be formed using any desired set of DOFs and therefore may be composed entirely of translational FRFs. This feature can be used to eliminate the need to impart moment excitation to the structure (as long as reciprocity can be assumed). This is beneficial both from a practical standpoint (since it is difficult to impart moment excitation) and because the numerical stability of the matrices involved can be improved by the omission of rotational data. This is because there is typically an order of magnitude of difference between the elements in the matrices which relate to rotations and translations (they have different units) and this can cause numerical ill-conditioning. The issue of exactly which DOFs should be used is discussed in more detail shortly. Also, it emerges that it is possible to populate the equation with more remote measurement DOFs than there are connection DOFs since:

$$\left[H_{cc}^{B}\right]_{nc\times nc} = \left[H_{ca}^{A}\right]_{nc\times na}\left(\left[H_{aa}^{A}\right]-\left[H_{aa}^{C}\right]\right)_{na\times na}^{-1}\left[H_{ac}^{A}\right]_{na\times nc}-\left[H_{cc}^{A}\right]_{nc\times nc} \qquad (4.4.11)$$

Where *nc* and *na* are the numbers of connection DOFs and remote DOFs, respectively. It may therefore be possible to exploit the over-determination implied

by Equation 4.4.11 in order to average out the effects of noise and other random perturbations.

A second useful feature of Equation 4.4.6 is that we may write:

$\left[H_{ca}^{A}\right]\left(\left[H_{aa}^{A}\right]-\left[H_{aa}^{C}\right]\right)^{-1}\left[H_{ac}^{A}\right]=\left[T\right]$ where $\left[T\right]$ is the coupled system matrix.

Therefore any individual element of the matrix $\left[H_{cc}^{B}\right]$ can be given by

$H_{jk}^{B}=T_{jk}-H_{jk}^{A}$. This means that it is not necessary to measure the full auto-FRF matrix of structure A at the connection points $\left[H_{cc}^{A}\right]$, but only to include a few (or indeed one) of the terms from its leading diagonal to allow the mass-normalisation of any resulting mode shapes. It is also worth noting that any element of $\left[T\right]$ will be given by:

$$T_{jk}(\omega)=\sum_{r=1}^{N^{A}}\frac{\phi_{jr}^{A}\phi_{kr}^{A}}{\omega_{r}^{2}-\omega+iD_{r}^{A}}+\sum_{r=1}^{N^{B}}\frac{\phi_{jr}^{B}\phi_{kr}^{B}}{\omega_{r}^{2}-\omega+iD_{r}^{B}} \qquad (4.4.12)$$

Thus, if the modes associated with the indirect testing fixture and test structure are easily distinguished from one another, it will be possible to mass-normalise the mode-shapes without measuring any elements of $\left[H_{cc}^{A}\right]$ at all.

It is also possible to substitute the matrix [*T*] into Equation 4.4.10 which yields

$$\left[H_{bc}^{B}\right]=\left[H_{ba}^{C}\right]\left[H_{ca}^{A}\right]^{-1}\left[T\right] \qquad (4.4.13)$$

from which it is clear that we need only measure a single row (or column) of the matrix $\left[H_{ba}^{C}\right]$. Once again, this means that there is no need to measure rotational responses (unless they are specifically required). Instead, for every additional DOF

which is to be included, excitation must be applied to each of the remote testing DOFs.

4.4.3 On the practical implementation of the uncoupling equations

Two advantages to the practical implementation of the indirect testing formulae have already been mentioned, namely that:

1) point rotational measurements are not required, as long as it is reasonable to assume reciprocity and also;
2) the full auto-FRF matrix for the connection DOFs of structure A need not be measured.

In addition to these advantages, there are a number of other features that may be used to the test engineer's advantage. First, if indirect excitation is to be used to perform a modal test on a structure, then the design of the test fixture is under the control of the test engineer. This means that the order of the matrices involved in the calculation can be controlled and limited which is beneficial in terms of the numerical stability of the calculations. Secondly, the test engineer also determines the choice of remote DOFs and, to a more limited extent, the choice of the coupling DOFs, so that these may be selected in a way that optimises the condition of the matrices involved. These features of uncoupling are explored in more depth in the numerical example that follows.

4.5 Numerical example

4.5.1 Purpose of the numerical tests

In order to investigate the principles of uncoupling as a possible route to the indirect testing of structures, the theory discussed in section 4.4 was applied to the simple frame structures shown in Figure 4.5.1. The objectives of the simulated tests were

threefold. The first was to determine whether acquisition of point rotations could be avoided as the theory implies; the second was to investigate if the selection of the remote excitation DOFs and the possibility of over-determination affected the results of the calculation in any way and; the third was to examine whether the formulae were robust enough to deal with noise on the FRF data. The overall aim of the tests was to determine the FRF matrix for the connection DOFs of structure B from remote measurements made on structures A and C.

4.5.2 Model data for the structures

All of the frames were modelled in ANSYS using Beam3 elements, having one rotational and two translational DOFs. All of the beam elements used had a 20×20mm cross section. The beams were modelled in aluminium, having the following material properties: Young's Modulus = 69 GN/m^2; Density = 2710 kg/ m^3, Poisson's Ratio = 0.33. Structures A and C were both constrained to be grounded at all DOFs at the base of the legs, while structure B was modelled as free-free. Structure C was composed of structure A, with structure B attached at nodes 7 and 12 (a 6 DOF attachment). Structures A, B and C had 48, 42 and 84 DOFs respectively.

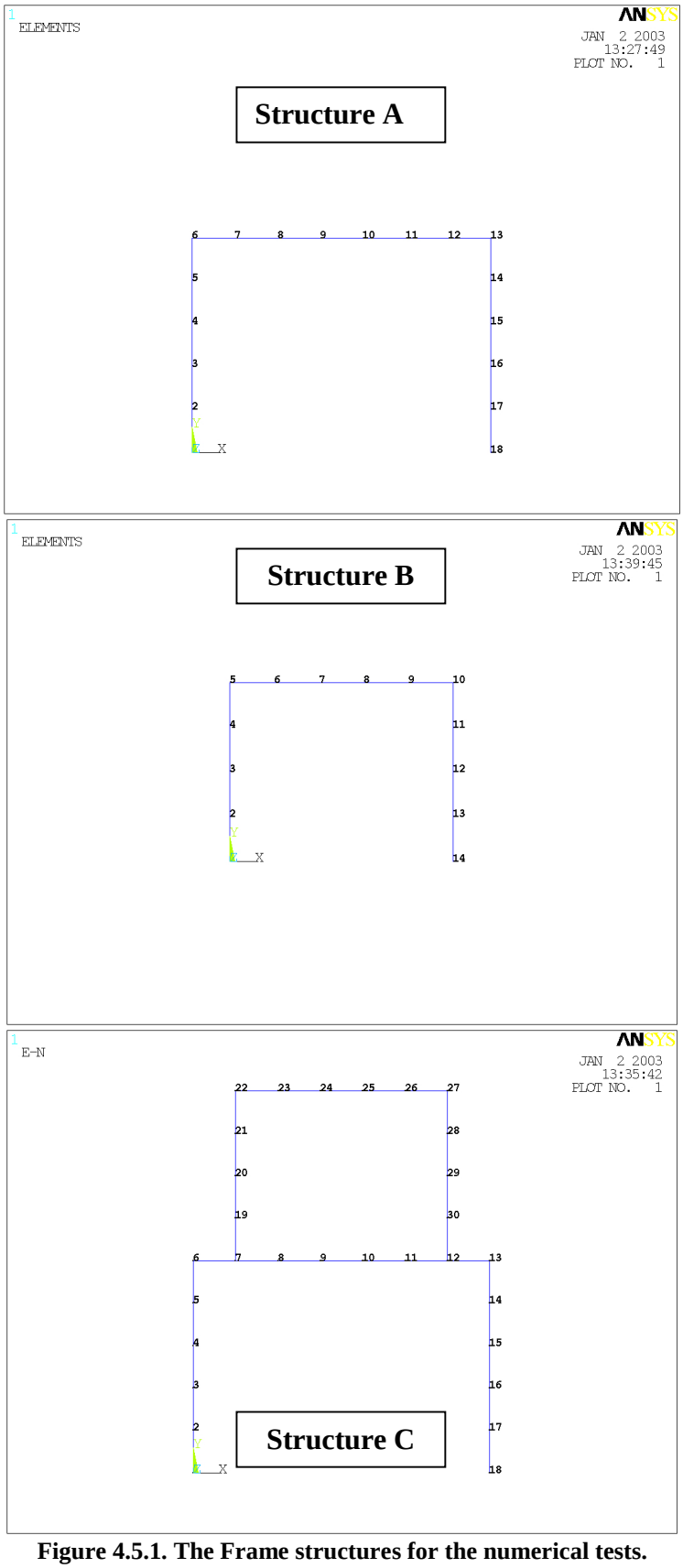

Figure 4.5.1. The Frame structures for the numerical tests.

4.5.3 Investigation into the selection of remote DOFs and the omission of Point RDOF measurements

In the first set of (numerical) tests, three remote nodes on structure A were arbitrarily selected. The results of a modal analysis encompassing all of the modes of structure A were then used to generate the translational FRF matrices associated with those nodes, ($[H_{aa}^{A}]$, $[H_{ac}^{A}]$, $[H_{ca}^{A}]$), in addition to the FRF matrix of the connection DOFs, ($[H_{cc}^{A}]$), which included both the translational and rotational DOFs. The same remote nodes were used for the generation of the relevant FRF matrix for structure C, ($[H_{aa}^{C}]$), which included only translational DOFs. The full FRF matrix for the connection DOFs of structure B (alone) ($[H_{cc}^{B}]$) was also generated in the same manner.

In order to ensure that the matrix $[H_{aa}^{C}]$ had been accurately calculated, the individual FRFs it contained were checked against FRFs calculated using Equation 4.5.1

$$[H_{aa}^{C}]_{check} = [H_{aa}^{A}] - [H_{ac}^{A}]([H_{cc}^{B}] + [H_{cc}^{A}])^{-1}[H_{ca}^{A}] \qquad (4.5.1)$$

After checking that the matrices were accurately calculated, the relevant data were then used as inputs to the uncoupling equation (Equation 4.4.6).

4.5.4 Results

Three example results are given (Figures 4.5.3, 4.5.4 and 4.5.5) for the three different node sets shown in Figure 4.5.2. Although the results shown represent only a tiny fraction of the possible ways in which 6DOFs can be chosen from the 28 DOFs[11]

[11] Only 28 DOFs are available if all the rotations and coupling DOFs are excluded.

available, they do illustrate how the calculated results can vary depending upon the selection of remote DOFs, a feature also noted by Maia et al (2000), op. cit, in their study on the properties of joints.

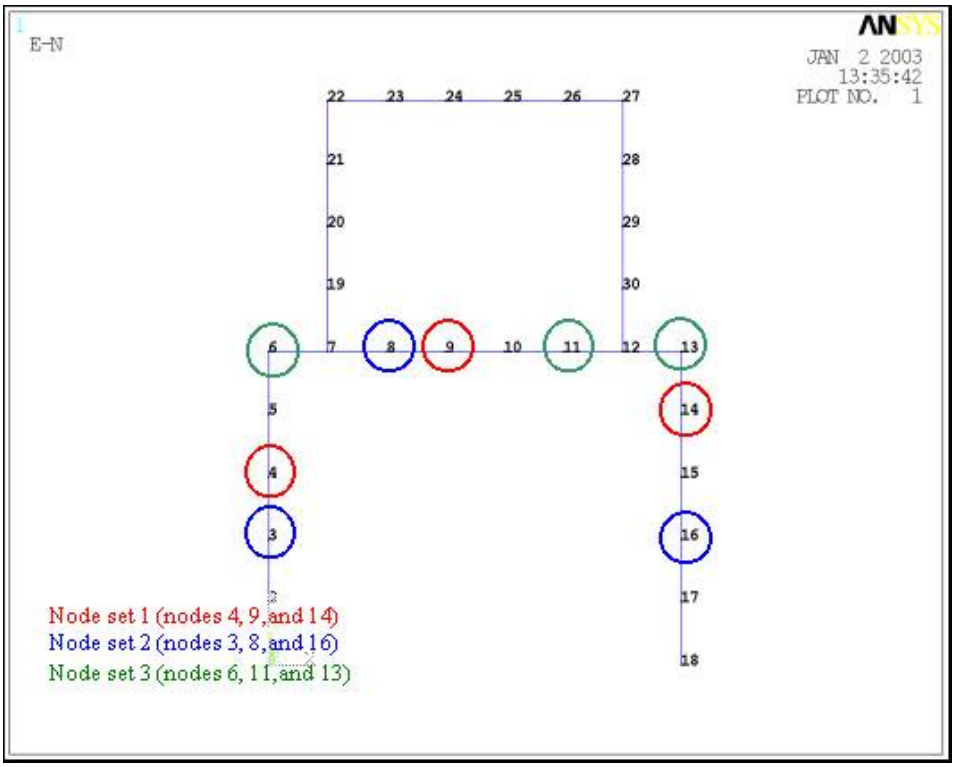

Figure 4.5.2. Nodes used in node sets 1, 2 and 3.

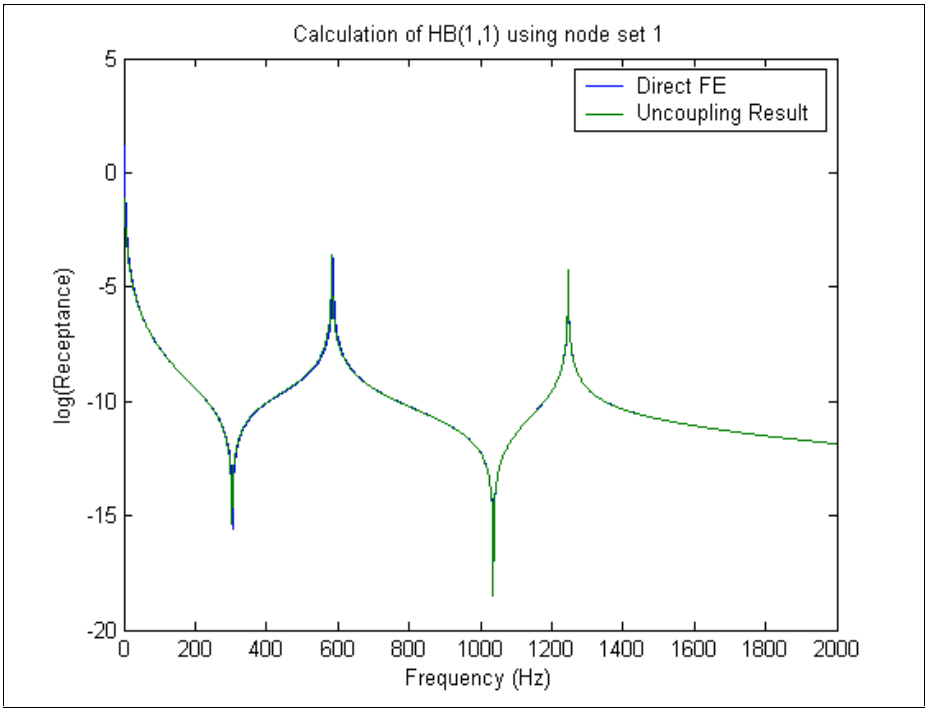

Figure 4.5.3. The result of the uncoupling calculation using node set 1.

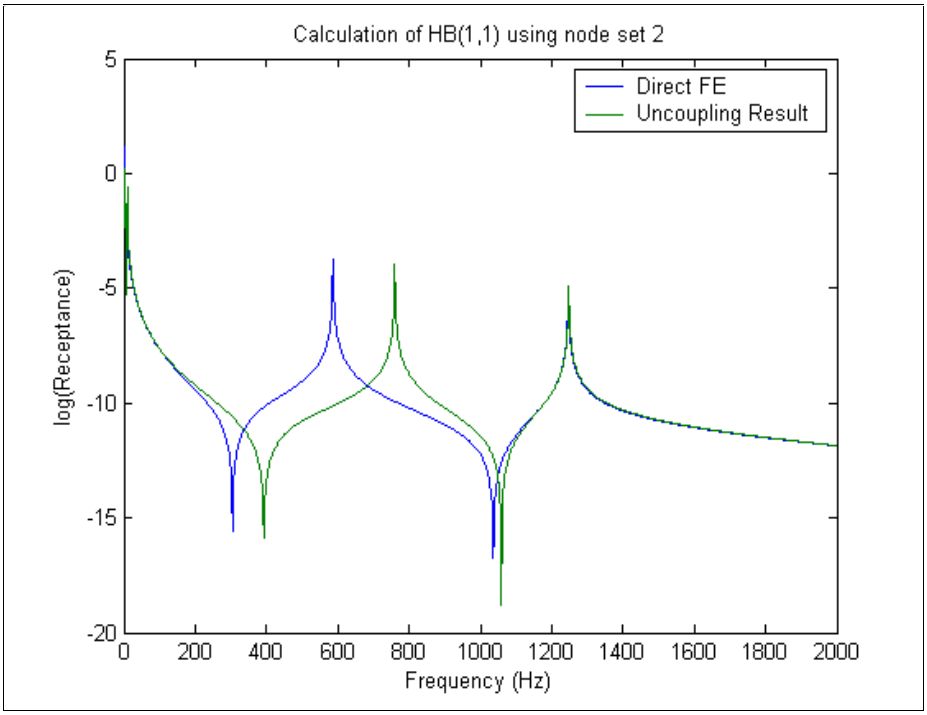

Figure 4.5.4. The result of the uncoupling calculation using node set 2.

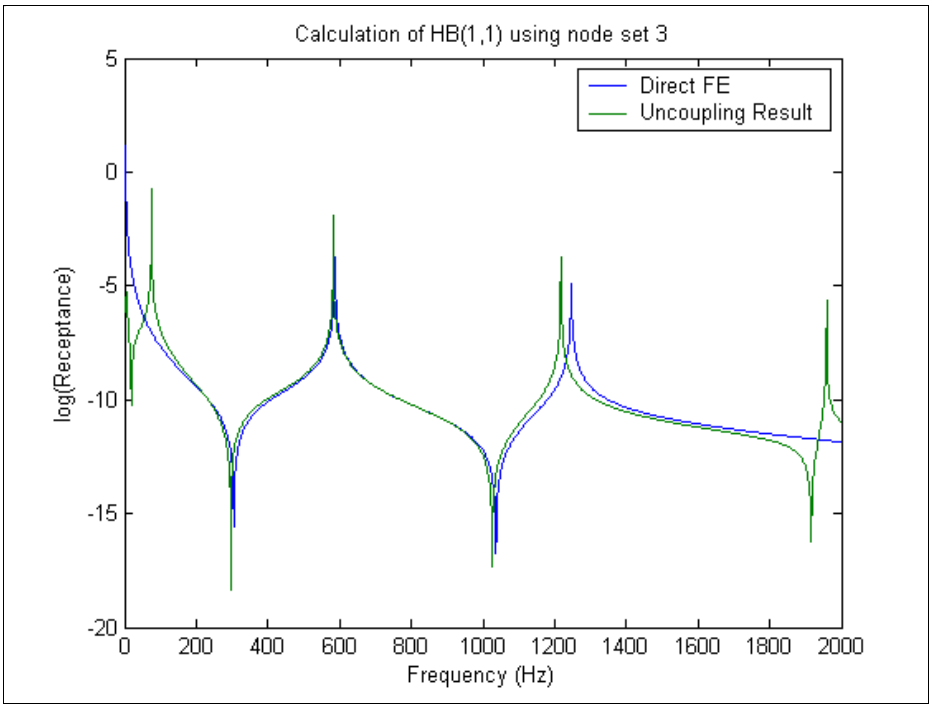

Figure 4.5.5. The result of the uncoupling calculation using node set 3.

In addition a fourth node set was constructed, which added an extra remote point to node set 2 as shown in Figure 4.5.6. Node set 2 was augmented since it provided a very poor estimation of the transfer function. The addition of the extra translational

DOFs associated with this point to the calculation produced the much-improved transfer function estimate shown in Figure 4.5.7.

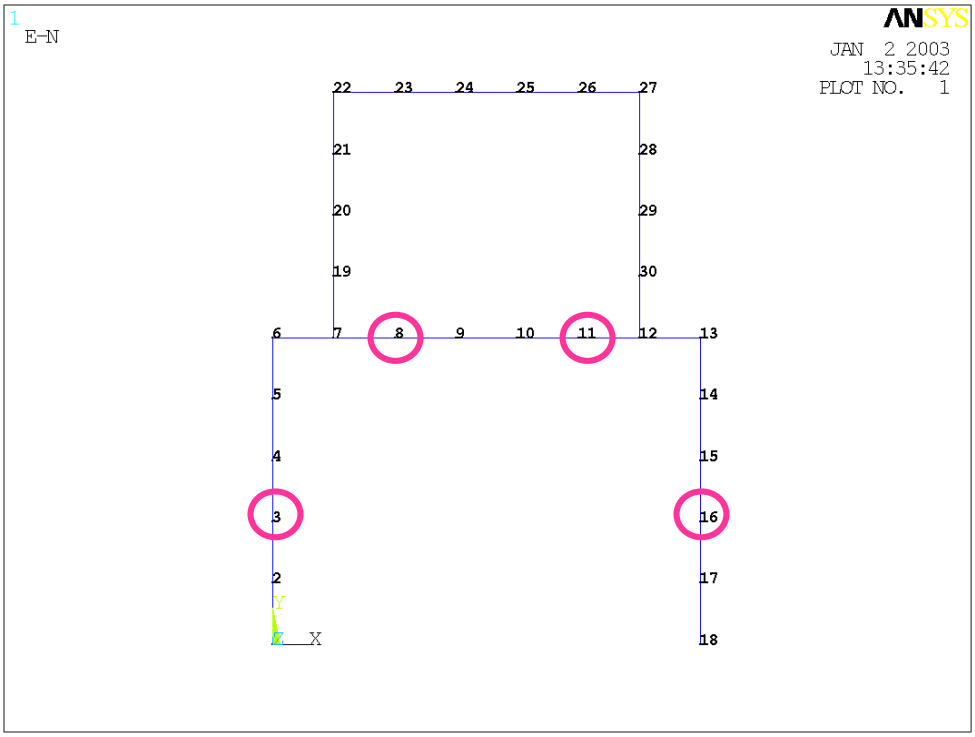

Figure 4.5.6. Fourth node set, incorporating an additional point, so to provide an over-determined set of FRFs for use in the uncoupling equation.

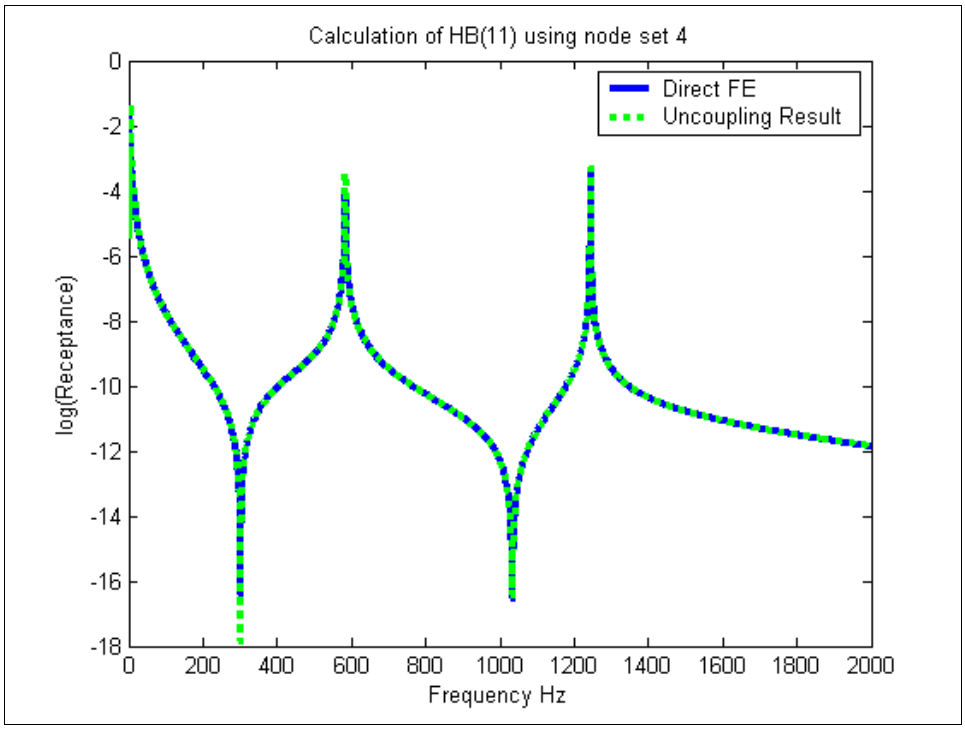

Figure 4.5.7. The result of the uncoupling calculation using the over-determined node set 4.

4.5.5 Investigation of the effects of noise on the indirect testing calculation

The FRF matrices involved in the indirect testing calculation were next contaminated with artificial noise. The noise was added by computing the inverse FFT of the FRFs and determining the peak values of the resulting time histories. A percentage of the peak value was then used to multiply a vector containing randomly generated numbers from a uniform distribution over the interval 0-1. This noise vector was then added to the time history vector. The noisy FRFs were then obtained by computing the FFT of the contaminated time history. Figure 4.5.8 shows an example of a noisy FRF generated by this method.

The noisy FRFs generated for the over-determined node set 3 (which had been identified as giving the best results so far) were then used in the uncoupling calculation. An example result for just 1% noise is shown in Figure 4.5.9. From this result it was clear that even small amounts of contamination had a catastrophic effect upon the result of the uncoupling equation. Interestingly, when the same amount of noise was applied to matrices involved in the coupling equation (Equation 4.5.1), the effect was not as severe, as illustrated by Figure 4.5.10.

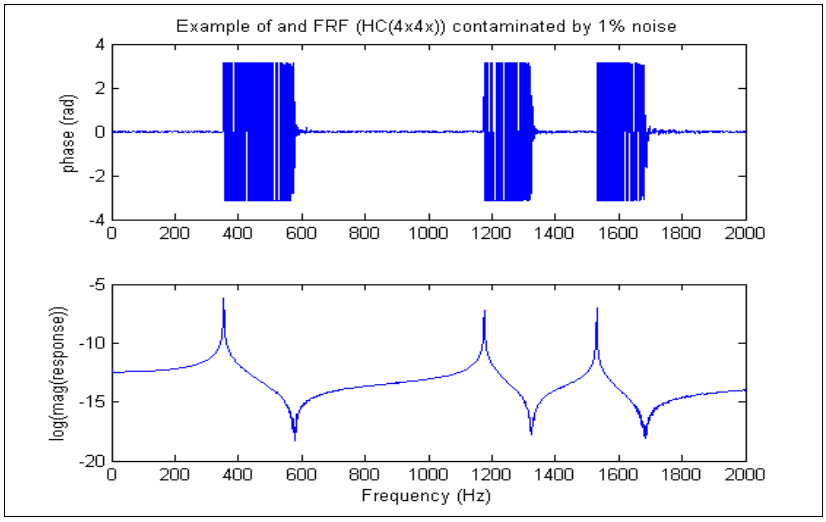

Figure 4.5.8. Example of an FRF contaminated by 1% "peak" noise.

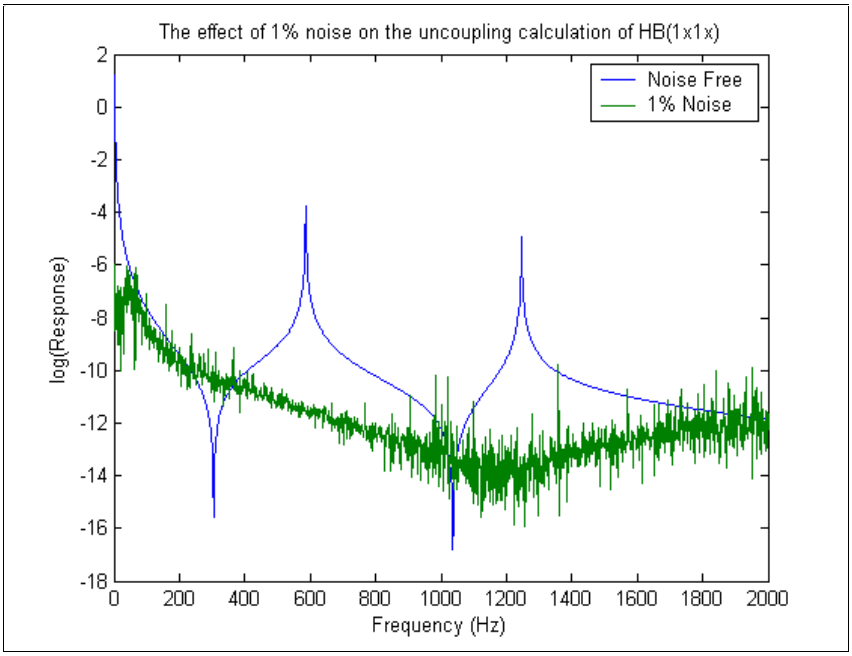

Figure 4.5.9. The effect of 1% "peak" noise on the uncoupling calculation.

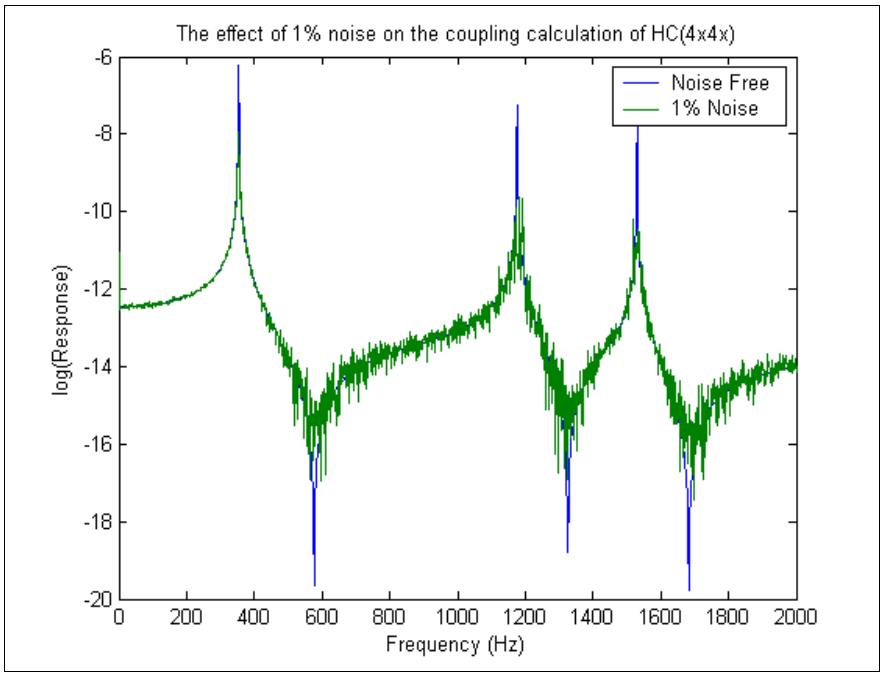

Figure 4.5.10. The effect of 1% "peak" noise on the coupling calculation

4.5.6 Discussion

The numerical example has shown that it is not necessary to include point rotation FRFs in the FRF matrices $\left[H_{aa}^{A}\right]$and $\left[H_{aa}^{C}\right]$ as implied by the theory (Section 4.4.2), however, it is clear from the results of the numerical tests that the uncoupling

equation is extremely sensitive to both the selection of the remote DOFs and to noise on the data set. Maia et al (2000), op. cit., had also noted these sensitivity problems but had not discussed their causes in any great detail. Figure 4.5.9 and Figure 4.5.10 demonstrate that the uncoupling problem can be considerably more sensitive to noise than the equivalent coupling calculation, which employs a notoriously sensitive formula as discussed in [77], for example. If indirect testing fixtures are to be successfully designed it is important that the reasons for the calculation's sensitivity problems are understood.

Sensitivity to small perturbations can be attributed to ill-conditioning of the matrices for inversion. Both truncation of numbers to a limited number of decimal places and noise can be regarded as perturbations on a matrix. The condition number with respect to inversion (γ) is defined as the ratio of the highest singular value of a matrix to the lowest, high condition numbers being associated with matrices that will behave erratically on inversion. Plotting this value (Figure 4.5.11) for the matrices associated with the four node sets used in previous examples (and which need to be inverted) reveals that they are all poorly conditioned. In fact, with the exception of node set one's behaviour at high frequency, each has a condition number in excess of 10000 across the entire frequency range. These high condition numbers help to explain the calculation's sensitivity to small perturbations. Furthermore, the fact that the selection of the remote DOFs influences the condition of the problem hints that at least part of the cause of the ill-conditioning can be attributed to physical as opposed to numerical effects.

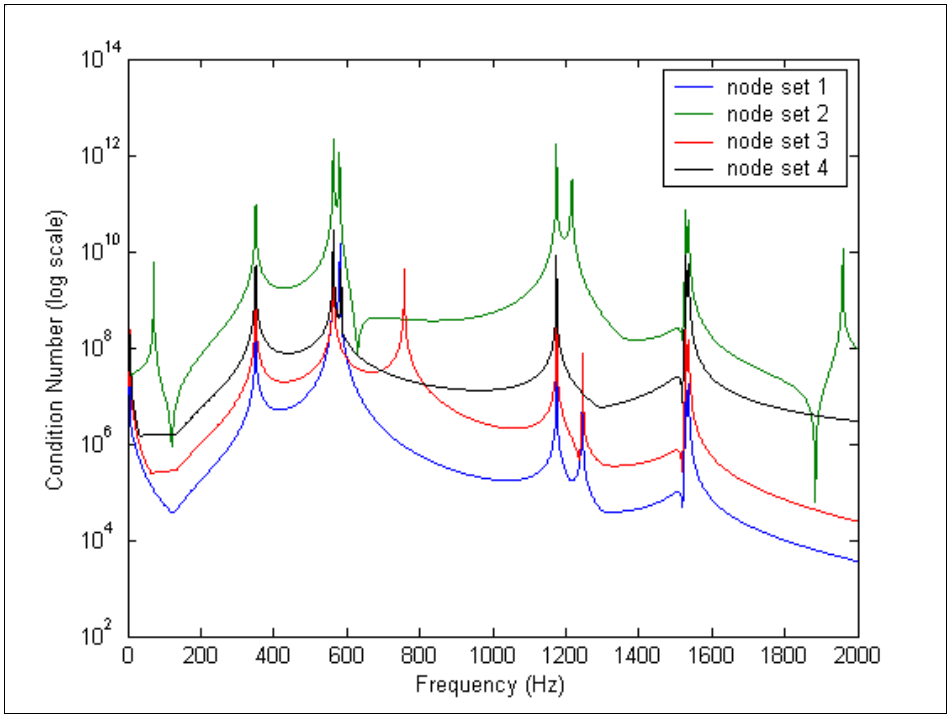

Figure 4.5.11. Condition number with respect to inversion against frequency plot for node sets 1, 2, 3 and 4.

The large variations in the transfer function estimates shown in Figure 4.5.3 to Figure 4.5.5 can be attributed to (small) round-off errors incurred when the FE solution is written in a truncated ASCII format. The fact that round-off errors exist becomes apparent when the difference between an FRF generated from the FE assembly model and the same FRF generated via the coupling calculation is plotted as in Figure 4.5.12. Although the log-scale used in this Figure tends to exaggerate what are very small differences, it does show that errors are present. Since these small round-off errors are sufficient to cause major errors in the calculated transfer functions, the effect of perturbations caused by noise are unsurprising.

Before progressing further with the use of the uncoupling equations, it is essential to understand the causes of ill-conditioning in the calculation. Since the FRF coupling

calculation has been available for many years, previous research into the problems associated with it provides a good starting point for the following discussion.

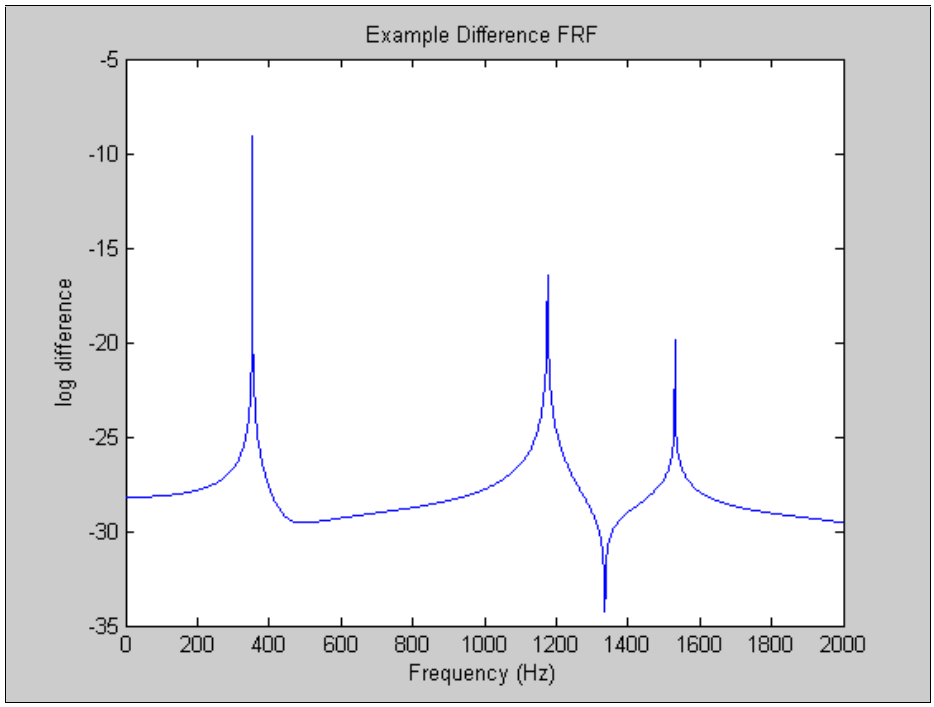

Figure 4.5.12. Example of the difference between an FRF calculated from an FE model of the assembled structure (structure C) and the same FRF generated by via FRF coupling of structures A and B.

Urgueira [77], described 3 reasons for the ill-conditioning of the FRF coupling calculation:

1. Fewer modes included in synthesised curves than coupling DOFs leading to a rank deficient synthesised FRF matrix that cannot be inverted at any frequency.
2. Closely spaced measurement locations, or measurements made on a very stiff region of the structure. In these cases, measurement resolution may mean that FRFs measured at different locations are recorded as identical.

3. FRF matrices will tend to become ill-conditioned close to natural frequencies of the structure due to the dominance of a single mode.

The first of these reasons is of little concern, and should not be encountered in practice since if it is necessary to curve-fit the raw FRF data, then residual compensation must be employed to approximate the effects of the out-of-range modes. Since it is the exclusion of the higher modes that leads to this problem, the inclusion of well-calculated residual terms can be used to overcome it.

The third type of ill-conditioning described by Urgueira derives from the fact that the FRF matrices are naturally ill-conditioned at resonance. Ill-conditioning can be viewed as the approach to singularity [84], and therefore is to be expected to occur near system resonances. Ewins op. cit. suggests that FRFs from lightly damped structures should be curve fitted to avoid the problems associated with this type of ill-conditioning.

The second reason for ill-conditioning of the coupling calculation is actually the most important when we consider the indirect testing of structures, and provides an explanation both for the calculations' sensitivity to the selection of remote measurement DOFs and a second, more serious problem, which will be discussed later.

Prior to Jetmundsen et al's improvements to the coupling calculation [76], if information about DOFs that were not involved in the coupling (the "slave DOFs") was required, it was necessary to ensure that these additional points were not too close

together, or measured at very stiff regions of the structure. This was due to the linear dependent rows and columns such measurements introduced into the matrices for inversion. With the development of the improved coupling formulation (Equation 4.3.3), this problem was removed and data about slave DOFs could be included in the calculation whether those data were linearly dependent or not. In the uncoupling calculation, however, since it is the FRFs relating to the slave DOFs that are used to generate the matrices for inversion, the correct selection of these DOFs is important, as there is a high probability that stiff regions of the structure will remain stiff, even after the attachment of the structure of interest. The question arises as to whether a set of optimum remote DOFs does exist, and, if so, whether these DOFs can be determined a priori.

In order to investigate whether an optimum set of remote DOFs existed, a Matlab script was prepared which ran through every possible combination of 6 translational DOFs from the 28 available (376740 possible permutations) and determined the mean of the condition number over the frequency range 0-2000Hz with 1.25Hz frequency resolution. The remote DOFs which generated the FRF matrix having the lowest mean condition number over the frequency range were selected and are shown in Figure 4.5.13. The condition number of the matrix for inversion based on these DOFs was compared with that which had previously been considered the best set (4x, 4y, 9x, 9y, 14x, 14y). The result is shown in Figure 4.5.14 from which it is clear that the selection of these remote DOFs has considerably improved the condition number of the matrix for inversion over the entire frequency range. However, the condition of the problem is still by no means good. Nonetheless it was considered important to

understand why these particular DOFs were selected in order to establish guidance criteria for the selection of remote DOFs in real applications.

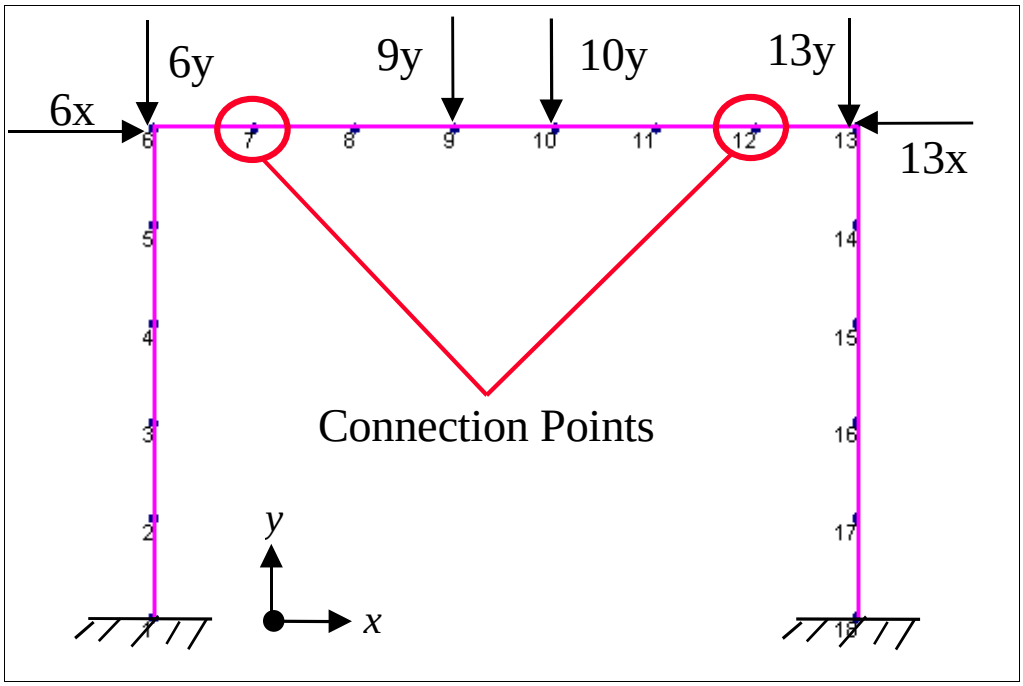

Figure 4.5.13. Optimum remote DOFs selected by iterative Matlab procedure.

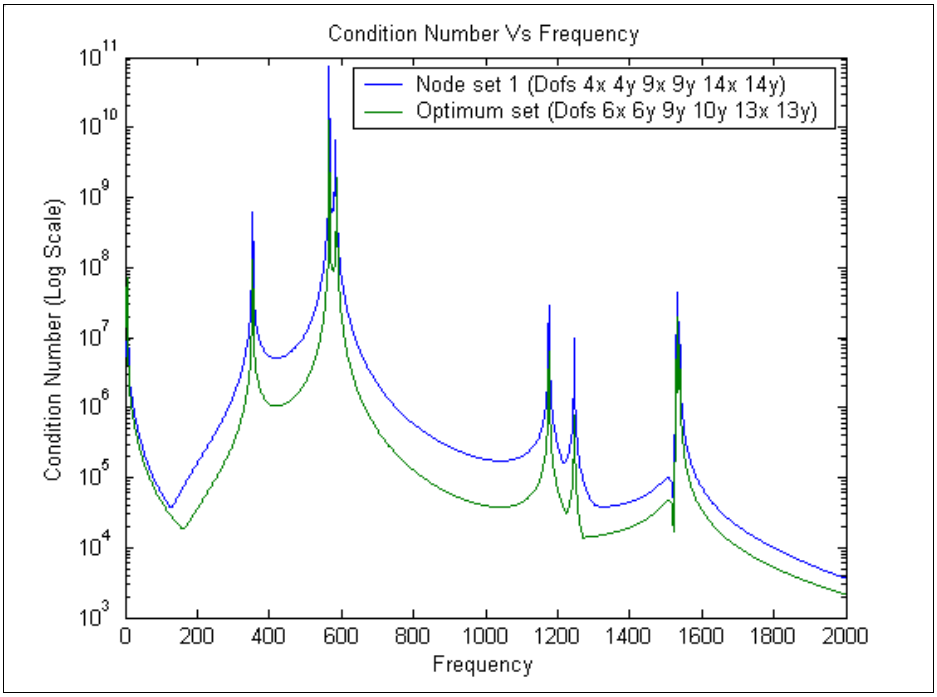

Figure 4.5.14. Condition number with respect to inversion against frequency plot for the selected optimum DOFs and previous node set .

In recent years the concept of Effective Independence (EI), developed by Kammer, [70], has been shown to be a useful tool for the modal tester in helping to determine where their measurement efforts should be concentrated. Its most common use is in the selection of a set of response measurement locations that will provide a unique description of each of a structure's mode shapes within a certain frequency range, an important consideration for the purpose of model correlation. The effective independence of structure A was calculated for its first two modes (these are the only modes which occur in the frequency range 0-2000Hz) using the MODPLAN tool provided in ICATS, the results of which are shown in Figure 4.5.15.

From Figure 4.5.15 (a) and (b) it is apparent that 4 of the 6 DOFs from the optimum set (9y, 10y, 6x and 13x) are at DOFs with a high EI. The other two DOFs (6y and 13y) however, both have very low EI values. The selection of these 2 DOFs can be attributed to the fact that the DOFs associated with nodes 7 and 12 cannot be selected as these are the coupling DOFs. Also, over the frequency range of interest, 8y and 11y will behave very in a similar way to 9y and 10y, respectively. As can be seen from Figure 4.5.15, all of the remaining possible DOFs all have a very low value of EI, and as such the two selected represent the best of a poor set. In a physical sense, for the purpose of indirect testing, the EI calculation is providing a set of DOFs that are not situated in regions that behave in a near rigid fashion across the frequency range of interest. It should be noted, however, that this is a near impossible task for this case.

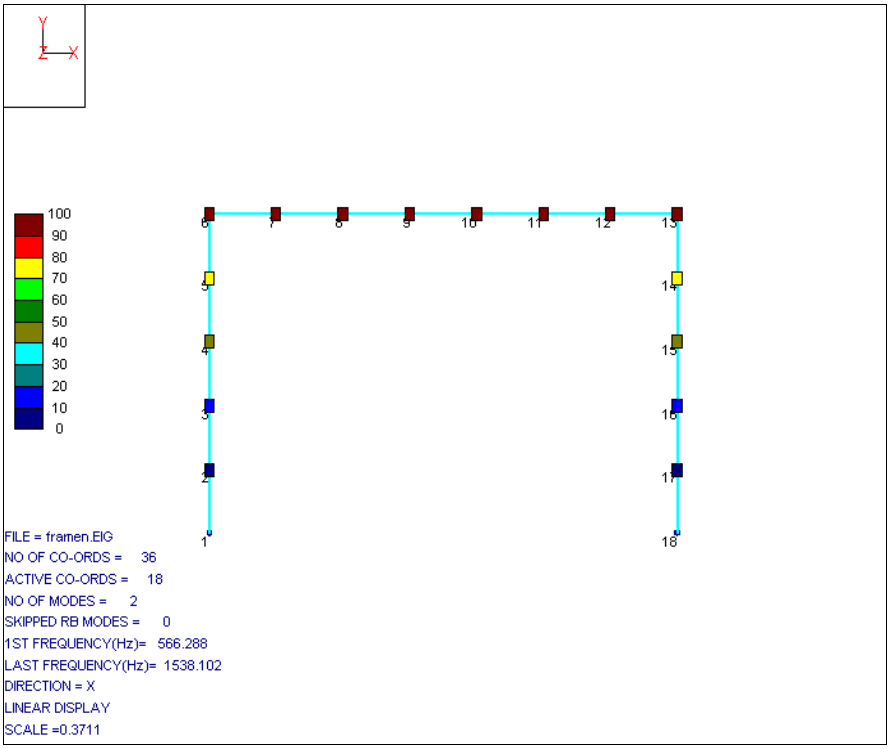

(a)

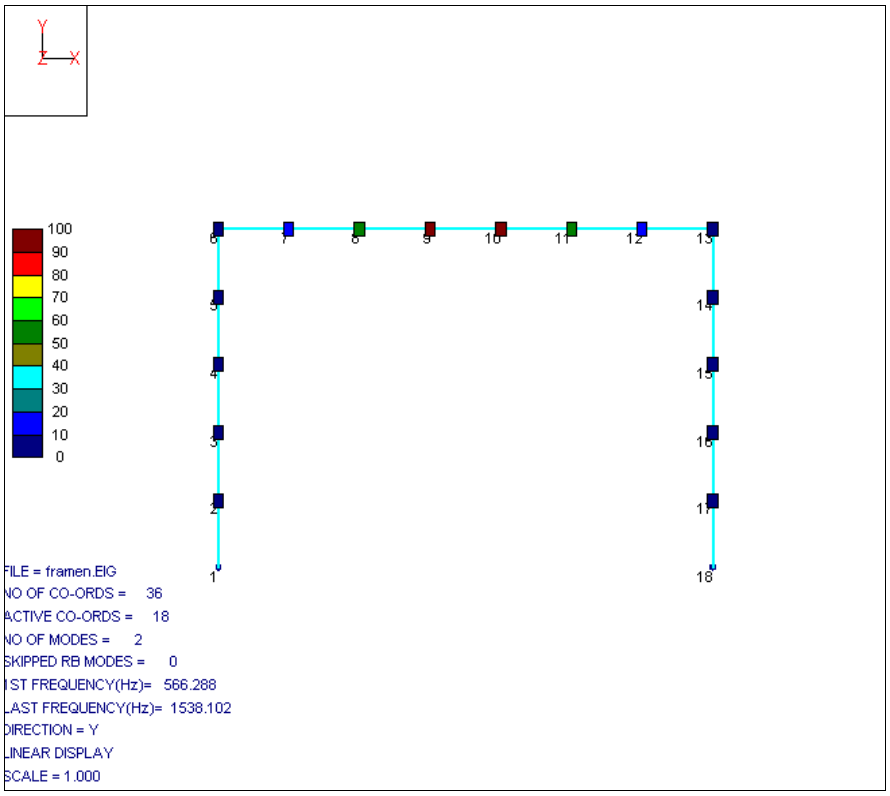

(b)

Figure 4.5.15. Results of effective independence calculation for the first two modes of structure A: a) *x* direction; b) *y* direction.

It has already been mentioned that although the selection of remote DOFs can contribute to the ill-conditioning of the problem, even selecting an optimal set of remote DOFs does not necessarily provide a well-conditioned problem. In fact, for the majority of the frequency range, even the optimum DOFs selected for this case still lead to a condition number in excess of 10000. Once again, the source of this additional, and more problematic, ill-conditioning can be attributed to the second cause of ill-conditioning identified by Urgueira, op. cit. In his work, when discussing the attachment of structures at rigid regions, Urgueira proceeds by considering simple spring-mass structures such as that shown in Figure 4.5.16 (a), in which the bold spring denotes one which is very stiff.

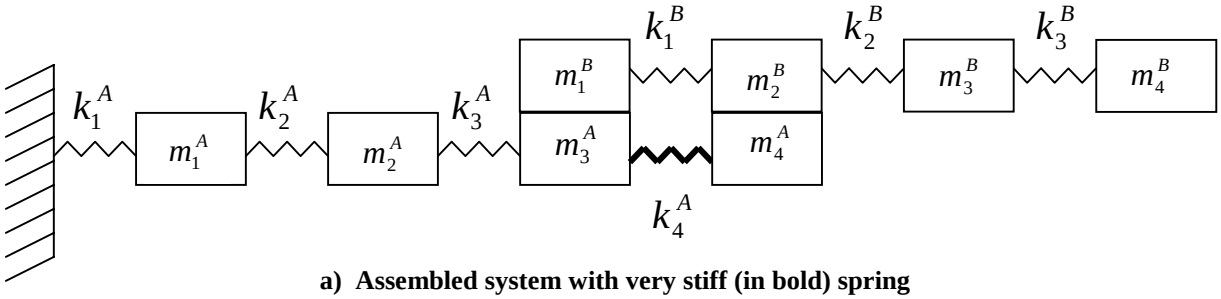

a) Assembled system with very stiff (in bold) spring

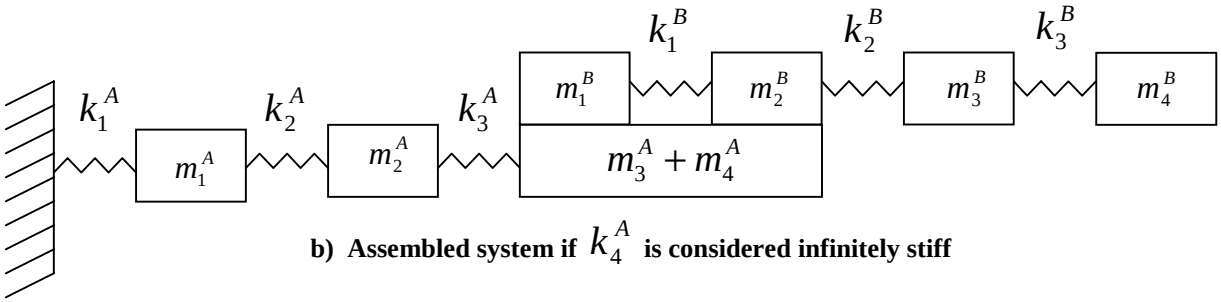

b) Assembled system if k_4^A is considered infinitely stiff

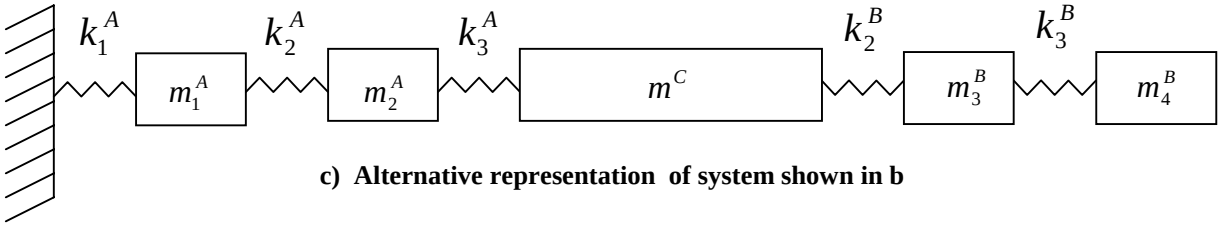

c) Alternative representation of system shown in b

Figure 4.5.16. Systems containing a stiff spring between two connection DOFs.

If Urgueira's argument is taken to its extreme, such that k_4^A is infinite, then the system can be redrawn as in Figure 4.5.16(b). In this case, the FRFs of the assembled structure (Figure 4.5.16(c)) at the connection points will be given by:

$$\left[H_{cc}^{C}\right]=\begin{bmatrix} H_{11}^{B} & H_{12}^{B} \\ H_{21}^{B} & H_{22}^{B} \end{bmatrix}\left(\begin{bmatrix} H_{33}^{A} & H_{33}^{A} \\ H_{33}^{A} & H_{33}^{A} \end{bmatrix}+\begin{bmatrix} H_{11}^{B} & H_{12}^{B} \\ H_{21}^{B} & H_{22}^{B} \end{bmatrix}\right)^{-1}\begin{bmatrix} H_{33}^{A} & H_{33}^{A} \\ H_{33}^{A} & H_{33}^{A} \end{bmatrix} \qquad (4.5.2)$$

since;

$$H_{33}^{A}=H_{34}^{A}=H_{43}^{A}=H_{44}^{A}$$

Therefore, in the coupling of systems A and B (using Jetmundsen et al's improved coupling formulation) the attachment of two DOFs to form a single DOF does not present a significant problem[12], as can be seen from the analytical solution. In fact, in this simple example, the condition of the matrix for inversion will be identical to the condition of the subsystem matrix $\left[H_{cc}^{A}\right]$, and will therefore only tend to suffer ill-conditioning problems in the vicinity of natural frequencies of that structure. If however, indirect testing is considered with structure A as the test fixture, then it is clear from an inspection of Figure 4.5.16 that the problem is always underdetermined irrespective of which remote DOFs are chosen. The ill-conditioning of the problem simply reflects the infinite number of ways in which the assembled mass, m^C, could be constructed and that the spring, k_1^B, is redundant in the assembly.

With respect to the simple frame structure problem, it is possible to see that the horizontal portion of structure A will behave almost rigidly in the x direction across

[12] Note that adding a singular matrix to a non-singular matrix **always** produces a non-singular matrix which will possess an inverse.

the frequency range (although the structure does sway in this direction). Therefore the two legs of structure B are almost grounded in this direction in the assembly, making the problem very poorly posed. It is also interesting to note the general downward trend of the condition number with frequency for node sets 1 and 2 (Figure 4.5.11), since this can be attributed to the increasing lateral flexibility of the cross member with frequency. This increasing flexibility means that the legs of structures B are less rigidly constrained at higher frequencies, making the problem increasingly well-posed.

In respect of indirect testing, this physical source of ill-conditioning represents the most serious problem in the successful application of the uncoupling equations. The problem seen here is akin to that encountered in the application of force determination via modal models [1], in that, although it is possible to use a pseudo-inverse to overcome the problem of under-determination, the solution provided by such a method will simply yield the solution with the minimum norm and is unlikely to have any bearing on physical reality.

4.6 The design of indirect test fixtures

4.6.1 Mathematical basis

Essentially, the design requirement for an indirect fixture is that the matrix for inversion ($[H^A_{aa}]-[H^C_{aa}]$) should be well-conditioned. Closer inspection of Equation 4.4.6, in addition to the properties of condition numbers provides mathematical insight into exactly how this should be achieved.

First we may write (using λ to denote the condition number) :

$$\lambda\left([H^A_{aa}]-[H^C_{aa}]\right)=\lambda\left([H^A_{ac}]\left([H^B_{cc}]+[H^A_{cc}]\right)^{-1}[H^A_{ca}]\right) \qquad (4.6.1)$$

The term $\left[H_{cc}^{B}\right]+\left[H_{cc}^{A}\right]$ is not completely within our control since even if $\left[H_{cc}^{A}\right]$ is singular, the sum $\left[H_{cc}^{B}\right]+\left[H_{cc}^{A}\right]$ can only be near singular if $\left[H_{cc}^{B}\right]$ is also near singular. What we can assert, however, is that if $\left[H_{cc}^{A}\right]$ is near singular, then $\left[H_{ac}^{A}\right]$ must be part of linearly dependent subset of the complete FRF matrix, $\left[H^{A}\right]$, and will therefore be ill-conditioned also. Furthermore, the same will apply if the matrix $\left[H_{aa}^{A}\right]$ contains linearly dependent or near linearly dependent terms. Suppose, for example, that:

$$\lambda\left(\left[H_{cc}^{B}\right]+\left[H_{cc}^{A}\right]\right)=1 \tag{4.6.2}$$

where λ is the condition number, then from the property of condition numbers

$$\lambda([A][B])=\lambda([A]) \quad \text{if} \quad \lambda(B)=1 \tag{4.6.3}$$

and

$$\lambda\left([A][A]^{T}\right)=\lambda([A])^{2} \tag{4.6.4}$$

Then it is apparent that efforts should be concentrated on ensuring that $\left[H_{ac}^{A}\right]$ is well conditioned and, as such, it is necessary to ensure that $\left[H_{cc}^{A}\right]$ and $\left[H_{aa}^{A}\right]$ do not contain linearly dependent terms. It must be noted, however, that in the vicinity of natural frequencies of the indirect testing fixture, ill-conditioning of the matrix for inversion will be unavoidable, particularly if the structure is lightly damped.

4.6.2 Practical implementation

From the previous discussion, it is clear that the design of indirect testing fixtures must be undertaken carefully and that particular attention needs to be paid to ensuring that the fixture does not constrain any relative motion of the structure of interest. The test fixture must also be flexible to allow well-conditioned matrices to be formed for the remote measurement DOFs. Two questions arise: first, how can the test fixture be designed so as not to constrain relative motion? and second, just how flexible must

the test fixture be? Initially it appears that there are two possible answers to the first of these questions, the most obvious of which is to separate the indirect test fixture in to *n* components, where *n* is the number of connection points. This solution is illustrated in Figure 4.6.1(a). The second answer is to introduce springs at each connection DOF thus allowing relative motion between the connections as illustrated in Figure 4.6.1(b). Of these two possible solutions, that shown in Figure 4.6.1(a) is preferable as there is no coupling between the two indirect testing systems. This reduces the number of off-diagonal terms in the FRF matrix, potentially improving its numerical stability and simultaneously reducing the number of measurements required.

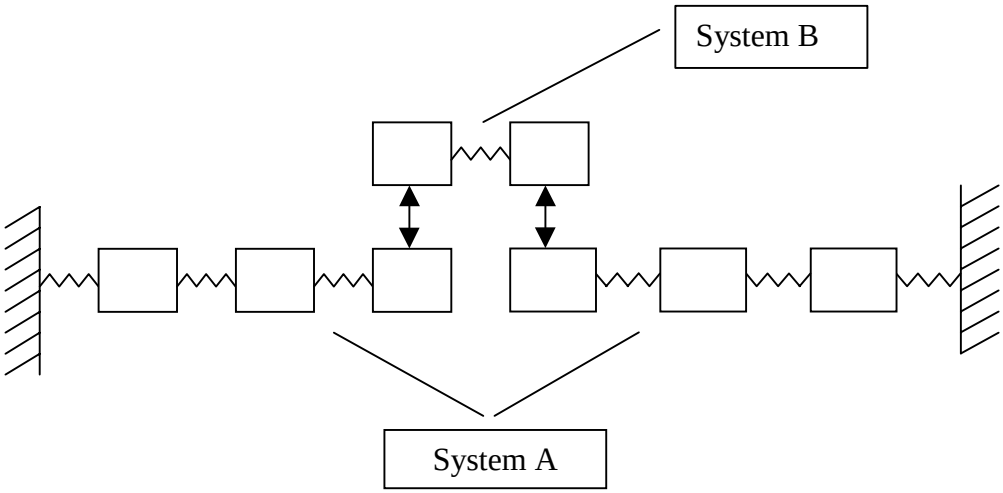

a) Indirect fixture as two separate components

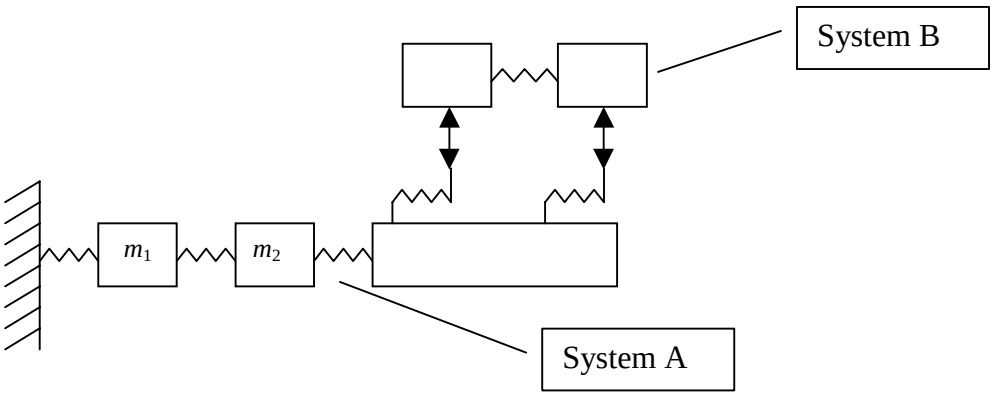

b) Indirect fixture with connection springs

Figure 4.6.1. Possible solutions to the problem of constraining relative motion

The second answer not only requires more measurements to be made, but also raises an additional question: How stiff should the connection springs be? This last question is most easily answered by considering the simple system shown in Figure 4.6.1(b). Irrespective of the stiffness of the springs used at the connection DOFs, the FRF matrix of structure A will only ever be of rank 3, reflecting the three-degrees of freedom it possess. Therefore, if the masses m_1 and m_2 are used as remote DOFs, $\left[H_{ac}^{A}\right]$ and its transpose will be linearly dependent, with $col1\left(\left[H_{ac}^{A}\right]\right) = col2\left(\left[H_{ac}^{A}\right]\right)$. The matrix product $\left[H_{ac}^{A}\right]\left(\left[H_{cc}^{B}\right]+\left[H_{cc}^{A}\right]\right)^{-1}\left[H_{ac}^{A}\right]^{T}$ will have rank 1, but will be of order 2, therefore it will be singular and will not posses an inverse. Since, $\left[H_{ac}^{A}\right]\left(\left[H_{cc}^{B}\right]+\left[H_{cc}^{A}\right]\right)^{-1}\left[H_{ac}^{A}\right]^{T} = \left[H_{aa}^{A}\right]-\left[H_{aa}^{C}\right]$, then the sum $\left[H_{aa}^{A}\right]-\left[H_{aa}^{C}\right]$ must also be singular. The problem is not, therefore, that there is no relative motion at the connection points, but rather, that the remote DOFs cannot tell whether relative motion does, or does not, exist.

The situation changes if combined spring-mass systems are used such that the system *A* is re-configured as shown in Figure 4.6.2. This ensures that the system FRF matrix has full rank at the outset, but is only really a variation on the design shown in Figure 4.6.1(a) without the practical benefits associated with fewer transfer FRF measurements that system affords.

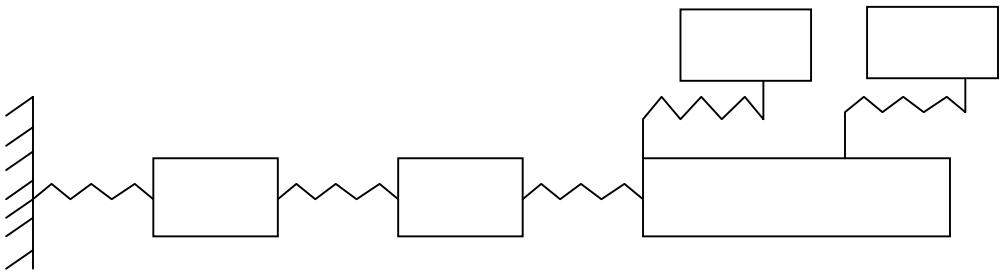

Figure 4.6.2. Redesigned indirect test fixture, incorporating additional masses.

The question of how flexible the test fixture must be is actually very easy to answer. It was demonstrated in section 4.5.6 that the DOFs with high EI values for modes in the frequency range of interest are closely related to those that are the most suitable for use in the uncoupling equation. In its more usual application, the EI calculation guides the selection of *n* DOFs so as to provide a linearly independent set of (*n*-1) mode shapes and thereby minimise the off-diagonal terms in the MAC matrix[13] [70]. Its role in the case in hand is similar, except that here the possibility exists that there are more connection DOFs than modes within the frequency range of interest. As was shown in section 4.5.6, this results in it becoming difficult to form a set of linearly independent equations with which to solve the uncoupling equation. Clearly, the ease of forming a linearly independent matrix, $\left[H_{aa}^{A}\right]$, will increase as the indirect test fixture becomes more flexible. To ensure a well-conditioned matrix, the fixture would require (at a minimum) as many modes in the frequency range of interest as there were connection DOFs. It should be noted however that these must be the "correct" modes, in the sense that they must encompass motion in each of the co-ordinate system directions. If the indirect test fixture contains more modes within the frequency range of interest than there are connection DOFs, the possibility of providing a **truly** over-determined matrix $\left[H_{ac}^{A}\right]$ exists, and it may be possible to benefit from the averaging effects such matrices provide. When deciding how many more modes than coupling DOFs should be included, two factors must be weighed against the expected benefits of over-determination: (i) the amount of effort required

[13] It is considered prudent to include a few more *n* DOFs than there are expected modes, so as to make use of over determination as a method for averaging out inevitable experimental inconsistencies.

to obtain the additional measurements and (ii) the fact that the additional resonances will inevitably lead to ill-conditioning in their vicinity.

4.6.3 Numerical example revisited

In the light of the observations made in the previous section, it is worth revisiting the numerical example of section 4.5 Although the objective here remains the same as before , that is, to determine the FRFs of structure B at its connection co-ordinates, the indirect testing fixture is designed to improve the numerical stability of the matrices involved.

First, the design is modified such that the fixture is in two pieces as shown in Figure 4.6.3. The improvement over the original design (design 1) of this modification (design 2) on the condition number of the matrix for inversion over the frequency range, can be seen in Figure 4.6.4.

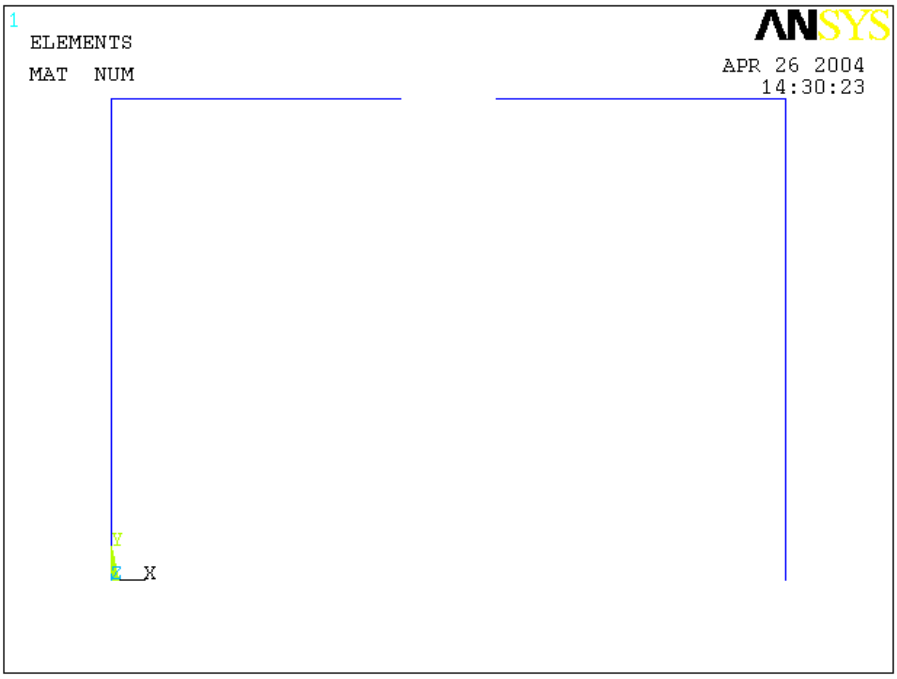

Figure 4.6.3. Indirect testing fixture redesigned as two separate components.

Next, the cross-section of the indirect testing fixture was reduced from 20mm by 20mm to 8mm by 8mm. This dimension was chosen since the first three modes of each half of the test fixture were at frequencies of 142Hz, 499Hz, and 1741Hz. Thus, the indirect test fixture possessed six modes in the frequency range 0-2000Hz. The condition number vs. frequency for this design (design 3) is shown by the red trace in Figure 4.6.4

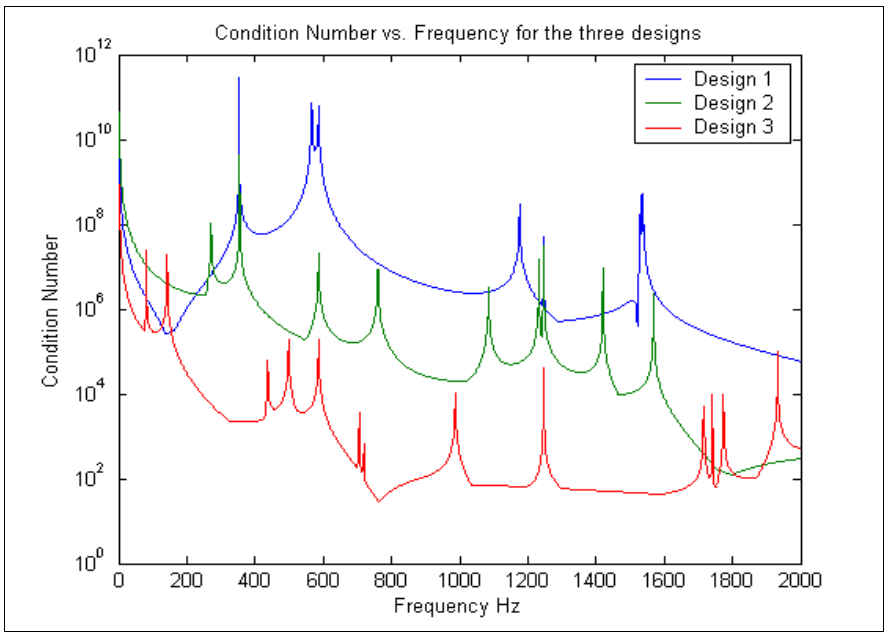

Figure 4.6.4. Condition number vs. frequency for the original, and improved designs.

The improvement in the condition of the problem drastically affects the calculation's stability, a fact clearly demonstrated by the final design's tolerance of 1% noise as illustrated in Figure 4.6.5.

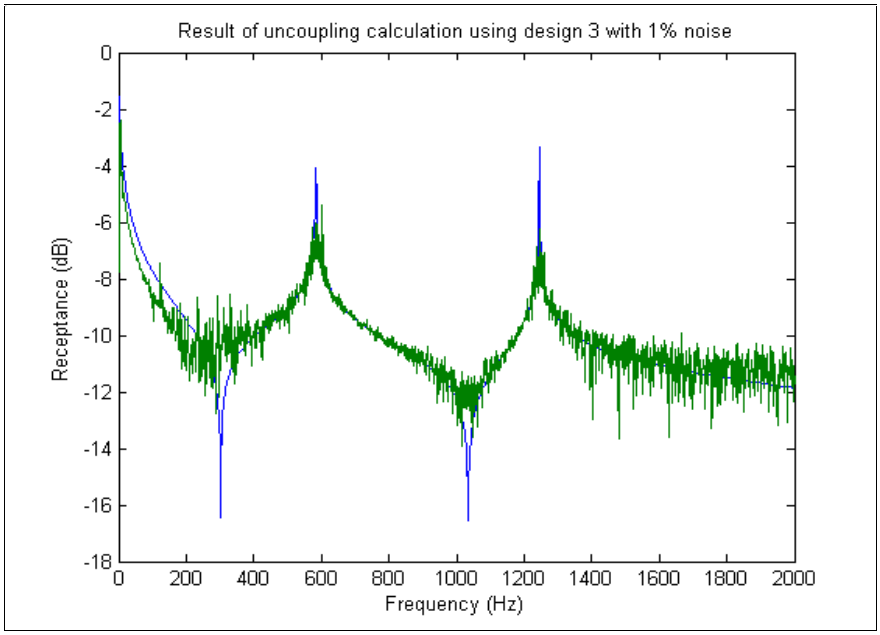

Figure 4.6.5. Estimation of HB1x1x by uncoupling using design 3, in the presence of 1% noise.

Although Figure 4.6.5 shows that the calculation is still sensitive to noise, the effect is no longer catastrophic, as it was in the case shown in Figure 4.5.9. A possible solution to the remaining sensitivity to noise is to employ a modal curve fitting routine and to use the curve-fitted results in the uncoupling calculation. This is a long established method in substructure coupling and is particularly useful where structures are lightly damped. In order to establish whether the ill-conditioning of the problem had been reduced sufficiently to allow this approach to be used, a virtual test was conducted.

FRFs contaminated with five percent noise by the method outlined in section 4.5.5 were generated for the DOFs shown in Figure 4.6.6 and were written to ICATS (.frf) format.

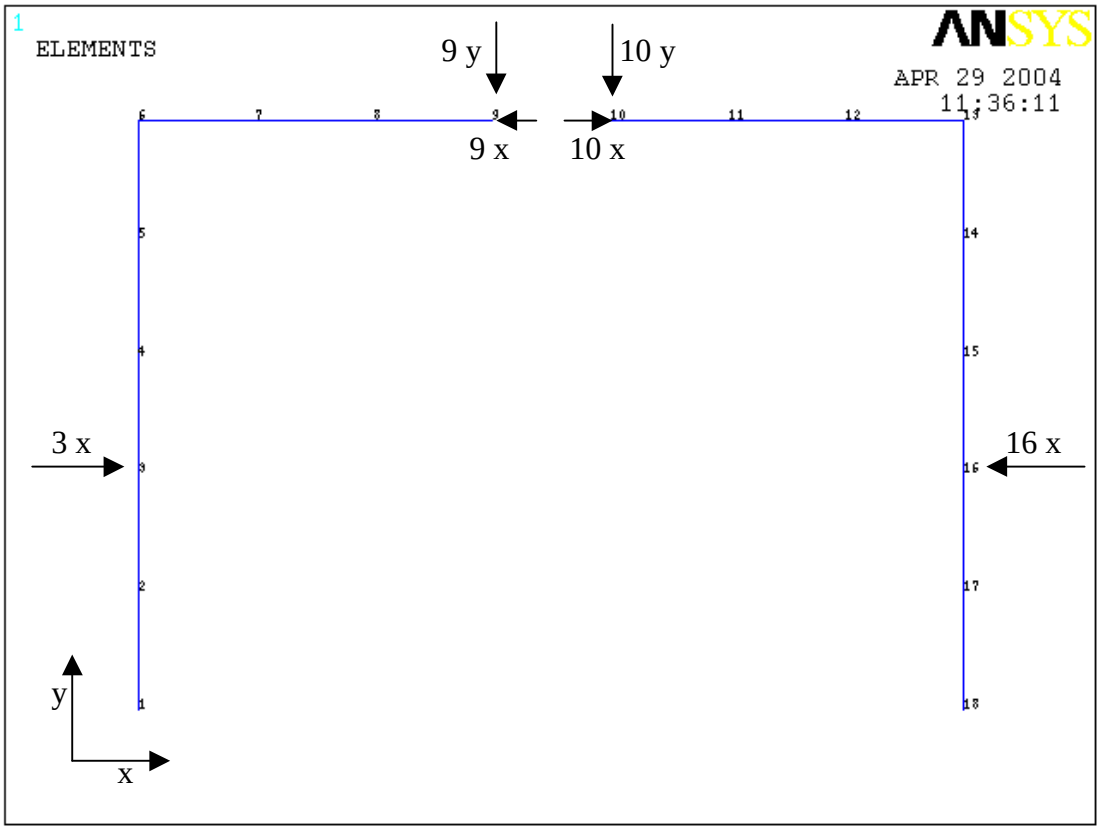

Figure 4.6.6. DOFs used for generation of FRFs for the virtual test

Examples of these FRFs are shown in Figure 4.6.7. The ICATS SDOF line-fitting algorithm was used to curve-fit the modes in each of the FRFs. The line-fitting method was used since it is well suited to FRFs from lightly damped structures [69] such as those which had been artificially generated. After each of the resonances in the FRF curve had been analysed, residual terms to compensate for the effects of the out-of-range modes were calculated using the pseudo-mode approach. In general, the FRFs regenerated from the results of the analysis were very close to the actual FRFs calculated from the FE data and Figure 4.6.8 (a) and (b) illustrate this. However, some of the regenerated curves did not compare well, especially at higher frequencies, where the effect of added noise made it difficult to locate anti-resonances for the residual estimation process. An example of such a curve is shown in Figure 4.6.8 (c). It is clear from Figure 4.6.8 (c) that although the regenerated curve is reasonably

accurate in the vicinity of the resonances, the same cannot be said for the off-resonant regions, particularly at high frequencies.

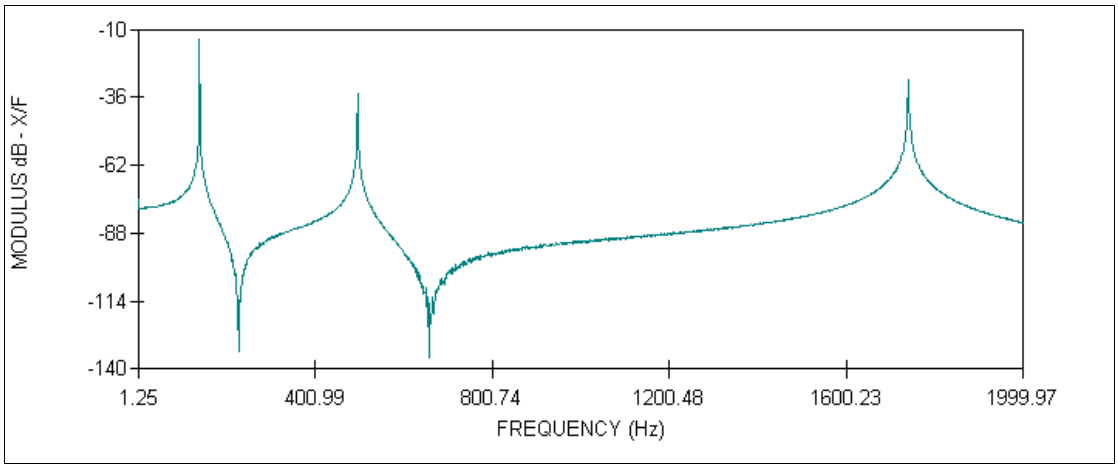

(a)

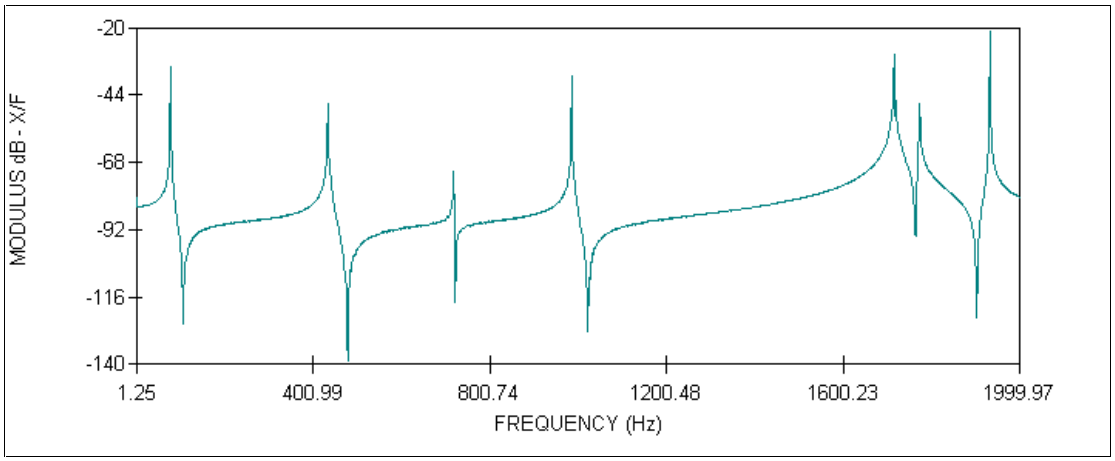

(b)

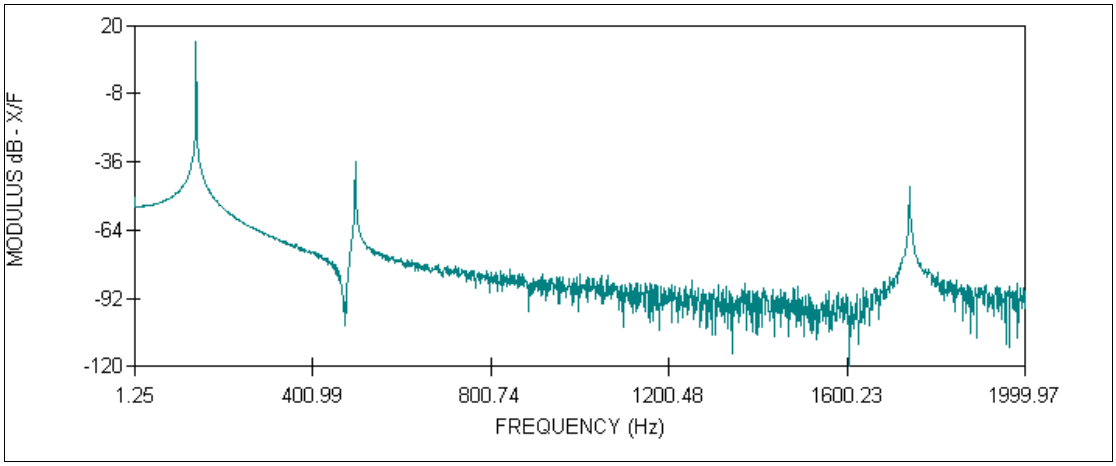

(c)

Figure 4.6.7. Example FRFs contaminated with 5% noise: a) H^{A}_{3x3x} **; b)** H^{C}_{3x3x} **; c)** H^{A}_{9x9x}

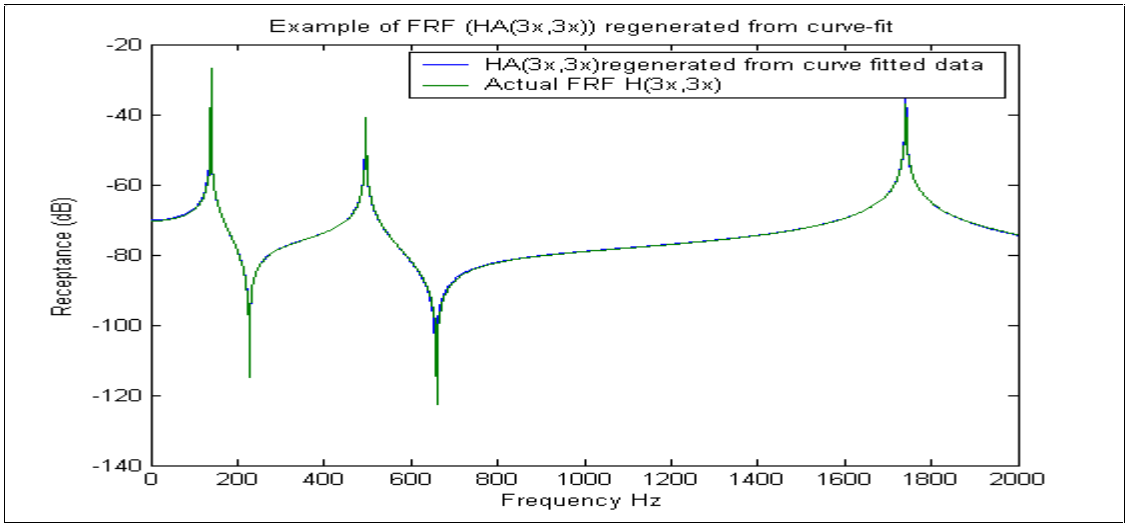

(a)

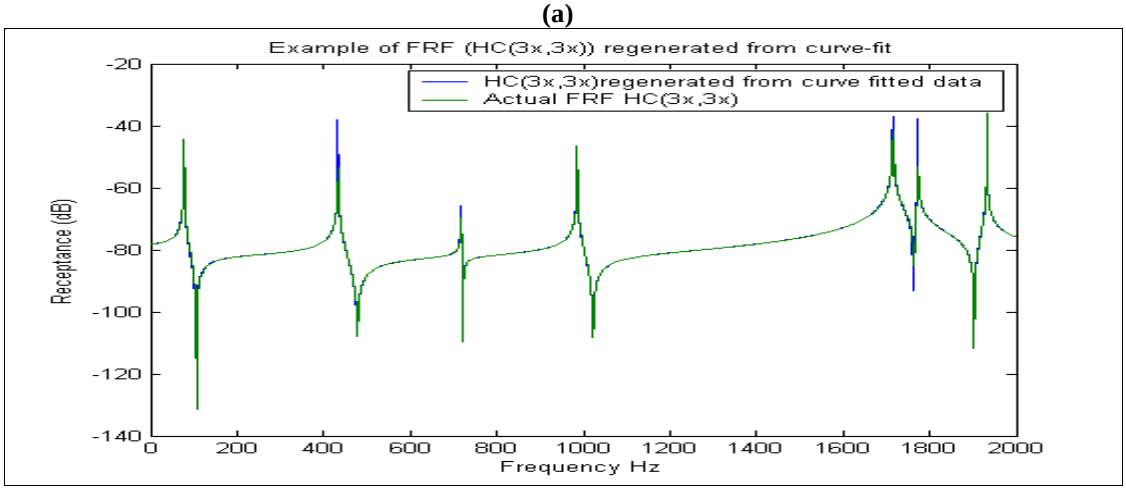

(b)

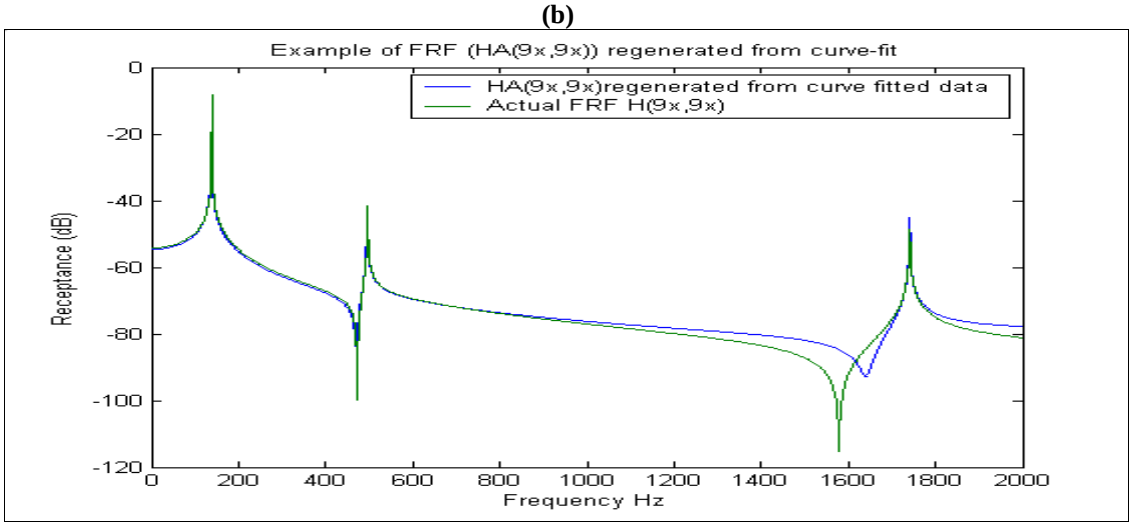

(c)

Figure 4.6.8. Example of FRFs regenerated from modal curve-fit data overlaid on the (true) FE curves: a) H^{A}_{3x3x} **; b)** H^{C}_{3x3x} **; c)** H^{A}_{9x9x}

The curves synthesised from the modal curve-fitting procedure were then used as input to the uncoupling equation (Equation 4.4.6). Figure 4.6.9 shows an element of

the coupled system matrix [T] given by, $T_{7x7x} = H^{A}_{7x7x} + H^{B}_{1x1x}$, and the equivalent element of this matrix calculated via FRF uncoupling.

The result shown in Figure 4.6.9 shows that the estimate of an element of the coupled system matrix, [T], obtained via uncoupling, contains most of the peaks and troughs associated with the actual curve. Although it also contains numerous "breakthroughs", these are all associated with the natural-frequencies of the indirect fixture and the assembled structure as shown in Figure 4.6.10. The breakthroughs are due to the ill-conditioning of the problem at resonant frequencies. In this study, although curve fitting has been used, no modal analysis process has been employed to form a consistent set of eigenvalues and eigenvectors from which to synthesise the curves. The regenerated data therefore contain small inconsistencies in the actual location of each natural frequency and in this example these inconsistencies have been sufficient to cause breakthroughs.

Figure 4.6.10 also clearly shows that the calculation is clearly predicting a new mode at around 600 Hz. A second "highly damped peak" is also visible at around 1200Hz. It is noted that these two "peaks" are close to the first two free-free natural frequencies of structure B at 584Hz and 1245Hz. Figure 4.6.11 shows the FRF $H^{B}_{1x,1x}$ calculated via the uncoupling method overlaid on the FRF for this DOF from the FE model of the structure.

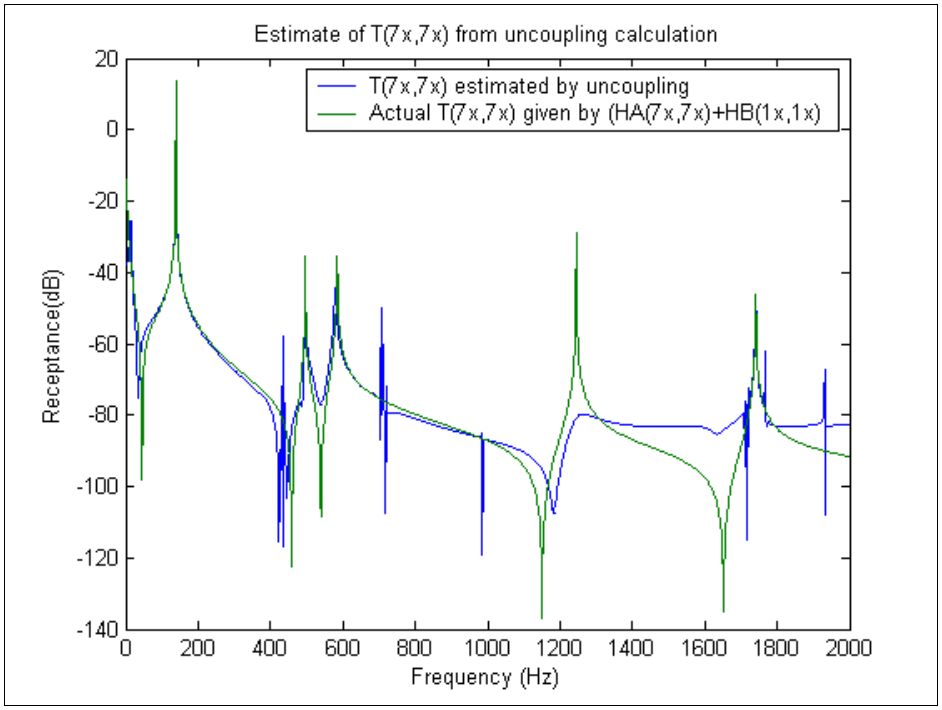

Figure 4.6.9. Estimate of $T_{7x,7x}$ calculate via uncoupling (blue) overlaid on the actual curve (green) given by $H^{A}_{7x7x} + H^{B}_{1x1x}$.

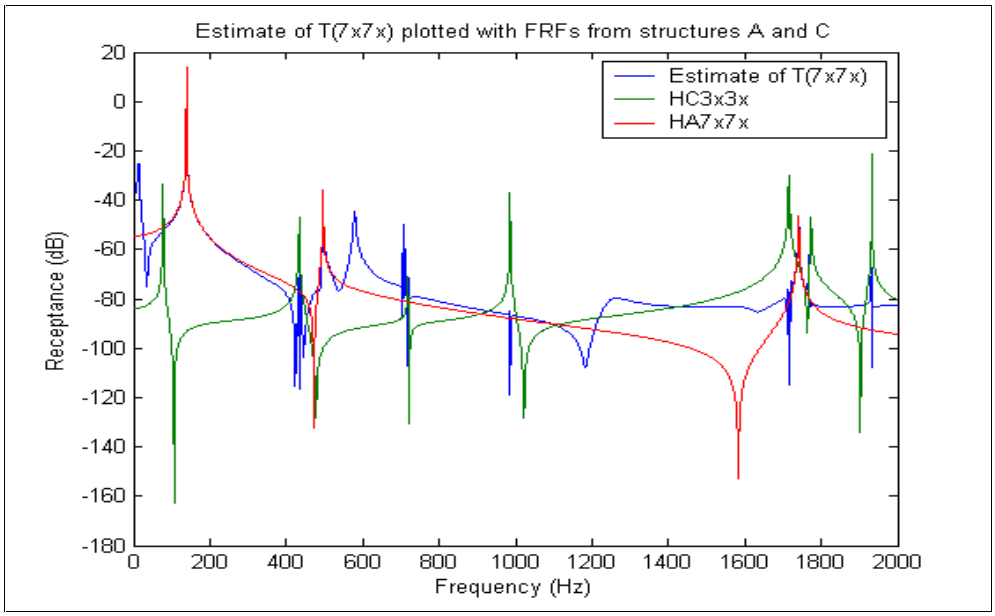

Figure 4.6.10. FRF plot illustrating how "breakthroughs" in the calculated curve occur at the natural frequencies of the test fixture and assembled structures.

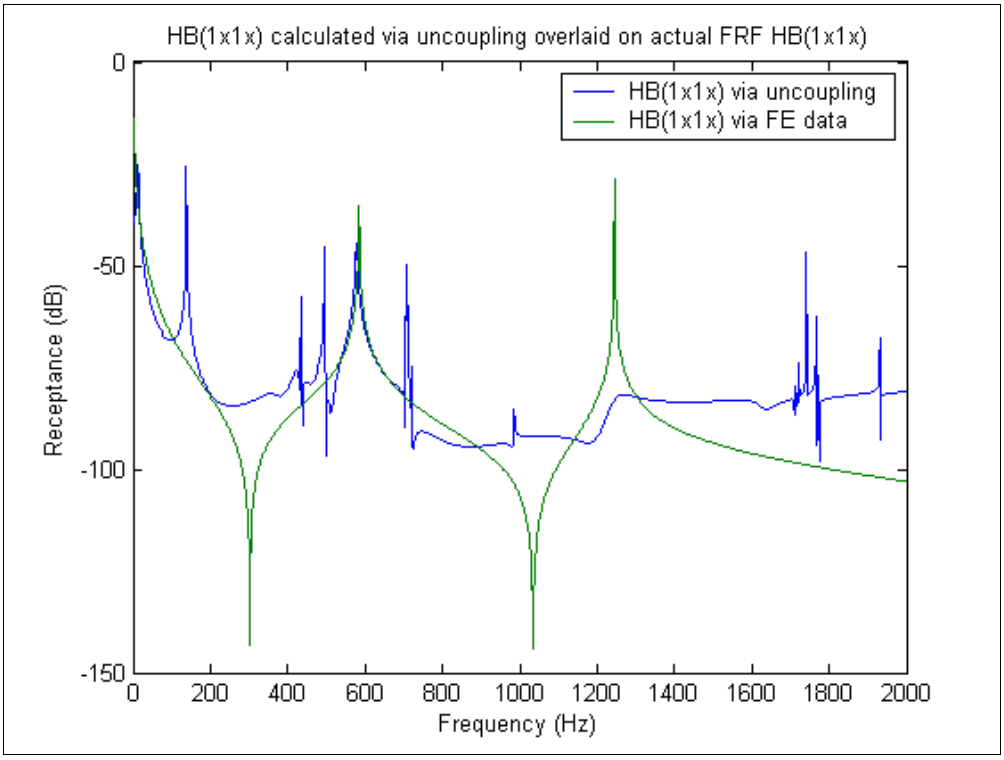

Figure 4.6.11. The FRF H^{B}_{1x1x} calculated using the uncoupling calculation overlaid on the actual FRF H^{B}_{1x1x}.

It is immediately clear that the inconsistency in the curve-fitted FRFs has led to the FRF predicted by the uncoupling equation being highly inaccurate at off-resonant regions. However, the first "true" peak in the calculated curve is similar to that of the actual FRF and could be curve-fitted as shown in Figure 4.6.12. By analysing one row of the auto-FRF matrix for structure B, $\lfloor H^{B}_{cc} \rfloor$, obtained from the calculation it was possible to complete a modal analysis for this mode, attempts to analyse the second "mode" were unsuccessful as the peak was not well defined. The natural frequency and mode shape extracted from the modal analysis were compared with the FE data. The mode was found to have a natural frequency of 578 Hz, 1.5% lower than the (true) FE natural frequency of 587Hz, and to have a MAC of 99.8% when compared to the first mode of structure B. This result gives a good indication that the

uncoupling calculation has “correctly” calculated this mode when curve-fitted data has been used.

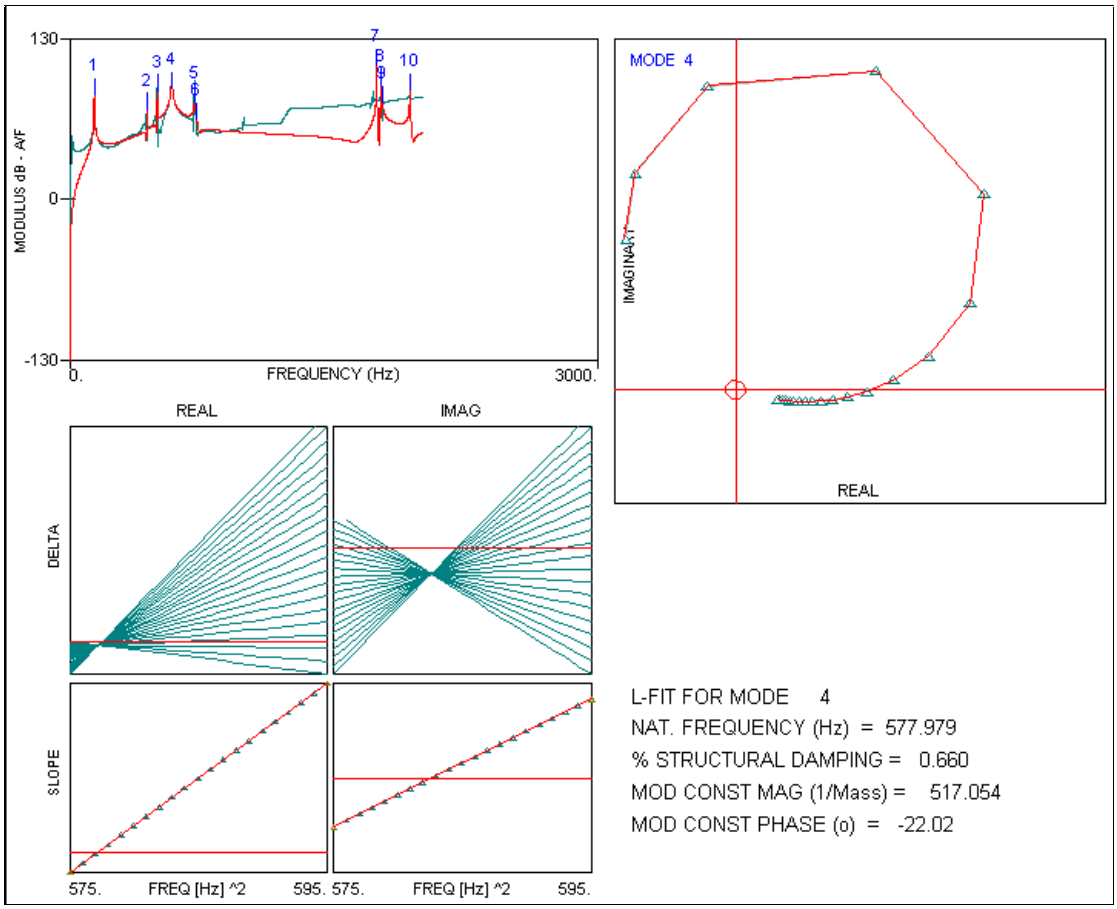

Figure 4.6.12. Curve fitting of the “true” resonance calculated using uncoupling

This virtual test demonstrates how, with careful design, indirect testing via the FRF coupling route is possible. Although in this case the second mode of the structure could not be identified, this is mainly due to the way in which the synthesised noise affects the higher frequencies of the FRFs, as shown in Figure 4.6.7. This leads to ambiguity in the curve-fitting process, especially in locating the anti-resonances. While this ambiguity is, to a certain extent, true-to-life, the synthesised noise added in the example seems overly severe, and point FRFs (such as that of Figure 4.6.7 (c)) showing such noise would be almost certainly be considered unacceptable in a modern modal test. In practice, it would be essential to obtain high quality FRFs, well

defined at both the resonances and anti-resonances, if the curve-fitting method was to be used successfully. It must also be said that the process used is extremely long, even for the 6DOF connection used in this case, it is was necessary to curve-fit 57 FRFs, even when reciprocity was exploited and the two parts of the test fixture were intially independent. For larger numbers of connection points, assuming 6DOF attachments at each, *n* independent components for the indirect test fixture and reciprocity, the number of FRFs required (*p*) is given by: $p = 24n + 18n^2$. Therefore, the task of measuring, curve-fitting and organising the data could not be undertaken lightly for more than three or four connection points.

4.7 Considerations for the practical implementation of the FRF uncoupling method

4.7.1 The choice of exciter

At the beginning of this chapter it was stated that the remote DOFs on the indirect test fixture could be excited using standard excitation techniques, such as impact hammer or electro-dynamic shaker. While in theory this remains true, in practice the excitation will almost certainly have to be applied using impact hammer excitation. Primarily, this is because of the expense involved in supplying as many shakers, and sources as there are remote measurement locations. This number of devices would be required to ensure that the FRFs of the measured components remained consistent, since there will always be a degree of structure-shaker interaction. Even if sufficiently consistent data could be measured by moving a shaker around the structure, the process would be extremely time-consuming for any more than a few connection points.

Although the use of an impact hammer provides a solution to the problem, since it is far easier to provide large numbers of sensors than exciters, its use does incur some costs. First, it is far more difficult to control the force level applied via an impact hammer than it is for a shaker. This may cause problems in obtaining well-defined anti-resonances, a requirement which was highlighted in the earlier virtual test. Secondly, the number of averages used when applying impact excitation is typically very much lower than that which is associated with shaker testing. The use of averaging for impact hammer excitation is also likely to "blur" the locations of the anti-resonances, which unlike the resonances, are sensitive to the location of the excitation. The combination of these two problems may mean that the FRF curves are not well defined across the entire frequency range.

4.8 A summary of the state-of-the-art in FRF based indirect testing

Before discussing an alternative to the FRF based indirect testing method it is worth reviewing the state-of-the-art in the use of FRF data for indirect testing applications and the contribution which this work has made to it.

The earliest and simplest of the FRF based indirect testing fixtures were explored by Maia et al,[86], in which they used FRF based techniques to remove simple free-free masses from structures. The Mass Uncoupling Method (MUM) was found to have a variety of applications including the determination of rotational responses and providing the full FRF matrix of translational FRF from measurement of a single row or column. The MUM was viewed as a useful method for determining some of the FRFs required for FRF based sub-structuring applications. Of course, similar techniques for measuring rotational responses were already used, all of which were based on the process described in [1], however, these methods use different

mathematical relationships to the those employed by the MUM. A good example of the similarity between the MUM technique and other rotational excitation / response measurement techniques can be found in [62].

Having developed the MUM technique Maia et al [66] went on to investigate more generalised uncoupling techniques making use of Equation 4.3.3. and developing Equation 4.4.6 in an effort to characterise the properties of joints via indirect measurements. Their work on joints characterisation showed some of the potential problems associated with the use of Equation 4.4.6, specifically, how the calculations result can vary depending upon the choice of remote excitation DOFs, and its sensitivity to noise. Interestingly, Dong and McConnell [74] used an identical formulation to that employed by Maia et al (the nomeclature differed slightly) in their efforts to determine FRFs relating to the RDOFs using an "instrumented cluster". Dong and McConnell also noted the calculations sensitivity to noise in their application. One of the main features of both Maia et al's and Dong and McConnells applications is that the FRF based indirect calculation is used only to infer information about a FRFs at a single connection point, which simplifies the problem considerably[14]. It is also worth noting that in neither [66] or [74] is there any requirement for the indirect measurement of FRFs relating to slave DOFs on the structure to which the indirect testing fixture is attached.

In this work the application of the indirect testing equations (Equations 4.4.6 and 4.4.10) has been extended to the case where the structure of interest is attached to the

[14] Even so the successful practical application of the technique is still extremely difficult.

indirect test fixture at more than one connection point. Also Equation 4.4.10 has been developed such that its theoretically possible to derive the free-free mode shapes of a structure of interest which is attached to the indirect test fixture with out directly applying a force to the structure of interest. It has been shown that, unlike the FRF sub-structuring equation, there is no need to measure point rotational FRFs (i.e moment in/angular response out) when the indirect testing equations are used. Furthermore this work has identified the physical cause of the calculations instability. It has shown how the "stiff-spring ill conditioning" phenomena identified by Urgueira [77] can first:

lead to ill-conditioning of the remote testing FRF matrix ($\left[H_{aa}^{A}\right]$) if the selection of the remote testing DOFs includes one or more linearly dependent DOFs, and second;

lead to an ill-conditioned connection FRF matrix ($\left[H_{cc}^{A}\right]$) which causes the deletion of connection DOFs on the structure of interest (the FRFs of which are contained in the matrix $\left[H_{cc}^{B}\right]$) and leads to an insoluble indirect testing equation.

Most importantly, through an understanding of the physics, this present work has shown that neither of the two problems discussed above are insurmountable. The first (ill-conditioning of the remote testing FRF matrix) can be overcome by ensuring that the indirect testing is flexible enough to possess as many modes as there are connection DOFs within the frequency range of interest. While ill-conditioning of the connection FRF matrix can be overcome by dividing the indirect test fixture into as many individual parts as there are connection locations, thus ensuring that relative motion between the connection DOFs on the structure of interest is not constrained.

It should be noted however that the successful practical application of these techniques will be difficult at least in part because of the large amount of consistent measurements that are required.

4.9 An alternative indirect testing method

4.9.1 Spatial uncoupling: the "model-and-remove" approach

Although, as mentioned earlier, it is not possible to obtain measurements of the spatial model directly, it **is** possible to develop a representative spatial model of a structure using the Finite Element method. Indeed, the generation of such FE models is one of the main reasons that a modal test is conducted in the first place! As such, the possibility of using spatial models for indirect testing should not be discounted.
The method by which spatial models could be used is as follows. First, a model of the indirect test fixture would be constructed and validated against test data. Second, a model of the assembly of the indirect test fixture and the structure of interest would be generated. This model would be validated against test data in which DOFs on the test fixture were used as the excitation/response locations. If response measurements were possible on the structure of interest, these data would also be included in the validation process. The majority of uncertainties within the assembly model would be associated with the structure of interest and the joints, so it would be these parameters that would be updated. Finally, once a sufficient level of correlation had been achieved, the test fixture would be removed from the model of the assembly leaving a valid model of the structure of interest.

A simple version of such an approach can be used to overcome the problem of mass-loading by transducers. If this approach is used, then the measurement transducers

and mass representative dummy transducers are attached to the structure at every DOF of interest. Each measurement requires that a transducer replace a dummy mass and vice versa, a process that (with care) ensures that the structure is mass loaded in a consistent way. The mass loading effect caused by measurement method is included in the FE model of the structure and once a sufficient level of correlation has been achieved between the test and FE data, the masses are removed from the model. In a more complex application, Mottershead et al, op. cit., also use an FE model of their "T-block" structure to allow the dynamic stiffness of the device to be included in their calculation. Hopkins et al, [81] , have also used a similar method to infer information about rotations for a sub-structuring application.

The above-mentioned applications all have two things in common, however. First, the indirect test fixture(s) are only ever attached at a single connection point(s). This simplifies matters considerably, since as was shown in the earlier study (Section 4.6.3) on the FRF uncoupling method, it ensures that relative motion between DOFs on the structure of interest is not constrained. Second, the indirect test fixtures are all very simple in terms of their geometry, allowing them to be modelled easily.
For more generalised spatial uncoupling, the FE models may need to represent more complex structures, particularly if the indirect test fixture is to be used as a means of supporting the structure-under-test. This increased complexity should not be regarded as a major barrier, however. Fotsch [82], for example, demonstrated that if models of single components are constructed which are faithful to the structure's geometry in every detail, then the model's predictions will lie within the uncertainty associated with the structure's manufacturing tolerances and the material properties used.

It is essential in considering the "model and remove approach" that the problems associated with the FRF uncoupling method be noted here also. Referring to Figure 4.5.16, it is possible to see that even if the substructure models are perfectly accurate in terms of the mass distribution, the solution is still non-unique since the spring stiffness k_1^B is redundant in the assembly. In this case, no information would be available against which the stiffness parameter could be checked, as the natural frequencies and mode shapes of the assembly would be insensitive to it.
It was also demonstrated earlier that the FRF-based indirect testing equation was also ill-posed if the indirect test fixture possessed fewer modes within the observed frequency range than there were coupling DOFs. In spatial indirect testing this problem will not exist so long as the indirect test fixture is free-free and does not constrain relative motion between connection points, as in the case of multiple added masses, for example. Problems will start to occur, however, when the indirect test fixture is grounded, as in the case of the earlier numerical example. In this case, as the test fixture becomes stiffer, the assembly behaves increasingly as if the structure of interest were grounded at its connection DOFs. This will make it increasingly difficult to disassemble the two structures, until at the point that the test fixture becomes infinitely stiff, it will be an impossible task, as the connection DOFs of the assembly will have been deleted.

One further problem which is exclusive to the use of spatial models derived via the FE method is that, while the mass and stiffness matrices are readily available, the same cannot be said of the damping matrix. In the real world, the level of prevalent damping can couple close modes together making it difficult to separate them using existing modal analysis techniques. This can make the correlation of the extracted

experimental modes with FE data, which does not account for the damping effects difficult. The analysis and correlation of close modes forms a subject in its own right, with papers such as [83] and [89] providing possible solutions. It will suffice to say here that if such close modes occur they are likely to make the validation of the FE models involved more time consuming and costly.

These problems aside, there are several potential advantages to the use of accurate FE models. The first is that it is not usually necessary to include rotational data to validate FE models, although the inclusion of such data can be of value. Secondly, far fewer measurements would be required in order to validate an FE model than would be required by the FRF uncoupling technique, which requires at least three FRF matrices of dimensions $nc \times nc$, where *nc* is the number of connection DOFs. Thirdly, since the ultimate aim of the tests is likely to be the validation of an FE model, then it is logical to try and achieve this with as little manipulation of the raw data acquired in the testing phase as possible.

4.10 Conclusions

4.10.1 Indirect modal testing of structures

It has been shown that the indirect testing of structures is possible, although careful consideration must be given to the design of the test fixture. The method can provide the mass-normalised mode shapes of the structure of interest, although only those for which the connections DOFs are not nodes will be excited. Nonetheless, the method may be extremely useful when no other test method is suitable. Two possible routes to indirect modal testing have been discussed, one using the raw data obtained from modal tests directly and the other which uses these data in conjunction with modal

analysis to validate FE models. The application of these techniques to real structures forms the basis of the next chapter of this work.

4.10.2 Ramifications for the inference of information on internal components

Although the problems of ill-conditioning associated with the indirect modal testing of structures can be designed out of indirect test fixtures, the same does not apply to the situation where we require information on components located inside an assembly. Indeed, the purpose of encasing a component inside another structure is often to isolate it from the environmental conditions that are experienced by the casing. Furthermore, the joints and connections used within assemblies typically include multiple redundancies to ensure the mechanical integrity of the joints. It has been shown that the inclusion of such redundant connections leads to the uncoupling problem becoming underdetermined and therefore insoluble. It must therefore be concluded that the accurate inference of the dynamic properties of internal components will be extremely difficult, unless the joints between the casing and the internal component are designed in a manner that does not overly constrain the internal component/components of interest.

CHAPTER 5. APPLICATION OF INDIRECT TESTING MODAL TESTING

5.1 Introduction

In this chapter the application of indirect testing to real structures is discussed. Two case studies are presented: the first explores the application of the FRF indirect testing method to free-free beams; and the second aims to determine the free-free properties of the AWE MACE Case structure (pictured in Figure 5.3.1 on page 188) using indirect modal testing. Although the first case study demonstrates that the theory of FRF uncoupling as a means of indirect testing is sound, it also highlights just how difficult the method is to apply in practice. Application of the FRF indirect testing technique is unsuccessful for the more complex MACE Case structure, which requires multi-point connection to the indirect testing fixture, making it a more demanding application of the technique. In order to determine the free-free properties of the MACE Case an attempt is made to use the model-and-remove approach. Standard modal testing techniques are used to provide data for the validation of high-fidelity FE "super models" of the indirect test fixture and the test fixture / MACE Case assembly. The test fixture is then removed from the FE assembly model and the resulting MACE Case model is shown to be valid over the frequency range 0-2000Hz.

5.2 Case study one: free-free beam

5.2.1 Background

The simple free-free beam provides an ideal test piece for indirect testing, the vibration properties of beams have been well defined mathematically for many years and the free-free boundary condition is the most simple to approximate in the laboratory introducing few uncertainties. Also, since the orthogonal modes of beams

are effectively de-coupled from one another, measurements can be made in only one or two of the three directions reducing the total number of measurements required for the indirect testing calculation. Even with these advantages however, the free-free beam still poses a significant challenge for FRF-based indirect testing since data relating to the RDOFs must be measured and because high quality FRF data is required. The aim of the experiment was to determine the free-free modes of a beam (beam B) based upon measurements made on two other beams (beam A and beam C) as illustrated in Figure 5.2.1.

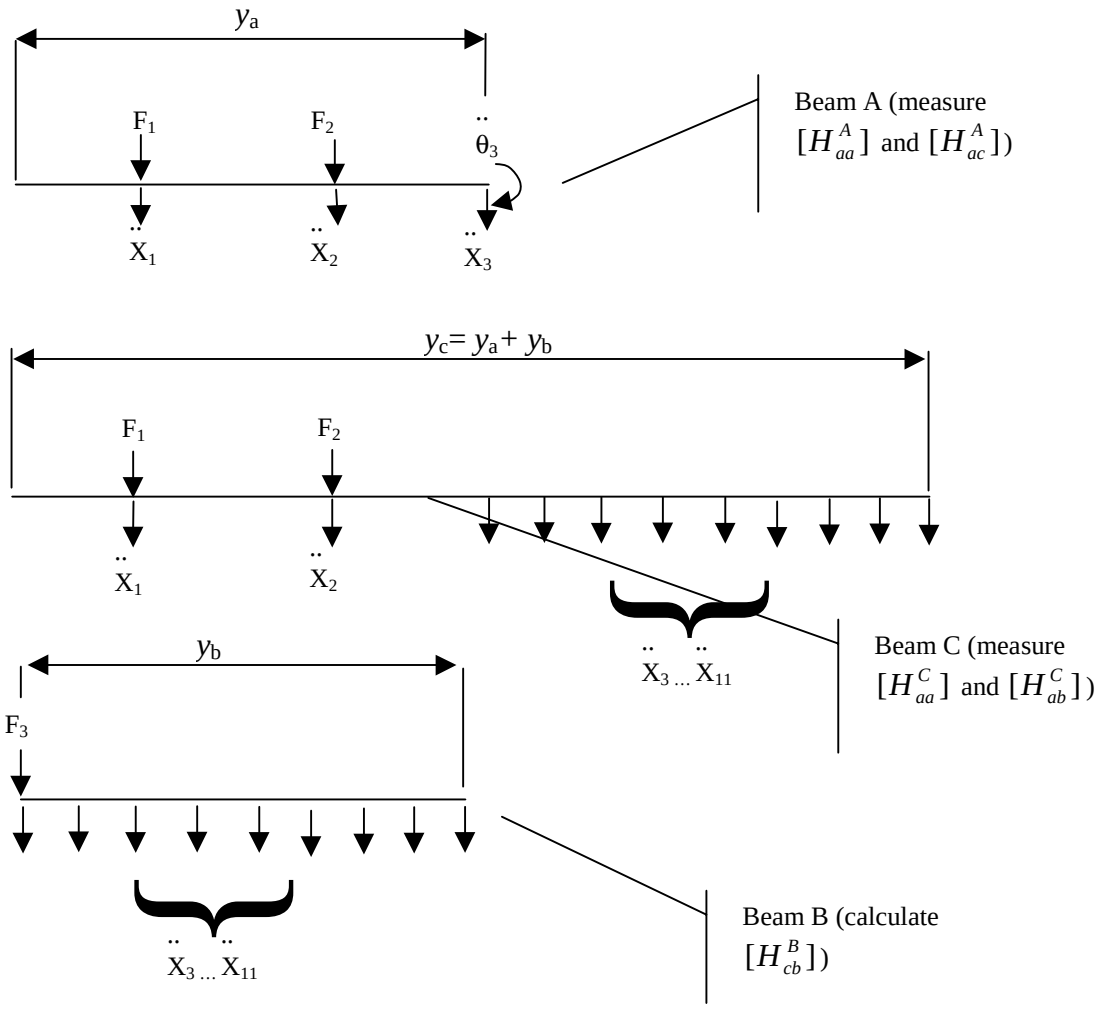

Figure 5.2.1. Illustration of the indirect testing of a beam (beam B) showing the required measurements on beams A and C.

5.2.2 Method and results

Two aluminium alloy bars, A and C were procured to the specifications given in Figure 5.2.2(a) and Figure 5.2.2(b). The experimental set-ups used for the measurements on beam A and beam C are shown in Figure 5.2.2 (a) and (b) respectively.

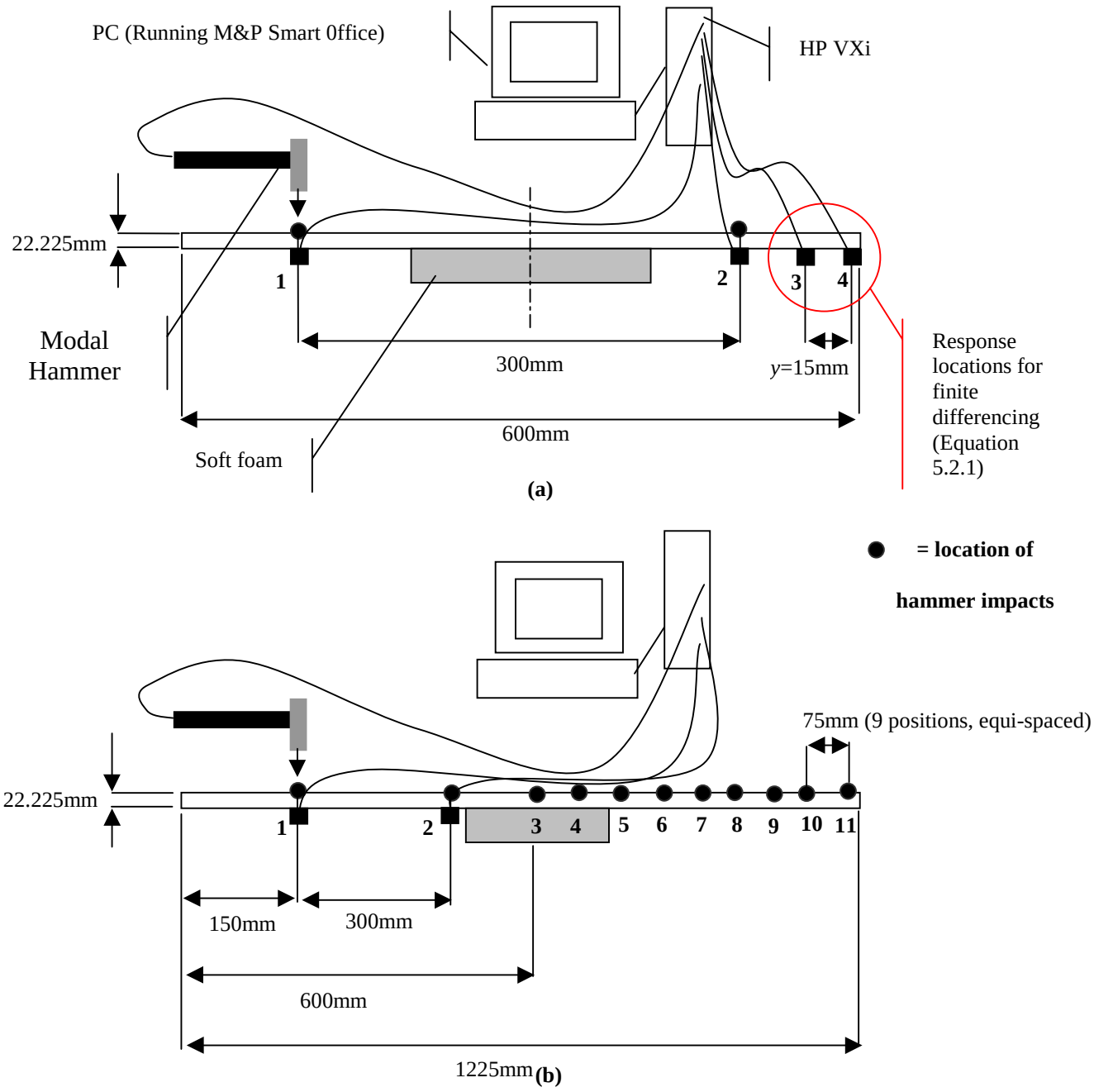

Figure 5.2.2. Test configurations use for the indirect testing of a beam: (a) experimental set-up for beam A; (b) experimental set-up for beam C.

The suspension of the beams on soft foam introduced damping sufficient to cause the response of the beam to die away within the measurement time of 1.27 seconds and the FRFs were estimated using 4096 spectral lines giving a frequency resolution of 0.78 Hz. Only a single impact at each location was used to excite the structure so that blurring of the anti-resonances due to measurement averaging was avoided. The FRFs relating to the translational responses at locations 3 and 4 were used to provide an estimate of the translational and rotational FRFs of beam A's tip according to Equation (5.2.1) - a and b respectively[15]. The FRFs resulting from the application of Equation a and b to the measured data are shown in Figure 5.2.3.

$$H_{xx} = \frac{H_{ax} + H_{bx}}{2} \qquad \text{(a)}$$

$$H_{x\theta} = \frac{H_{ax} - H_{bx}}{y} \qquad \text{(b)} \qquad (5.2.1)$$

The raw data was read into Matlab and used to populate the matrices $\left[H_{aa}^{A}\right]$, $\left[H_{aa}^{C}\right], \left[H_{ac}^{A}\right]$ which were then used to calculate the coupled system matrix [T] using Equation 4.4.6. Figure 5.2.4 shows the estimate of $T_{3x,3x}$ obtained from the indirect testing calculation.

[15] Note: The transfer FRFs calculated using these equations are referred to as H_{1x3x}^{A}, H_{2x3x}^{A}, $H_{1x3\theta z}^{A}$ and $H_{2x3\theta z}^{A}$.

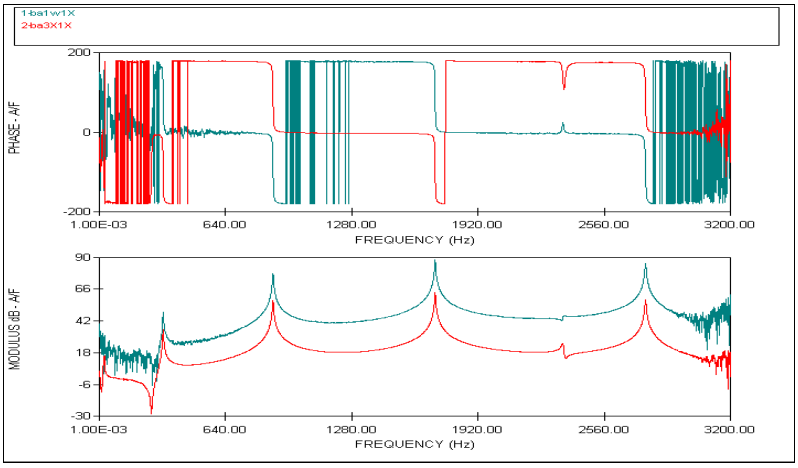

(a)

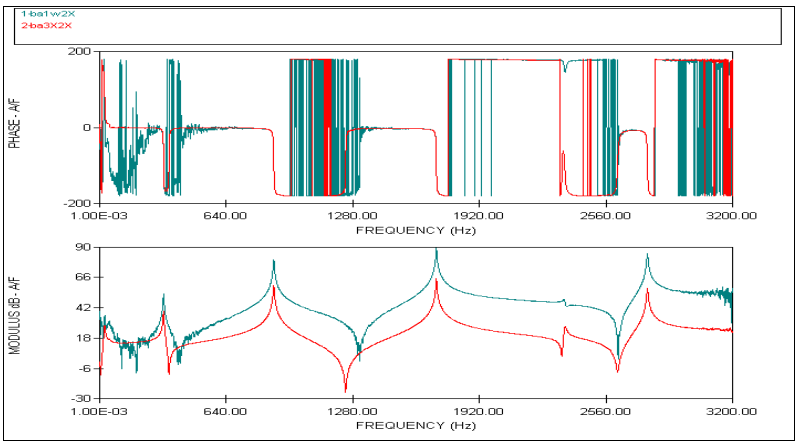

(b)

Figure 5.2.3. Estimates of translational (red) and rotational (green) FRFs: (a) $H^{A}_{1x,3x}$ and $H^{A}_{1x,3\theta z}$; (b) $H^{A}_{2x,3x}$ and $H^{A}_{2x,3\theta z}$

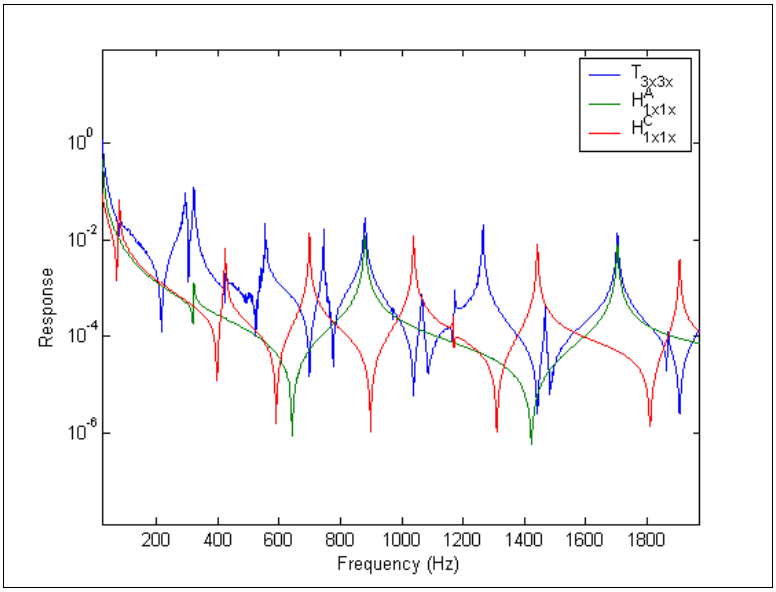

Figure 5.2.4. Estimate of $T_{3x,3x}$ (overlaid on $H^{A}_{1x,1x}$ and $H^{C}_{1x,1x}$) showing at least 4 new resonant peaks.

The estimate of $T_{3x,3x}$ in Figure 5.2.4 shows at least four new resonant peaks. It is also interesting to note that the resonances of H^{C}_{1x1x} are all at frequencies corresponding to anti-resonances of $T_{3x,3x}$. Despite the apparent smoothness of the curve $T_{3x,3x}$ attempts at modal parameter extraction on the new peaks it showed were not successful because the data was noisy in the vicinity of the new peaks (as shown in Figure 5.2.5). The noise on the new peaks is a consequence of the calculation being naturally ill-conditioned at frequencies in the vicinity of the new resonances.

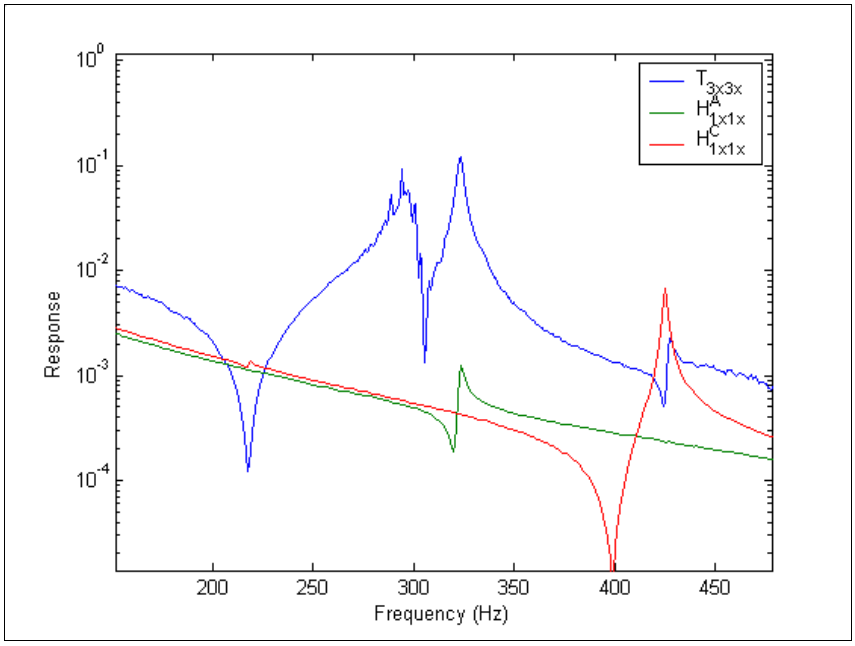

Figure 5.2.5. Zoomed portion of Figure 5.2.4 showing an example of noise on the new peaks.

As discussed in Chapter 4, even small amounts of noise on the FRF data used in the indirect testing calculation can have a catastrophic result when the problem becomes ill-conditioned. For this reason the FRFs obtained in the experiments were curve-fitted using the line-fitting modal parameter extraction method provide in the ICATS Modent software. High and low residuals terms were then calculated for each FRF using the pseudo-mode approach. Examples of the curve fitted estimates (shown in red) of the measured FRF data (shown in green) are shown in Figure 5.2.6.

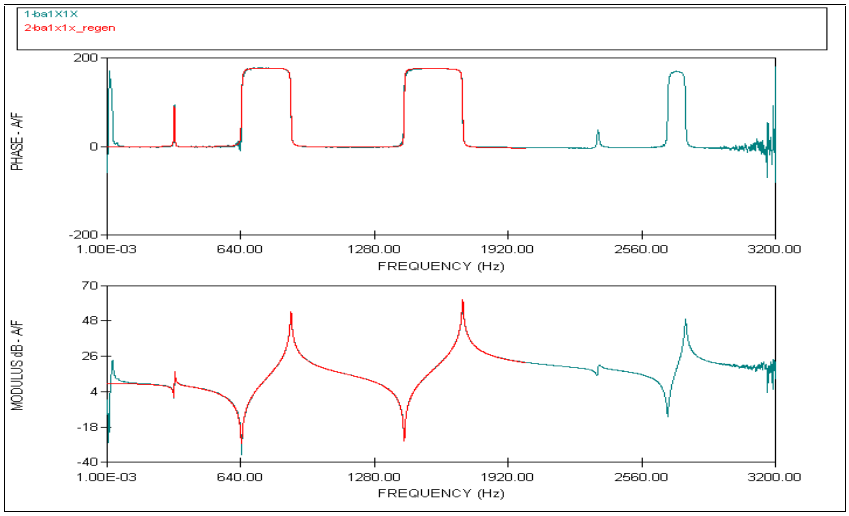

(a)

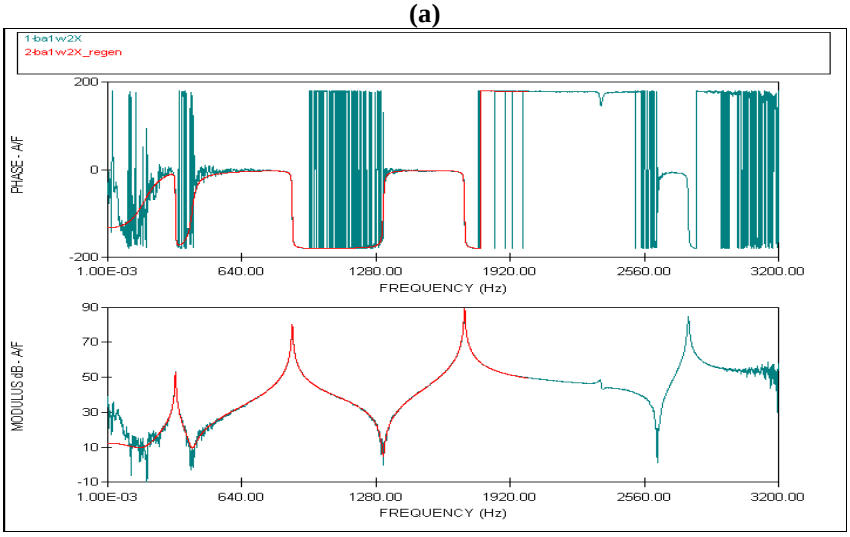

(b)

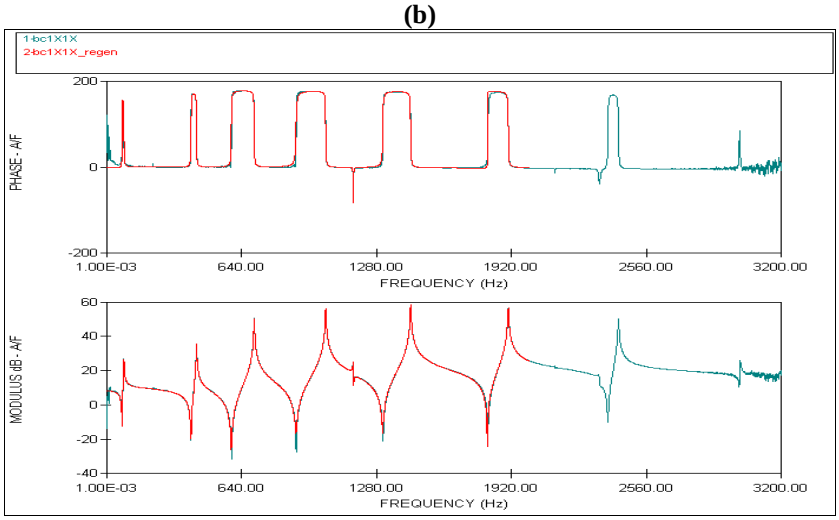

(c)

Figure 5.2.6. Example of modal curve fits (red) overlaid on raw FRF data (green) for FRFs: (a) $H^{A}_{1x,1x}$**; (b)** $H^{A}_{1x,3\theta z}$**; (c)** $H^{C}_{1x,1x}$

After curve fitting the FRFs were regenerated within Matlab over the frequency range 0-2000Hz with a resolution of 0.5Hz and were used to form the matrices $\left[H_{aa}^{A}\right]$, $\left[H_{ac}^{A}\right]$, $\left[H_{aa}^{C}\right]$ and $\left[H_{ab}^{C}\right]$for the indirect testing equations (Equations 4.4.6 and 4.4.10). Figure 5.2.7 shows the estimate of an element of the coupled system matrix ($T_{3x,3x}$) computed using the curve fitted data, overlaid on the curve fitted data for H_{1x1x}^{A} and H_{1x1x}^{C}. Figure 5.2.7 shows that when applied to the curve-fitted data the indirect testing calculation has predicted what appear to be three new resonant peaks at the locations indicated.

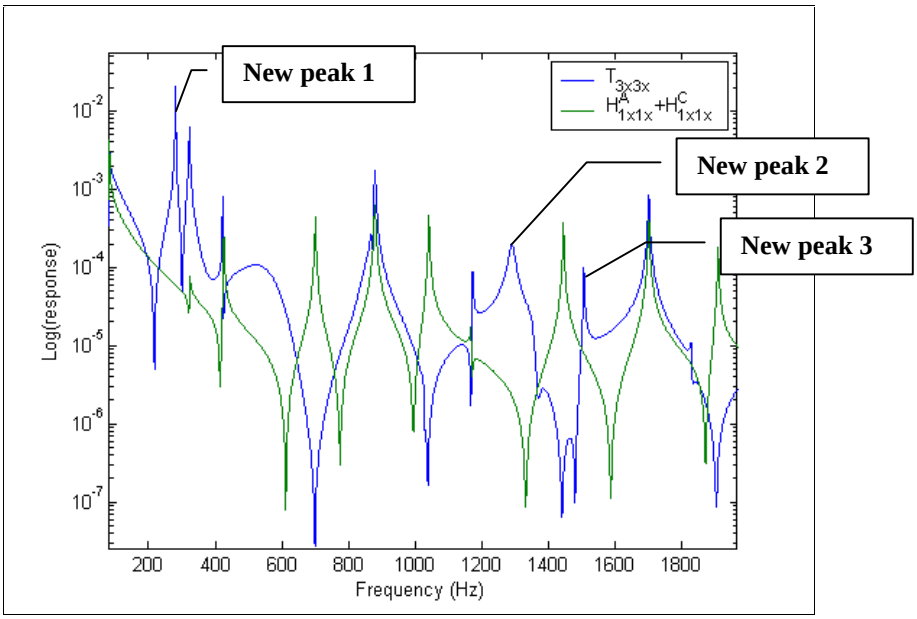

Figure 5.2.7. Estimate of $T_{3x,3x}$ overlaid on the curve given by $H_{1x,1x}^{A} + H_{1x,1x}^{C}$

Figure 5.2.8 shows a few examples of the 9 FRFs computed via the indirect testing equations for beam B. These FRFs were analysed using the Global-M curve fitting modal parameter extraction method provided in the ICATS Modent suite. The first two peaks were readily analysed however, Global-M analysis of the third peak would not converge. The mode shapes extracted from modal analysis of the first two peaks are shown in Figure 5.2.9. The mode shape shown in Figure 5.2.9(a) is clearly the

first bending mode of a free-free beam and has a natural frequency of 280 Hz, 5% lower than the theoretical natural frequency (295Hz) for the first bending for an aluminium alloy[16] beam of dimensions 625mm×22.225mm×22.225mm . The second mode (Figure 5.2.9 (b)) at 1291 Hz is similar to the third bending of a beam although there is some distortion at node 10. However the error in frequency against the theoretical value for the third bending mode (1596 Hz) is around 20% . Given the lack of confidence in the mode shape and the large frequency error, the second mode was considered to be caused by inaccurate data being used in the indirect testing calculation.

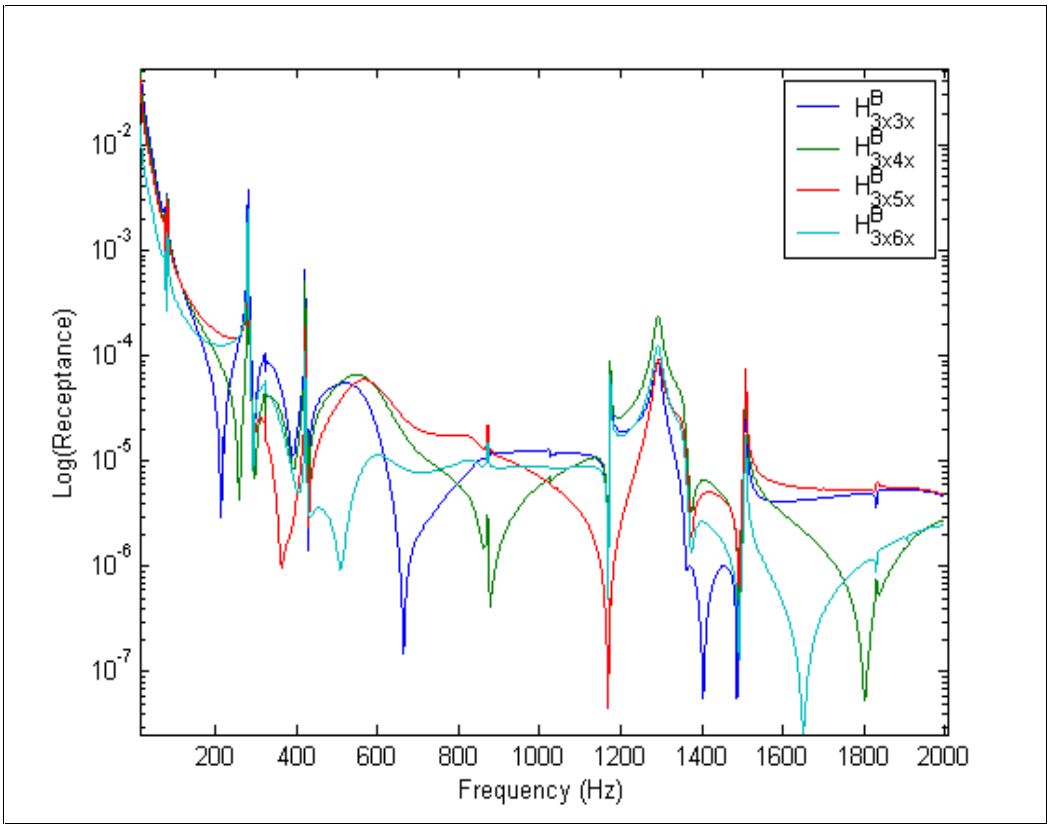

Figure 5.2.8. Example estimates of the free-free FRFs of beam B calculated via the indirect testing method.

[16] With the assumed material properties $E=69\times10^9$ N/m^2, $\rho=2710$ kg/ m^3.

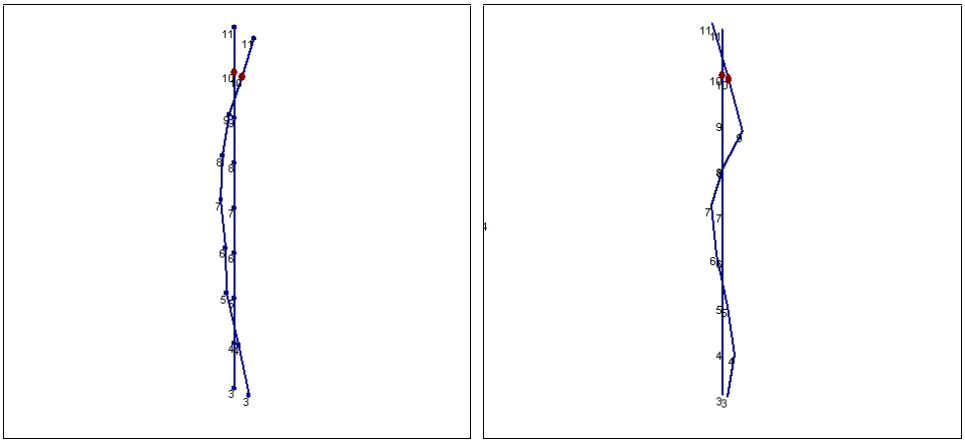

(a) **(b)**

Figure 5.2.9. Examples of mode shapes obtained from modal analysis of FRFs obtained via the indirect testing calculation: (a) mode at 280 Hz; (b) mode at 1291 Hz.

5.2.3 Discussion

From the results presented in the previous section it appears that while the indirect testing method has worked well at frequencies up to the first bending mode of beam B it is less than successful at higher frequencies. Since the dynamic characteristics of beams are well defined analytically it is possible to use virtual testing to understand why the calculation fails to accurately predict the higher modes of beam B.

The first possibility for the calculation's inaccuracy at high frequency could of course be the ill conditioned nature of the FRF-based indirect testing method. However, in this case the structure under test (beam B) is not overly constrained by the test fixture (beam A) and the selected remote measurement DOFs are well separated and do not behave in a near-rigid fashion across the frequency range. Therefore the two major sources of ill-conditioning of the indirect coupling calculation discussed in Chapter 4 do not apply to the present case. This fact is borne out by the generally smooth nature of the estimate of $T_{3x,3x}$ given in Figure 5.2.4 from which it is clear that the measurement noise has not had a catastrophic effect on the result of the calculation.

Also, it is possible to estimate the actual condition of the problem using the numerically "perfect" data provided by FE models[17] of beam A and beam C. The condition number with respect to inversion against frequency plot for the remote measurement locations at distances 150mm and 450mm along the beam is shown in Figure 5.2.10. This plot shows that the problem is reasonably well conditioned across the frequency range, and except close to natural frequencies of the sub-structures, the condition number is generally less than 1000.

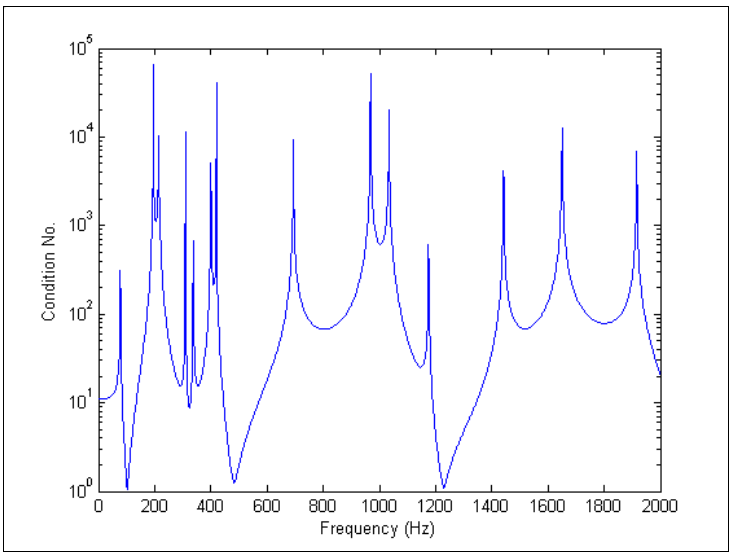

Figure 5.2.10. Analytically derived condition number with respect to inversion Vs. Frequency plot for the uncoupling of beam A and beam B.

A second likely source of error is the estimation of the rotations via the finite difference method (Equation (5.2.1)), which as discussed in Chapter 4 is prone to transverse sensitivity errors. However, when the FRFs relating to these RDOFs were computed from the FE model of structure A, it was found that they compared well (in terms of their overall shape) to the measured rotations as shown in Figure 5.2.11.

[17] The beams were modelled in Ansys using beam3 elements, having material properties: ρ = 2710 kg/m^3; E=69GN/m^2 and μ=0.33.

Such good results are not really surprising because the orthogonal modes of beams are essentially uncoupled meaning there is little or no cross-axis motion for the transducers to pick-up. Good comparisons between the analytical and experimental results were also obtained for the translational FRFs computed using Equation 5.2.1 (and indeed all the other measured FRFs) , which are also shown in Figure 5.2.11.

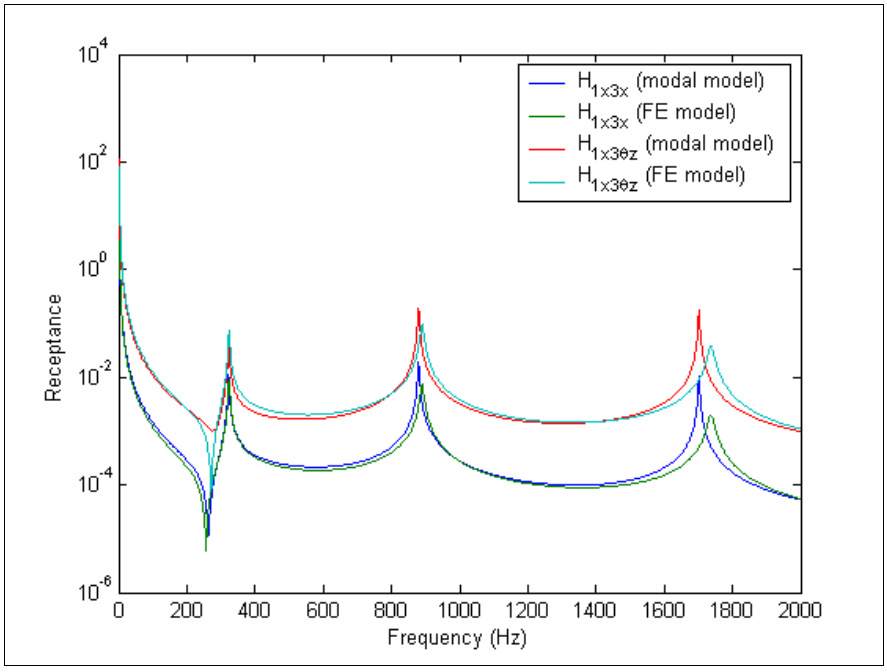

(a)

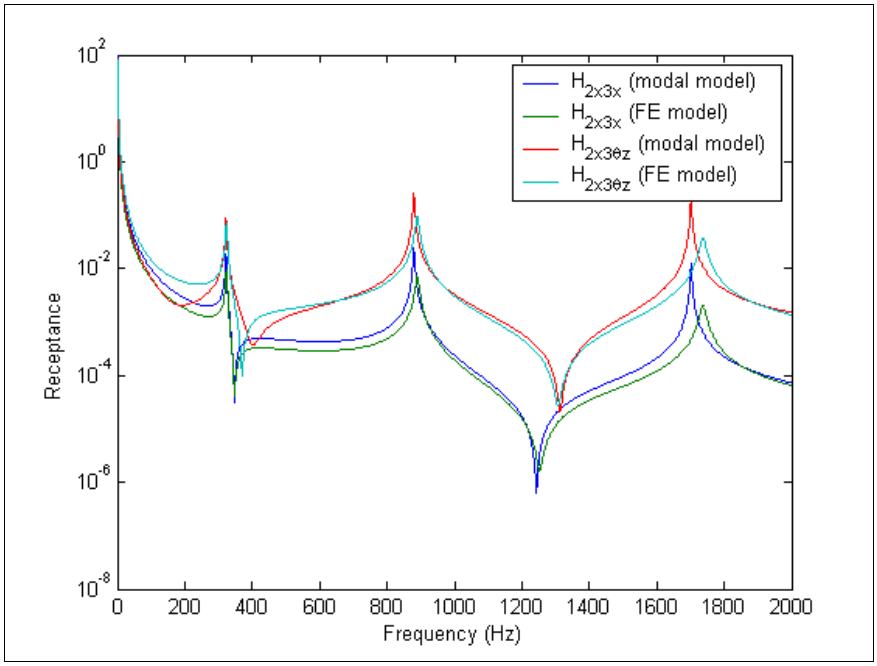

(b)

Figure 5.2.11. Examples of curve-fitted translational and rotational FRFs derived using Equation 5.2.1 overlaid on FRF curves derived from an FE model.

Having eliminated the two most obvious sources of error in the calculation as the main factors in the poor performance of the indirect test at high-frequency, attention turned to the precise conditions of the test and the assumptions which had been made. The most significant assumption made by the indirect testing method is that of reciprocity, which conveniently allows the problems associated with the measurement of point rotations (moment input, angular acceleration output) to be avoided. From examination of the reciprocity plot of Figure 5.2.12 it is clear that while a good level of reciprocity has been achieved with the test method (almost certainly a level sufficient for DTA level 3 and 4 modal testing applications) the transfer function estimates do not overlay exactly.

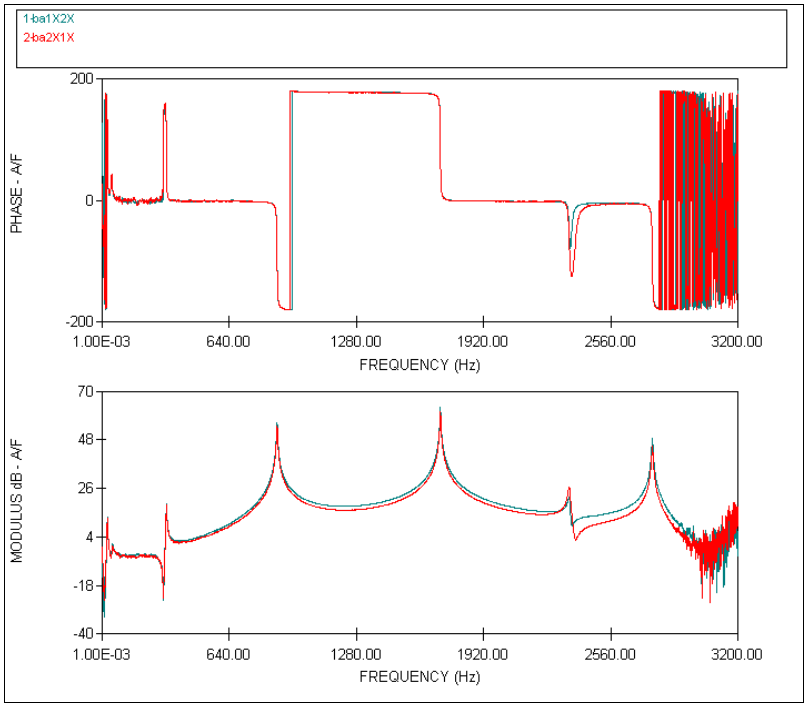

Figure 5.2.12. Example of reciprocity achieved with the test configuration, H^{A}_{1x2x} (green) and H^{A}_{2x1x} (red).

In fact the FRFs H^{A}_{1x2x} and H^{A}_{2x1x} estimates tend to drift apart with increasing frequency, as the assumption that the force is applied exactly at the reference co-ordinate becomes increasingly less realistic. It is interesting to consider just how the indirect testing equation behaves when perfect reciprocity is assumed rather than

achieved with the test configuration. For example, consider the case illustrated in Figure 5.2.13 in which the forces are applied at positions A and D, and responses are measured at points B and C.

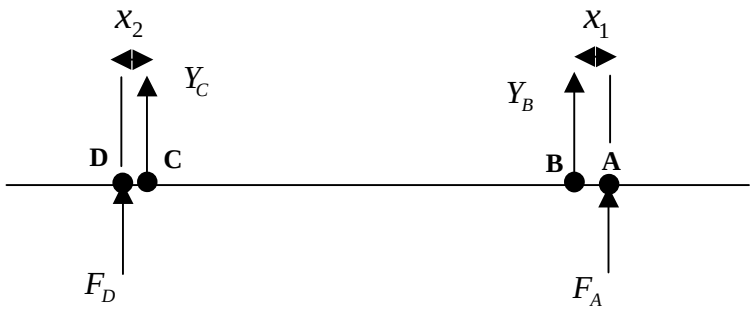

Figure 5.2.13. Illustration of how incorrect assumptions relating to excitation and reference locations lead to reciprocity errors.

It is clear that the transfer function , $\frac{Y_b}{F_a}$, will be a good approximation to the point FRF, $\frac{Y_b}{F_b}$, over a limited frequency range (the extent of this frequency range will be related to the distance x_1 and the proximity of the points A and B to nodes/anti-nodes). The transfer function , $\frac{Y_c}{F_a}$, will also be a good approximation to, $\frac{Y_c}{F_b}$, over the same limited frequency range but the fact remains that, $\frac{Y_b}{F_d} \neq \frac{Y_c}{F_a}$. In the simple case of Figure 5.2.13 the amount of error between the transfer FRFs is dependant upon the excitation frequency and the errors in the distances (x_1 and x_2) between the intended excitation locations (points B and C) and the actual excitation locations (points A and D). Essentially, as far as the indirect testing calculation is concerned, the beam's length will appear to vary with frequency, a natural consequence of describing the beam by its (inaccurately) observed behaviour. The effect of not achieving a good level of reciprocity in the test, but (erroneously) assuming it in the indirect testing calculation is readily simulated using finite element models of the beams A and C.

Beam A was modelled such that certain "key" nodes were positioned at the locations shown Figure 5.2.14. These key node locations were also replicated in the model of the longer beam C.

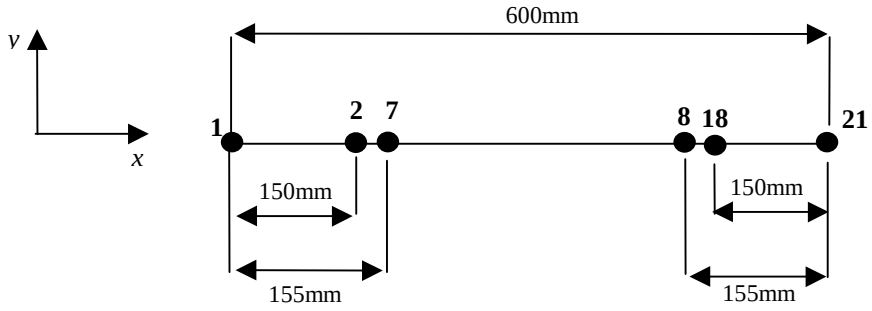

Figure 5.2.14. Key node locations (finite element model numbering) for the virtual test investigation into the effects of assuming reciprocity.

The assumed point FRFs H^{A}_{2y7y} and H^{A}_{18y8y} were calculated, as was a single transfer FRF H^{A}_{2y18y}. These FRFs are overlaid on the true point and transfer FRFs H^{A}_{7y7y}, H^{A}_{18y18y} and H^{A}_{7y18y} in Figure 5.2.15, in which a frequency dependent error, resembling the "residual error" is clearly visible. It should also be noted that the assumed point FRFs (H^{A}_{2y7y} and H^{A}_{18y8y}) are clearly plausible within the frequency range, with anti-resonance following resonance in the expected fashion. Assumed point and transfer FRFs were also generated for the same co-ordinates on beam C. The assumed point and transfer FRFs were then used to populate the Auto-FRF matrix for beam A ($\left[H^{A}_{aa}\right]_{est}$) and Beam C ($\left[H^{C}_{aa}\right]_{est}$) such they were given by:

$$\left[H^{A}_{aa}\right]_{est}=\begin{bmatrix} H^{A}_{2y7y} & H^{A}_{2y18y} \\ H^{A}_{18y2y} & H^{A}_{7y18y} \end{bmatrix} \text{ and } \left[H^{C}_{aa}\right]_{est}=\begin{bmatrix} H^{C}_{2y7y} & H^{C}_{2y18y} \\ H^{C}_{18y2y} & H^{C}_{7y18y} \end{bmatrix}$$

The cross-FRF matrix ($\left[H^{A}_{ac}\right]_{est}$) was calculated assuming excitation at 2*y* and 8*y* and was given by: $\left[H^{C}_{ac}\right]_{est}=\begin{bmatrix} H^{A}_{2y21y} & H^{A}_{2y21\theta z} \\ H^{A}_{8y21y} & H^{A}_{8y21\theta z} \end{bmatrix}$

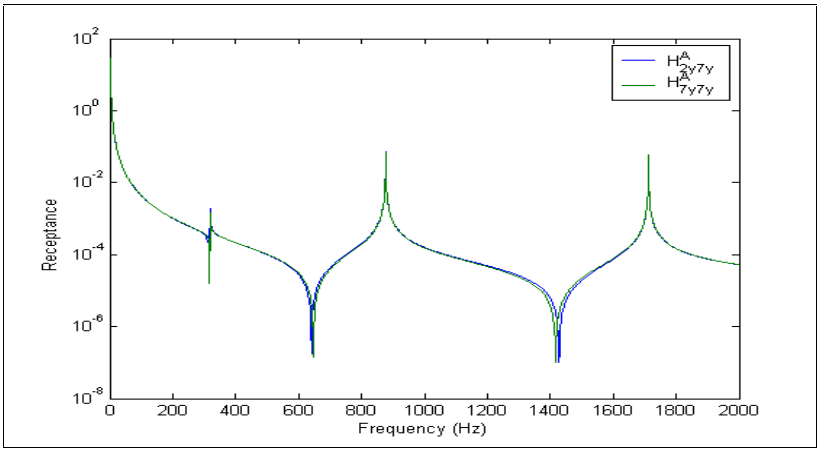

(a)

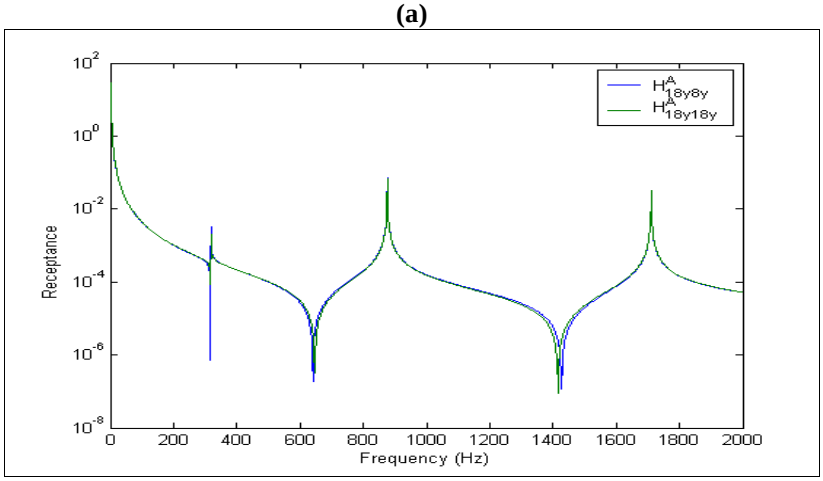

(b)

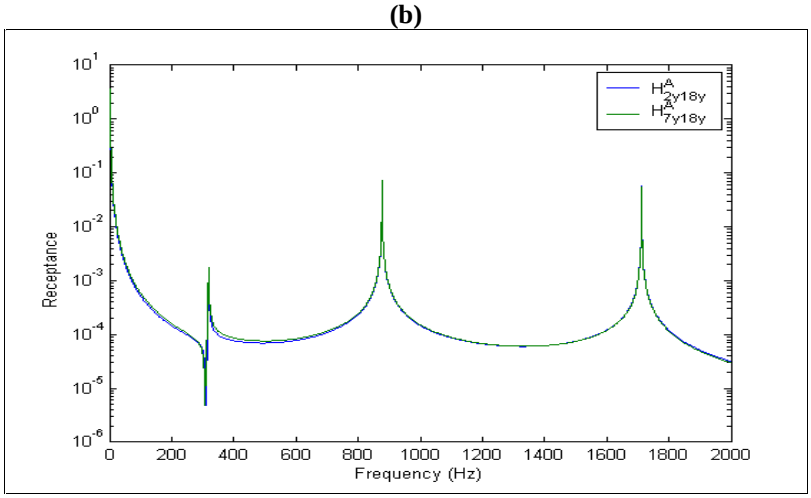

(c)

Figure 5.2.15. Examples of analytical FRFs including reciprocity errors (blue) overlaid on true FRF curves (green).

These FRF matrices were then used as inputs to the indirect testing calculation (Equation 4.4.6) in order to calculate the estimated coupled structure matrix $[T_{est}]$.

Figure 5.2.16 shows the estimate of $T_{est3y,3y}$ resulting from this calculation overlaid on the true curve $T_{3y,3y}$ computed using the correct auto and cross-FRF matrices:

$$\left[H_{aa}^{A}\right]=\begin{bmatrix} H_{7y7y}^{A} & H_{7y18y}^{A} \\ H_{18y7y}^{A} & H_{18y18y}^{A} \end{bmatrix};\ \left[H_{aa}^{C}\right]=\begin{bmatrix} H_{7y7y}^{C} & H_{7y18y}^{C} \\ H_{18y7y}^{C} & H_{18y18y}^{C} \end{bmatrix}\ \text{and};\left[H_{ac}^{C}\right]=\begin{bmatrix} H_{7y21y}^{A} & H_{7y21\theta z}^{A} \\ H_{18y21y}^{A} & H_{18y21\theta z}^{A} \end{bmatrix}$$

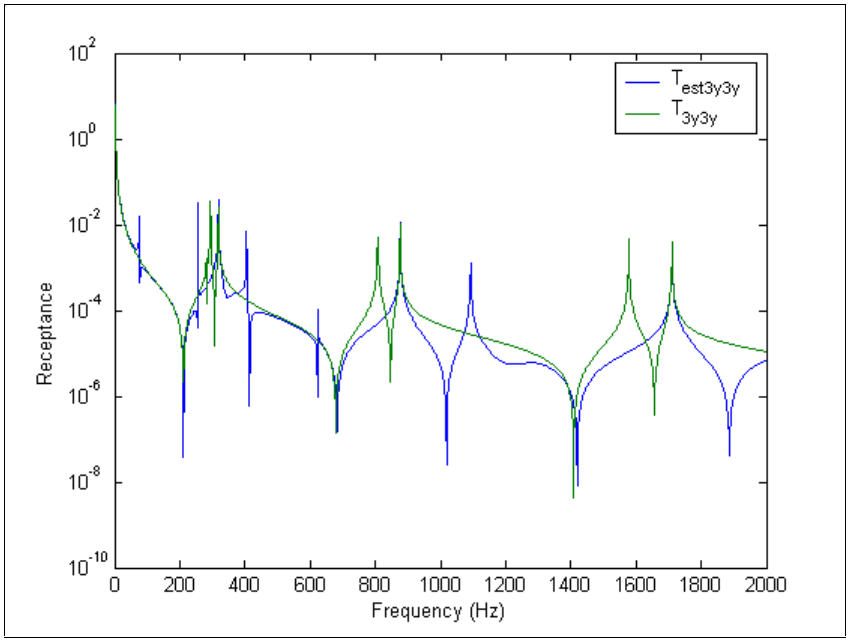

Figure 5.2.16. Estimate of an element ($T_{est3y3y}$)of the coupled system matrix [T_{est}] overlaid on the true curve (T_{3y3y}).

It is clear from Figure 5.2.16 that serious errors in the estimation have been introduced as a result of assuming reciprocity, with the calculation failing to predict all of the new peaks as well as generating spurious ones, in a manner similar to that seen in the real experiment.

5.2.4 Conclusions.

The mode shape obtained in Figure 5.2.9(a) demonstrates that indirect testing can work although its successful application is extremely difficult. In addition to the careful design of the test fixture, as discussed in Chapter 4, the FRF-based indirect testing method also requires extremely accurate measurements. The requirement for

measurement accuracy stems from the fact that the results of the indirect testing calculation can **only** be relied upon while the assumption of reciprocity holds true. One way in which a sufficient level of reciprocity might be achieved across the entire frequency range would be to test the beams A and C using two shakers and impedance heads, in an effort to ensure "true" point and transfer FRFs. As discussed in Chapter 4 however, the use of shaker excitation for the purpose of indirect excitation is of limited practical applicability and cannot be viewed as a general solution to the sensitivity of the calculation to reciprocity errors.

5.3 Case study two: the MACE Case

5.3.1 Background

The Modal Analysis Correlation Exercise (MACE) assembly (see Figure 5.3.1) was developed by the AWE as a test vehicle for modal testing and FE methods in the 1990s. The MACE Case (highlighted in Figure 5.3.1) is conical having a cone angle of 4°. It incorporates three slots (included so that the structure was not completely axi-symmetric) and a number of internal flanges to which additional components can be attached to create the full MACE assembly.

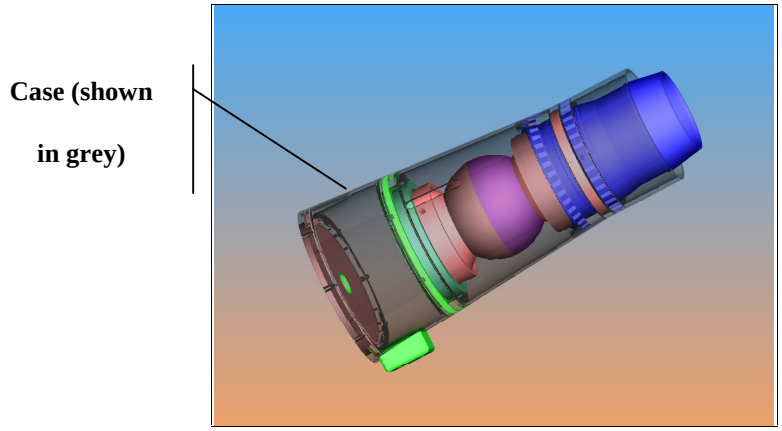

Figure 5.3.1. The MACE assembly.

The MACE Case was selected as the structure under test for the present study into indirect excitation methods as it was considered to have a reasonably complex geometry and because it could be attached to an indirect test fixture in a similar manner to the actual structures for which the methods developed in this thesis are intended. The free-free modal properties of the MACE Case, obtained using standard excitation and response methods, were also well documented [68] so that comparisons with previous test results were possible.

The objective of the indirect testing experiments conducted on the MACE Case were to determine its free-free modes over the frequency range 0-2000Hz, based upon measurements made while the structure was attached to a fixed-base indirect test fixture.

5.3.2 Indirect testing of the MACE Case using FRF uncoupling technique

5.3.2.1 Design of the Indirect Testing Fixture (ITF)

Based upon the theory reported in Chapter 4, the essential requirements of an indirect test fixture are that it is sufficiently flexible that it does not prevent relative motion of the structure under test at the connection DOFs and that it should possess at least as many modes within the frequency range of the test as there are coupling DOFs. The MACE Case was to be attached to the structure at 4 connection locations, a 24 DOF coupling. In Chapter 4 it was shown that the ideal solution was to design the test-fixture as *n* separate components where *n* is the number of connection points, which reduced the number of measurements required and improved the indirect coupling calculation's numerical stability. In practice, however, this was found to be impractical, since in addition to the requirement for flexibility, there was also a

requirement for mechanical strength, since the indirect test fixture had to be load-bearing. Simple inverted L-shaped designs (such as those used in the virtual test of Section 4.6.3) give rise to high bending stresses at the junction between the vertical and horizontal elements and at the leg/ground interface. The introduction of diagonal braces (see Figure 5.3.2) reduces the bending stress at the vertical/horizontal junction, but increases the stiffness in the *x* and *y* directions.

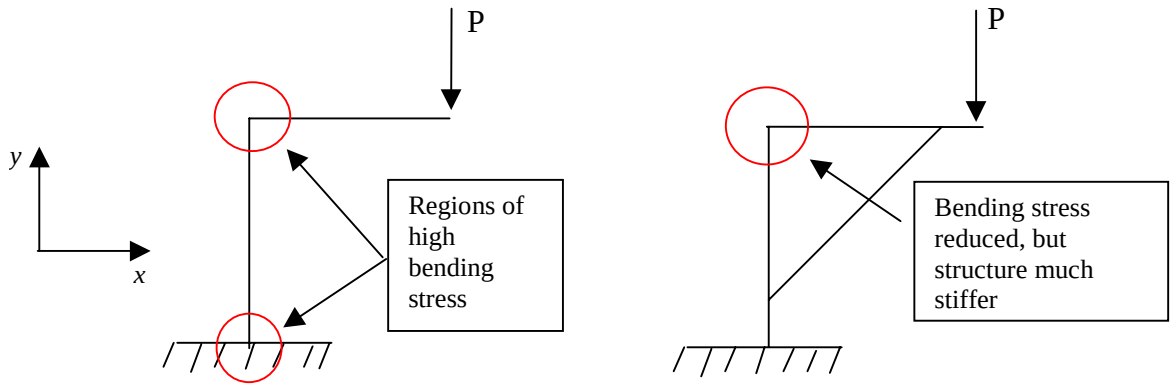

Figure 5.3.2. Problems in meeting the flexibility and strength requirements for the ITF when designed as 4 individual components.

For the MACE Case, the conflicting requirements for both mechanical strength and flexibility of the ITF finally gave rise to the design given in Figure A.1.1 of Appendix 1. When rigidly grounded the FE model of the test fixture was found to posses 39 modes within the frequency range of interest and many of these were found to show relative motion between the connection locations in both the *x* and *y* directions (see Figure 5.3.3 for example) . Most importantly, relative motion between the connection points was observed at frequencies much lower than the first natural frequency of the free-free MACE Case (determined as 585Hz in previous experiments as part of the MACE project) and which was known to be the “first ovaling” (2 nodal diameters, no nodal lines) mode of the case. It was therefore concluded that the frame was

sufficiently flexible not to overly constrain relative motion of the Case between the connection points. The design was not optimal however, since it consisted of 1, and not 4 components, meaning that 3 full matrices of dimensions 24×24 were required for the indirect testing calculations.

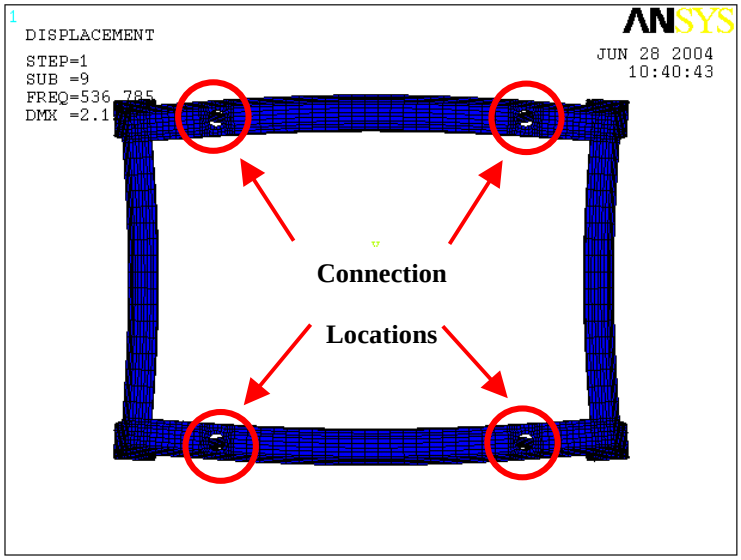

Figure 5.3.3. Example mode (536 Hz) of rigidly grounded ITF showing relative motion between the connection locations.

Attention was also paid to the design of the bolts (see Figure 5.3.4) used to connect the MACE Case to the ITF, which included a 1.5mm thick, 12mm diameter flange incorporated to ensure point contact at the connection locations.

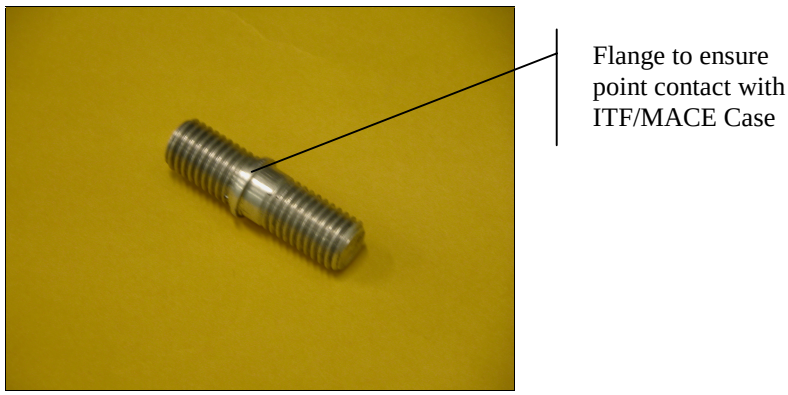

Figure 5.3.4. Purpose designed bolt for connecting the MACE Case to the ITF.

5.3.2.2 Attempts at FRF-based indirect testing of the MACE Case

With the design of the frame complete, attempts were made to determine the free-free modes of the MACE Case using the FRF coupling method as illustrated in Figure 5.3.5. Initial experiments were conducted in an attempt to determine the coupled structure matrix [T] **only** and so no measurements of DOFs on the MACE Case were made.

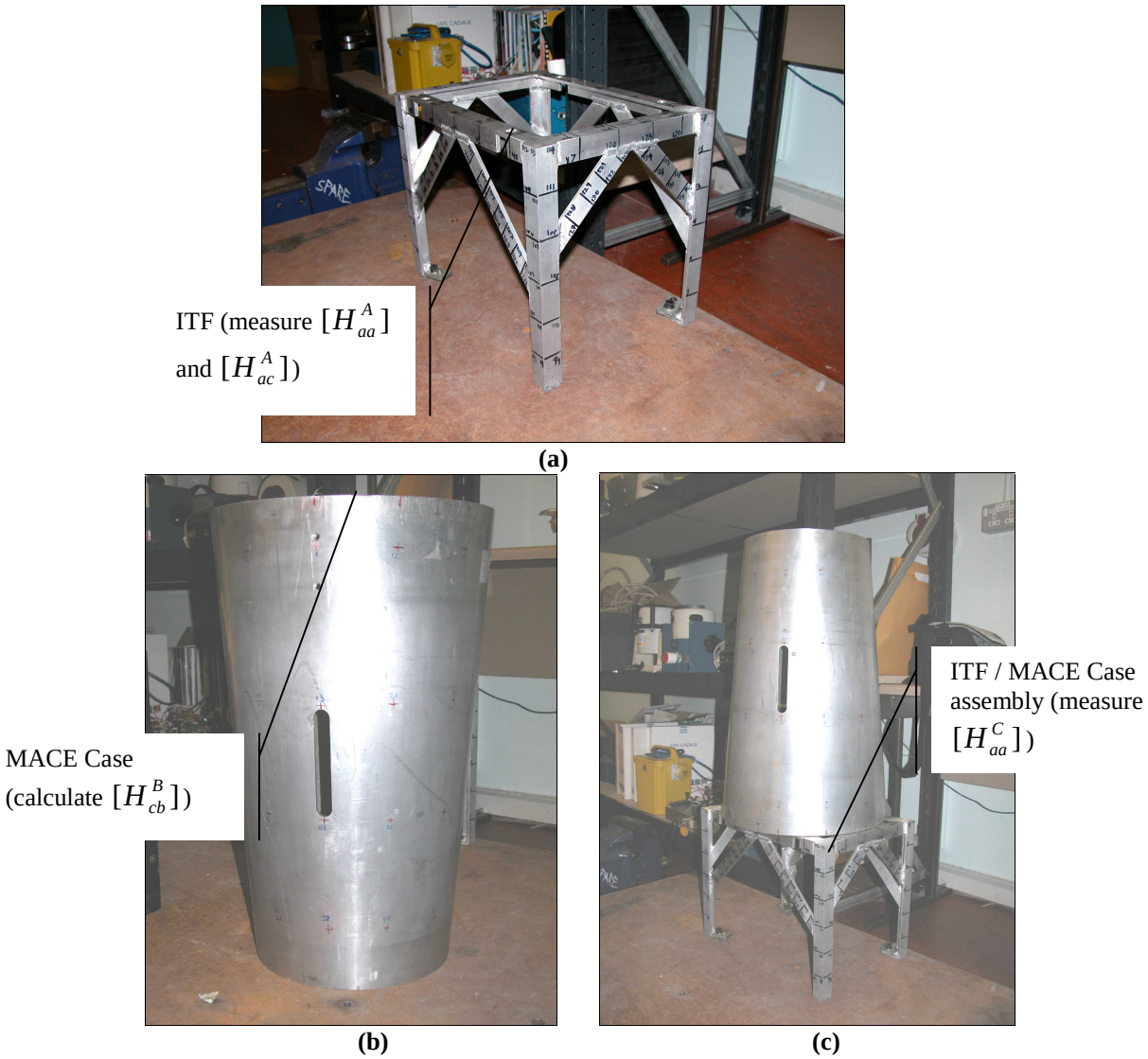

Figure 5.3.5. Indirect testing of the MACE Case: (a) the Indirect Testing Fixture (ITF); (b) the MACE Case; (c) the ITF/MACE Case assembly.

Efforts to use the EI calculation to determine the optimum remote measurement DOFs were hampered by the fact that many of the DOFs with high values of EI were either

inaccessible when the MACE Case was placed upon the test fixture or because they were situated on the extremely compliant diagonal cross-braces (see Figure 5.3.6).

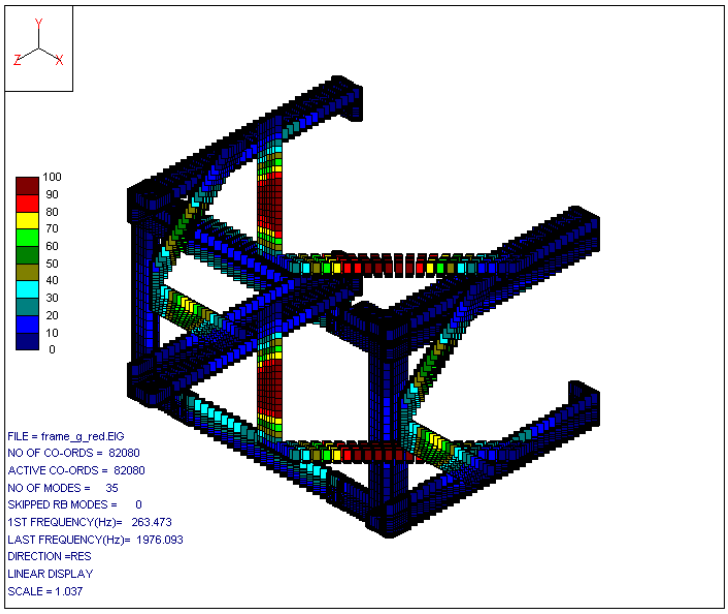

Figure 5.3.6. Plot of EI showing how the best remote measurement DOFs are located on the diagonal cross braces of the ITF.

The FRF-based indirect testing method requires excitation at every remote excitation DOF and it was found to be extremely difficult to get measurements to trigger when hammer excitation was applied to the cross-braces, or obtain a flat force spectrum over the range 0-2000Hz. After some experimentation to determine locations on the ITF which were sufficiently stiff to allow hammer excitation to be imparted both before and after the MACE Case was attached to it, the remote measurement locations were selected as those shown in Figure 5.3.7.

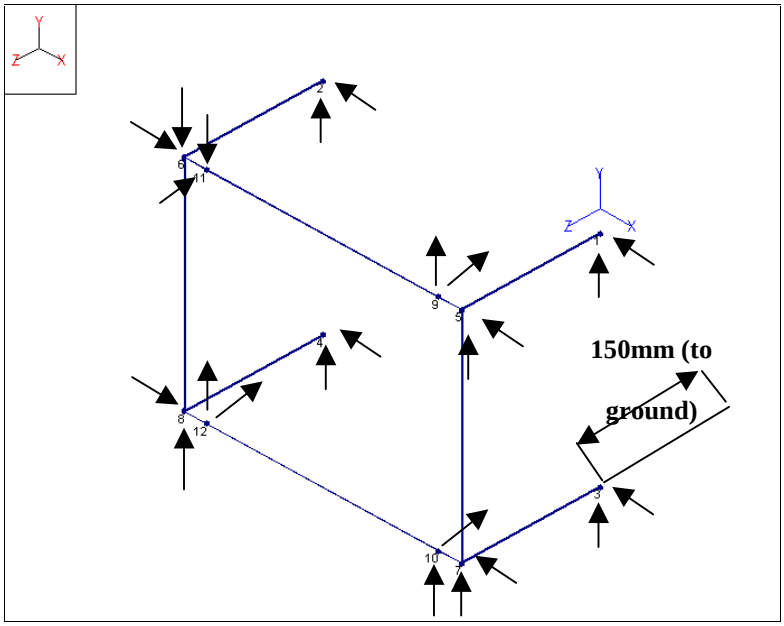

Figure 5.3.7. Measurement geometry for FRF-based indirect testing.

The 900 FRF measurements[18] required to populate the three 24 by 24 matrices $\left[H_{aa}^{A}\right]$, $\left[H_{aa}^{C}\right]$and $\left[H_{ac}^{A}\right]$ were then made. Examples of the FRFs obtained from measurements on the ITF and on the ITF/MACE Case assembly are shown in Figure 5.3.8. As in the previous case study (Section 5.2) the required translational and rotational FRFs for the matrix $\left[H_{ac}^{A}\right]$were derived using the finite difference method (Equation 5.2.1). The raw FRF Data was read into Matlab and was used as input to the indirect testing calculation (Equation 4.4.6). Figure 5.3.9 shows an example element of the matrix [T] calculated using the raw FRF data. It is clear from Figure 5.3.9 that the FRF-based indirect testing method has provided less than satisfactory results that warrant little further analysis using, for example, modal curve fitting routines (note the similarity between Figure 5.3.9 and Figure 4.5.9, for example). Attempts to repeat the experiment taking even greater care over each measurement yielded similar results.

[18] Note that reciprocity was assumed so that 900 and not 1728 FRF measurements were required!

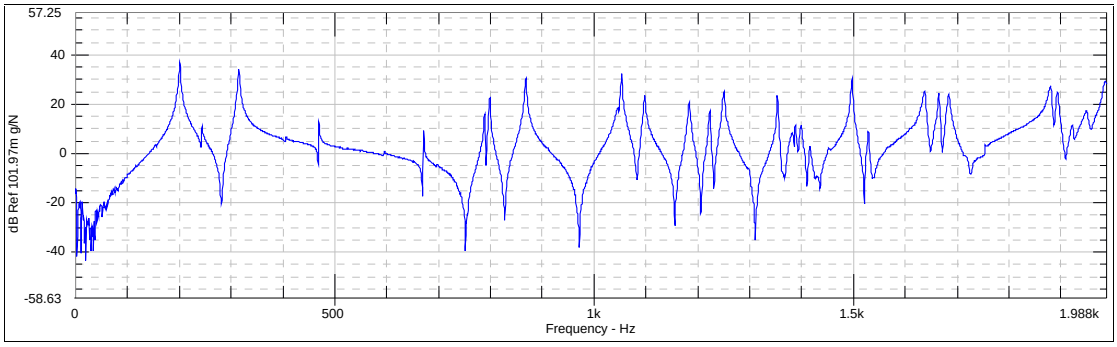

(a)

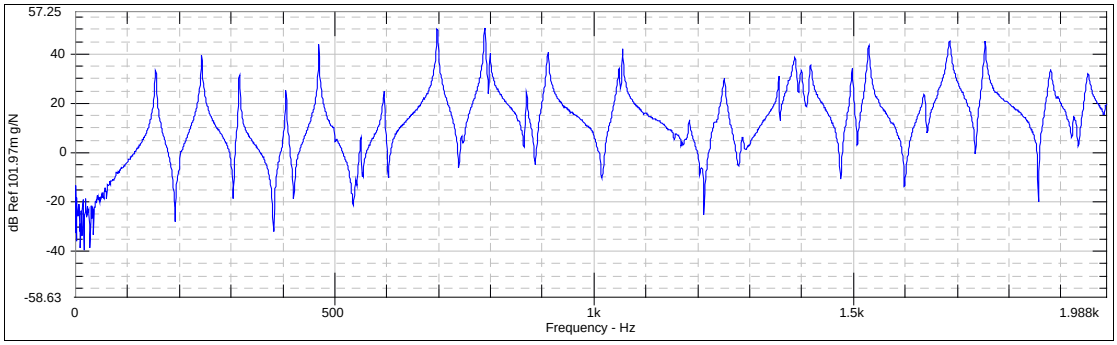

(b)

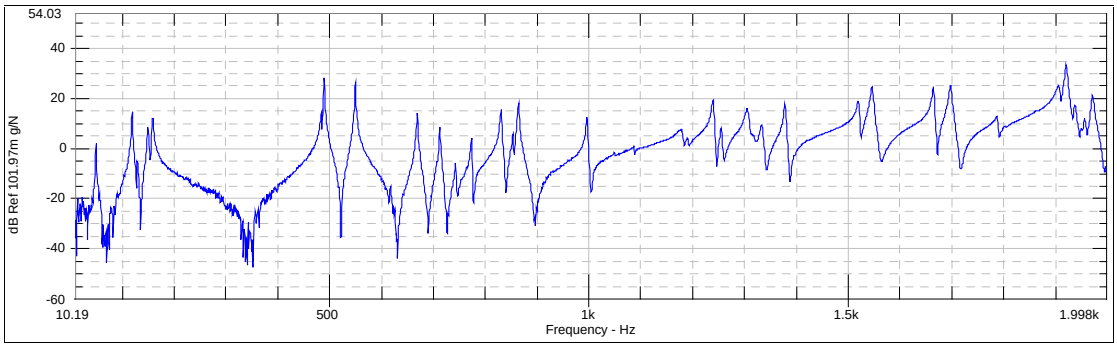

(c)

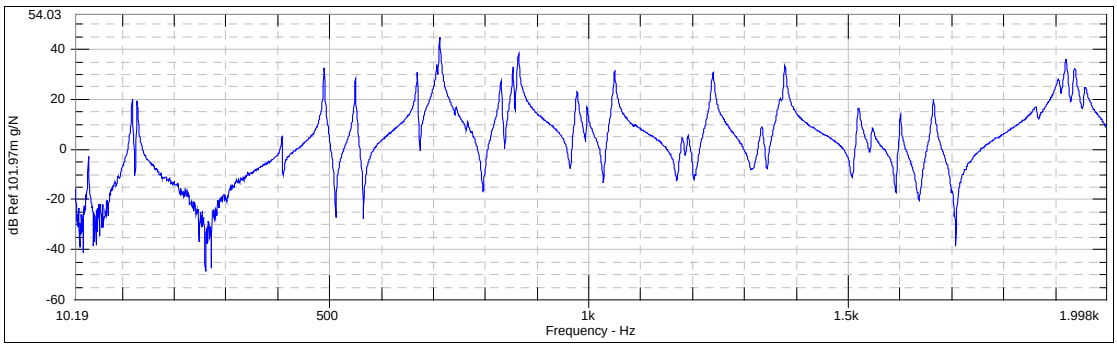

(d)

Figure 5.3.8. Example FRFs from test on the ITF and ITF/MACE Case assembly: a) H^{A}_{1x1x}; b) H^{A}_{1y1y}; c) H^{C}_{1x1x}; d) H^{C}_{1y1y}.

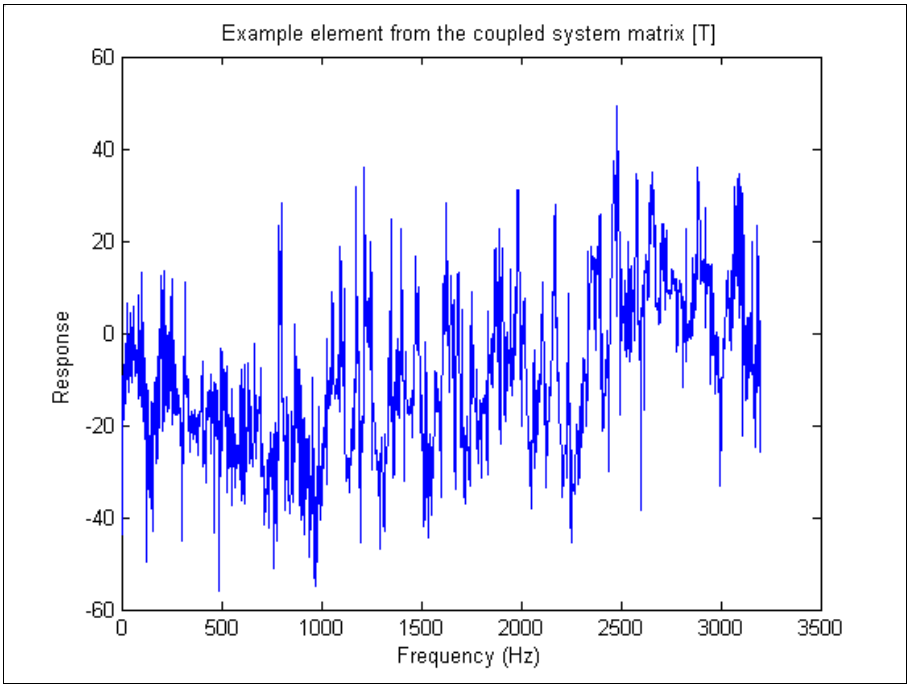

Figure 5.3.9. Example estimate of an element of the coupled structure matrix [T] .

Unlike the case of the simple beam reported in Section 5.2 it is not possible to cite one major cause for the failure of the method. Rather, the poor estimate of the coupled system matrix [T] the calculation provides is likely to be a combination of a number of factors, including: ill-conditioning due to sub-optimal remote locations; unsatisfactory levels of reciprocity achieved with the test configuration; and poor estimates of rotational FRFs. Although the FRF indirect testing method had been unsuccessful in meeting the objective of the experiment, it was clear from the results that an alternative method of indirect testing would be required to determine the free-free modes of the MACE Case.

5.3.3 Development and application of the model and remove approach

5.3.3.1 General comment

As discussed in Chapter 4, an alternative to the FRF-based indirect testing approach is to use spatial models generated using the FE method, the so called “model and remove approach”. The requirements for the ITF remain similar to those for the FRF-

based method, in that the test fixture **must not** overly constrain relative motion between the connection DOFs of the Structure Under Test (SUT). However, the model and remove approach differs from the FRF-based approach in the sense that it describes both the ITF and the ITF/SUT in terms of their physical properties (length, width and density, for example) not their observed behaviour. In order for the model and remove approach to be successful it is therefore essential that the FE models used provide an accurate physical description of the actual components: the models **must** be valid over the frequency range of interest.

5.3.3.2 Application of the model and remove approach to the MACE Case

The importance of adopting a structured approach to model validation is discussed by Ewins in [1]. In the present case study, the validation process was divided into four distinct phases. These phases, along with a brief description of their purpose in the overall process were:

1) Generation of a valid FE model of the ITF under free-free boundary conditions. This phase of the process allows any errors or shortcomings in the ITF model to be identified and corrected.
2) Generation of a valid FE model of the ITF under fixed-free boundary conditions. This phase of the process was included so that the non-trivial and unknown connection stiffness associated with ITF's feet / ground interface could be included in the model and updated until the FE model matched the test data.
3) Generation and validation of the FE assembly model of the ITF and MACE Case. This phase was intended to isolate errors associated with the MACE Case model and to update the unknown connection stiffnesses at the ITF/MACE Case interfaces if necessary.

4) Removal of the ITF FE model from the FE assembly model leaving a valid FE model of the MACE Case under free-free boundary conditions.

The next four sections of this Chapter detail the objectives, method and results obtained during each phase of the model validation process in turn.

5.3.3.3 Validation of the free-free ITF model

The objective at this stage was to obtain a valid model of the ITF structure in a free-free configuration. Grounding (the term being used loosely here) a structure represents a significant change from the free-free configuration and therefore the validation criteria need to be strict, such that when the model is grounded the dominant uncertainties are associated with the non-trivial connection stiffnesses. In the current study the criteria under which the model would be considered valid were that over the frequency range 0-2000Hz, the error between the analytical and test frequencies for correlated mode pairs would not exceed 5%. The analytical and test modes would be considered correlated if a MAC value of 80% or greater was achieved. These represent reasonable levels of agreement given modelling and test uncertainties [2].

The initial FE model of the ITF (shown in Figure 5.3.10) was used to produce a test strategy for the structure. The best suspension and hammer excitation points were calculated (for the 36 modes in the frequency range 0-2000Hz) using the ICATS Modplan software with the resulting plots shown in Figure 5.3.11.

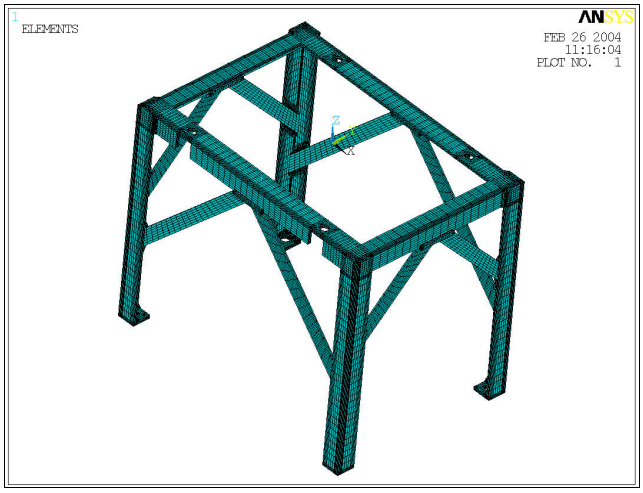

Figure 5.3.10. The initial FE model of the ITF.

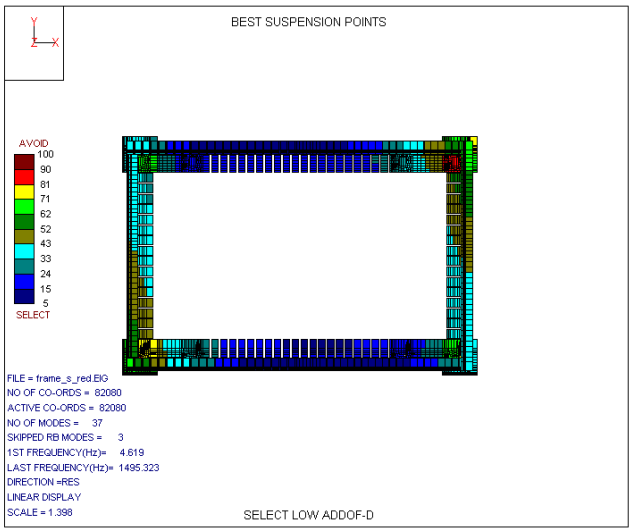

(a)

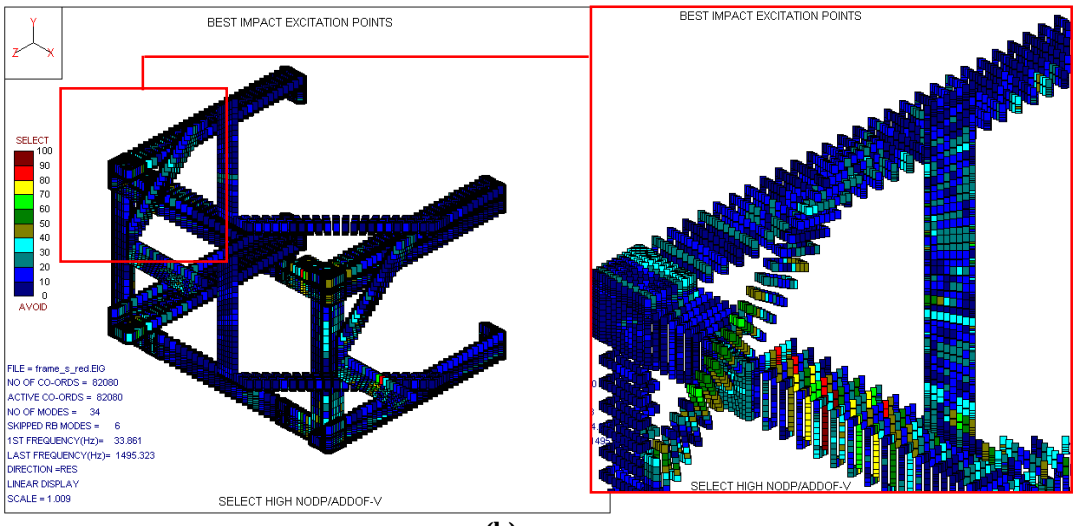

(b)

Figure 5.3.11. Test planning for the ITF: a) Best Suspension locations (shown in dark blue) and ; (b) best impact locations (shown in maroon/red).

Also, the best accelerometer locations were selected using the iterative, ADDOF-A weighted, EI calculation provided in the ICATS Modplan software, [69]. This calculation computes the weighted value of EI for a given set of eigenvalues and then removes the DOF associated with the eigenvalue that contributes least to the global rank of the mode shape matrix. The EI calculation is then repeated on the reduced set of eigenvectors and the lowest ranking DOF is rejected. The process of DOF rejection is continued until the eigenvector matrix possess a rank (at least) equal to the number of modes within the frequency range. It is good practice to terminate the iterative process early so that there are a few more DOFs than modes as this allows some averaging of random errors by virtue of over determination. Figure 5.3.12 shows DOFs selected by the iterative EI calculation, when used to determine the best accelerometer locations for the ITF. As can be seen from Figure 5.3.12 the calculation has, in general, selected well separated DOFs although there are a few regions where clustering of DOFs occurs. Of these clustered DOFs only those which were separated by a distance of 5mm or greater were included in the test geometry shown in Figure 5.3.13. Despite the somewhat arbitrary final selection of the measurement DOFs the selected test geometry provided a good Auto-MAC with no off-diagonal elements having a value greater than 60% (Figure 5.3.14).

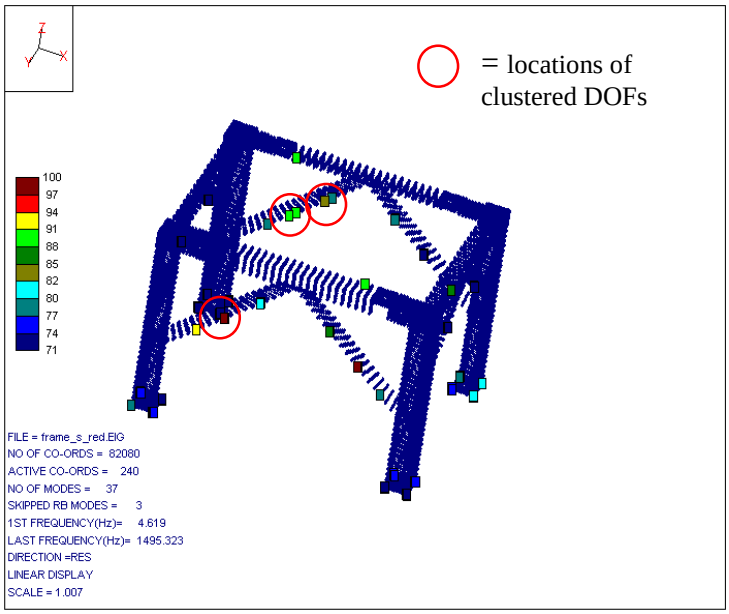

Figure 5.3.12. Best accelerometer locations for the ITF in a free-free configuration.

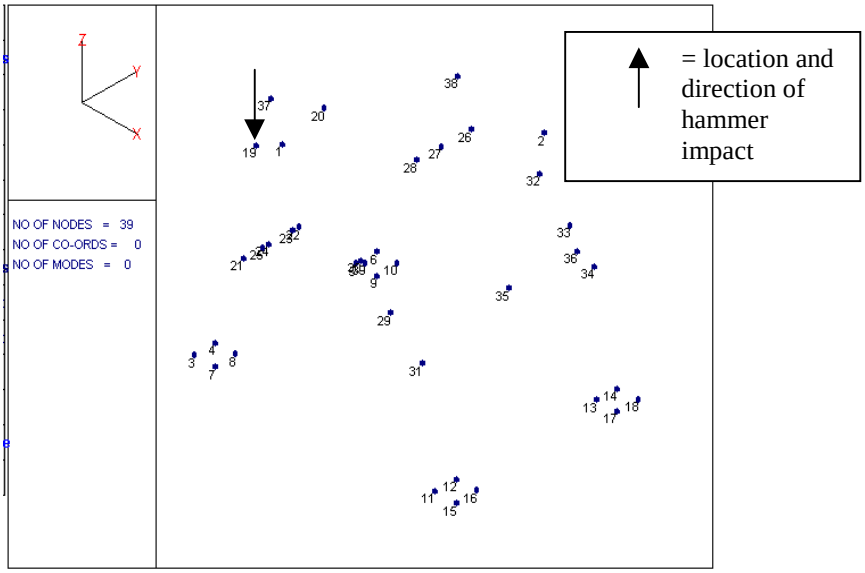

Figure 5.3.13. The final test geometry for the free-free ITF.

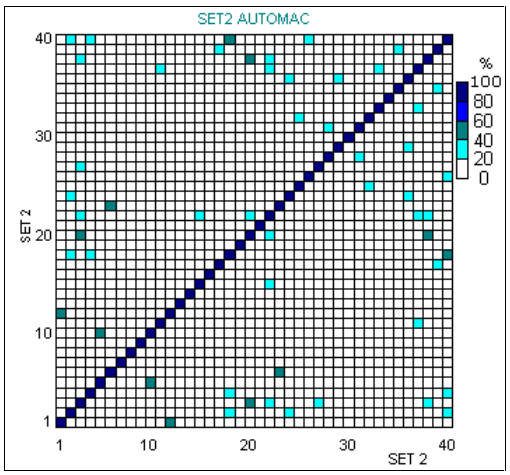

Figure 5.3.14. Analytically derived Auto-MAC for the final test geometry.

Having completed the test planning phase, the structure was suspended from the four connection holes (see Figure 5.3.3) using elastic bands. Hammer impacts were applied at the location shown in Figure 5.3.14 and a single Endeveco type 7253 tri-axial accelerometer was moved around to each of the measurement co-ordinates shown in Figure 5.3.13. Standard pre-test checks for mass-loading, reciprocity and overall data quality were completed with satisfactory results prior to making the actual measurements. The FRFs were measured over the frequency range 0-2000Hz with a frequency resolution of 0.78Hz. The average of three measurements was used to provide smoothing for each FRF. The resulting FRF data were analysed using the Global-M modal parameter extraction method. Figure 5.3.15 shows the Auto-MAC of experimentally derived modes, and provides a good example of what can be achieved using careful test planning.

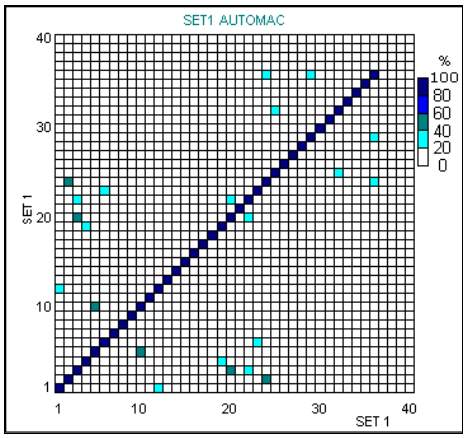

Figure 5.3.15. Auto-MAC of the experimentally obtained mode shapes.

The MAC and natural frequency plot comparing the experimental data (set 1) to the FE results (set 2) is shown in Figure 5.3.16, from which it is clear that although the first 8 modes shapes are well correlated the majority of higher mode shapes are not. Also, there are large errors between the analytical and test frequencies for the correlated mode pairs.

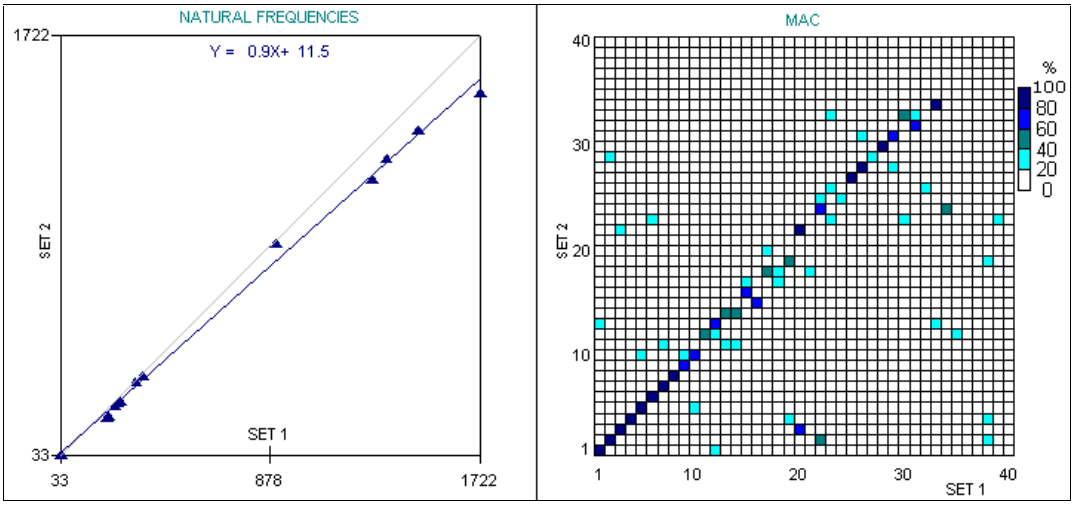

Figure 5.3.16. Correlation between the experimental (set 1) and analytical (set 2) mode shapes achieved with the initial FE model.

Since the Auto-MAC for the test data (Figure 5.3.15) showed that there was only trivial spatial aliasing, it was considered that the source(s) of error(s) lay with the model. The model was reviewed and an error was found in the dimension of the legs (as illustrated in Figure 5.3.17) which were found to be some 4mm too wide. This error was corrected and the modes obtained from it were compared to the test data, the resulting MAC and natural frequency plot is shown in Figure 5.3.18.

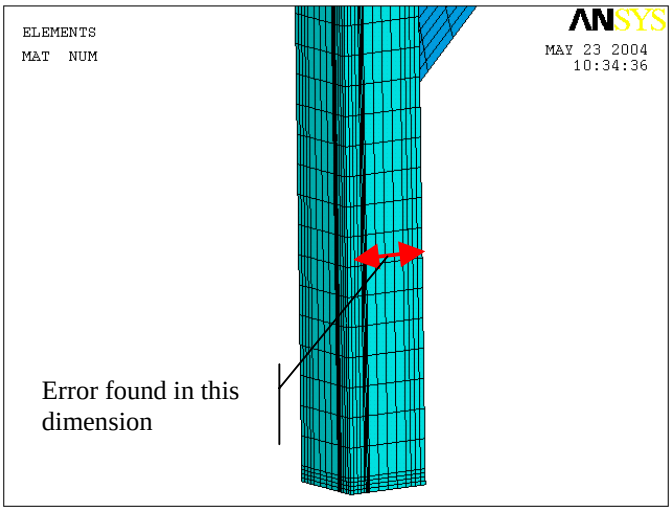

Figure 5.3.17. Detail of the ITF model showing the dimension which required correction.

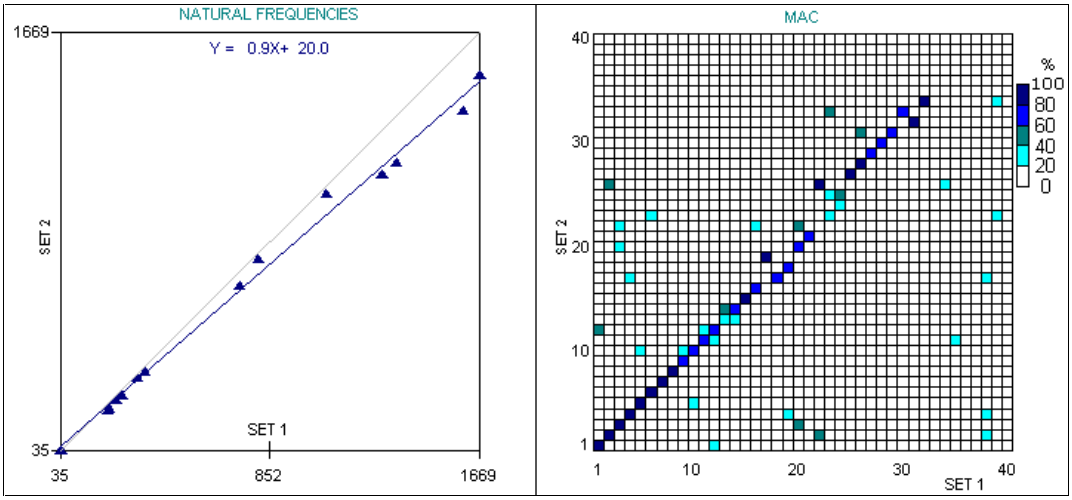

Figure 5.3.18. Correlation between the experimental (set 1) and analytical (set 2) mode shapes achieved with the improved leg FE model.

Although the MAC plot shows a general improvement the frequency error between the correlated mode pairs is worse. This was attributed to the fact that the correction of the leg dimension error had introduced a 12% discrepancy between the FE calculated and actual mass (FE mass =1.79kg , actual mass =2.048kg). One possible source of the error between the predicted and actual mass was that the weld fillets used to fabricate the ITF structure together had not been included in the model. Since the ITF was fabricated from Aluminium, some of the welds (particularly those used to fix the cross-braces to the legs) were large as shown in Figure 5.3.19 (a).

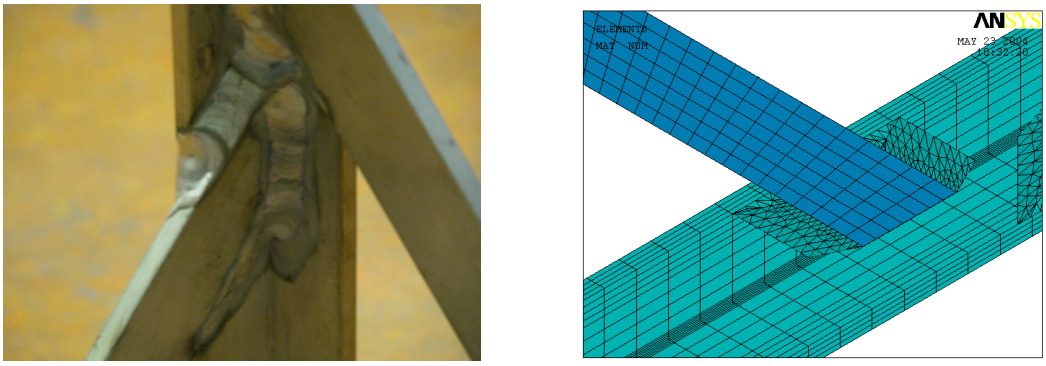

(a) **(b)**

Figure 5.3.19. Close up of ITF showing large welds used to secure the cross braces (a) and approximation to these welds included in the FE model.

Approximations of the major welds were included in the model (Figure 5.3.19 (b)) and the results obtained from an eigensolution of the new model were compared to the test data. Figure 5.3.20 shows the results of this correlation which although much better both in terms of the MAC and natural frequencies of the correlated mode pairs still includes large errors. It should be noted that this result was achieved using the design variable approach to modal updating, altering the stiffness of the welds in an attempt to minimise the difference between the analytical and experimental natural frequencies. While altering the weld stiffness may be considered physically meaningful, it has clearly not been successful in this case because the model is not capable of correctly representing the structure's physics.

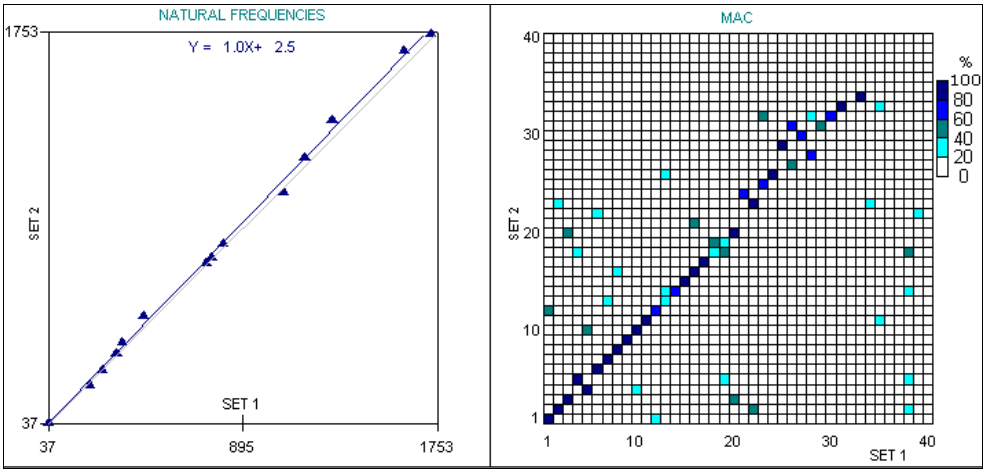

Figure 5.3.20. Correlation between the experimental (set 1) and analytical (set 2) mode shapes achieved with the FE model (legs corrected and approximations to major welds).

Interestingly the inclusion of the welds had not remedied the error in the mass, although it had brought the predicted and actual mass closer (FE mass =1.87kg, actual mass = 2.048kg). In order to determine exactly what was causing the mass discrepancy the structure's dimensions were checked. The measurement of the ITF identified an error in the dimension of the cross-brace of the model which had been modelled approximately 3mm too thin in the dimension shown in Figure 5.3.21 (a) and also established that the (measured) mean thickness of the cross-braces was

5.1mm and not 4.7625mm (3/16'') as specified in the drawing (see Figure A.1.1 in Appendix 1). The mean thickness of the Aluminium L-section was also found to be 5.2mm as opposed to 4.76mm. These dimension errors were corrected in the model and approximations to all of the welds were included (see Figure 5.3.21(b)).

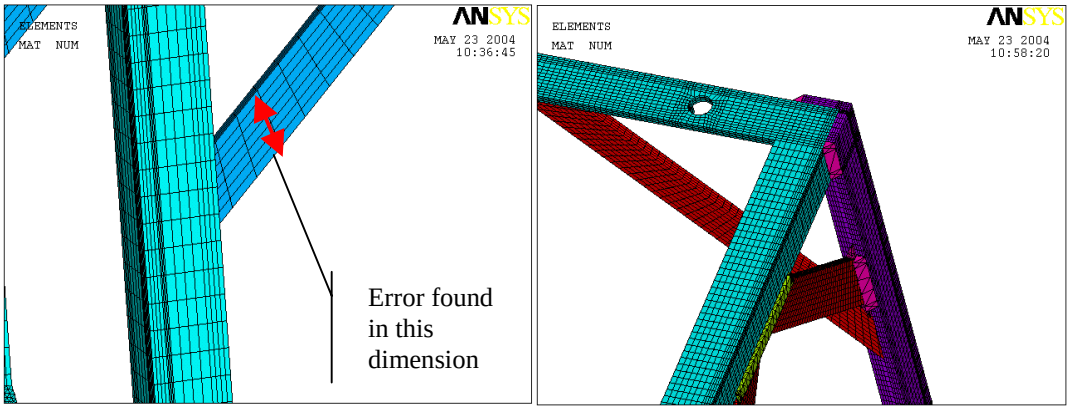

(a) **(b)**

Figure 5.3.21. Close-ups of the ITF model, showing region where dimensional error was found (a) and the inclusion of all welds (b).

The predicted and actual mass were found to differ by less than 1% (FE mass = 2.043kg actual mass 2.048kg). The results obtained from modal analysis of this model were compared to the test results. Figure 5.3.22 shows the initial correlation between the thus corrected (and physically accurate) model and the experimental data. After manually updating the Young's Modulus of the material used for the welds[19] (from 69 GN/m^2 to 69MN/m^2 in three iterations) the correlation between the model and the test data shown in Figure 5.3.23 was achieved.

[19] It is likely that reducing the Young's Modulus of the weld material is compensating for the use of a coarse 4-node tetrahedral mesh for the welds.

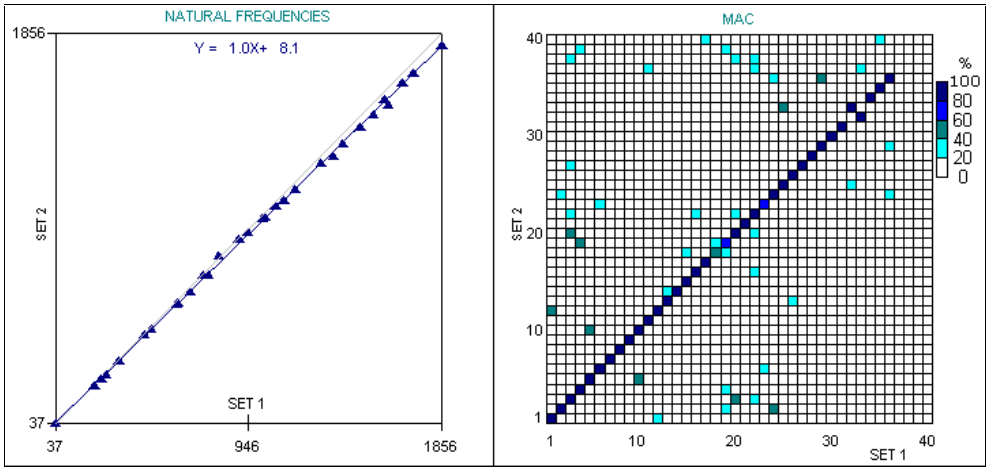

Figure 5.3.22. Correlation between the experimental (set 1) and analytical (set 2) mode shapes achieved with the FE model (all errors corrected, all welds included (E=69 GN/m^2) and mean values of measured thickness used).

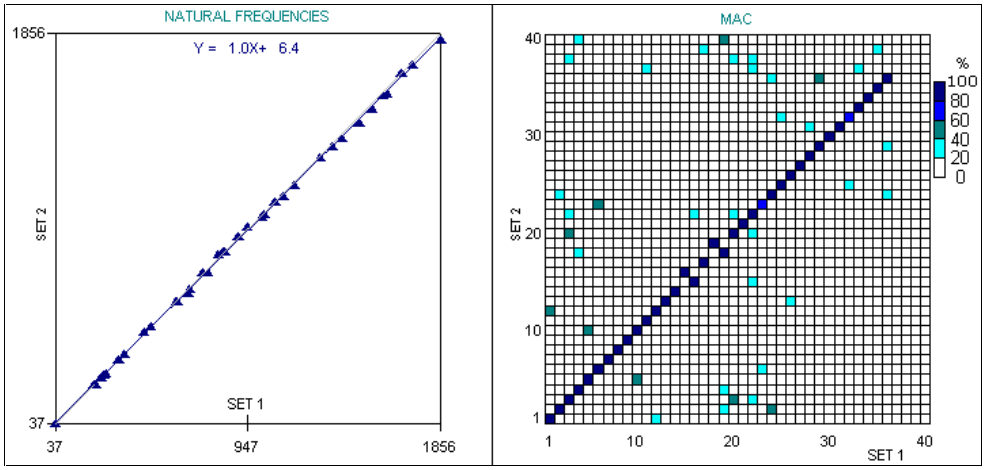

Figure 5.3.23. Correlation between the experimental (set 1) and analytical (set 2) mode shapes achieved with the FE model (all errors corrected, all welds included (E=69 MN/m^2) and mean values of measured thickness used).

Every mode of the model had a MAC in excess of 78% when compared with the test data and was within three percent of the measured natural frequency[20] (the mean error in frequency for the first 36 modes was 1.1%). Table A1.1 in Appendix 1 gives the

[20] Although the MAC plot shows some mode switching between modes 15,16 and 18,19 these are associated with close modes of the structure. The natural frequencies obtained from the test data for modes 15 and 16 were 733 Hz and 746 Hz (3% difference) respectively. For modes 18 and 19 the natural frequencies were 830 Hz and 835 Hz (0.6 % difference) respectively.

actual values associated with the final correlation achieved for the free-free ITF model. Since the objectives of the free-free ITF model validation had been met the next phase (validation of the fixed-free ITF model) could begin.

5.3.3.4 Validation of the fixed-free ITF model

The model validation criteria for the fixed-free ITF model were identical to the validation criteria for the free-free model (MAC of 80%, natural frequencies within 5%) over the frequency range 0-2000Hz. An attempt was made to determine the best response locations for the fixed-free test configuration using the ICATS Modplan software, the results of which are given in Figure 5.3.24. In the case of the fixed-free ITF the iterative EI calculation failed to provide a satisfactory result, clustering the measurement locations (Figure 5.3.24(a)) resulting in the unsatisfactory Auto-MAC with some high-valued off-diagonal terms as shown in Figure 5.3.24(b). The clustering of the measurement DOFs was such that the approach to the clustering problem discussed in Section 5.3.3.3 simply resulted in there being fewer measurement DOFs than modes. The clustering of the EI method in this case led to the use of the spatially dense measurement geometry shown in Figure 5.3.25(a) which was demonstrated to provide the Auto-MAC shown in Figure 5.3.25(b).

FRF measurements were then made on the fixed-free ITF using the same method described in Section 5.3.3.3. The Auto-MAC of the modes extracted from the FRF data (using the Global-M parameter extraction method) is shown in Figure 5.3.26 from which it is clear that despite the large number of DOFs included in the test geometry, the test data is incapable of separating two pairs of modes (one at around 480 Hz and one at 1400 Hz).

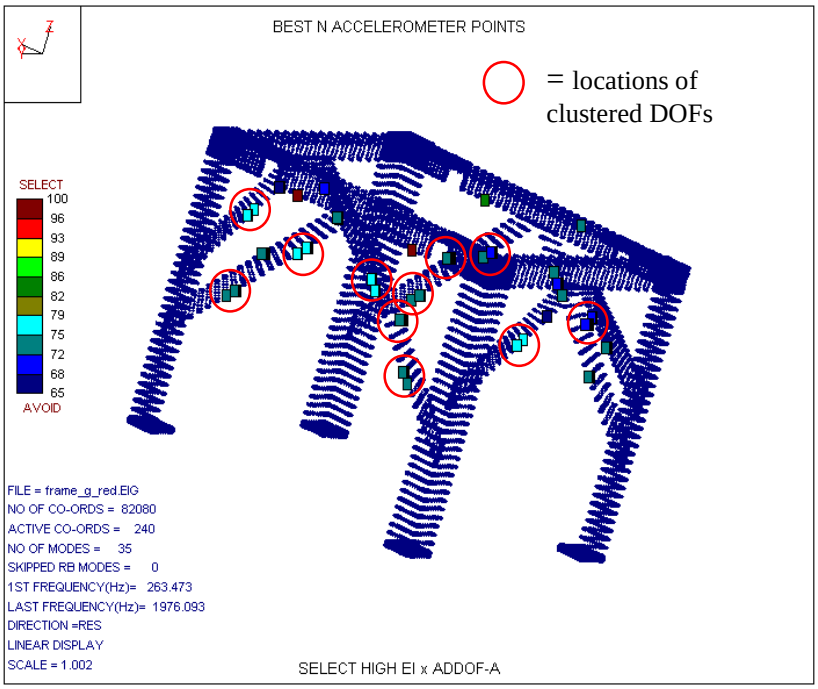

(a)

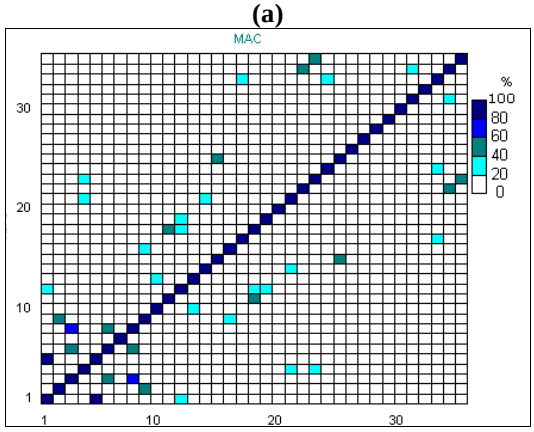

(b)

Figure 5.3.24. a) Best accelerometer locations for the ITF in fixed-base configuration showing clustering of measurement locations; b) analytical auto-MAC for the EI determined, best measurement locations.

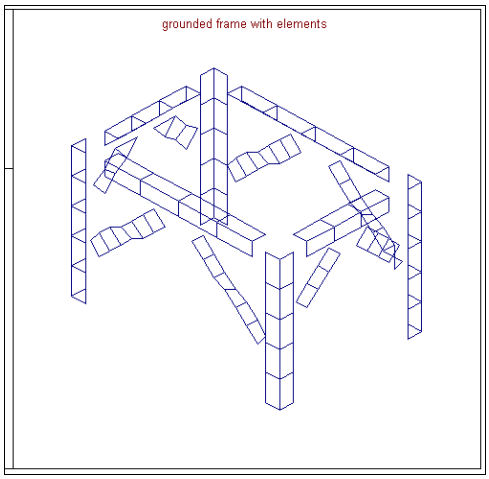

(a)

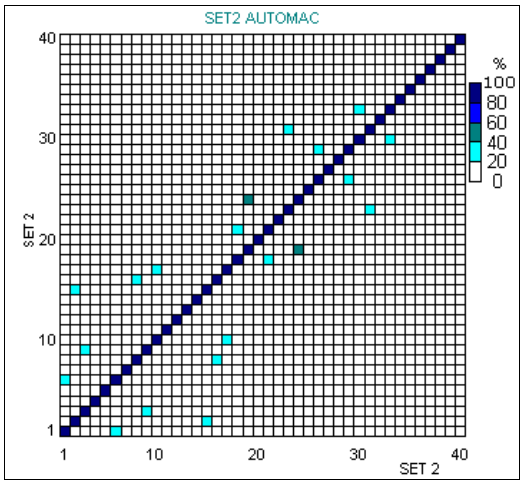

(b)

Figure 5.3.25. Final test geometry (a) and its corresponding (analytical) auto-MAC (b).

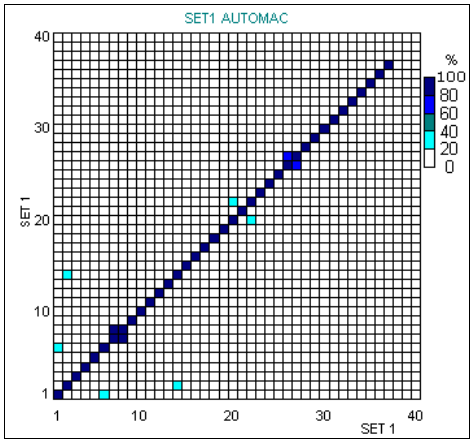

Figure 5.3.26. Auto-MAC of the experimentally derived modes.

Compliant elements were introduced at the base of the feet to represent the non-trivial connection stiffness at the leg ground interface (see Figure 5.3.27). These elements were assigned isotropic material properties with an initial Young's Modulus of $69GN/m^2$. The first natural frequency predicted by this initial fixed-free model was 253Hz, some 40% different from the first test natural frequency of 142Hz. The Young's Modulus of the compliant elements was then manually reduced in the model, until after four iterations a value of $69MN/m^2$ was found to match the first natural frequency of the model and test modes to within 3%. The results from this model were compared to the test results giving the MAC and natural frequency plot shown in Figure 5.3.28. From the results shown in Figure 5.3.28 it is clear that while the correlation between the fixed-free FE and test models is reasonable to around 1210 Hz, the results above this frequency are poor. It is likely that the reason for this poor correlation is the assumption of isotropic material properties for the compliant elements.

In reality the structure was clamped to a seismic block as shown in Figure 5.3.27(b). One method which might be employed to represent this clamping method would be to use orthotropic material properties for the compliant elements. This method would

allow the connection stiffness in the *z* direction to be considerably higher than that of the *x* or *y* directions and would increase the number of parameters available for updating [90]. However, it is important to recognise that increasing the numbers of parameters for updating simply increases the number of assumptions made about the structure's behaviour and better, more physically realistic results would be obtained by modelling the connection mechanism (shown in Figure 5.3.27 (b)) in detail. Time allowing[21], the detailed modelling of the physics of the joint would have been the approach adopted, however, for the present case study, the validation criteria were relaxed such that a valid model of the MACE Case was only sought over the frequency range 0-1000Hz. As can be seen from Table A.1.2 of Appendix 1, the relaxed validation criteria for the fixed-free ITF model have been met using the simple isotropic material model for the leg/ground interface elements.

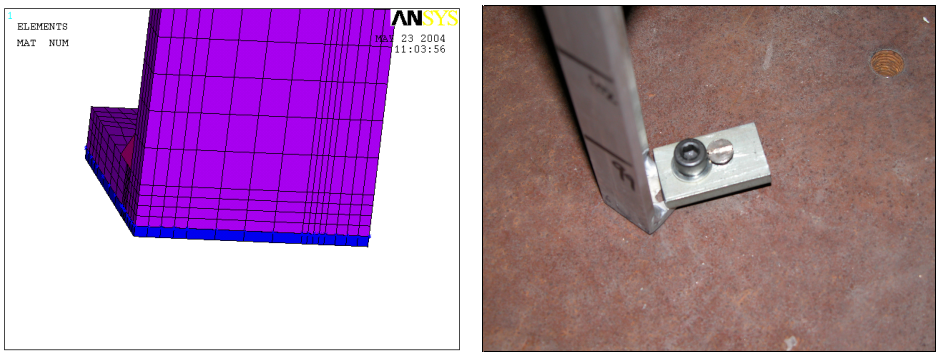

(a) **(b)**

Figure 5.3.27. a) Close up of ITF showing the compliant elements (blue) used to represent the leg/ground interface stiffness; b) actual clamping arrangement used to fix the ITF to the seismic block.

[21] The run times to obtain the first 42 modes of the fixed-free ITF were approaching 8 hours via the Lanchoz solution method, meaning it could take upward of one and a half days to complete a solution and correlate it with the test data.

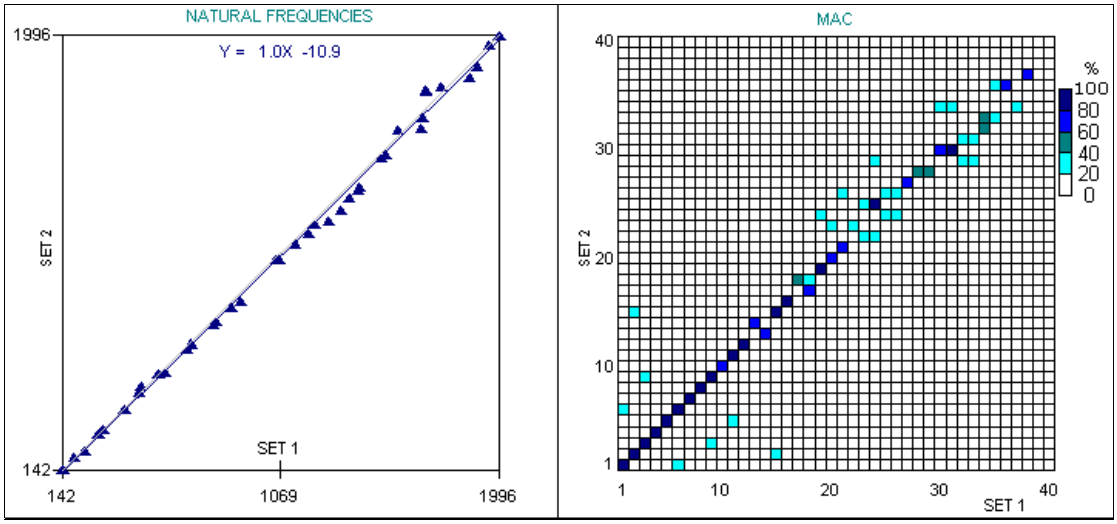

(a)

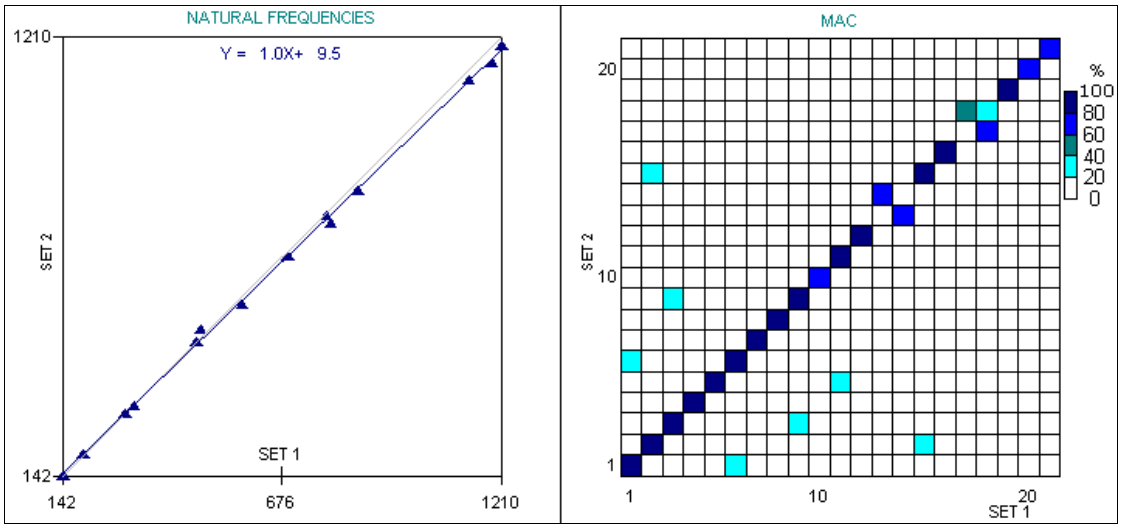

(b)

Figure 5.3.28. Natural Frequency and MAC plot for the experimental and analytical ITF (in fixed base configuration) modal models: (a) all modes included; (b) modes 1-21 (0-1210Hz) included.

5.3.3.5 Validation of the ITF/MACE Case assembly model

In the third stage of the model and remove approach a high fidelity FE model of the MACE Case was coupled with the validated FE model of the ITF in a fixed-free configuration. The MACE Case model (Figure 5.3.29 (a)) included every major geometric feature including the key-way, bolt-holes (with the exception of threads), internal chamfers and fillets. The MACE Case model was coupled to ITF using brick element representations of the bolts, bonded-always contact was assumed at the frame/bolt and bolt/MACE Case interfaces (shown in Figure 5.3.29 (c)).

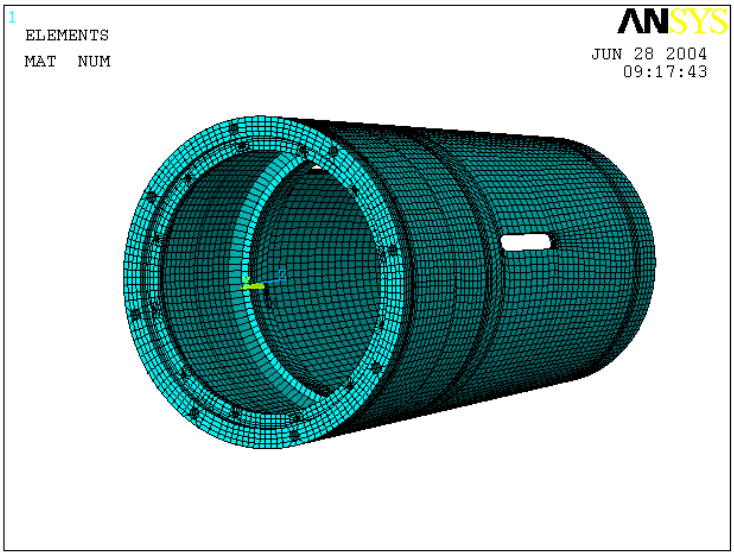

(a)

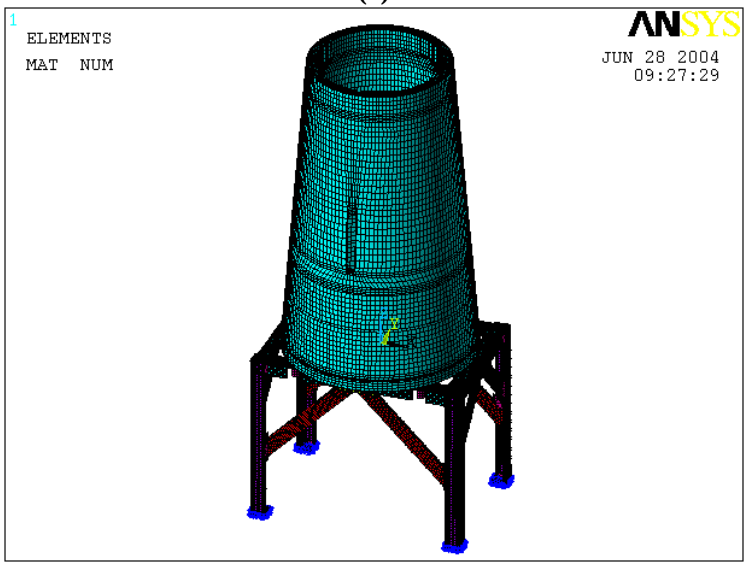

(b)

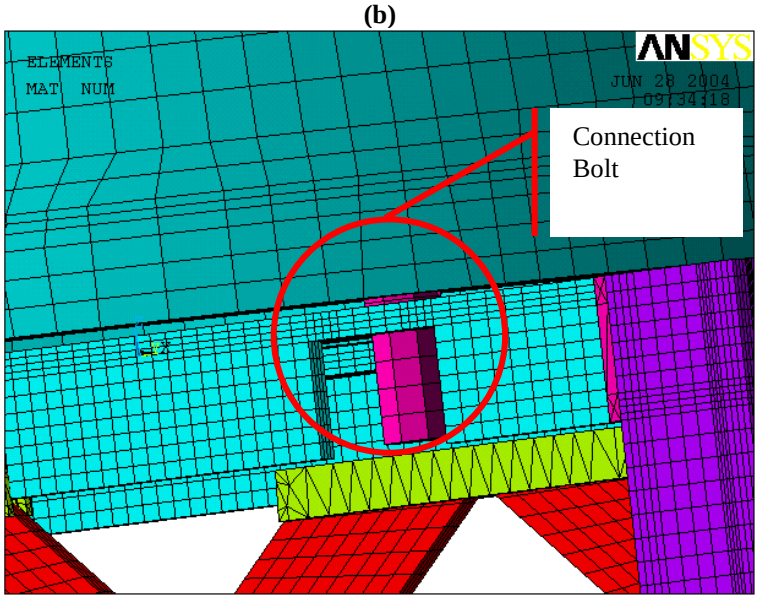

(c)

Figure 5.3.29. a) MACE Case model; b) ITF/MACE Case assembly model; c) detail of assembly model showing ITF/MACE Case interface and representation of a connection bolt.

In the case of the assembly, the actual structure was available for testing long before an FE model became available. Modal tests (originally intended as precursor trials) were conducted in which a tri-axial accelerometer was attached at point 233 on the ITF (see Figure 5.3.30) and a roving hammer excitation applied at each of the co-ordinates shown in Figure 5.3.30.

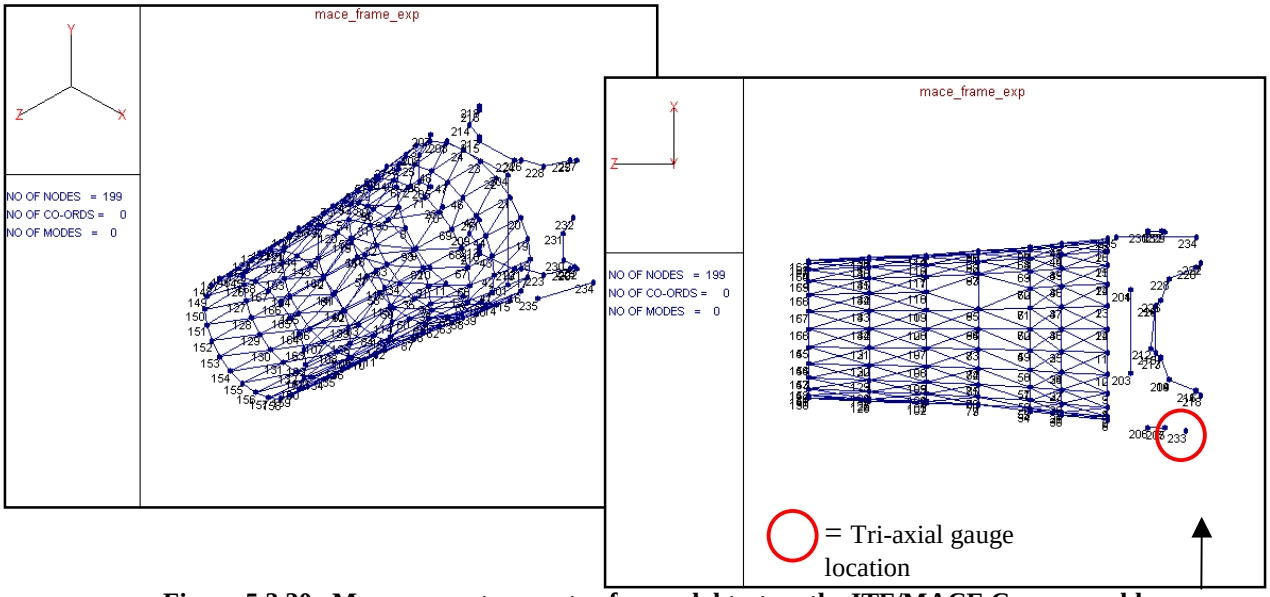

Figure 5.3.30. Measurement geometry for modal test on the ITF/MACE Case assembly.

The FRFs obtained from the test contained numerous resonances as illustrated by the example FRF of Figure 5.3.31.

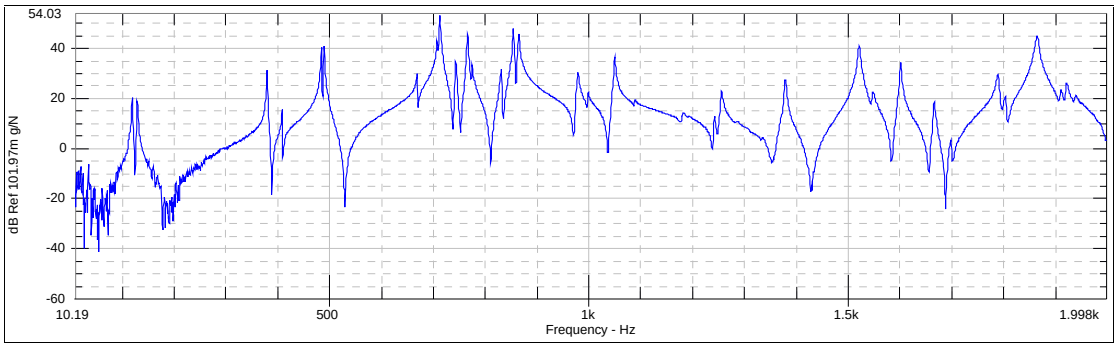

Figure 5.3.31. Example of an FRF taken from the ITF/Mace case assembly showing multiple resonances.

After analysis it was found that only a few of the modes involved any significant motion of the MACE Case (such as that shown in Figure 5.3.32, for example), and

these will be referred to as the Case modes . After the initial FE model had been analysed the results were quantitatively compared using the MAC, as shown in Figure 5.3.33.

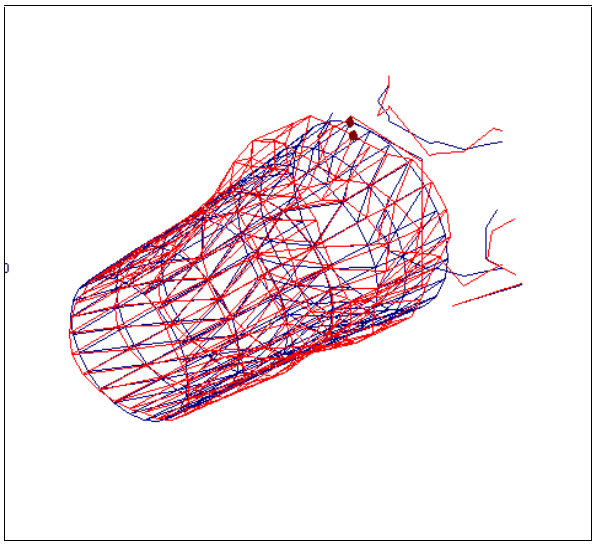

Figure 5.3.32. Example Case mode at 1805Hz.

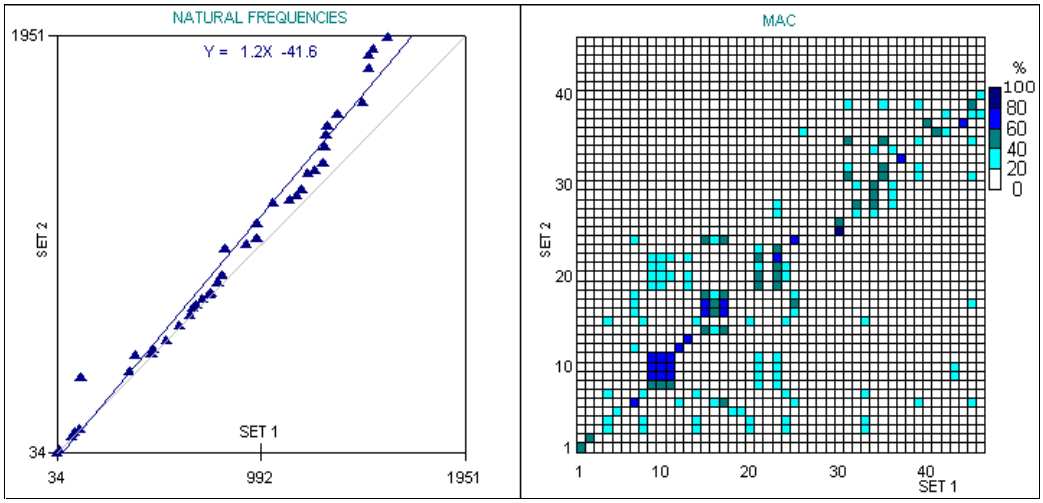

Figure 5.3.33. Natural Frequency and MAC plot for the experimental (set 1) and analytical (set 2) modal models of the ITF/MACE Case assembly model.

Although this initial correlation seems poor, a review of the mode shapes revealed that (See Figures A.1.2 to A.1.5 of Appendix 1, for example) all of the Case modes were similar in terms of the motion of the Case, but, that the motion of the frame was not similar in the two models. It was also noted that natural frequencies were very similar, and were all within 5% of the natural frequencies from the test. Furthermore,

Case modes beyond the upper validation frequency of the FE model of the ITF (1210 Hz) were also very similar in terms of their mode shapes and were also very close in frequency (see Figures A.1.6 to A.1.7 of Appendix 1). In fact, when only the Case modes were included for comparison the MAC and natural frequency plot shown in Figure 5.3.34 was achieved. Omitting all of the co-ordinates on the ITF from the MAC calculation gave the improved MAC plot of Figure 5.3.35.

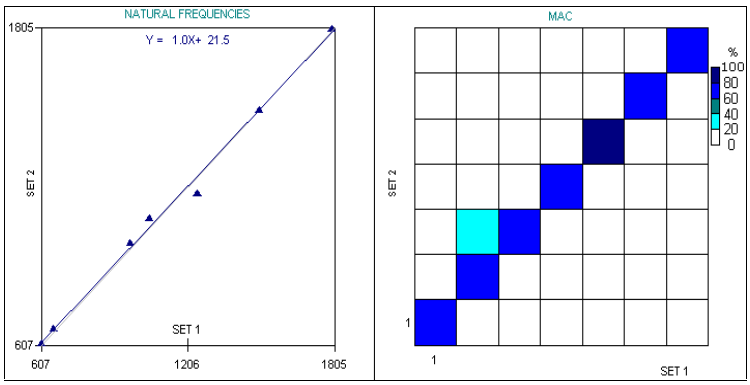

Figure 5.3.34. Natural frequency and MAC plot of assembled structure (Case modes only, all measured DOFs included)

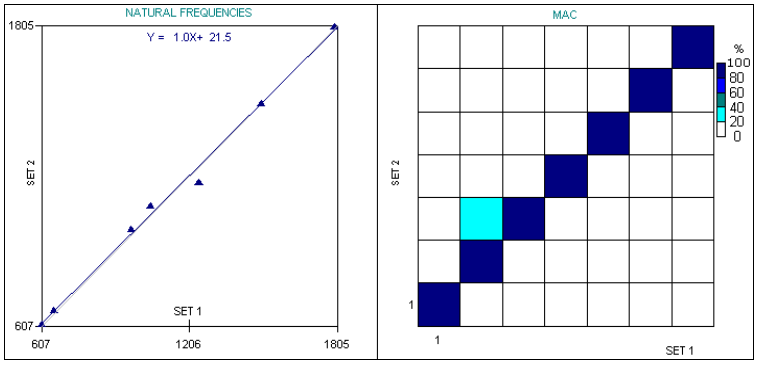

Figure 5.3.35. Natural frequency and MAC plot of assembled structure (DOFs on Case only, Case modes only).

In order to understand this somewhat unexpected result, a sensitivity study was conducted in order to determine whether the Case modes were sensitive to the non-trivial connection stiffness. The initial value of Young's modulus for the compliant elements (69MN/ m^2) was halved, and then doubled in the FE model. Figure 5.3.36 shows the percentage difference in natural frequency between these two runs and the

results obtained with an interface stiffness of 69MN/ m^2. It should be noted that while for the Case modes Figure 5.3.36 is comparing correlated mode pairs, the assembly modes (particularly the higher modes) are not necessarily like for like comparisons. The result shown Figure 5.3.36 suggests that the natural frequencies of the Case modes are insensitive to the leg/ground interface stiffness, although (as expected) the assembly modes predominantly involving motion of the frame are.

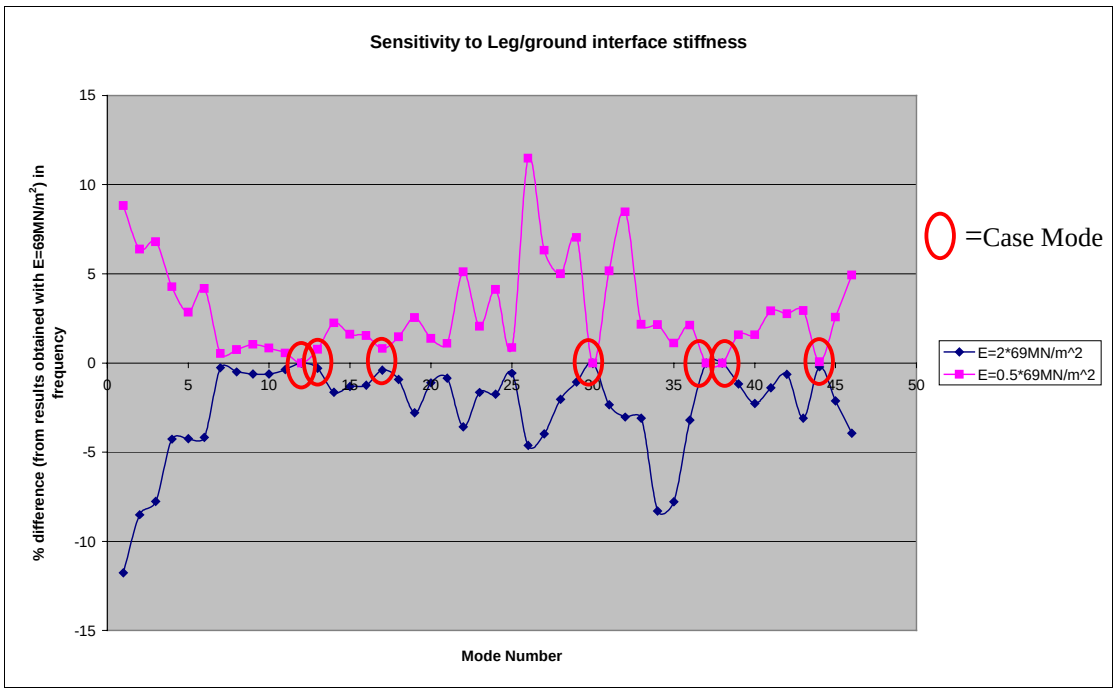

Figure 5.3.36. % change in frequency of the first 46 Modes of the ITF/MACE Case assembly caused by halving and doubling the original leg/ground interface stiffness (69MN/m^2).

The physical cause of this insensitivity to the leg/ground interface stiffness are obvious when we consider the simple spring-mass system of Figure 4.5.16 (repeated here for convenience as Figure 5.3.37). In Chapter 4, the case in which the spring stiffness k_4^A became infinite was considered and it was shown how this led to an ill-posed problem if structure A was used as the indirect testing fixture. However, if structure B is used as the indirect test fixture then it is clear that the problem is actually over-determined (for the purpose of FRF-based indirect testing) and that structure A will be insensitive to changes in stiffness between the connection DOFs.

Although, quite obviously, the MACE Case is not infinitely stiff, it **is** much stiffer than the ITF and so insensitivity to changes in the stiffness between the connection DOFs is to be expected.

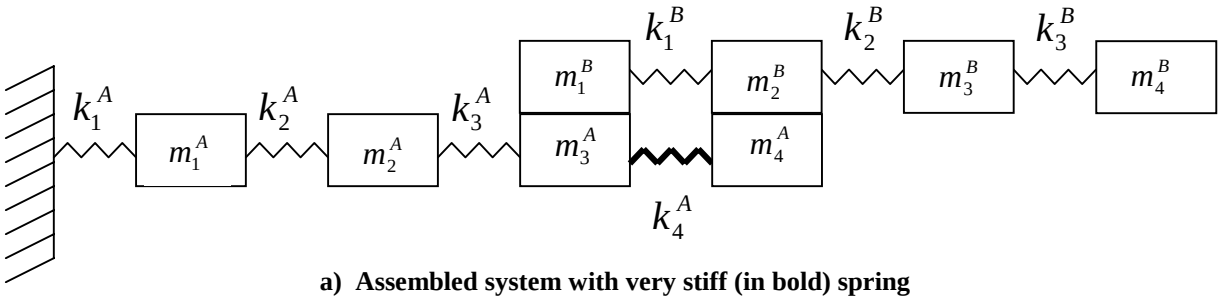

a) Assembled system with very stiff (in bold) spring

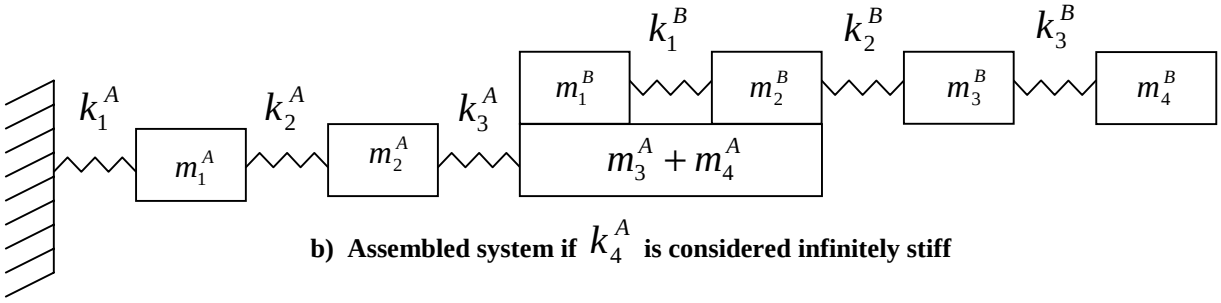

b) Assembled system if k_4^A is considered infinitely stiff

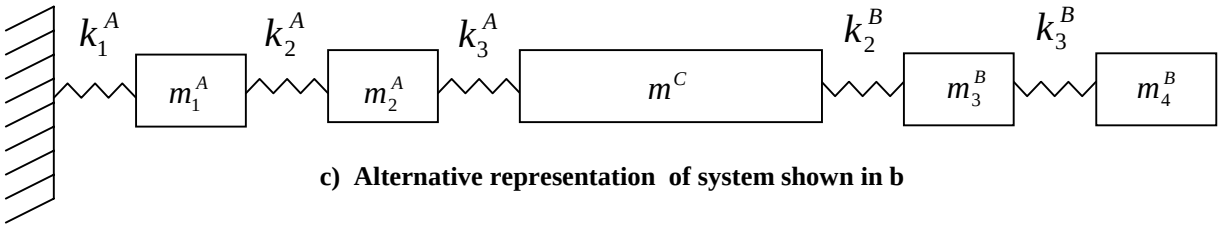

c) Alternative representation of system shown in b

Figure 5.3.37. Systems containing a stiff spring between two connection DOFs.

A similar sensitivity study was conducted for the MACE Case / ITF interface by altering the stiffness of the attachment bolts (see Figure 5.3.29). The results of this sensitivity study are given in Figure 5.3.38. It is noted that while the natural frequencies of both the Case modes and assembly modes are reasonably insensitive to the ITF/ MACE Case interface stiffness, doubling the stiffness has considerably less effect than halving it. This feature suggests that as long as the interface stiffness is "stiff enough" then the results of the assembly model will be reliable.

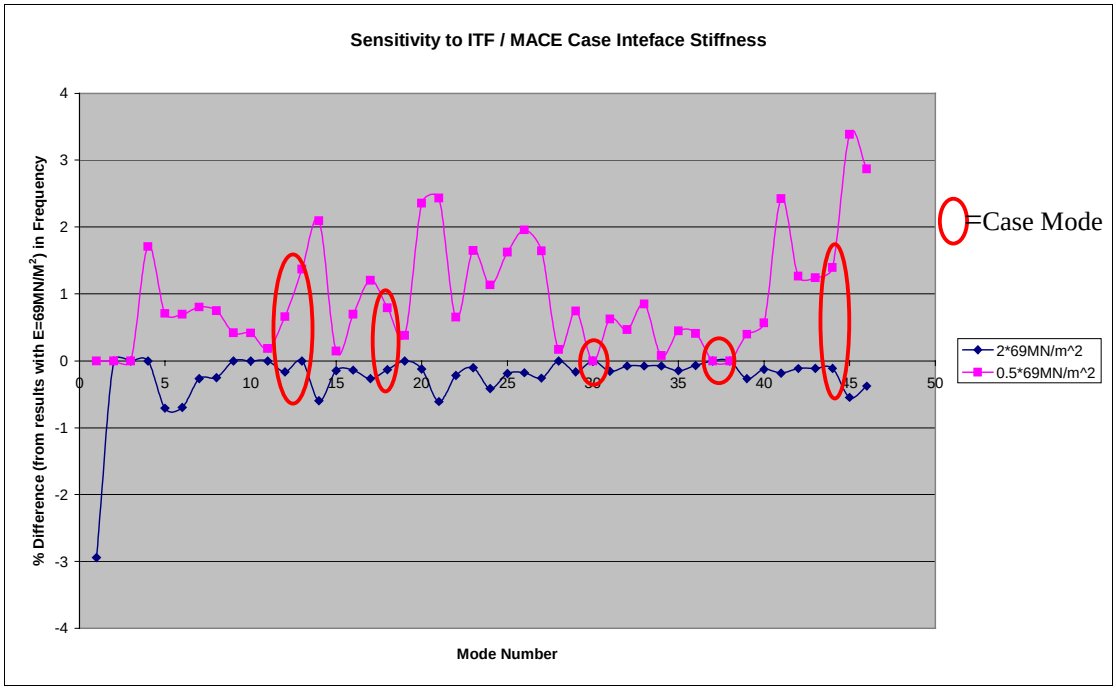

Figure 5.3.38. % change in frequency of the first 46 Modes of the ITF/MACE Case assembly caused by halving and doubling the original ITF/ MACE Case interface stiffness (69GN/m^2).

Given the good natural frequency correlation between the experimental data and FE assembly model and based upon the results of the two sensitivity studies it was concluded that the FE model of the MACE Case was valid over the frequency range 0-2000Hz. The error in frequency between correlated mode pairs of the free-free MACE Case FE and experimental modal models was expected to be less than 5%.

5.3.3.6 Comparison of the free-free MACE Case model with experimental data.

The MACE Case was suspended in a free-free configuration and a modal test was conducted using hammer excitation. The results of modal analysis of the test data were compared to the results obtained from running the FE model of the Case in a free-free configuration. The natural frequency and MAC plot obtained from this correlation are shown in Figure 5.3.39. Although the test has missed some of the

structure's conjugate mode pairs, the correlation between the test and analysis models is good with a maximum frequency error between correlated mode pairs of just 3%.

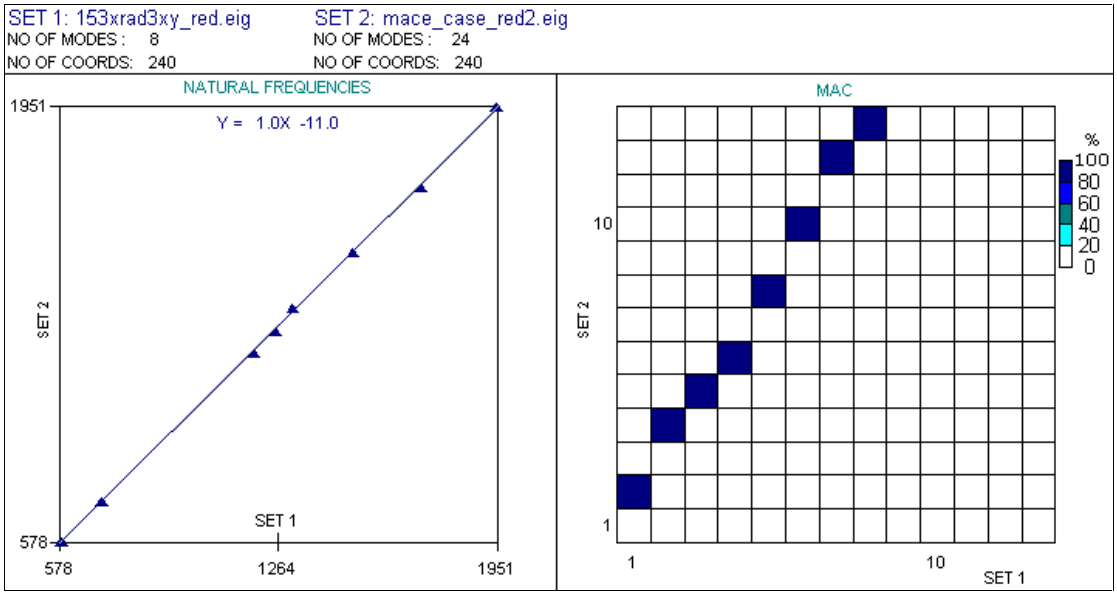

Figure 5.3.39. Natural frequency and MAC plot showing for the free-free MACE Case. Set 1=Experimental model , set 2= FE model.

5.3.3.7 Case study two: conclusions

When applied to the MACE Case, the FRF-based indirect testing method has been unable to determine any of the modes of the MACE Case, even when every effort has been made to ensure the quality and consistency of the measured data. Even for just 4 connection locations (24 coupling DOFs) the application of the method was extremely time consuming, requiring many hours to set up, make the measurements and process the acquired data. Efforts to optimise the remote measurement locations were not successful primarily because the DOFs selected by the iterative EI measurement were situated at flexible regions on the structure at which it was difficult to apply hammer excitation. The use of non-optimal indirect testing DOFs is likely to have made the problem very poorly conditioned (as discussed in Chapter 4) increasing the calculation's sensitivity to noise and other perturbations. In addition, the ITF was not ideal as the need for both flexibility and strength were found to impose conflicting requirements on the design. The ill-conditioning of the indirect testing calculation

introduced by both the use of sub-optimal measurement locations and a less than satisfactory design are likely to have been the primary reasons for the failure of the method in this case study.

Due to the failure of the FRF-based indirect testing method an alternative approach based on spatial models was used. It has been demonstrated that by employing test-planning test techniques, in conjunction with careful modal testing and high-fidelity FE modelling, that it is possible to obtain a valid model of a structure via the model and remove approach. In hindsight, this case study seems almost too simple an application of the model and remove approach, as the MACE Case is only a single component and not an assembly. However, it is important to understand that this is only the case because care was taken to ensure that the results of the modal tests were unambiguous and that the FE models used were faithful to the structure's geometry in almost every detail.

In order to extend the "model and remove approach" to more complex assembly models it would be necessary to adopt the method used to the validate of the free-free ITF model, which formed one of the most time consuming stages of this case study. Although none of the technology used at the free-free validation stage was new, the approach adopted to the problem of updating the ITF model does represent a significant advance. It is common in the field of model updating to continue expanding the number of updating parameters, such as thickness, stiffness and densities, for example, until a set to which the model is sensitive can be found and altered until the maths fits the physics. This approach to model updating is unusual in the field of mathematical modelling, in which it is not common to improve a model's

validity simply by increasing the number of assumptions it includes. If, as in the case of the ITF, updating parameters are viewed as assumptions, then it becomes logical to reduce their number to as few as possible, measuring unnecessarily "unknown" parameters wherever possible and saving techniques such as design variable or inverse eigen-sensitivity methods for variables which are **truly** unknown. Although it was not of a particularly complex geometry the ITF was extremely resonant, exhibiting 36 modes over the frequency range 0-2000Hz. Ensuring that the ITF model was an accurate representation of the actual structure meant that **all** of the FE calculated modes for the range 0-2000Hz were well correlated and within 2% of the experimental natural frequencies.

With hindsight, virtual testing of the ITF/ MACE Case assembly prior to commencing the tests could have saved a considerable amount of time by identifying the Case modes insensitivity to the ITF leg/ground interface stiffness. Identifying this insensitivity would have reduced the importance of obtaining a valid model of the fixed-free ITF over the frequency range 0-2000Hz and the virtual tests could have been used to set the validation criteria for both the fixed-free ITF and assembly models. The fact that the Case modes were insensitive to the leg/ground interface stiffness was extremely beneficial in this case, meaning that the vast majority of the assembly modes could be ignored at the assembly model validation phase of the indirect testing procedure.

In general, the model and remove approach to indirect testing has been successfully demonstrated in this case. Provided that the indirect testing fixture does not constrain relative motion between the connection DOFs of the structure under test information

relating to the stiffness of these regions will be available. The method also requires considerably less data and data manipulation than does the FRF-based indirect testing method and there is no need to measure RDOFs. For more complex assembly models (and in particular those which contain internal/hazardous components) it is suggested that any sub-component which can be subjected to a modal test **is** tested (either directly if possible or indirectly when necessary) and that the FE assembly model is gradually constructed from valid sub-component "super models" such that for the final indirect test uncertainties relate only to problem components. This "super-modelling" approach to the construction of the assembly model may appear computationally expensive with today's technology, however, the potential to construct extremely high-fidelity models already exists. By way of an example, Figure 5.3.40 shows a FE model of the MACE Case constructed to test the capabilities of Sandia National Laboratory's massively parallel "Salinas" code.

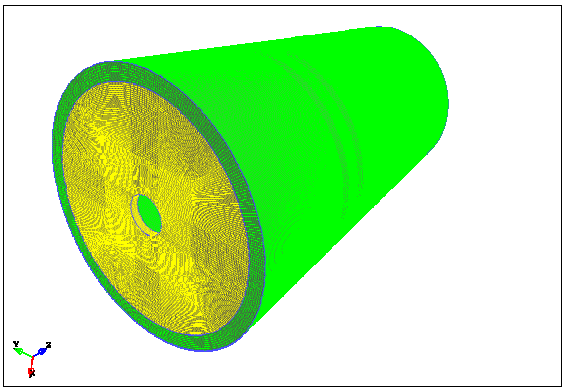

Figure 5.3.40. FE Model of MACE Case/Seal Plate Assembly containing approximately 2 million 20 node brick elements (courtesy of Trevor Hensley (AWE)).

Even with this extremely fine mesh (1942312, 20-node brick elements) the first 30 modes of the Case were extracted in just 1.5 hours using 800 processors of the AWE "Blue Oak" supercomputer. Of course, the real value of such computing power lies not with the capability of generating very large FE models, but rather, with the capability of reducing the number of assumptions such models include.

CHAPTER 6. CONCLUSIONS AND RECOMMENDATIONS FOR FURTHER STUDY

6.1 Conclusions

6.1.1 Overview

As discussed in Chapter 2, the specific objectives of this research were:

1) to investigate of the LDV in conjunction with non-intrusive excitation methods to make measurements for DTA level 3 and 4 applications;
2) the extension of CSLDV methods for application to structures with highly curved surfaces, and;
3) the development of the theory of indirect testing as a possible alternative to completely non-contacting testing, and as a means of inferring information about the dynamic characteristics of internal components.

This Chapter discuses how the research presented in this thesis has met these objectives and the contribution it has made to the state-of-the art.

6.1.2 Minimally-invasive modal testing using impact hammer excitation and LDV response measurement

The application of minimally-invasive impact hammer excitation and non-contacting LDV response measurements has been used to meet the requirements for DTA level 3/4 measurements and fulfil the first of the specific requirements. Impact hammer excitation and LDV response measurement represents an ideal method for the modal testing of many delicate and critical structures. It has been shown via the case study of Chapter 2 that the combination of these two existing technologies is capable of providing the high quality FRF data required for DTA level 3 and 4 applications.

Although this is not a major breakthrough, it does serves as a reminder that before resorting to more exotic, completely non-contacting excitation methods, which compromise the ability to make force measurements, we would be well advised not to rule-out completely the use of hammer impact excitation. The technique is particularly suitable for individual component tests, in which there are likely to be few doubts as to the linear behaviour of the structure at modal excitation levels. It is also worth noting that hammer excitation introduces few hazards[22] since, unlike shaker testing, there is no need for high voltage power supplies or amplifiers. The required test equipment could be developed for remote operation, using pneumatic hammers and either manually repositioning the laser probe between measurements or taking advantage of a scanning LDV's mirror positioning system, this would provide an intrinsically safe method for testing hazardous components.

6.1.3 Application of CSLDV method to axi-symmetric structures

In order to allow the continuous LDV scanning of some of the structures of specific interest which are cylindrical/conical, a new method for the scanning of axi-symmetric structures has been developed. The technique is applicable for any axi-symmetric structure and although it requires fixed-free boundary conditions, it is capable of providing a succinct polynomial representation of an axi-symmetric structures ODS, even if the ODS does not exhibit symmetry because of slight mistuning. Furthermore, the spatial resolution of the scanned image is competitive with that which could be achieved with holography and is better than that of FE models. It is also important to recognise that images such as those shown in Figures 3.3.15 and 3.3.17 could not be obtained using holographic techniques because of the

[22] Levels of electrical charge in close proximity to the test item will be of the order of pC.

line-of-sight requirements of holography systems. The ODS measured using the cylindrical CSLDV technique are easily mapped into a Cartesian co-ordinate system for visual or numerical comparison against FE results, although currently a qualitative eigenfunction comparison is not possible because the circumferential scan frequency is too low to provide adequate side-band separation. One limitation to the cylindrical CSLDV technique is that the polynomial representation may require many coefficients in order to represent an essentially simple, sinusoidal ODS. It is possible however, to circumvent this problem for higher-order ODSs by completing the scan as a series of segments, thereby reducing the number of side-bands required to describe each segment. Breaking the scan into segments in this way may also allow for a full side-band modal analysis (as demonstrated on planar surfaces by Marterelli [3]) since reducing the maximum angle of rotation allows higher scan-frequencies to be employed.

6.1.4 The indirect modal testing of structures

The main contribution to the technical requirements established in this thesis comprise the two new methods for the indirect modal testing of structures which have been developed: the FRF-based method; and the so called "model-and-remove" approach. Both of these methods have been demonstrated to work in practice and it has also been shown that they are both susceptible to "stiff-spring ill-conditioning" as described by Urgueira [77] and discussed in Chapter 4. Furthermore, understanding the physical causes of the indirect testing calculation has allowed the design of indirect testing fixtures to be improved. In the FRF-based approach, stiff-spring ill-conditioning can cause the indirect testing calculation to behave erratically for two reasons:

1) by causing singularity of the remote DOF FRF matrix $\left[H_{aa}^{A}\right]$ if two or more remote measurement DOFs exhibit near-identical motion over the measured frequency range; and/or

2) by causing singularity of the connection DOF matrix $\left[H_{cc}^{A}\right]$ leading to the deletion of one or more DOFs in the coupled system matrix $\left[H_{cc}^{C}\right]$ when the indirect test-fixture is attached to the structure under test.

It has been shown that the first of these reasons for the instability in FRF-based calculations can be avoided by ensuring that the indirect test fixture exhibits at least as many modes as there are connection DOFs. This allows Kammer's EI calculation, [70], to be used in order to select the remote measurement DOFs such that they provide a well conditioned FRF matrix across the frequency range of interest. However, it has also been shown that the second reason for the indirect testing equations' instability can be avoided by careful consideration of the design of the test fixture. Without careful design it is likely that the indirect test fixture will overly constrain the structure-under-test at the connection DOFs, and when this occurs it will **always** lead to an under-determined set of indirect testing equations, possessing an infinite number of solutions. With an understanding of the physics, it is possible to ensure success by eliminating cross-connectivity in the connection DOF FRF matrix $\left[H_{cc}^{A}\right]$.

The possibility that there can be an infinite number of solutions to the indirect testing equation has serious ramifications for the inference of information on the behaviour of internal components from external observations since it is common to include "dynamically redundant" connections in joints. Where such redundant connections

are used to couple an internal component to its housing, the results of indirect inference of the internal component's behaviour must be treated with extreme caution. A statement which applies equally if the model-and-remove approach to indirect testing has been employed. In the case of the model-and-remove approach, the modes of the assembly will be insensitive to the stiffness of the internal structure between the co-ordinates that have been deleted. There will therefore be no information available about these regions against which the sub-component model can be checked.

It has also been shown that the FRF-based indirect testing method is extremely sensitive to measurement reciprocity errors. This is because the method describes the structures of interest by their behaviour and it is therefore of the utmost importance that their behaviour is accurately observed. In the case of FRF-based indirect testing, assuming or forcing reciprocity on data which do not exhibit it will lead to the calculation yielding results for a system which is not physically realisable.

The model-and-remove approach has been demonstrated to be the more easily practicable and stable of the two indirect testing methods developed in this thesis. Since the model-and-remove approach to indirect testing relies on validated spatial models developed using the FE method, it can take advantage of the wealth of research aimed at the modal level validation of FE models and is, in fact, a new application of modal testing, rather than a new modal testing method. In the case study of Section 5.3, the method reduced what was an extremely difficult case for FRF-based indirect testing method, to a relatively simple problem. This was achieved by utilising Fotsch's philosophy of ensuring that each component was modelled in all of its detail, and by taking advantage of insensitivity of the assembled structure to the

leg/ground interface stiffness. It is noted that the FRF-based indirect testing method's requirement for a test fixture which exhibits at least as many modes as coupling DOFs meant there was an abundance of data against which to check that the FE model of that structure was valid and also that the effect of the test fixture on the dynamic behaviour of the MACE case was minimal[23]. This is an interesting feature of the case study, since it illustrates how the meeting of the requirements for a well-conditioned problem in the FRF-based indirect testing method is also beneficial when indirect testing is approached using spatial models. With careful design of the indirect testing fixture the model-and-remove approach is applicable to most structures, although further research is required into its application to more complex assemblies. It is the author's belief that by adopting a "super-modelling" approach to the problems posed by assemblies, in conjunction with the modal level validation of every component / sub-assembly which **can** be tested individually, that the proposed model-and-remove method represents the optimal method of testing the structures for which the research in this thesis is intended.

6.1.5 The use of LDV for indirect test measurements

It should be noted that neither the FRF based or model and remove approaches to indirect testing have any specific response transducer requirements. In the case of the structures of specific interest, the LDV will can be used to collect FRF measurements from a surface to which it is impossible to attach a contacting transducer. Trials have demonstrated that a good signal level is achieved when the LDV is used to make measurements on the untreated surface's of the structures of interest and so the LDV

[23] The natural frequency of the "first ovaling" mode of the MACE case, for example, was changed by the addition of the indirect testing fixture from 585 Hz to 607 Hz, a 3.6 % increase.

can simply be used as alternative to contacting accelerometers in either the model and remove or FRF based indirect testing method.

6.2 Recommendations for further study

6.2.1 Application of FRF-based indirect testing for sub-structuring applications

Although the practical implementation of FRF-based indirect testing is extremely difficult (particularly when the structure-under test is connected to the test fixture at more than one co-ordinate) it may still provide a useful tool in FRF-based sub-structuring. One notable feature of the FRF-based indirect testing method is that it **does not** require the measurement of point rotations nor does it rely on the usual finite difference method in order to determine information about the point rotational FRFs at the connection DOF. Also, the calculation inherently allows for flexibility of the test-fixture and does not, as in the case of many RDOF measurement techniques, assume a rigid test fixture. Against these potential benefits is the fact that the method requires extremely accurate measurements. However, the requirement for measurement accuracy is a feature of many RDOF measurement methods including the usual rigid block methods.

6.2.2 Stiff spring ill-conditioning

Often, when attempting DTA level 4 applications, such as sub-structuring, force determination, assembly modelling or, indeed, indirect testing, a point is reached where the analyst concedes defeat, citing the ill-conditioning of the problem as the major reason for their calculations' unsatisfactory performance. It is noted, for example, that predicting the response of a cantilevered beam based upon measurements on a free-free beam is an arduous task requiring the accurate measurement of many more modes than those required to predict the free-free

response of two beams added together [85]. Also, in force determination examples such as the example given in [1] and illustrated in Figure 6.2.1 below, it is found that no unique solution exists because the problem is ill-posed since an attempt is being made to determine three unknowns, based on five measurements, when only two independent variables (the block's translational and rotational degrees of freedom) are available.

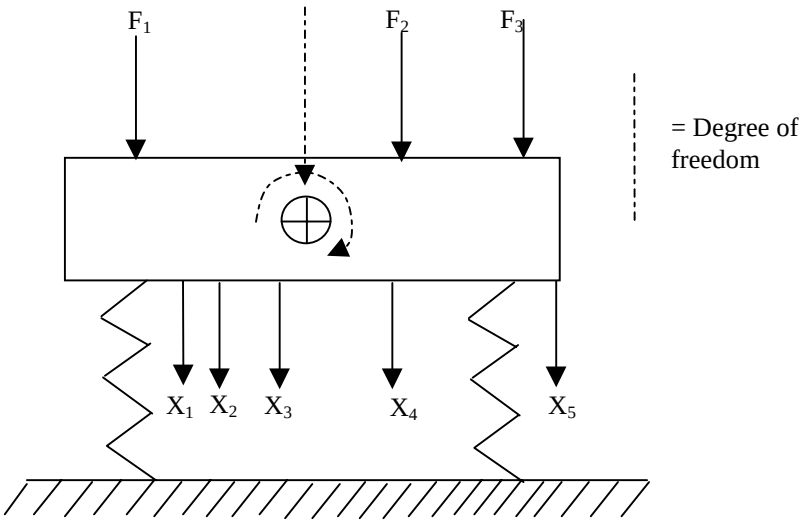

Figure 6.2.1. Ill-posed force determination example: it is not possible to uniquely determine the three applied forces, even though five response measurements are made since the system only possesses two degrees of freedom.

Similar problems are of course also found in indirect testing, as illustrated in Chapter 4, and sub-structuring, when situations such as that illustrated in Figure 6.2.2 are encountered.

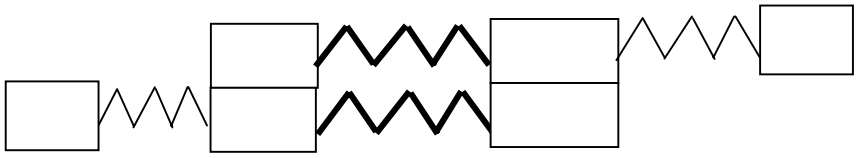

Figure 6.2.2. The sub-structuring problem becomes ill-conditioned when both structures include FRFs measured at one or more apparently redundant co-ordinates.

In this work, examples were considered in which the stiff springs became infinitely stiff, something which never happens in real structures, but which **can** appear to happen when measurement data are truncated to a limited number of significant figures. When data are truncated in this way, shallow curves become straight lines and what may be two or more DOFs in reality appear to be one: a problem which leads to "dynamically indeterminate systems" in all of the examples given thus far. It is also worth noting that stiff-spring ill-conditioning may be responsible for the problem of "clustering" in the EI calculation. As FE meshes become increasingly fine, the distance between nodes becomes smaller and the nodes are therefore connected by stiffer springs. The EI calculation includes an inversion of the predictor matrix (usually denoted as [A]) and while this matrix is always of full rank, this is not a guarantee that the matrix is well conditioned. Also, the numerical data with which the calculation is provided has usually already been truncated from the FE model's (16 or 32 bit) precision to six decimal place ASCII text format and so some information has already been lost. It is also worth mentioning here that the test plans produced by the EI method inherently assume that measurements can be made to 6 decimal place accuracy. An interesting feature of stiff spring ill-conditioning is that it can lead to insensitivity to stiffness parameters, such as in the case of the ITF/MACE case assembly, some assembly modes are not affected by joint stiffnesses. It has been known for some time that certain modes of sub-components are critical when that sub-component is included in an assembly, while other modes that sub-structure exhibits are not and it is possible that stiff spring ill-conditioning contributes to this behaviour. It is felt that further research into how this form of ill-conditioning affects each of a structure's different representations (spatial, modal or response) may lead to better understanding of why certain calculations, which although are theoretically

possible, do not work in practice and why it found that the responses of some sub-assemblies are easier to predict than others.

6.3 Closure

The new methods that have been discussed in this thesis for measuring the dynamic properties of structures which are difficult to measure using standard modal testing techniques either for technical or regulatory reasons are already beginning to be applied to the actual structures for which the research presented in this thesis was intended. Although some development work is still required for widespread application of the methods , this thesis has presented the basis upon which experimental data can be obtained from these critical structures and against which FE models of them can be validated.

REFERENCES

[1] Ewins, D.J. 2000. "Modal Testing 2", Research Studies Press.

[2] Dynamic Test Agency. 1996. "Primer on Best Practice in Dynamic Testing", Chameleon Press.

[3] Martarelli, M., 2001. "Exploiting the Laser Scanning Facility for Vibration Measurements", Ph.D. Thesis, Imperial College London.

[4] Polytec Product Guide, "Scanning Vibrometer", Ref. No. PSV-E-7-9803-5000.

[5] Bell, J.R.; Rothberg S.J. 2000. "Laser Vibrometers and Contacting Transducers, Target Rotation and Six Degree of Freedom Vibration: What Do We Really Measure?" *J. Sound & Vibration*. 237(2). pp245-261.

[6] Polytec Product Guide "Polytec Compact 3D Laser Vibrometer CLV-3D".

[7] Polytec Product Guide, "Scanning 3D LDV".

[8] Castellini, P., Revel, G.M. 1999. "Tracking Laser Vibrometer Measurements for Estimation of Excitation Level in Rotating Structures", Proc. 17th Int. Modal Analysis Conf., pp. 1005-1011.

[9] Castellini, P., Cupido, E. 2001. "Vibration Measurements on Wind-Screen Wipers by Tracking Laser Doppler Vibrometer", Proc 19th Int. Modal Analysis Conf., pp. 457-463.

[10] Stanbridge, A.B., Ewins, D.J. 1994. "Measurement of Translational and Angular Vibration using a Scanning Laser Doppler Vibrometer", 1st International Conference on Vibration Measurements by Laser Techniques, Ancona, Italy, Proc. SPIE Vol. 2358. Shock Vib. 3(2) 141-152 1996.

[11] Stanbridge, A.B., Ewins, D.J. 1996. "Measurement of Total Vibration at a Point using a Conical-Scanning LDV", 2nd International Conference on Vibration Measurements by Laser Techniques, Ancona, Italy, Proc. SPIE Vol. 2868, pp. 126-136.

[12] Stanbridge, A.B.,Martarelli, M., Ewins, D.J. 1999. "Measuring Area Mode Shapes with a Scanning Laser Doppler Vibrometer", Proc 17th Int. Modal Analysis Conf., pp. 980-985.

[13] Stanbridge, A.B., Ewins, D.J. 1996. "Using a Continuously Scanning LDV for Modal Testing", Proc 14th Int. Modal Analysis Conf., pp. 816-822.

[14] Stanbridge A. B., Martarelli, M., Ewins, D.J., 2002, "Measuring Strain Response Mode Shapes with a Continuous-Scan LDV", *Shock and Vibration*, **9** (1-2), pp 19-27.

[15] Stanbridge, A.B., Martarelli, M., Ewins, D.J. 1999. "The Scanning Laser Doppler Vibrometer applied to Impact Modal Testing", Proc 17th Int. Modal Analysis Conf., pp. 986-991.

[16] Slangen, P., Berwart, L., de Veuster, C., Golinval, J.C. Lion, Y. 1994. "Digital Speckle Pattern Intererometry (DSPI): A Fast Procedure to Detect and Measure Vibration Mode Shapes", Vibration Measurements, Proc. SPIE 2358, pp. 102-110.

[17] Wang, Z., Walz, T., Ettemeyer, A. 2000. "3D-PUSLESPI Technique for Measurement of Dynamic Structure Response", Proc. 18th Int. Modal Analysis Conf., pp. 1362-1368.

[18] Crawforth, L., Munce, A.C., Moser, M.A. 1993. "Quantitative Measurement of Dynamic Deformations Using Pulsed Holographic Interferometry", Proc. 11th Int. Modal Analysis Conf., pp. 130-137.

[19] Van der Auweraer, H., Steinbichler, H., Haberstok, C., Freymann, R., Storer, D. 2000. "Integration of Pulsed-Laser ESPI with Spatial Domain Modal Analysis: Results From the Salome Project. Proc. 4th Int. Conf. On Vibration Measurements by Laser Techniques. pp 313-322.

[20] Sciammarella, C.A. 1982. "The Moiré Method – A Review", *Experimental Mechanics*, vol. 22(11) pp. 418-433.

[21] Mitchell, A.K., Harvie, F.L. 2000. "Modal Testing of Large Structures Using Projected Grid Moiré", Proc. 18th Int. Modal Analysis Conf., pp. 1063-1069.

[22] Patton, M.E., Trethewey, M.W. 1987. "A Survey and Assessment of Non-Intrusive Modal Testing Techniques for Ultra-lightweight Structures", *Int. J. of Analytical and Experimental Modal Analysis.*, **2** (4), pp. 163-173.

[23] Brown, D.L., Halvorsen, W.G., 1972. "Application of Coherence Functions to Acoustic Noise Measurements", Inter-Noise Proc 1972. pp 233-245.

[24] Forssen, B., Crocker, M.J. 1983. "Estimation of Acoustic Velocity, Surface Velocity, and Radiation Efficiency by use of the 2-Microphone Technique", *J. Acoust. Soc. Am.* **73** (3), pp. 1047-1053.

[25] Okubo, N., Nakane, N., Miyano, H., Nogiwa, Y. 1985. "3-Dimensional Acoustic Intensity Measurement by use of 4 Microphones", Proc. 3rd Int. Modal Analysis Conf., pp. 652-659.

[26] Smiley, R.G. 1985. "Relating Acoustic Intensity Measurements and Modal Analysis Test Results", Proc. 3rd Int. Modal Analysis Conf., pp. 665-667.

[27] Musson, B.G., Stevens, J.R. 1986. "Comparison of Modal Test Results from Non-Contacting and Conventional Response Measurements", Proc. 4th Int. Modal Analysis Conf., pp. 1487-1493.

[28] Oliver, D.E., Gilbey, J., Webber, W.R.S. 1986. "Non-Contact Stress Pattern Analysis of Structures with Complex Waveforms", Proc. 4th Int. Modal Analysis Conf., pp. 1181-1186.

[29] Hillary, B., Ewins, D.J. 1984. "The use of Strain Gauges in Force Determination and Frequency Response Function Measurements", Proc. 2nd Int. Modal Analysis Conf., pp. 627-634.

[30] Song T.X., Zhang P.Q., Feng W.Q., Huang T.C. 1986. "The Application of the Time Domain Method in Strain Modal Analysis", Proc. 4th Int. Modal Analysis Conf., pp. 31-37.

[31] Debao, L., Hongcheng, Z., Bo, W. 1989. "The Principle and Techniques of Experimental Strain Modal Analysis", Proc. 7th Int. Modal Analysis Conf., pp. 1285-1289.

[32] Okubo, N., Hirano, T. 1987. "Dynamic Strain Analysis of a Substructure by use of the experimental Modal Analysis and the Finite Element Method", Proc. 5th Int. Modal Analysis Conf., pp. 1669-1673.

[33] H. Joseph Weaver, Jennifer K. Dowdell. 1984. "Modal Parameter Estimation Via Shaker Vs Speaker Excitation", Proc. 2nd Int. Modal Analysis Conf., pp. 887-893.

[34] Musson, B.G., Stevens, J.R. 1985. "Comparison Of Acoustic And Mechanical Excitation For Modal Response Measurements", Proc. 3rd Int. Modal Analysis Conf., pp. 124-130.

[35] Elliott, K.B., Robinson, J. 1988. "Estimation of Distributed Acoustic Loads", Proc. 6th Int. Modal Analysis Conf., pp. 1199-1206.

[36] Castellini, P., Esposito, E., Miandro, F., Paone, N., Santolini, C., Tomasini, E.P. 1999. "Non-Invasive Measurements of Structural Damage by Laser

Scanning Vibrometer: An Experimental Comparison Among Different Exciters", Proc. 17th Int. Modal Analysis Conf., pp. 692-698.

[37] Parloo, E., Verboven, P., Guillaume, P., Van Overmeire, M. 2001. "Sensitivity-Based Mass Normalisation of Mode Shape Estimates from Output-Only Data", Int. Conf. on Structural System Identification, 5-7 Sept 2001, University of Kassel (Ger), Vol.2, pp. 627-636.

[38] French, M., Knittel, J., Wyszynski, A. 1996. "Applications of Laser Methods to Automotive Seat Modal Testing", 2nd International Conference on Vibration Measurements by Laser Techniques - Advances and Applications, pp. 112-118.

[39] Wilson, C.J., Bogy, D.B. 1996. "An Experimental Modal Analysis Technique for Miniature Structures", *J. of Vibration and Acoustics*, **118**(1), pp. 1-9.

[40] Patton, M.E., Tretheway M.W. 1989. "A Non-Contacting Excitation Technique for Modal Analysis", Proc. 7th Int. Modal Analysis Conf., pp. 894-900.

[41] Bucher, I., Rozenstain, M. 2001. "Determination of External Forces – Application to the Calibration of an Electromagnetic Actuator", Proc. DETC'01, Pittsburgh, pp. 1-8.

[42] Forch, P., Gahler, C., Nordmann, R., 1996, "Modal Testing in Rotating Machinery Using Active Magnetic Bearings", 6th Int. Conf. On Vibrations in Rotating Machinery, Oxford, 9-12 Sept.

[43] Saldner, H.O. 1994. "Calibrated Non-Contact Exciters for Optical Modal Analysis", Vibration Measurements, SPIE Vol. 2358, pp. 227-237.

[44] Koss, L.L., Tobin R.C. 1983. "Laser Induced Structural Vibration", *J. of Sound and Vibration*, **86**(1), pp. 1-7.

[45] Philip, W.R., Booth, D.J., Perry N.D. 1995. "Single Pulse Laser Excitation of Structural Vibration Using Power Densities Below the Surface Ablation Threshold", *J. of Sound and Vibration*, **185**(4), pp. 643-654.

[46] Castellini, P., Revel G.M., Scalise, L., De Andarde, R. M. 2000. "Laser Pulses in Modal Analysis an Experimental and Numerical Investigation. Proc. 18th Int. Modal Analysis Conf., pp. 1611-1617.

[47] Castellini, P., Revel G.M., Scalise, L. 2000. "Application of Lasers for Non-Contact Excitation and Measurement of Vibration", 4th International Conference on Vibration Measurements by Laser Techniques - Advances and Applications, pp. 280-291.

[48] Zhang, P.Q., Tang, X.L., Shan, B.X. 1998. "Analytical and Experimental Modal Analysis for Operational Validation and Calibration of a Miniature Silicon Sensor", *J. of Sound and Vibration*, **214**(5), pp. 903-913.

[49] Chou, Y.F., Wang, L.C. 1999. "Modal Testing for Microstructures", Proc. 17th Int. Modal Analysis Conf., pp. 1783-1788.

[50] McConnell, K.G., 1995. "Vibration Testing", John Wiley & Sons.

[51] Private communication with Prof. D.J. Ewins, regarding the work of J. Woodhouse (Cambridge University). 2001.

[52] Filiatrault, A., Cherry, S. 1987. "Modal Parameter Estimation of a Steel Moment Resisting Frame from Base Excitation", Proc. 5th Int. Modal Analysis Conf., pp. 374-380.

[53] G.F. Mutch G.F., Vold, H. 1984. "The Dynamic Analysis of a Space Lattice Structure Via the use of Step Relaxation Testing", Proc. 2nd Int. Modal Analysis Conf., pp. 368-377.

[54] Sinapius, J.M. 1996. "Identification of Free and Fixed Interface Normal Modes by Base Excitation", Proc. 14th Int. Modal Analysis Conf., pp. 23-31.

[55] Chen, J.S., Su, C.P., Chou, Y.F. 1995. "Modal Analysis of Miniature Structures", Proc. 13th Int. Modal Analysis Conf., pp. 969-975.

[56] Der Auweraer, H.V., Hermans, L. 1999. "Applications of Structural Model Identification During Normal Operating Conditions: An Overview of the Eureka Project Synopsis". Proc. 17th Int. Modal Analysis Conf., pp. 27-34.

[57] Abdelghani, M., Goursat, M., Biolchini, T., et al. 1999. "Performance of Output Only Identification Algorithms for Modal Analysis of Aircraft Structures", Proc. 17th Int. Modal Analysis Conf., pp. 224-230.

[58] Ren, W. X, Zong, Z. M., 2002, "Output Only Modal Parameter Identification of Civil Engineering Structures", *Struct. Eng. Mech.* **17**(3-4) pp. 429-444.

[59] Hermans, L., Van der Auweraer H., Mevel, L. 1999. "Health Monitoring and Detection of a Fatigue Problem of A Sports Car", Proc. 17th IMAC pp 42-48.

[60] Brincker, R; Andersen, P., 2002, "A Way of Getting Scaled Mode Shapes in Output Only Modal Testing", Proc. IMAC 21, pp. 141-145.

[61] Liu, W.; Ewins, D.J., 2000, "The Importance of RDOF in FRF Coupling Analysis", Proc. IMAC 19. pp 1160-1166.

[62] Yoshimura, T.; Hosoya, N., 2000, "FRF Estimation of Rotational DOFs by Rigid Block Attachment Method", ISMA25 Proceedings, pp. 1021-1027.

[63] Mottershead, J.E., Kyprianou A., Ouyang, H.; In Print; Structural Modification, Part 1: Rotational Receptances", Submitted for publication in *J. of Sound and Vibration* 2004.

[64] Salter, J.P., 1969 "Steady State Vibration", Kenneth Mason.

[65] Jorgensen, B.R; Woehrle, T; Eli, M; Chow, CT., 1999, "Modal Response of Interior Mass Based Upon External Measurements", Proc. IMAC 17, pp. 2038-2041.

[66] Maia N.M.M; Silva J.M.M; Silva P.L.C.G.C., 2000, "Identification of the dynamics behaviour of joints using sub-structuring methods". Proc 18th Int. Modal Analysis Conf, pp 923-929.

[67] Unpublished AWE reports/data. Ind P. R., "Hybrid Modelling".

[68] Unpublished AWE reports/data. Reece, C., "Modal Coupling Research Program (MCRP)".

[69] ICATS 2003 (Modent / Modesh / Modplan) User Manual.

[70] Kammer, D. C.; "Sensor Placement for On-Orbit Modal Identification and Correlation of Large Space Structures," Journal of Guidance, Control, and Dynamics, **14**(2), 1991, pp. 251-259.

[71] Montgomery D. E.; West R. L., "Three-dimensional experimental spatial dynamic response of a reciprocating Freon compressor", First International Conference on Vibration Measurement by Laser Techniques, Proc. SPIE, **2358**, 200-211, 1994.

[72] Stanbridge, A.B., 2003, "Scanalxyplot", Matlab Script, Imperial College London.

[73] A.B. Stanbridge, P. R. Ind, D.J. Ewins., 2004, "Measuring Vibration of Cylindrical Surfaces using a Continuous-Scan LDV". Sixth International

Conference on Vibration Measurement by Laser Techniques, Proc. SPIE, pp-249-259.

[74] Dong, J.; McConnell K. G., 2002, “Extracting Multi-Directional FRF Matrices with “Instrument Cluster”, Proc. IMAC 20, pp. 751-764.

[75] Bishop, R.E.D.; Johnson D.C., “The Mechanics of Vibration”,Cambridge University Press, 1960.

[76] Jetmundsen, B.; Bielawa, R.L.; Flannelly, W.G., “Generalized Frequency Domain Substructure Synthesis”, J. of the American Helicopter Society, pp. 55-64, 1960.

[77] Urgueira, A.P.V, 1989, “Dynamic Analysis of Coupled Structures Using Experimental Data” PhD Thesis, Imperial College London.

[78] Ansys (V.8) User Manual 2004.

[79] Trethewey, M.W., Sommer, H.J., “Measurement of Rotational DoF Frequency Response Functions with Pure Moment Excitation”, Proc. Int. Conf. On Structural Dynamics Testing, Madeira, 3-5 June 2002.

[80] Ewins, D. J., 1980, “On predicting Point Mobility Plots from Measurement of other Mobility Parameters”, *J. of Sound and Vibration*, 70, 69-75.

[81] Hopkins R.N.; Carne, T.G.; Dohrmann C.R.; Nelson, C.F.; O’Gorman, C.C., 2004, “Combining Test-based and Finite Element-based Models in NASTRAN”, Proc. IMAC 22, pp 217-222.

[82] Fotsch, D.W., 2001, “Development of Valid FE Models For Structural Dynamics Design”, PhD Thesis, Imperial College, London.

[83] Walther, H; Kmetyk, L; Holzmann, W; Segalman, D., 2004, “Model Correlation with Closely Spaced Modes” Proc. IMAC 22, pp 233-240.

[84] James. G, 1993, “Advanced Modern Engineering Mathematics”, Addison-Wesley

[85] Private communication regarding FRF sub-structuring with Prof. D.J. Ewins. 2003.

[86] Maia, N.M.M, Silva, J.M.M, Ribeiro, A.M.R. 1997. “Some Applications of Coupling/Uncoupling Techniques in Structural Dynamics. Part 3. Estimation of Rotational Frequency-Response-Functions using MUM”, Proc. 15th IMAC, pp-1453-1462.

[87] A. B. Stanbridge & D. J. Ewins, “Modal Testing using a Scanning Laser Doppler Vibrometer”, *Mechanical Systems and Signal Processing*, **13**(2), 255-270, 1999.

[88] Yasuda, C; Riehle, P. J., Brown D. L. and Allemang R. J., 1986, “An Estimation Method for Rotational Degrees of Freedom using a Mass Additive Technique”, Proccedings of IMAC IV, pp. 691-699.

[89] Mares, C; Mottershead, J.E; Friswell, M., 2001, “Vibration Tests Using Fictitious Modifications”, International Conference on Structural System Identification, Kassel, Germany, pp. 617-626.

[90] Mares, C; Mottershead, J. E; Friswell, M. I, 2003, “Results Obtained by Minimising Natural Frequency Errors and Using Physical Reasoning”, *Mechanical Systems and Signal Processing*. 17 (1), pp 39-46.

APPENDIX 1: INDIRECT TESTING OF THE MACE CASE

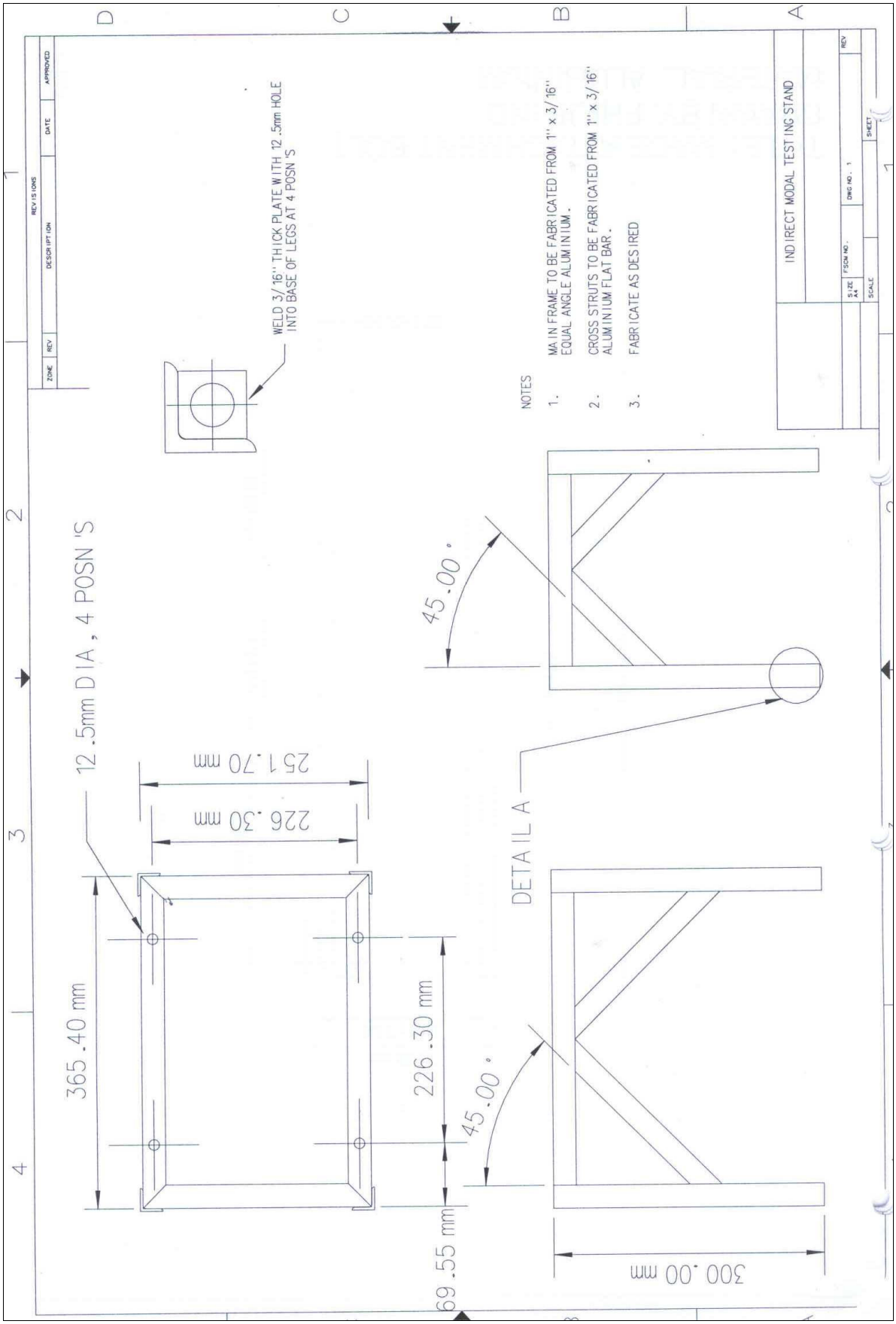

Figure A.1. 1. Final design for the indirect test fixture.

MODE No. (Exp/FE)	Experimental Natural Frequency (HZ)	FE Natural Frequency (HZ)	MAC	Error (%)
1/1	37.6	38.5	90.1	2
2/2	220.3	216.7	95.0	2
3/3	226.9	221.9	96.7	2
4/4	253.1	249.6	97.2	1
5/5	266.9	263.8	97.7	1
6/6	275.3	272.4	97.3	1
7/7	336.4	336.5	96.4	0
8/8	364.1	364.0	96.4	0
9/9	455.7	462.5	97.2	1
10/10	487.3	494.1	97.3	1
11/11	608.0	605.8	94.7	0
12/12	611.7	608.2	91.7	1
13/13	662.5	649.1	87.9	2
14/14	671.8	666.3	83.4	1
15/16	733.2	742.7	95.4	1
16/15	756.3	740.6	95.7	2
17/17	807.2	827.2	95.4	2
18/19	830.8	839.5	85.8	1
19/18	835.4	838.5	90.0	0
20/20	901.2	909.0	93.4	1
21/21	943.3	954.4	84.3	1
22/22	1012.1	1003.0	81.1	1
23/23	1023.8	1017.7	79.2	1
24/24	1072.8	1070.1	92.5	0
25/25	1111.36	1098.3	89.9	1
26/26	1165.8	1148.4	93.1	1
27/27	1288.6	1278.4	93.1	1
28/28	1345.8	1330.4	95.2	1
29/29	1390.6	1366.8	86.0	2
30/30	1471.0	1443.6	91.3	2
31/31	1534.2	1508.2	94.8	2
32/32	1584.2	1571.3	78.9	1
33/33	1604.5	1575.5	89.0	2
34/34	1669.8	1670.9	85.2	0
35/35	1722.2	1710.8	91.8	1
36/36	1856.7	1827.6	84.1	2

Table A.1- 1. First 36 natural frequencies and MACs for the final free-free indirect test fixture model.

MODE No. (Exp/FE)	Experimental Natural Frequency (HZ)	FE Natural Frequency (HZ)	MAC	Error (%)
1/1	144.7	142.2	96.8	2
2/2	193.1	196.9	95.9	2
3/3	236.0	230.2	92.2	3
4/4	295.2	293.0	91.3	1
5/5	316.0	311.8	98.2	1
6/6	406.5	401.55	94.7	1
7/7	468.3	469.4	92.3	0
8/8	477.7	483.2	86.6	1
9/9	550.2	548.7	87.8	0
10/10	579.3	559.0	78.5	3
11/11	672.23	659.5	82.8	2
12/12	691.1	679.9	90.5	2
13/14	783.5	775.2	78.3	1
14/13	794.8	780.6	79.3	2
15/15	859.8	837.8	91.9	3
16/16	899.9	878.9	83.9	2
17/18	1046.7	1040.1	58.2	1
18/17	1062.4	1036.7	67.5	2
19/19	1130.4	1106.0	88.3	2
20/20	1187.2	1149.6	76.4	3
21/21	1210.8	1190.7	72.5	2

Table A.1- 2. First 21 natural frequencies and MACs for the final fixed-free indirect test fixture model.

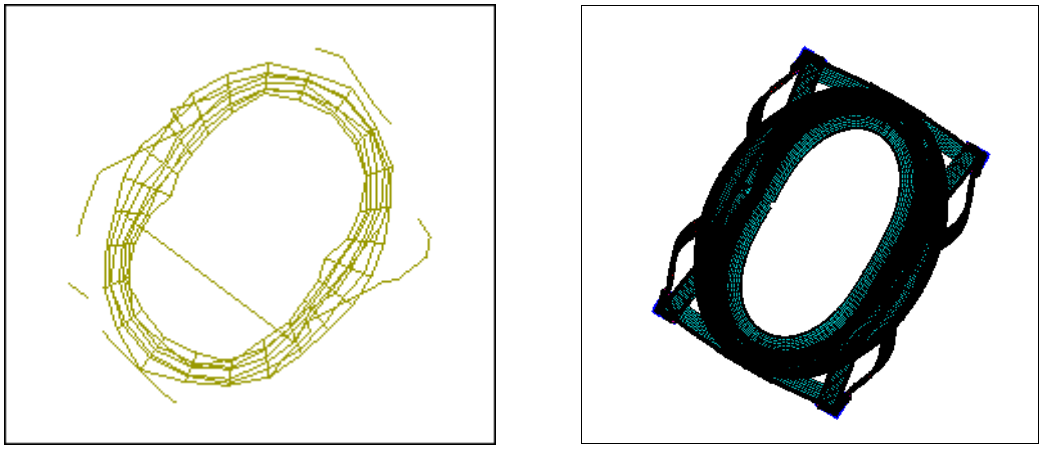

(a) (b)

Figure A.1. 2. (a) Experimental mode at 618 Hz. (b) FE mode at 607 Hz.

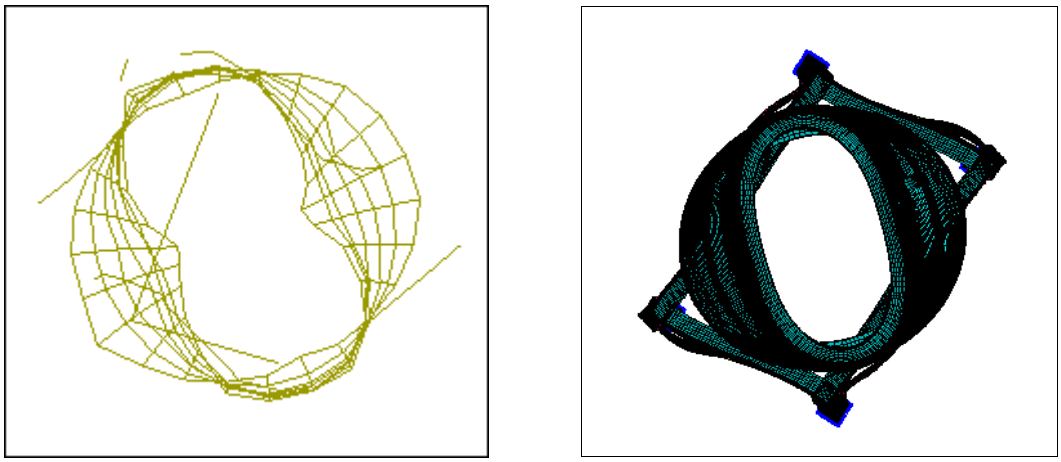

(a) (b)

Figure A.1. 3. (a) Experimental mode at 670 Hz. (b) FE mode at 657 Hz.

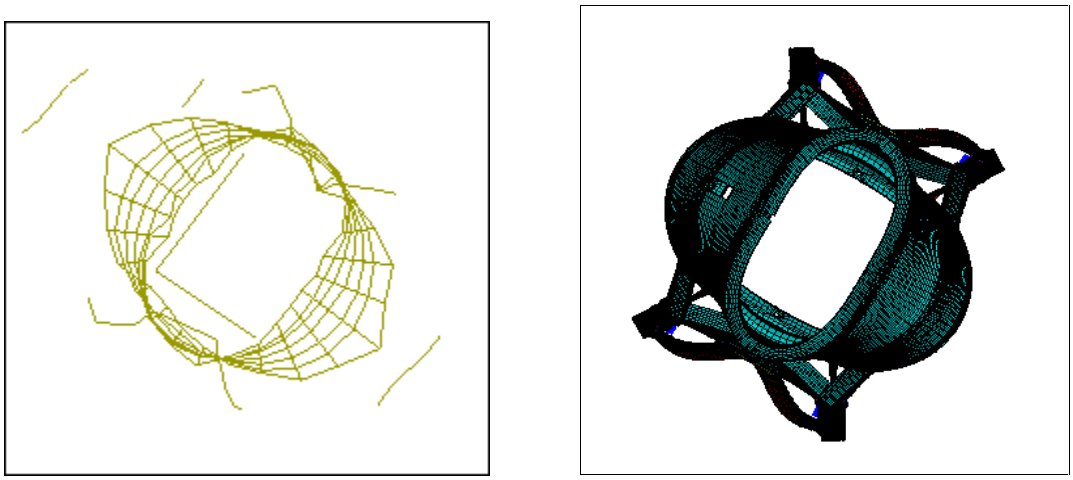

(a) (b)

Figure A.1. 4. (a) Experimental mode at 994 Hz. (b) FE mode at 970 Hz

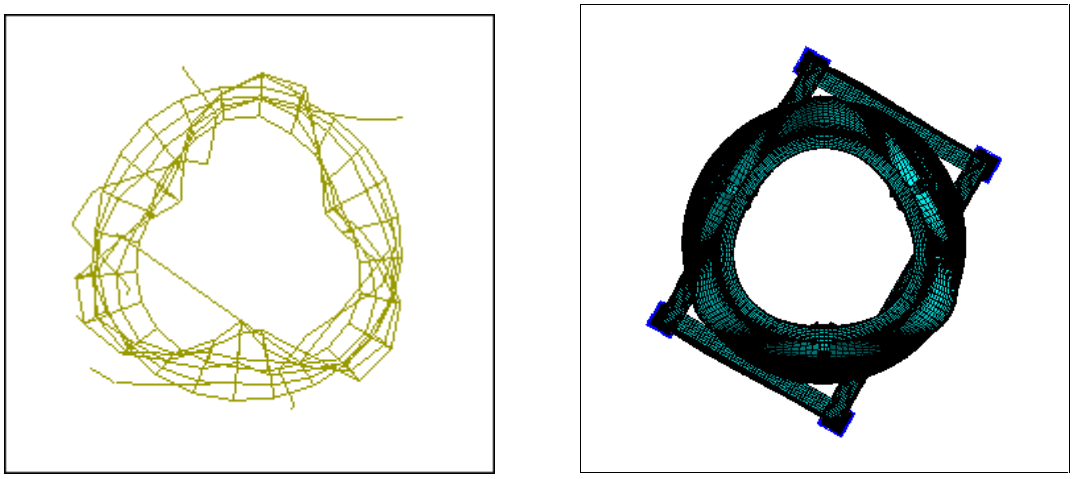

(a) **(b)**

Figure A.1. 5. (a) Experimental mode at 1243 Hz. (b) FE mode at 1243 Hz

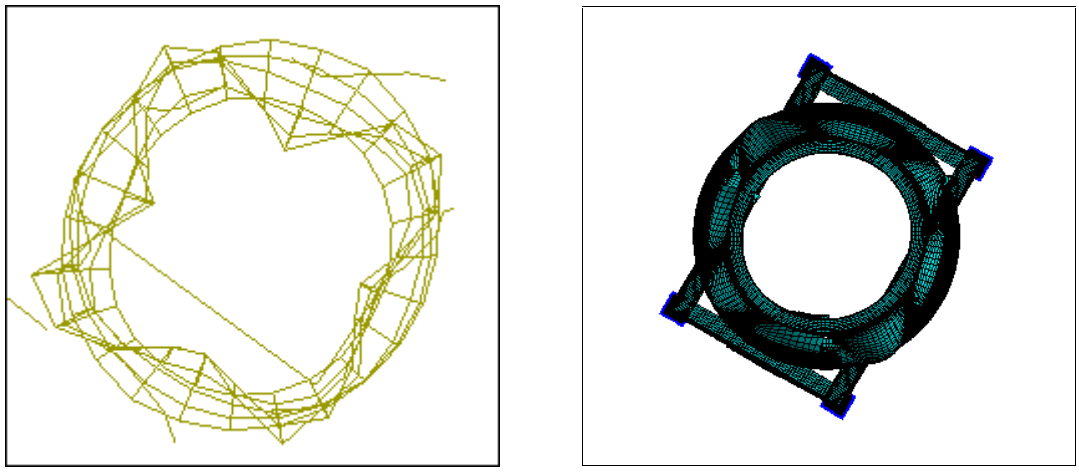

(a) **(b)**

Figure A.1. 6. (a) Experimental mode at 1497 Hz. (b) FE mode at 1495Hz

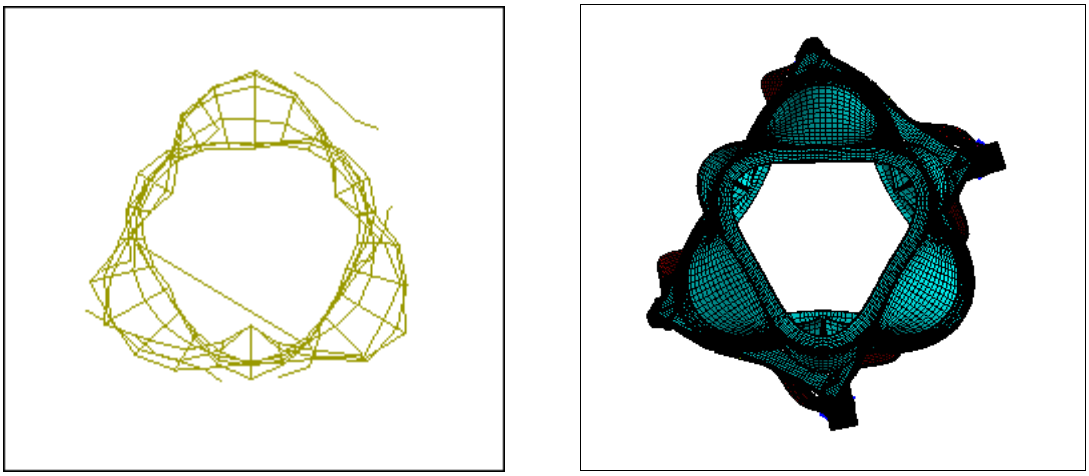

(a) **(b)**

Figure A.1. 7. (a) Experimental mode at 1805 Hz. (b) FE mode at 1792 Hz